Short- and long-term acclimation of plants to different growth light conditions

Inaugural-Dissertation

For attaining the titel of Doctor (Dr. rer. nat.)
in the Faculty of Mathematics and Natural Sciences
at Heinrich-Heine-Universität Düsseldorf

Presented by

Tobias Schumann

From Viersen, Germany

Düsseldorf, December 2015

From the Institute of Plant Biochemistry,
Heinrich-Heine-Universität Düsseldorf

Printed with permission from the Faculty of Mathematics and Natural Sciences,
Heinrich Heine University Düsseldorf

Supervisor: Prof. Dr. Peter Jahns

Co-Supervisor: Prof. Dr. Georg Groth

Date of Oral Examination: 17th of February 2016

Der Gewalt fehlt es an Stärke, wenn der Verstand die Oberhand gewinnt.

STATEMENT OF DECLARATION

I, Tobias Schumann, hereby declare that I have fully and independently written the submitted dissertation without additional unauthorized support and consultation beyond that permitted and specified in the dissertation to include the necessary and appropriate cited literary resources. The dissertation in its present or similar form has not been previously submitted under the same or otherwise specified institution and department name. Previous unsuccessful oral examinations have not been registered or attempted.

Düsseldorf, December 15th 2015

Table of Contents

1 Introduction

Photosynthetic organisms provide the basis for oxygenic life on earth. During oxygenic photosynthesis, plants and other phototrophic organisms absorb and utilize light energy to reduce carbon dioxide (CO_2) to carbohydrates. As a byproduct, molecular oxygen is released through oxidation of the primary electron donor H_2O. During this process, light energy is converted into chemically available energy in form of ATP and reducing equivalents (NADPH) which are then used for the biosynthesis of organic compounds. During their whole life cycle, photosynthetic organisms have to cope with a number of environmental stress factors, such as drought, temperature and light. Unlike green algae and cyanobacteria, which are able to avoid stress via movement, land plants are sessile organisms and therefore unable to escape stress conditions. Thus, a complex network of defense mechanisms has evolved to protect the plant and to ensure the survival of plants under adverse environmental conditions. Most abiotic factors (e.g. temperature and water availability) change on a rather long time scale on a daily or seasonal basis, but particularly the light intensity can vary within seconds to minutes over orders of magnitudes due to cloud movement or shading in dense plant communities. The ability to acclimate to long- and short-term changes in the environmental conditions is thus essential for the survivability and fitness of plants.

1.1 The chloroplast: site of photosynthesis in plants and green algae

In green algae and plants, photosynthesis takes place in chloroplasts. Chloroplasts are semi-autonomous organelles which supposedly originate from cyanobacterial ancestors (Cavalier-Smith, 2000). Nowadays, 95 % of the chloroplast genes are nucleus encoded (Schleiff and Becker, 2010), however many chloroplast multi-protein complexes contain both, chloroplast and nucleus encoded subunits. Chloroplasts in plants are mainly localized to the mesophyll and parenchyma tissue.

The chloroplast consists of two envelope membranes which are residuals of endosymbiosis (Lee et al., 2014). An inner membrane system, the thylakoid membrane, separates the stromal space from the thylakoid lumen (Figure 1.1). Light harvesting and CO_2 fixation are spatially divided within the chloroplast: the light reaction is localized in the thylakoid membrane, whereas the carbon assimilation is localized in the chloroplast stroma. Notably, the majority of plant membranes are build up by glycolipids, as opposed to animal or yeast membranes that are composed of phospholipids. Three species of glycolipids, MGDG, DGDG, and SQDG account for more than 80 % of the chloroplasts lipids (Webb and Green, 1991; Dörmann and Benning, 2002; Kirchhoff et al., 2002; Pribil et al., 2014). The advantage of using glycolipids instead of phospholipids is related to the often limiting availability of

phosphate (Dörmann and Benning, 2002). Mutant plants affected in MGDG or DGDG synthesis, showed severe changes in the chloroplast ultrastructure (Dörmann et al., 1995; Jarvis et al., 2000). Mutants lacking DGDG were also shown to be affected in the amount of photosynthetic protein complexes (Härtel et al., 1997), the rate of water oxidation (Reifarth et al., 1997), and the conversion of the xanthophyll cycle pool (Härtel et al., 1998).

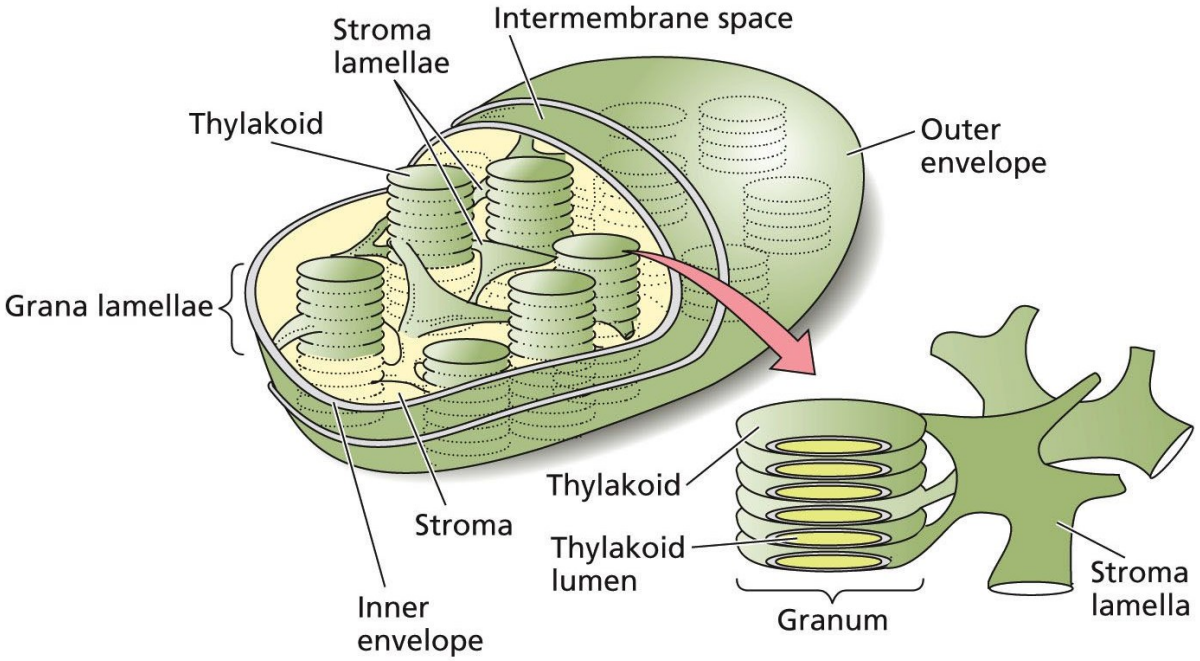

Figure 1.1 Schematic image of a chloroplast. The chloroplast contains three membranes, an outer and inner envelope membrane and the thylakoid membrane, which separates the stroma from the thylakoid lumen. The thylakoid membrane is organized in stacked (grana) and unstacked (stroma lamella) regions (from: Taiz/Zeiger, 2007).

The thylakoid membrane is structurally and functionally diverted into stacks of thylakoid membranes, so called grana, and unstacked areas, so called stroma lamellae. Protein super-complexes involved in photosynthetic electron transport are embedded in the membrane, however photosystem II (PSII) and photosystem I (PSI) are laterally segregated due to the differentiation of grana and stroma lamellae (Danielsson et al., 2004). PSII is localized in the grana stacks, whereas PSI is excluded from the stacks due to its bulky stromal protrusions. Hence, PSI is localized in the margin regions of a granum and in the stroma lamellae, like the ATP synthase, which is restricted to grana margins and stroma lamellae as well, due to the bulky stroma-attached F1 portion. Only the cytochrome b_6f (Cyt b_6f) complex is homogeneously distributed among grana and stroma lamellae (Avenson et al., 2008).

The 2D structure of the thylakoid membrane is known since many years and can easily be analyzed with transmission electron microscopy. However, the 3D structure of a granum is still under debate. Whether a helical structure features the granum (Mustárdy and Garab, 2003), or whether the granum rather consists of interacting stroma lamellae in a fork-type model (Arvidsson and Sundby, 1999; Shimoni et al., 2005) remains to be shown.

1.2 The photosynthetic electron and proton transport

The photosynthetic linear electron transport chain (LET) involves three major protein super-complexes (PSII, Cyt b_6f, and PSI), which are integrated in the thylakoid membrane, as well as two mobile electron carriers, Plastoquinone (PQ) and plastocyanin (PC), that connect the protein complexes. Light energy, which is captured in the light harvesting complexes (LHC) of PSII and PSI, is used to induce charge separation in the reaction centers (RCs) of PSII and PSI and thereby facilitating electron transport along a redox gradient.

In PSII, charge separation induces the oxidation of water at the lumenal side and the reduction of the mobile membrane-located electron carrier PQ at the stromal Q_B site. After uptake of two protons from the stroma, PQ is reduced to plastohydroquinone (PQH_2) and PQH_2 delivers the electrons to Cyt b_6f, where one electron is passed forward to the lumen localized electron carrier PC. The second electron is used for re-reduction of PQ at Cyt b_6f in the so called Q-cycle. PC transports the electron to the PSI RC P700. In PSI, charge separation leads to the transfer of electrons to ferredoxin (Fd) and finally the ferredoxin-NADP-reductase (FNR) transfers the electrons to $NADP^+$ (Figure 1.2).

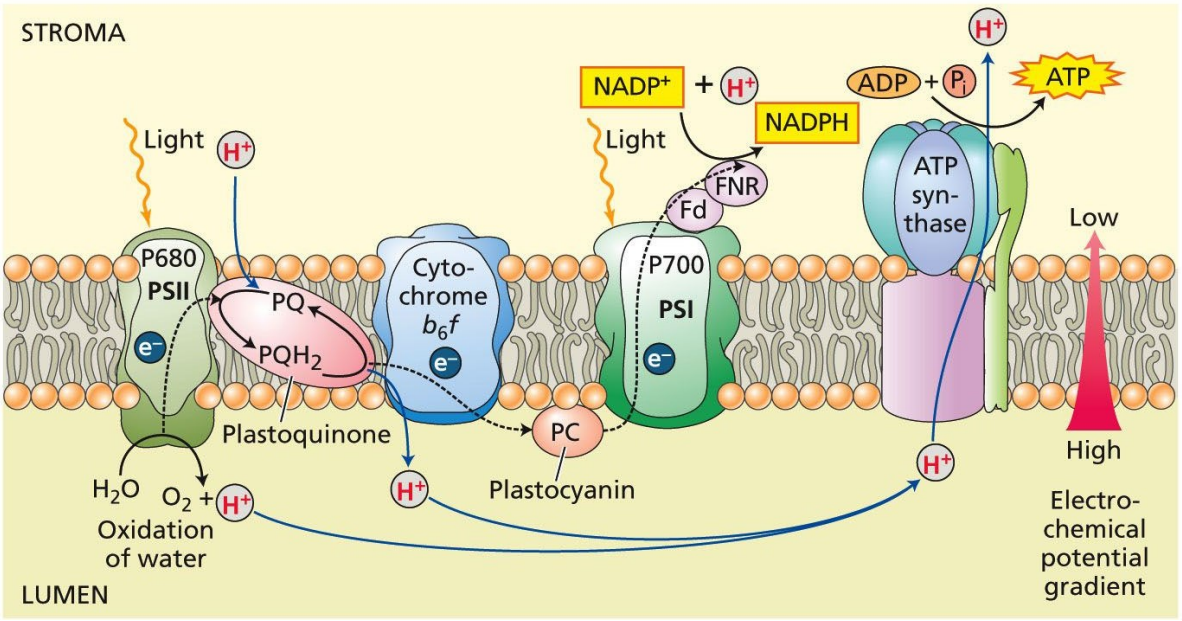

Figure 1.2 Photosynthetic electron and proton transport. From PSII, electrons are transferred to the mobile carrier PQ, which transports the electrons to the Cyt b_6f complex. They are then further transferred to PC which transports the electrons to PSI. There, energy is transferred onto the electrons, and they are ultimately transferred to $NADP^+$. Missing electrons at PSII are refilled by electrons originating from water, which was split in oxygen and hydrogen at the oxygen evolving complex. Upon linear electron transport the lumen is acidified due to the release of protons at the oxygen evolving complex and due to a proton input from the Q-cycle. The proton gradient contributes to the *pmf* and is used for ATP synthesis by the ATPase (from Plant Physiology, 4th Edition).

During linear electron transport, two reactions lead to an acidification of the lumen: (i) the splitting of water into oxygen and protons at the oxygen evolving complex of PSII and (ii) the oxidation of PQH_2 at Cyt b_6f. The accumulation of protons in the thylakoid lumen together

with the movement of ions gives rise to an electrochemical gradient across the thylakoid membrane, the so-called proton motive force (*pmf*). The energy stored in this gradient is used by the ATP synthase to generate ATP. Both components of the total *pmf*, the proton gradient (ΔpH) and the transmembrane electric field (ΔΨ) represent equivalent driving forces for ATP synthesis (Wiedenmann et al., 2008). Upon illumination of dark-adapted chloroplasts, the initial *pmf* is composed of the ΔΨ component only, but within a few minutes of illumination the contribution of ΔΨ to the *pmf* decreases due to the activation of ion channels (Avenson et al., 2005). The total *pmf* as well as the partitioning of *pmf* into ΔΨ and ΔpH can be estimated under *in vivo* and *in vitro* conditions by measurements of the electrochromic shift (ECS) (Kramer and Sacksteder, 1998; Kramer et al., 2003; Klughammer and Schreiber, 2008) (for methodological details see section 2).

1.3 Protein complexes involved in photosynthetic electron transport

1.3.1 PSII and LHCII

PSII is multi-protein complex embedded in the stacked grana regions of the thylakoid membrane. It is organized as a functional dimer, each consisting of the reaction center (RC) proteins D1 and D2 and further 27-28 subunits (Dekker and Boekema, 2005). Several lipids (Guskov et al., 2009) and pigments, namely chlorophylls and carotenoids, especially β-carotene (β-Car) (Telfer, 2002) are bound to the PSII RC (Umena et al., 2011). These pigments serve light harvesting and photoprotective function, whereas the bound lipids mainly serve structural purposes.

The PSII RC is surrounded by an internal antenna (CP43 and CP47) and external light harvesting antenna that consists of light harvesting complex (LHC) monomers that form a minor antenna, and LHCs that form functional trimers (major antenna). The primary function of the LCHs is to harvest light energy and transfer it to the PSII RC, where physical energy in converted into redox energy via charge separation. Charge separation takes place at the P680, which is the primary electron donor that transfers its electron to pheophytin and finally to Q_A. Electrons originating from water oxidation at the oxygen evolving complex (OEC) are immediately re-reducing the oxidized P680.

All Lhcb proteins belong to the family of chlorophyll a/b binding proteins (CAB-proteins) (Green et al., 1991). They are encoded in the nucleus, thus the apo-protein needs to be imported into the chloroplast, where it is inserted in the thylakoid membrane upon assembly. Lhcb proteins spontaneously fold upon binding of pigments, however the presence of xanthophylls is mandatory for correct folding (Plumley and Schmidt, 1987; Paulsen et al., 1990). A model for the structure of the Lhcb1 monomer and the localization of the pigments is shown in Figure 1.3.

The protein backbone of Lhcb proteins consists of three transmembrane α-helices (termed A-C, Figure 1.3) and two short α-helices (D and E, Figure 1.3) at the lumen side of the membrane (Liu et al., 2004). The lumen exposed helix E is supposed to become protonated upon lumen acidification, which might lead to pH-regulated conformational changes in the antenna of PSII (Liu et al., 2004). The pigment binding sites are termed V1, L1, L2, and N2, as derived from their carotenoid binding specificity. At the V1 site, either violaxanthin (Vx) or zeaxanthin (Zx) is bound. L1 and L2 bind two luteins (Lut), which are mandatory for the correct folding of the LHC (Jahns et al., 2001).

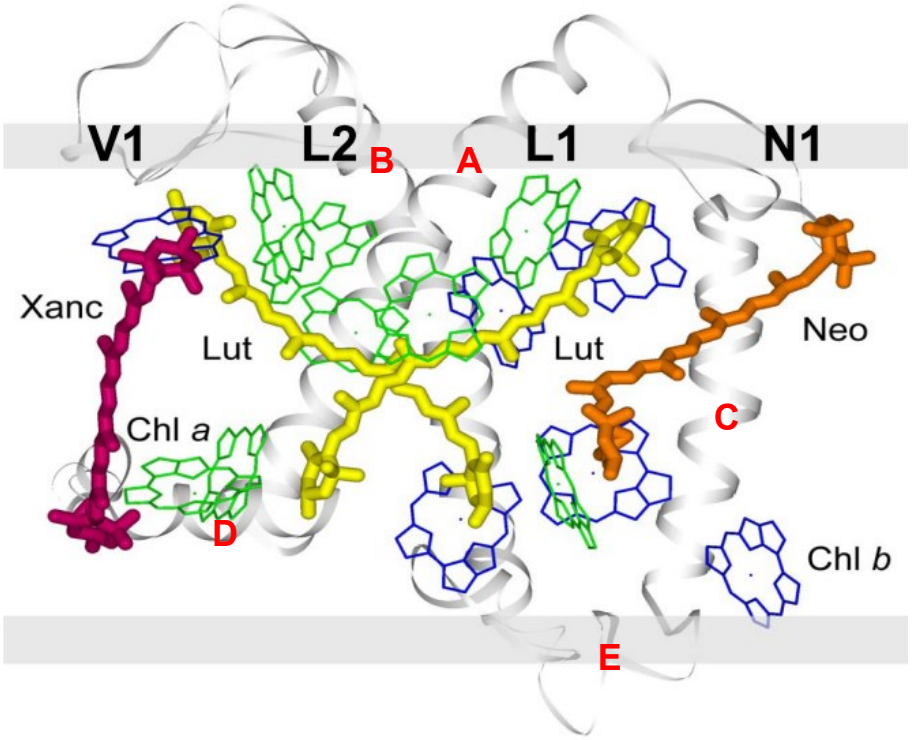

Figure 1.3 Model of a light harvesting complex of PSII. One LHCII contains five α-helices, three of them traverse the thylakoid membrane (A, B, C), whereas helices D and E are short and facing the lumen. Besides 8 Chl a and 6 Chl b, LHCII binds 1 molecule Nx at the N1 binding site. Two Lut (at L1 and L2) are forming the backbone of the LHCII. At the V1 site either Vx (at dark or low light acclimated states) or Zx (in a light acclimated state) is bound.

At the more peripheral N1 site, neoxanthin (Nx) is bound. Additionally, 8 Chl a and 6 Chl b are bound to each Lhcb monomer, which further stabilize the protein (Standfuss et al., 2005). The Chl molecules are responsible for the absorption of blue and red light, but also Lut contributes to light harvesting by transferring absorbed excitation energy to Chl (Siefermann-Harms, 1985; Peterman et al., 1997; Formaggio et al., 2001; Croce et al., 2001).

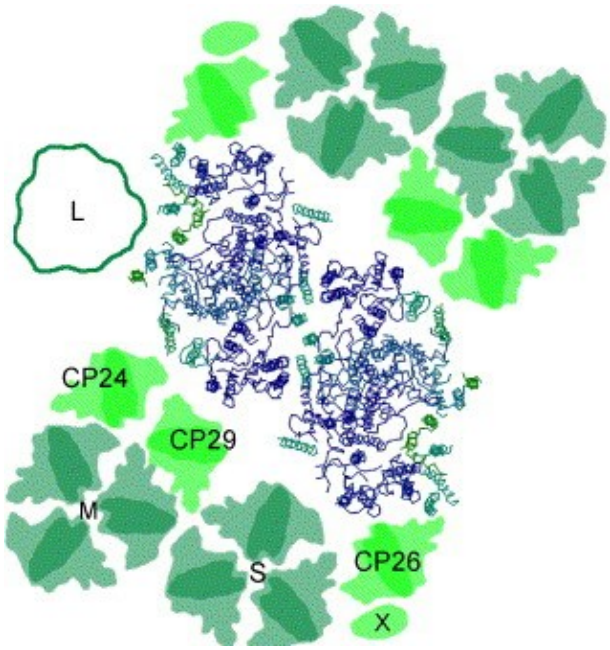

Figure 1.4 Model of the PSII reaction center with major antenna proteins attached. The reaction center dimer (blue) is surrounded by the minor antenna proteins CP24, CP26, and CP29 (light green). Attached to the minor antenna are the major light harvesting complex trimers (dark green). These trimers can be either strongly bound (S), moderately bound (M), or loosely bound (L). Adapted from (Dekker and Boekema, 2005).

In total, six different Lhcb proteins, termed Lhcb1-6, are found to be associated with PSII. Lhcb1, Lhcb2 and Lhcb3 form functional hetero-trimers, which are connected to the PSII RC via the minor antenna proteins Lhcb4, Lhcb5 and Lhcb6 (Figure 1.4). These proteins fulfil different roles in light harvesting and dissipation of excess energy (Horton et al., 2008). Lhcb proteins can generally be modified via protonation or phosphorylation, however to a different degree (Bergantino et al., 1998; Allen, 1992). Despite the different functions of single Lhcbs in fully functional PSII, the overall high similarity of the Lhcb proteins allows (at least partially) for functional complementation when single antenna proteins are missing (Ruban et al., 2003), .

1.3.2 Cytochrome b_6f complex

The Cyt b_6f complex is the bottleneck of photosynthetic electron transport due to its slow turnover rate in PQ reoxidation (Schöttler and Tóth, 2014). In comparison to PSII, Cyt b_6f occurs in sub-stoichiometric amounts and is the major point of control for photosynthetic electron flux (Anderson, 1992; Haehnel, 1984; Hope, 2000). Like PSII, also Cyt b_6f is organized as a functional dimer. The main components of each monomer are the 34 kDa cytochrome f protein to which a c-type cytochrome is bound and the cytochrome b_6, which has a molecular mass of 25 kDA and binds a high and low potential heme. Furthermore a Fe_2-S_2 cluster is bound to the so-called Rieske protein (Bendall, 1982; Whitmarsh and Cramer, 1977; Hauska et al., 1983). Reduced PQH_2 interacts with the Cyt b_6f complex at the

Rieske protein, where it is sequentially oxidized, thereby releasing two protons into the thylakoid lumen. Stoichiometrically, one electron per PQH_2 is recycled during the Q-cycle, whereas the other is transferred to PC. The rate of PQH_2 oxidation depends on the lumen pH (Finazzi, 2002), and is slowed down at acidic pH thereby limiting linear electron flow from PSII to PSI (Jahns et al., 2002).

1.3.3 Photosystem I and LHCI

PSI is a large monomeric super-complex (about 600 kDa) composed of 17 subunits binding in total about 200 cofactors, including Chl, carotenoids, lipids, and three Fe_2S_4 cluster (Amunts and Nelson, 2008; Qin et al., 2015). Due to its bulky stromal protrusions (Amunts and Nelson, 2008; Junge et al., 2009), PSI is sterically hindered to enter grana stacks and is therefore exclusively localized in the grana margins and stroma lamellae (Albertsson, 2001). Its reaction center contains a special Chl a pair, P700, which functions as the primary electron donor. Upon electron transport, $P700^+$ is reduced by accepting an electron from the mobile electron carrier PC. However, $P700^+$ is only a weak oxidant, so that oxidized P700 is relatively harmless compared to $P680^+$ in PSII. This makes PSI a very efficient and relatively harmless quencher for excess excitation energy (Ort, 2001; Schöttler et al., 2011).
Unlike PSII, PSI and Cyt b_6f complexes are not only involved in the linear electron transport, but also in the cyclic electron flow between PSI and Cyt b_6f. During cyclic electron flow around PSI (CEF1) (Kramer et al., 2004a), electrons that were transferred from PSI onto Fd are further transferred to PQ and not to the FNR, which is the case in linear electron transport. CEF1 occurs during periods of unbalanced ATP consumption, however the exact mechanism and the impact of CEF1 is still under debate.
Like PSII, also PSI consists of a light harvesting antenna, however its size is conserved and invariable, as opposed to the light harvesting antenna of PSII. The PSI antenna consists of in total four different Lhca proteins that form two heterodimers, i.e. Lhca1 and Lhca4 form one dimer, and Lhca2 and Lhca3 the other (Ben-Shem et al., 2003; Amunts et al., 2007; Amunts et al., 2010). Each Lhca protein consist of three alpha-helices and one amphipathic fourth helix in the lumen (Qin et al., 2015). Unlike Lhcb proteins, mutual complementation of the Lhca proteins is not possible (Klimmek et al., 2005; Morosinotto et al., 2005), because of their structural differences, i.e. in the length of the alpha helix (Qin et al., 2015).

1.3.4 ATPase

The ATPase, also known as ATP synthase or CF_0CF_1, drives ATP synthesis by using the *pmf*, which is build up during photosynthetic electron transport. The *pmf* was firstly introduced by Peter Mitchell in the 1960s. It consists of the electric field and the proton gradient in the following relation:

$$pmf = \Delta E - 59\ (pH_i - pH_o),$$

with ΔE being the transmembrane electric potential, $pH_i - pH_o$ resembling the ΔpH, assuming a constant proportionality at 25 °C of 59 mV per pH unit (Mitchell, 1961).
The ATPase consists of a membrane integrated, hydrophobic part, the CF_0 domain, which is composed of three subunits: a, b, and c. Polypeptides a and b are located at the periphery of a barrel shaped ring that is in plants formed by 14 identical subunits of polypeptide c through which protons are transported during ATP synthesis (Seelert et al., 2000; Vollmar et al., 2009). The CF_1 head domain consists of 3 alternating α- and β-subunits and 1 γ, δ, and ε subunit respectively. *pmf* driven proton flux from the lumen to the stroma drives conformational changes in the α- and β-subunits resulting in the formation of ATP from ADP and P_i in a stoichiometry of 4.67 protons per molecule of ATP. Hence a full turn produces three ATP at the cost of 14 protons.

1.4 Coping with excess light: non-photochemical quenching (NPQ)

Plants are sessile organisms that have to cope with excess light during major parts of their lifetime. Under most natural conditions, the antenna proteins of both photosystems absorb more light than can be utilized in photosynthesis (Müller et al., 2001), favoring the formation of ROS and thus photo-oxidative damage of cell components. In general, two reactions contribute to the light-induced formation for ROS: Firstly, energy transfer of from ^{3}Chl* to O_2 in the antenna of PSII leading to the formation of highly reactive singlet oxygen ($^1O_2$*) (Vass and Styring, 1993; Hideg et al., 1998). Secondly, electron transfer to O_2 leading to the formation of superoxide radicals ($O_2^{\cdot-}$), predominantly at the acceptor side of PSI in the so-called Mehler reaction (Mehler, 1951). While superoxide radicals can be efficiently detoxified through conversion to hydrogen peroxide by the water-water cycle (Asada, 2000), singlet oxygen formation represents the major source for photo-oxidative damage in plants (Triantaphylidès and Havaux, 2009). However, ROS are not only harmful toxins damaging the chloroplast, but also serve as important signaling molecules (Mittler et al., 2004; Triantaphylidès and Havaux, 2009) that are involved in the communication between the chloroplast and the nucleus (Foyer and Noctor, 2009; Galvez-Valdivieso and Mullineaux, 2010). Detoxifying high levels of ROS is costly and the risk of damage to proteins and lipids in the chloroplast is high. Therefore, effective mechanisms have evolved to minimize the amount of light-induced ROS formation. Among those, the dissipation of excess light energy as heat, commonly termed non-photochemical quenching (NPQ), is an efficient way to reduce the formation of both $^1O_2$* and $O_2^{\cdot-}$. The overall NPQ processes comprise various mechanisms that directly compete with the use of excitation energy in photosynthesis. Hence, the onset of NPQ mechanisms needs to be strictly regulated and restricted to periods

of excess light conditions. Constitutively active NPQ mechanisms under limiting light conditions would drastically decrease the light use efficiency and thus would have a negative impact on plant fitness.

Chl a fluorescence has been shown to provide an excellent measure for estimating photochemical and non-photochemical processes in photosynthetic organisms. Pioneering work in the 1960s applied Chl a fluorescence analysis to single cell organisms, such as cyanobacteria and green algae in order to perform mutant screening (Bennoun and Levine, 1967, Papageorgiou and Govindjee, 1968a, 1968b), while later research was extended to intact leaves and isolated chloroplasts or thylakoids of land plants (Murata and Sugahara, 1969; Wraight and Crofts, 1970; Krause, 1973; Krause et al., 1982) (Murata, 1969). Nowadays, commercially available fluorometers, such as the pulse amplitude modulated (PAM) fluorometer (Schreiber et al., 1986), which are easy to operate also by non-specialists, are frequently used for numerous applications to study photosynthesis in the lab and in the field. For the characterization of NPQ processes, usually fluorescence quenching analysis by the saturation pulse saturation method are performed (Krause and Jahns, 2003). A typical Chl fluorescence quenching analysis measured with intact leaves by using a PAM fluorometer is shown in Figure 1.5. Due to the pulsed measuring light (1-100 kHz, 3-5 µmol photons m^{-2} s^{-1}) the detected Chl fluorescence is less prone to scattering, which leads to an increased signal to noise ratio. Additionally, the light intensity is sufficiently low to prevent linear electron transport. The minimum fluorescence (F_0) is observed after turning on the measuring light. A short and strong actinic light flash, or saturation pulse (SP, 200 ms, 4000-6000 µmol photons m^{-2} s^{-1}) is applied to the leaf. The flash leads to a complete reduction of the Q_A, however neither high rates of electron transport nor non-photochemical quenching mechanisms are activated during this short illumination time. At that point PSII RC is in a “closed state”, and the maximum fluorescence (Fm) can be obtained. The maximum quantum efficiency in a dark acclimated state is calculated by dividing the variable fluorescence ($Fv = Fm-F_0$) by Fm. Typically the Fv/Fm value of dark acclimated land plants is around 0.83 (Björkman and Demmig, 1987; Johnson et al., 1993). An actinic light source of variable intensity is turned on after determination of the maximum quantum yield, which induces an initial fluorescence rise. With the full activation of photosynthesis (electron transport, Calvin-Benson cycle) and NPQ processes, the fluorescence typically declines within 10-15 min to a steady level.

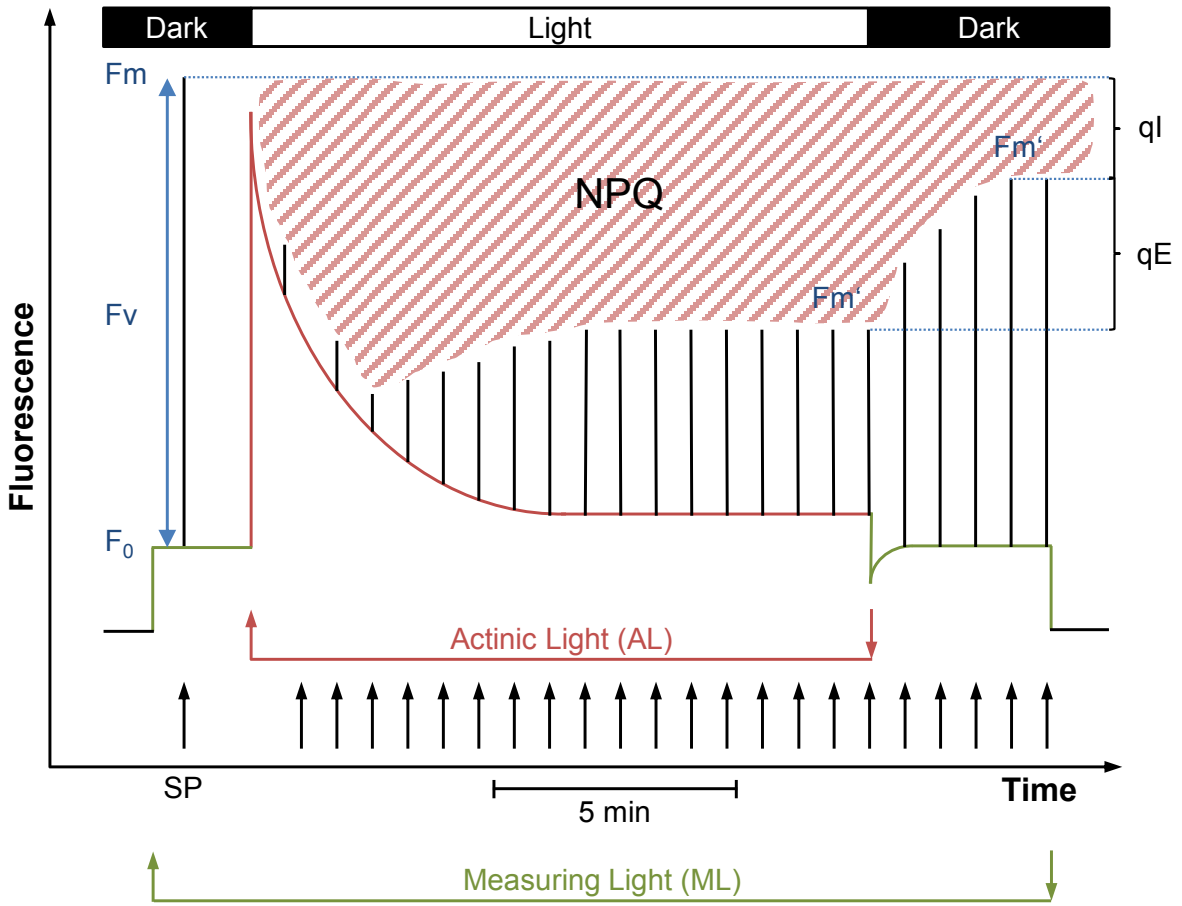

Figure 1.5 Typical chlorophyll a fluorescence curve. Important parameters are indicated. After an initial saturation pulse in the dark, an actinic light source in turned on (Actinic Light on). Saturation Pulses (SPs) are subsequently applied throughout the whole measurement. The recovery of variable fluorescence is measured in a dark period following the illumination (Actinic Light off). By turning on the measuring light, F_0 is obtained. The maximum fluorescence (Fm) is obtained by applying a SP in the dark. The fluorescence ranging from F_0 to Fm is termed variable fluorescence (Fv). After a first reduction of maximum fluorescence in the light, steady state fluorescence is reached (Fm'). In the subsequent dark phase fluorescence rises due to the deactivation of NPQ processes, until a temporarily maximum is reached (Fm').

During the whole measurement, SPs are applied typically every 1-2 min to determine the maximum fluorescence (Fm') during the actinic light phase and the subsequent dark phase . The extent of NPQ can be calculated for each SP as (Fm/Fm' - 1). On basis of their dynamics (induction and relaxation) and the analysis of specific mutants, different NPQ mechanisms have been extensively characterized during the past 20 years.

1.4.1 Energy-dependent quenching (qE)

The most rapid component of the NPQ is the energy-dependent quenching, or qE. It has been shown that the qE induction is strongly dependent on the PsbS subunit of PSII (Li et al., 2000). qE is strictly regulated by the lumen pH, which is sensed by two glutamate residues of the PsbS protein (Li et al., 2004). In the qE-inactive dark state, PsbS exists as a dimer, while it monomerizes upon protonation of PsbS and thus leads to the light activation of qE (Bergantino et al., 2003). It has been proposed that light-induced activation of PsbS induces

conformational changes in the antenna of PSII that lead to the detachment of the trimeric LHCII complexes. Upon detachment, the function in the LHCII is switched from a light harvesting state into an energy-dissipation state (Horton et al., 2008). The exact quenching mechanism in the detached LHCII antenna is still under debate. Disagreement exists whether Chl-Chl interactions (Miloslavina et al., 2008; Müller et al., 2010) or Chl-Car interactions (Holt et al., 2005; Ruban et al., 2007) lead to the deactivation of the ^{1}Chl*. However, it is widely accepted that the quenching in the antenna of PSII is modulated and enhanced in the presence of the carotenoid zeaxanthin (Demmig-Adams et al., 1990; Johnson et al., 2008a).

1.4.2 The protective role of zeaxanthin

The xanthophyll Zx is formed in the xanthophyll cycle upon de-epoxidation of Vx via the intermediate antheraxanthin (Ax) (Jahns et al., 2009). Xanthophylls are either bound to LHC complexes (see Figure 1.3) or present as free pigments in the thylakoid membrane (Havaux and Niyogi, 1999; Aspinall-O'Dea et al., 2002; Dall'Osto et al., 2005). The xanthophyll cycle pigments (VAZ pigments) are interconverted by two enzymes that are regulated in a light-dependent manner, particularly by the lumen pH. The light-induced acidification of the lumen activates the luminal Vx de-epoxidase (VDE) (Hager, 1969), which catalyzes the conversion from Vx via the intermediate Ax to Zx in the presence of the cofactor ascorbate (Yamamoto et al., 1977). Within 15-30 minutes of illumination, the maximum of convertible xanthophylls are converted into Zx (Jahns, 1995; Wehner et al., 2004; Nilkens et al., 2010). Under low light (LL) conditions or in darkness, Zx is reconverted to Vx by the stromal enzyme Zx epoxidase (ZEP), which requires several cofactors, such as Fd, O_2, NADPH and FAD. However, the reconversion is about one order of magnitude slower, compared to the de-epoxiation reaction. Generally, non-protein bound xanthophylls are converted faster compared to protein bound xanthophylls, due to the restricted accessibility of the respective enzymes to the protein-bound xanthophylls.

Zx has a dual role in protecting the chloroplast from photo-oxidative damage. As a free pigment, Zx detoxifies ROS, thus resembling the function of tocopherol (Havaux et al., 2007). However, Zx bound to the antenna proteins of PSII is involved in the deactivation of ^{1}Chl*, thereby preventing the formation of ^{3}Chl* and thus the formation of ROS. The deactivation of ^{1}Chl* takes place in the minor antenna complexes, as well as in the detached LHCII trimers (see below, section 1.4.4). The specific contribution of Zx to the overall NPQ induction upon binding to LHC complexes is termed qZ (Holzwarth et al., 2009). In addition, the presence of Zx in the LHCII complexes leads to an enhanced qE-type quenching, possibly by increasing the pK of qE-activation (Johnson et al., 2008b; Johnson and Ruban, 2009; Crouchman et al., 2006).

1.4.3 Time resolved measurements and decay associated spectra

For a detailed understanding of the mechanisms involved in the NPQ processes under *in vivo* conditions, analysis of energy dissipation by ultra-fast fluoresecence measurements is required (Holzwarth and Jahns, 2014). Commercially available photospectrometer are not appropriate to obtain information about energy dissipation processes that are faster than several µsec. However, a special setup, using a high intensity argon laser, allows for time resolved measurements and thus to discriminate between several dissipation processes. The pulsed laser beam (1 ps^{-1}) illuminates a special red dye, which emits light at a wavelength between 610 and 710 nm. With the help of filters and shutters, the light intensity, as well as the exact excitation wavelength (usually 663 nm) can be adjusted, according to the required measuring conditions. The measuring beam is focused to a rotating cuvette containing the leaf sample. Rotation of the cuvette prevents possible chlorophyll bleaching caused by the high intensity of the laser beam and allows for sufficient averaging of repetitive measurements. In order to close all RC during a saturation pulse, an additional high intensity blue LED is used. After passing the sample, the measuring beam is guided to a computer controlled monochromator that splits the emitted light into defined wavelength. The intensity of each wavelength is obtained and deconvoluted in an A/D converter and finally analyzed in a multichannel analyzer.

The samples are typically measured at 11 different wavelengths in the range from 678 to 750 nm in different acclimation states: Firstly, samples are measured in a dark acclimated state. The PSII RCs are then closed via DCMU treatment to obtain the maximum fluorescence. Finally, the fluorescence is measured after 30 minutes of illumination that allow for a fully light-acclimated state under steady state conditions. The decay kinetics obtained at all wavelengths are finally fitted in a global analysis (Wagner et al., 1996). This analysis gives rise to so-called decay-associated spectra (DAS), which carry both, spectral and kinetic information. The kinetics were fitted on basis of established models for the energy transfer and the according rate constants in PSII and PSI. These models have been developed from studies with isolated components (Miloslavina et al., 2006; Slavov et al., 2008) . This so-called target analysis was exclusively performed in the workgroup of Prof. Dr. Alfred Holzwarth (MPI of chemical energy conversion in Mülheim a.d. Ruhr).

This analysis was used to develop a model, which allows for the exact discrimination between PsbS-dependent qE processes and Zx-dependent qZ processes.

1.4.4 qE and qZ are integrated in a two sited quenching model

With the help of time resolved measurements and target analysis a two sited quenching model was derived from the comparative analysis of leaves from Arabidopsis wild-type and mutant plants (Holzwarth et al., 2009) as shown in Figure 1.6. In a dark acclimated state, the

LHCII trimers and monomers are attached to the PSII RC. The green color indicates the binding of the xanthophyll Vx. Upon illumination, a biphasic dissipation process takes place. In a first step, LHCII trimers detach from the PSII RC, forming aggregates that dissipate energy in the quenching center 1 (Q1). This process is strictly dependent on the PsbS protein and is assigned to the pH-regulated qE type quenching. A second quenching center (Q2) is established in the minor antenna of PSII upon the exchange of Vx to Zx. This process is strictly dependent on the presence of Zx, and thus termed qZ (Figure 1.6). The binding of Zx to the LHCs of PSII is indicated by a red color in Figure 1.6. Also in detached LCHII trimers, Zx is bound, that accelerates the quenching in Q1.

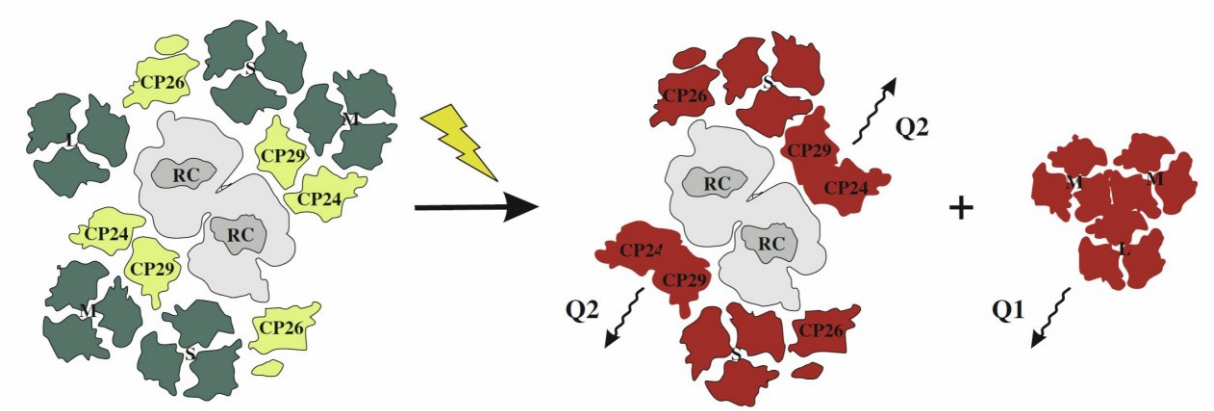

Figure 1.6 Model of two quenching centers that are formed during illumination. In a dark acclimated state (left) Vx is bound to the minor and major antenna complexes of PSII, indicated by the dark and light green color. Upon illumination, lumen acidification and PsbS induced conformational changes lead to a detachment of the major LHCIIs that form a quenching center apart from PSII (Q1). The formation of a second quenching center (Q2) in the minor antenna of PSII RC depends on the formation of Zx (indicated by the red color) (Holzwarth et al., 2009).

1.4.5 Photoinhibition (qI)

During extended periods of high light (HL) stress the capacity of rapidly reversible quenching (qE and qZ) is limited and the over-excitation leads to the formation of ROS. To minimize the excitation pressure on PSII and PSI, the D1 protein of PSII is damaged in a process called photoinhibition (qI). This directed damage inactivates the PSII RC and thus reduces not only the formation of ROS, but also linear electron transport. However, in order to re-establish maximum quantum efficiency, the damaged D1 protein needs be replaced. Without an efficient repair mechanism the sustained damage of the PSII RC would drop the photosynthetic yield constantly below 5 % (Melis, 1999). In case of moderate light stress, damaged D1 protein can be quickly repaired and the efficiency of PSII can be quickly restored. However, under severe HL stress, or in combination with other stresses, the repair machinery required for D1 turnover is slowed down, which leads to a longer deactivation of PSII. This stroma localized repair machinery, which involves multiple enzymatic reactions, replaces the damaged protein. Because of its size, the machinery is sterically hindered to enter the grana stacks, where PSII is localized (Kirchhoff, 2014). Phosphorylation of LHCII

and the PSII RC by the STN8 kinase (Bonardi et al., 2005; Vainonen et al., 2005) are crucial steps during the repair process. Depending on the extent of HL stress, the repair of PSII RCs requires more than 30 minutes (Nilkens et al., 2010) and qI is thus the slowest component of NPQ.

1.4.6 State transition (qT)

State transition (qT) describes a process that balances the relative excitation of the two photosystems by reversible migration of LHCII trimers from PSII to PSI. This migration depends on the phosphorylation of the LCHII by the redox regulated serine/threonine kinase STN7 (Bellafiore et al., 2005), which is activated when the PQ pool is mainly reduced. In state 1 (oxidized PQ pool), LHCII complexes are not phosphorylated and bound to PSII. Upon phosphorylation of a fraction of LHCII, the induced negative charge leads to the migration of LHCII to the margin regions of the thylakoid membrane towards PSI, where it associates to the antenna of PSI, which gives rise to state 2. Thus the transition from state 1 to state 2 increases the antenna size of PSI and reduces the antenna size of PSII, thereby fine-tuning the distribution of excitation energy between the two photosystems. During qT, the PSI antenna can be enlarged by up to 25 % (Ruban and Johnson, 2009).

1.5 Long- and short-term responses of plants to different light conditions

Plants have the ability to cope with a variety of environmental factors. Depending on the length of the stimulus, long- and short-term responses are differentiated. Long-term responses are apparent from a broad phenotypic plasticity of a species upon growth under different stress conditions. Especially light is a highly variable parameter, showing large changes in intensity not only on a diurnal or seasonal basis, but often within a few seconds due to sun flecks or clouding (Ganeteg et al., 2004; Hirth et al., 2013). Since excess light is the source of photo-oxidative damage, efficient short- and long-term acclimation to varying light conditions are essential for plant fitness.

1.5.1 Long-term responses

Long-term acclimation responses occur in the time range of days (Beisel et al., 2010) to months (Schofield et al., 1998; Rachmilevitch et al., 2008). Typically, such responses are directly visible from changes in the plant architecture such as leaf area, leaf thickness, or rosette diameter (Ballaré, 1999; Weston et al., 2000).

Long-term acclimation responses of *Arabidopsis thaliana* have been largely characterized under controlled laboratory conditions only. Leaves from LL grown plants are characterized by long petioles that form less compact rosettes than normal light (NL) grown plants (Mishra

et al., 2012). LL plants are further characterized by a lower Chl a/b ratio than NL plants, mainly due to the increased accumulation of LHCII complexes (Leong and Anderson, 1984; Wild et al., 1986), which serve for optimal light use efficiency under limiting light conditions (Anderson and Osmond, 1987; Chow et al., 1990). Related to the high LHCII content, the thylakoid membrane of the chloroplasts from LL plants mainly forms appressed grana stacks (Anderson, 1986). In contrast, the VAZ pool size is reduced in LL plants compared to plants grown at higher light intensities (Demmig-Adams and Adams, 1992), in accordance with the limited NPQ capacity that is observed in LL plants (e.g. (Mishra et al., 2012).

HL grown plants, on the other hand, are characterized by more compact rosettes, consisting of large leaves with short petioles (Mishra et al., 2012). Especially in combination with additional stresses, the color of leaves from HL plants can turn reddish due to the accumulation of anthocyanins (Page et al., 2012), which reduce the light absorption by chloroplasts. Typically, acclimation to HL leads to decrease of the light harvesting antenna of PSII, resulting in an increase of the Chl a/b ratio (Leong and Anderson, 1984; Wild et al., 1986). On the level of electron transport, particularly the amount of the Cyt b_6f complex is upregulated in response to HL (reviewed by (Anderson, 1992; Schöttler and Tóth, 2014). Accompanied with this increase in RCs, also the amount of RubisCO is increased (Björkman, 1981; Seemann et al., 1987) which together ensures overall high rates of photosynthesis (Walters and Horton, 1994), as evident from an increased rate of LET and CO_2 assimilation in comparison to NL and LL plants (Leong and Anderson, 1984, de la Torre and Burkey, 1990a, 1990b). The thylakoid membrane structure of HL plants is dominated by non-appressed regions of stroma lamellae (Lichtenthaler et al., 1981; Lichtenthaler and Schindler, 1992). The NPQ capacity is increased in HL plants, which is based on an increased amount of PsbS (Ballottari et al., 2007) and the VAZ pool size (Demmig-Adams and Adams, 1992) in comparison with NL plants.

So far, little research has been conducted on plants grown under natural light (NatL) conditions in temperate zones. Studies on the acclimation to fluctuating light have been investigated mainly on trees and/or subtropical plants growing in the understory of a canopy (Ögren and Sundin, 1996). Only a few studies examined the effect of cloud movement (Knapp and Smith, 1989) and the effect of moving leaves (Roden and Pearcy, 1993), focusing mainly on the importance and responses of plants to sun flecks. In densely covered canopies, sun flecks not only provide the majority of available light energy for photosynthetic carbon assimilation (Pearcy and Calkin, 1983; Chazdon, 1986), but also give rise to absorption of excess excitation energy, which ultimately leads to the formation of harmful ROS. The response of plants to sun flecks strongly depends on the duration and intensity of the flecks (Chazdon and Pearcy, 1986), which also applies to artificially generated sun flecks under controlled lab conditions (Yin and Johnson, 2000). Typically, plants grown under

fluctuating light, possess a photosynthetic capacity which exceeds the one observed in plants grown under constant light conditions, both under LL and HL conditions (Pollard, 1970). Additionally, fluctuating light conditions were shown to induce reorganization of pigment-protein complexes, resulting in an accelerated NPQ induction (Alter et al., 2012; Kono and Terashima, 2014). The size and the de-epoxidation state of the VAZ pool were shown to be increased in plants exposed to sun flecks (Alter et al., 2012). Obviously, plants exposed to sun flecks or fluctuating light resemble characteristic features of HL grown plants.
Thus, acclimation of photosynthesis to different light environments comprises changes in the chloroplast structure and changes in the stoichiometry of the proteins involved in photosynthetic electron transport and carbon assimilation (Walters, 2005). However, photosynthetic acclimation is not restricted to long-term responses only, since dynamic regulation of *de novo* synthesis of proteins or directed degradation (Walters and Horton, 1994; Yang et al., 1998) occurs on a shorter time scale and thus allows for adjustment of the photosynthetic machinery in the short-term.
A significant role in both, grana structure and light harvesting is directly related to the LHCII complexes. In particular the antenna size of PSII is highly dynamic and acclimates to the according light condition, as shown in Figure 1.7. The minimal unit of PSII is the C_2S_2 complex, which can be found in HL plants (Kovacs et al., 2006). This complex only consists of the two core units (C_2) and two strongly bound LHCII (S-timers, S_2) that are unable to contribute to qT. In plants acclimated to moderate light intensities (NL), the PSII unit can be described as $C_2S_2M_2$, in this case the PSII recruits two more LHCIIs that are only moderately bound (M-trimers, M_2) to the RC. These M-trimers are supposed to become phosphorylated and detached from PSII upon qT (Dekker and Boekema, 2005; Caffarri et al., 2009). Acclimation to LL conditions may further lead to the synthesis of additional LHCII complexes that are only loosely bound to the RC (L-trimers) and thus to the formation of $C_2S_2M_2L$ complexes. However, the amount of LHCIIs and hence the composition of PSII-LHCII super-complexes that accumulate upon acclimation differ among plant species (Dekker and Boekema, 2005; Yakushevska et al., 2001).

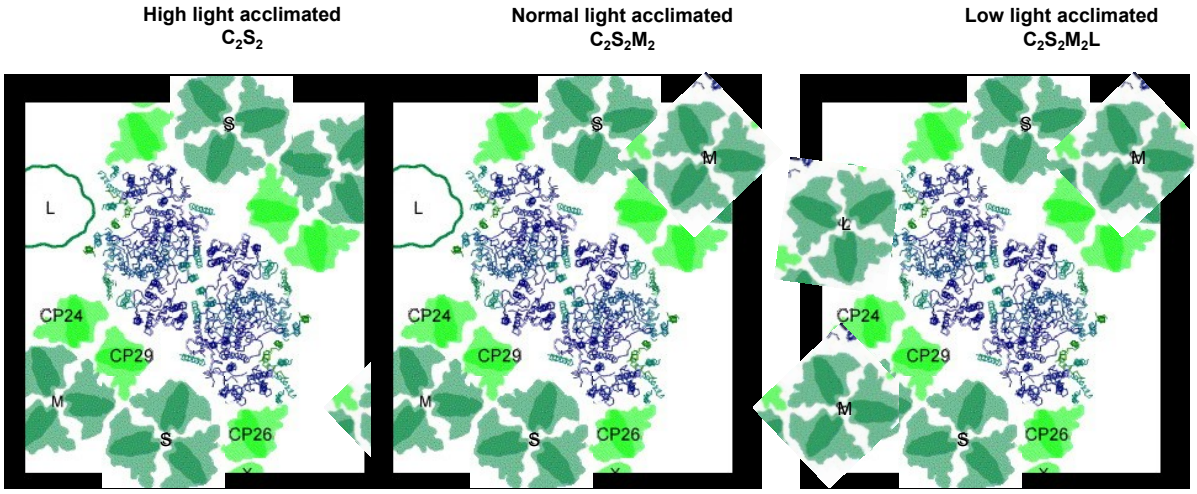

Figure 1.7 Model of the PSII reaction center with major antenna proteins attached. The reaction center dimer (blue) is surrounded by the minor antenna proteins CP24, CP26, and CP29 (light green). Attached to the minor antenna are the major light harvesting complex trimers (dark green). These trimers can be either strongly bound (S), moderately bound (M), or loosely bound (L).PSII RC and the LHC antenna are shown for HL (A), NL (B) and LL (C) acclimated plants. Adapted from (Dekker and Boekema, 2005).

Depending on the amount of LHCII proteins, the extent of grana stacking may vary (Lichtenthaler et al., 1981; Chow et al., 2005). This is mainly due to the accumulation of Van-der-Waals forces and the attraction of complementary charges that are present between LHCs in opposing thylakoid membranes (Chow et al., 2005). Less stacked grana, as found in HL acclimated plants, were shown to unstack upon illumination (Herbstova et al., 2012; Kirchhoff, 2013), which might be possible due to the overall weaker attraction forces resulting from the smaller LHC antenna (Figure 1.7).

1.5.2 Short-term responses

Short-term responses typically occur on a time-scale of seconds to minutes (Rachmilevitch et al., 2008) or few hours (Schofield et al., 1998). Since restructuring of existing tissues, membranes or protein complexes is costly, short-term acclimation is a cost efficient way of coping with changing environmental factors. Plants have developed a number of strategies to respond to varying light conditions. On the cellular level, chloroplast movement represents an efficient way to adjust the overall absorption cross section of chloroplasts (Wada et al., 2003). The movement of chloroplasts can either be described as accumulation response in case of limiting light, or as avoidance response under excess light conditions (Wada et al., 2003). Within the chloroplast, acclimation of light utilization is typically coupled to the light reactions of photosynthesis thereby balancing the production of ATP and NADPH in relation to the ATP/NADPH demand. As a consequence, the signaling for short-term acclimation processes is influenced by a variety of stresses that directly or indirectly effect the photosynthetic efficiency (Anderson et al., 1995). Key signals involved in short-term light

acclimation are the pH of the thylakoid lumen (Takizawa et al., 2007) and the redox state of the chloroplast (Küchler et al., 2002; Pfannschmidt, 2003; Oelze et al., 2008). The lumen pH is a direct measure for the saturation of photosynthetic electron transport which does not only reflect generally saturating light conditions but also any limitation of electron transport through limited utilization of NADPH and ATP in downstream assimilation processes. A drop of the lumen pH below a threshold of about 6.0 rapidly activates the synthesis of Zx (through activation of the VDE) and energy dissipation (through activation of PsbS). The redox state of the chloroplast is known to regulate kinases, such as STN7 or STN8. STN7 phosphorylates LHCII and thus leads to qT, a mechanism for short-term balancing of excitation energy between PSII and PSI. STN8 phosphorylates the PSII core and is involved in the repair cycle of the D1 protein that is damaged upon qI. Generally, NPQ processes are effective means of short-term acclimation towards excess light especially in environments with fluctuating light conditions.

However, acclimation is not only possible on protein level but is also reflected by the dynamics of the thylakoid membrane. Upon illumination, the thylakoid lumen was shown to swell (Kirchhoff et al., 2011), presumably due to the transport of Cl^- ions through voltage gated Cl^- channels in the thylakoid membrane (Spetea and Schoefs, 2010). Furthermore unstacking of the grana was observed, giving rise to more efficient diffusion of proteins and protein complexes (Kirchhoff, 2013), which ultimately accelerates electron transport and supports NPQ mechanisms such as qE and qT due to the increased diffusion speed of both, mobile electron carriers and LHCs. Furthermore, unstacking of the membrane simplifies the access of the PSII repair machinery to damaged PSII D1 units, thereby increasing the repair efficiency (Kirchhoff, 2014). By enhancing diffusion of molecules such as LHC complexes that can undergo qT upon phosphorylation, cyclic electron flow around PSI, which generates ATP and by that balances the ATP/NADPH ratio, is enhanced. This gives rise to a faster regulation in the short-term in response to changes in the ATP/NADPH demand under different light conditions (Kono et al., 2014).

1.6 Aim of the thesis

The work of this thesis was part of a collaborative research project initiated together with the group of Prof. Dr Alfred Holzwarth at the Max-Planck-Institute for Chemical Energy Conversion (Mülheim a.d.Ruhr). Starting point of the work was the identification of two different quenching sites (Q1 and Q2, Figure 1.6) that contribute to NPQ under *in vivo* conditions (Holzwarth et al., 2009). The long-term objective of the collaborative work was, to determine, whether the two quenching sites (Q1 and Q2) are differentially activated in plants with different NPQ capacities, and to understand the underlying physiological acclimation strategies. For that, ultrafast fluorescence spectroscopy (carried out at the MPI Mülheim) was

combined with the physiological and biochemical characterization of plants acclimated under different light environments, which are known to result in decreased or increased NPQ capacities in comparison with plants grown under standard (NL) lab conditions. The initial approach was the characterization of the NPQ processes in *Monstera delicosa* plants grown either under LL or natural HL conditions. Monstera plants grown under natural HL represent a very interesting biological system, since these plants develop a very high NPQ capacity under natural HL conditions (Demmig-Adams et al., 2006). For future studies, however, the use of Monstera plants is limited by the lack of specific mutant lines. Therefore, the studies were further extended to Arabidopsis plants that were grown either under controlled lab conditions at three different light intensities (LL: 25, NL: 100, HL: 500 µmol photons m^{-2} s^{-1}), or under natural (fluctuating) light conditions. The acclimation of Arabidopsis to different growth conditions was analyzed by characterizing morphological and physiological properties in comparison with the NPQ characteristics.

2 Materials and Methods

2.1 Plant growth

Arabidopsis thaliana (ecotype Colombia-0) wild type and mutant plants were cultivated in small growth pots with 5 plants per pot. For all growth conditions seeds were first stratified for 2 days in 0.1 % agarose and then put on well-watered soil (BP substrate, Klasmann-Deilmann GmbH, Geerste, Germanay). Low light (25 µmol photons m^{-2} s^{-1}) and high light (500 µmol photons m^{-2} s^{-1}) plants were transferred into the according light intensities after two weeks of growth at NL (100 µmol photons m^{-2} s^{-1}). Plants were grown under short day conditions with 14/10 h day/night cycle. Growth temperature was about 20 °C. All plants were fertilized with either Lizetan® granulate (Bayer CropScience, Langenfeld, Germany) or Celaflor® granulate (Scotts Celaflor GmbH, Mainz, Germany).

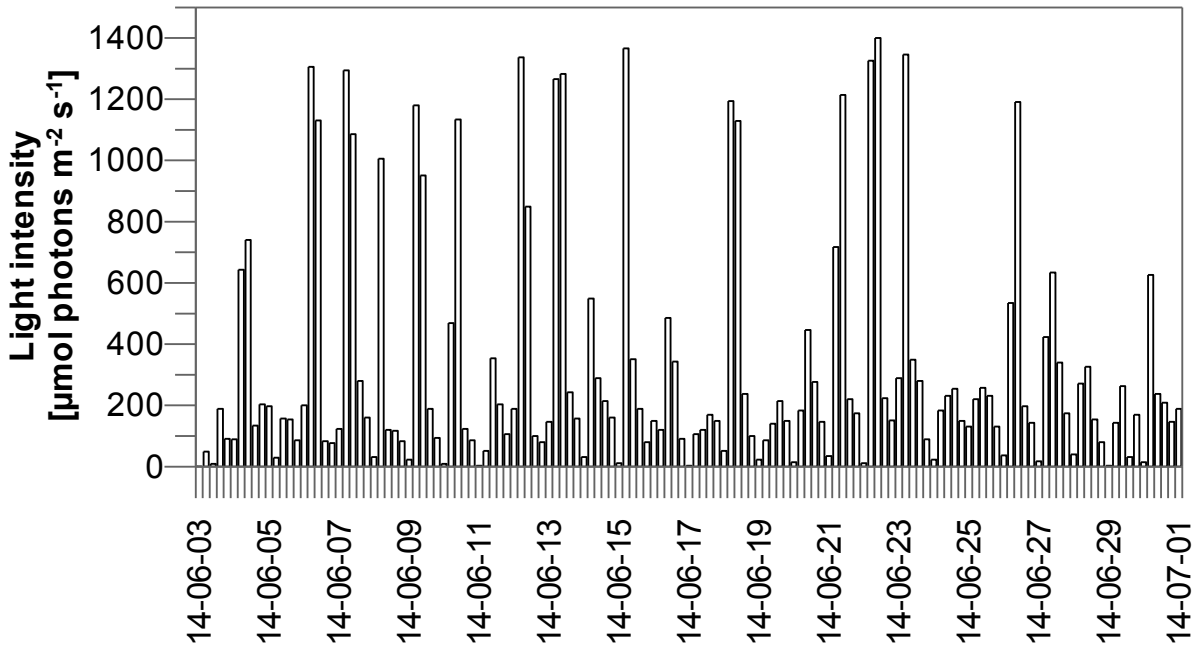

Figure 2.1 Typical cause of light intensities over one month of growing season, measured with a light sensor located between the plant pots. Light intensities are shown at 06:00, 09:00, 12:00, 15:00, and 18:00 o'clock for each day between the 3rd of June till the 1st of July.

Furthermore, plants grown under natural, fluctuating light conditions (NatL) were cultivated. Exclusively wild type plants were used for this growth method. After two weeks of controlled growth conditions at 100 µmol photons m^{-2} s^{-1}, plants were put on a balcony outside of the lab, facing east (Düsseldorf, North-Rhine Westphalia, 51°11'18.5"N 6°48'00.5"E). Plants were watered manually, since rainfall onto the plants was prevented by the roof. Note that full sunlight exposure was only given before noon due to shading of the plants by surrounding

buildings. The median light intensity was at 150 µmol photons m^{-2} s^{-1}, with a 95 % quantile of 1230 µmol photons m^{-2} s^{-1} at its upper range (see Figure 2.1).

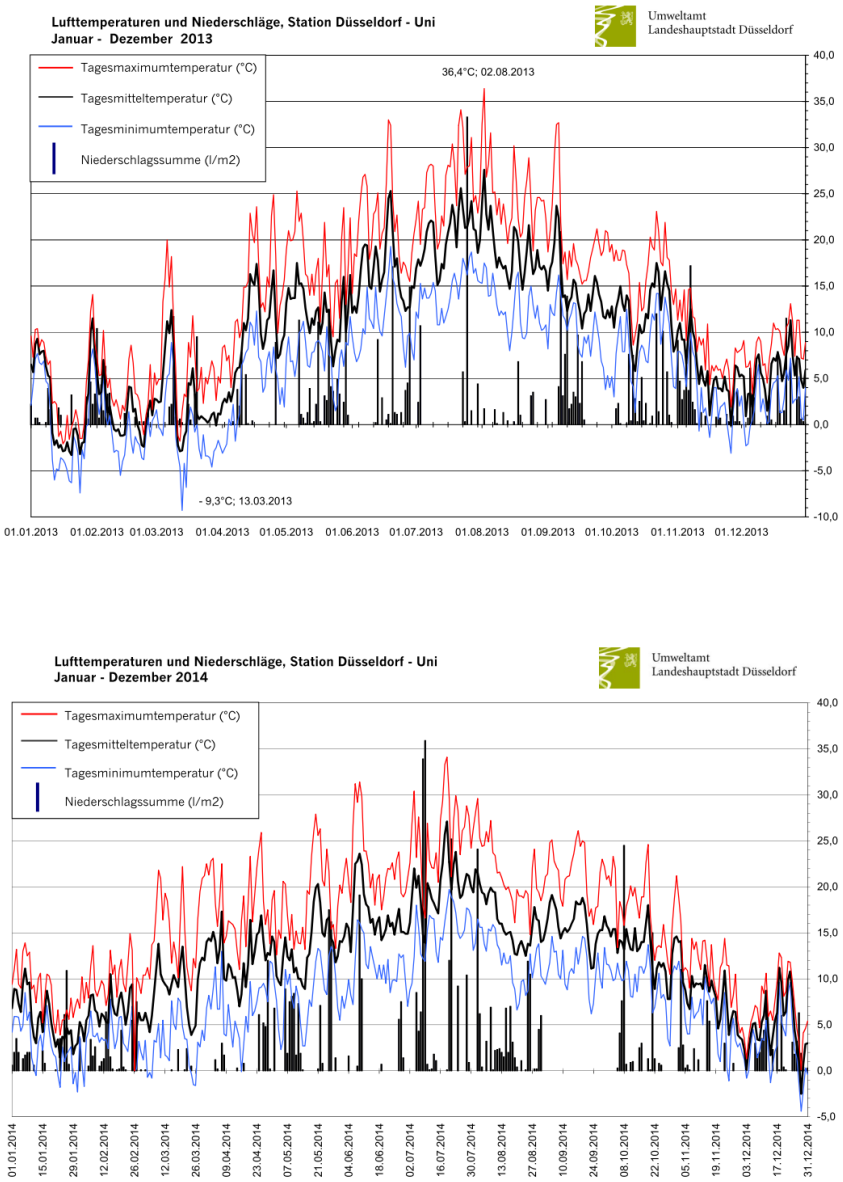

Figure 2.2 Records of temperature and rainfall in the years 2013 and 2014. Data was obtained at the weather station at the Heinrich-Heine-University Düsseldorf.

Growth season was from April till October 2013 and 2014 with temperatures between 15 and 25 °C on average for both growth seasons (see data from the City Environmental Office of Düsseldorf Figure 2.2).

2.2 Pigment analysis

For pigment quantification, a reversed phase HPLC (High performance liquid chromatography) system was used (Gilmore and Yamamoto, 1991; Färber et al., 1997). The

reversed phase system consists of a stationary, apolar phase, in this case a silica gel column with a pore size of 3-5 µm, and a mobile phase containing liquids with different polarity. In order to elute all pigments from the column, a stepwise gradient of two different mobile phases was used. Composition and gradient of the mobile phase are shown in table 2.2. Once the sample is injected into the flow of the liquid phase, pigments bind to the column with different affinities, dependent on their polarity. More polar substances are binding less well and are eluted earlier from the column as less polar substances.

Table 2.1 Components and distributors of the HPLC system.

HPLC component	Distributor
Solvent degasser Gastorr 104	Schambeck
Pump L-7100	Hitachi/Schambeck
Precolumn LiChroCART 4-4	Merck
Column LiChroCART 250-4	Merck
Separation material LiChrospher 100 RP-18.5 µm	
UV/VIS-Detector L-7420	Hitachi/Merck
Autosampler L-7200	Hitachi/Merck
Injection valve 7125 with 20 µl sample loop	Cotati
Peltier sample cooler for L-7200	Merck
Interface D-7000	Hitachi/Merck

Table 2.2 Elution program for the separation of pigments.

Elution program	Time (min)
100 % solvent A	0 - 9
linear gradient to solvent B	9 - 12.5
100 % solvent B	12.5 - 18
linear gradient to solvent A	18 - 19
100 % solvent A	19 - 23

Solvent A: Acetonitil:Methonol:Tris-buffer in the ratio of 87:10:3
Solvent B: Methanol:n-Hexan in the ratio of 4:1
Tris-buffer: 0.1 M Tris/HCl (pH 8.0), filtered (0.2 µm pore size, Schleicher und Schüll).

The eluted pigments then pass a UV/VIS-detector unit, where they are quantified photometrically at 440 nm. The peaks are identified using specific retention times and finally quantified by taking specific conversion factors into account, which were formerly determined

with the help of calibration curves for each pigment (see table 2.3). For more detailed information regarding the HPLC setup see table 2.1.

Table 2.3 Retention times and specific conversion factors of the eluted pigments.

Pigment	Retention time (min)	Conversion factor (area mol^{-1})
Neoxanthin	3.3	2990
Violaxanthin	4.2	3375
Antheraxanthin	6.3	3006
Lutein	8.5	2877
Zeaxanthin	9.4	1980
Chlorophyll b	13.6	842
Chlorophyll a	14.2	1056
β-Carotene	16.7	2595

2.2.1 Pigment content normalized on fresh weight

The fresh weight was determined on intact leaves or leaf discs, which were immediately shock frozen in liquid nitrogen and mortared with a bead-mill system (Retsch®, Haan, Germany) for 30 sec at 30 Hz. For pigment extraction, 1 ml of 100 % acetone was added to each sample and stored overnight at -20 °C. The next day, the samples were centrifuged and filtered through a 0.2 µm membrane filter (GE Healthcare, Buckinghamshire, UK) and stored at -20 °C until measurement.

2.2.2 Conversion of Xanthophylls

The conversion of the xanthophylls was carried out in leaf discs, using a strong actinic white light source. A cooling cuvette and an additional fan were used to reduce heating of leaves. Leaf discs were illuminated at 340, 850 or 2000 µmol photons m^{-2} s^{-1}, respectively. Samples were taken before illumination (time point 0), and after 2, 5, 10, 20 and 30 minutes of illumination. After 30 minutes the samples were transferred into darkness to monitor the VAZ re-conversion in the dark. During a 30 min relaxation phase samples were taken after 2, 5, 10, 20 and 30 minutes, also. The taken samples were quickly dried and immediately transferred into 2 ml reaction tubes, which were immediately shock frozen in liquid nitrogen. For further sample preparation see 2.2.1.

2.3 Thylakoid isolation from *Arabidopsis thaliana* leaves

5-10 grams of leaf material was harvested and washed twice with water and additionally once with demineralized water and kept in the fridge for 10-30 minutes. Afterwards leaves were shredded using a Waring blender (Waring Comercial, Connecticut, USA) under addition of 25 to 50 ml isolation medium (Medium A). The homogenate was filtered through two layers of mull and one layer of nylon gaze (20 µm). The filtrate was centrifuged at 1010 x *g* (Universal 32t, Hettich, Germany) for 5 minutes at 4 °C and pellets were resuspended in shock medium (Medium B) in order to break the remaining intact chloroplasts open and yielding a homogenous thylakoid suspension. After adding the same volume of resuspension medium (Medium C) the sample was centrifuged again and finally resuspended in a 1:1 mixture of media B+C. The thylakoids were kept on ice in the dark until further use.

Table 2.4 Media composition for thylakoid isolation from *Arabidopsis thaliana* leaves

Isolation medium* **(Medium A)**	**Shock medium (Medium B)**	**Resuspension medium (Medium C)**
330 mM Sorbitol	5 mM $MgCl_2$	660 mM Sorbitol
44 mM MES (NaOH pH 7.4)		80 mM HEPES (NaOH pH 7.6)
10 mM NaCl		10 mM NaCl
1 mM $MgCl_2$		5 mM $MgCl_2$
1 mM $MnCl_2$		2 mM KH_2PO_4
5 mM EDTA		
5 mM EGTA		

* add freshly 0.1 % (w/v) BSA and 330 mg/L Sodium-ascorbate

Chlorophyll content was determined using a method adapted from (Arnon, 1949), measuring the absorption at 645 and 663 nm with a photospectrometer (Ultrospec 100 pro, Amersham Biosciences). 5-10 µl of isolated thylakoids were added to 1 ml of 80% Acetone and centrifuged at maximum speed for 2 min. According to the following formula the chlorophyll content was calculated:

$$Chlorophyll\ content\ \left(\frac{mg}{ml}\right) = \left(\frac{(A_{645} * 20.2 + A_{663} * 8.02}{1000}\right) * \frac{Volume_{total}}{Volume_{sample}}$$

2.4 Chloroplast isolation from *Arabidopsis thaliana* leaves

2-5 grams of plant material were used for the preparation. After carefully washing once with distilled water, leaves were kept in the fridge for 2 hours in order to stabilize the membranes. Meanwhile 4 falcon tubes were prepared, each containing 5 ml of Percoll and 5 ml of 2x Isolation buffer and kept in the fridge for further use. After 2 hours, 25 ml of 1x Isolation

buffer (and freshly added 0.1 % (w/v) BSA and 330 mg/L sodium ascorbate) were added to the leaves and homogenized for 3 sec with low speed in a well sharpened Waring blender (Waring Comercial, Connecticut, USA). The homogenate was then gently filtered through one layer 50 µm Petex polyester mesh (Sefar, Thal, Switzerland). The filtrate was carefully loaded onto the formerly prepared falcon tubes. Then, samples were centrifuged for 10 minutes at 4 °C with 2000 x *g* (Universal 32t, Hettich, Germany). After the centrifugation intact chloroplasts were localized at the bottom of the falcon tube, whereas broken chloroplasts are found in a smear in the upper part of the Percoll cushion. The supernatant was discarded and the broken chloroplasts were removed with a soft tissue. Intact chloroplasts were resuspended in 1 ml (+ 15 ml) of 1x Isolation buffer by gently shaking of the tubes and pooled afterwards. The chloroplast suspension was centrifuged for 5 min at 4 °C with 2000 x *g*. After carefully discarding the supernatant chloroplasts were resuspended in a final volume of 100 to 250 µl of 1x Isolation buffer. Chlorophyll content was determined as mentioned (see 2.3).

Isolation Buffer 2x

600 mM Sorbitol
40 mM HEPES (KOH, pH 7.6)
2 mM $MgCl_2$
2 mM $MnCl_2$
10 mM EDTA
10 mM EGTA
20 mM $NaHCO_3$

2.5 Determination of Chl content normalized on the amount of chloroplasts

The chlorophyll concentration of isolated chloroplasts (see 2.4) from LL, NL, HL and NatL was determined as previously described (see 2.3). Dilutions of 1:10, 1:20, 1:50, and 1:100 of the chloroplast suspension were prepared for chloroplast counting. 50 µl of the chloroplast solution was transferred onto a Baumannsche counting chamber and the number of chloroplasts was quantified via counting 4 out of 16 squares of the counting chamber. Each square contained a volume of 0.004 µl, resulting in 0.064 µl for the whole chamber. To normalize the data, counts were divided by 0.064 and multiplied by 1000, yielding in the total number of chloroplasts per ml. Only chloroplast isolations with high amounts of intact chloroplasts were used for the calculation to minimize bias that would result from broken chloroplasts.

The amount of Chl per chloroplast was calculated as follows:

$$\frac{mol\ chlorophyll}{chloroplast} = 0.9 * 10^{-6} * \frac{c}{n},$$

with c = chlorophyll concentration of the chloroplast solution in mg Chl per ml; n = number of calculated chloroplasts per ml solution; where 0.9 * 10^{-6} corresponds to the molecular weight of Chl (M = 900 g/mol).

2.6 Isolation and quantification of total protein extract

One leaf per plant was harvested and mortared using a motorized pistil (Heidolph RZR 2051control, Heidolph Instruments GmbH & Co.KG, Schwabach, Germany) while adding 200-300 µl of protein extraction buffer. Samples were centrifuged for 10 minutes at maximum speed and the supernatant was transferred into a new reaction tube.

Total protein concentration was quantified using the BioRad D_C Protein Assay (Biorad, Munich, Germany) according to manufacturer's guideline. This assay is based on a method developed by (Lowry et al., 1951), which uses colorimetric means in order to quantify proteins in a solution. During the reaction aromatic residues in the protein, introduced by tryptophan and tyrosine, are oxidized by the Folin agent and can be measured at 750 nm. After determining the protein concentration, samples were adjusted with protein sample buffer to either 1-2 mg/ml total protein.

Protein extraction buffer	**Protein sample buffer**
50 mM Tris/HCl (pH 7.6)	50 mM Tris/HCl (pH 7.6)
1 M Urea	1 M urea
1.6 % SDS	1.6 % SDS
	1 % (v/v) β-mercaptoethanol
	12.5 % (v/v) glycerin
	0.05 % bromophenol blue

2.7 SDS-PAGE and Westernblot analysis

Protein samples were obtained as described previously (see 2.6) and 8-20 µg total protein extract were loaded onto the SDS gel (Table 2.5). For separation, a discontinuous gel system as described by Leammli was used (Laemmli, 1970). Before loading, the samples were preheated for 5 min at 95 °C. Proteins were separated using an initial voltage of 50 V for the stacking gel and 120 V for the separation gel. Empty pockets were filled with sample buffer in order to keep a homogenous running front during the separation. Band sizes were identified using the PageRulerTM (Fisher Thermo Scientific, Waltham, USA) protein ladder.

Table 2.5 Stacking and separation gel composition for SDS PAGE.

Components	Stacking gel (5 %)	Separation gel (13.5 %)
Acrylamide (30:1:1)	1.7 ml	13.5 ml
Tris/HCl pH 8.8	-	6.5 ml
Tris/HCl pH 6.8	2.5 ml	-
ddH_2O	5.6 ml	12.1 ml
SDS (10 %)	200 µl	300 µl
APS (10 %)	100 µl	200 µl
TEMED	8 µl	10 µl
Bromphenol blue	10 µl	-

Laemmli buffer
25 mM Tris/HCl (pH 7.5)
150 mM glycine
0.1 % SDS

Sensitive Coomassie staining solution
25 % (v/v) 2-propanole
10 % (v/v) acetic acid
0.5 g/L Coomassie brilliant blue G-250

Proper loading of the samples on the gel was checked with a sensitive Coomassie staining. After destaining with water, gels were used for Westernblot analysis. The Westernblot was performed using a semi-dry blotting chamber (Peqlab Biotechnologie GmbH, Erlangen, Germany). A discontinuous blotting system was used for transfer of the proteins onto a PVDF membrane (Immun-Blot® PVDF, BIORAD, Hercules, USA). The setup for the transfer was as follows (from anode to cathode): Three layers of Whatman paper previously incubated in Anode buffer I, followed by three layers of Whatman paper previously incubated in Anode buffer II. The PVDF membrane, also incubated in Anode buffer II was put onto the six layers of Whatman paper, topped by the SDS gel, incubated in Cathode buffer. Finally the stack was finished by topping three layers of Whatman paper, previously incubated in Cathode buffer.

Anode buffer I
25 mM Tris (pH 10.4)

Anode buffer II
300 mM Tris (pH 10.4)

Cathode buffer
25 mM Tris (9.4)
40 mM 6-amino capronic acid

Protein transfer was verified by staining of the PVDF membrane with Ponceau staining solution. All steps were performed at room temperature. The membranes were then washed

2 x with TBS-T buffer each for 10 min. The membrane was blocked by with a 5 % (w/v) milk powder solution (solved in TBS-buffer) while shaking for 1 h. After blocking, membranes were washed 1 x with TBS-T buffer and further incubated with the primary antibody for 1 h. Either anti-D1 antibody (Agrisera, Vännäs, Sweden) in a dilution of 1:4000, or anti-PsbS antibody (Pineda Antikörper Service, Berlin, Germany) in a dilution of 1:8000 were used. After washing with TBS-T buffer, the membranes were finally incubated with the secondary antibody (dilution 1:10000), also for 1 h. After washing 3 x with TBS-T buffer (10 min), membranes were incubated with picoLUCENT^{TM} (G Biosciences, St. Louis, USA) agent. Fluorescence was detected using the LAS-4000 mini (Fujifilm, Tokyo, Japan). Band intensity was quantified using the freeware Image Studio Lite (LI-COR Biosciences, Lincoln, USA).

TBS buffer:	**TBS-T buffer:**	**Ponceau staining solution:**
10 mM Tris/HCl (pH 7.5)	1 x TBS buffer	3 % (w/v) 2,4,6-Trichloranisol (TCA)
150 mM NaCl	0.2 % Triton X-100	0.2 % (w/v) Ponceau S
	0.05 % Tween-20	

2.8 Spectroscopy

2.8.1 Fluorescence measurements

Fluorescence was measured in intact leaves for 30 min at 340, 825, and 1950 µmol photons m^{-2} s^{-1} actinic light intensity, followed by 30 min of relaxation. The leaves were placed on a glass plate and a drop of water was placed on the cut end of the leaf to prevent additional effects on the fluorescence by drought stress. Measuring light intensity was 7 µmol photons m^{-2} s^{-1}. Saturation pulses (200 ms, 4000 µmol photons m^{-2} s^{-1}) were applied as follows:
Saturation pulses during actinic light phase: 10 x 3'', 10 x 6'', 17 x 30'', 20 x 60''
Saturation pulses in the dark period: 10 x 6'', 8 x 30'', 25 x 60''
For measuring transient NPQ, 53 µmol photons m^{-2} s^{-1} were used for NL, HL, and NatL plants. For LL plants 13 µmol photons m^{-2} s^{-1} were used. Fluorescence was measured for 10 minutes with actinic light, followed by 5 min of relaxation in the dark. Saturation pulses were applied every 60 sec. NPQ was calculated as (Fm/Fm' - 1) (Krause and Jahns, 2004).

qL, as the coefficient of photochemical quenching, provides information about the reduction state of PSII. Values range between 0 (PSII closed, oxidized) and 1 (PSII open, reduced). qL was calculated as follows: $qL = (Fm'-F)/(Fm'-F_0') \times F_0'/F$
Additionally, electron transport rates were determined, derived from the effective quantum yield of PSII (Y(II)), according to Genty (Genty et al., 1989).

Y(II) = (Fm'-F)/Fm', ETR = Y(II) x I x a x f, with I = light intensity (µmol photons m^{-2} s^{-1}), f = fraction of absorbed light by PSII (0.5), and a = fraction of absorbed light by the leaf (0.84).

2.8.2 PSI oxidation state (P700)

PSI oxidation state can be monitored by measuring absorption changes at 730 and 870 nm. The oxidation state depends on the PSI excitation (oxidation) and reduction by electron transfer from PC (reduction). Oxidized P700 thus resembles congestion in the LET. Light curves with the following actinic light intensities were measured: 53, 166, 340, 825, and 1950 µmol photons m^{-2} s^{-1}. Two minutes per light step allowed for full acclimation to the according light intensities. The oxidation state was measured both, with increasing and decreasing light intensities and the data was pooled for analysis.

2.8.3 Measurement of the proton motive force and the proton conductance

The proton motive force (*pmf*) was measured using the DUAL-PAM 100 device, with P515 emitter and detector units. By analyzing absorption changes between 515 and 525 nm in the Dark-Interval-Relaxation-Kinetic (DIRK) (Sacksteder and Kramer, 2000), partitioning of the *pmf* was estimated. A typical DIRK signal of a NL grown plant in the light- (340 µmol photons m^{-2} s^{-1}) dark transition is shown in Figure 2.3. Due to proton efflux through the ATPase in the dark-light transition, the ECS signal is characterized by an undershoot compared to the steady state dark ECS shortly after illumination (Figure 2.3 A).

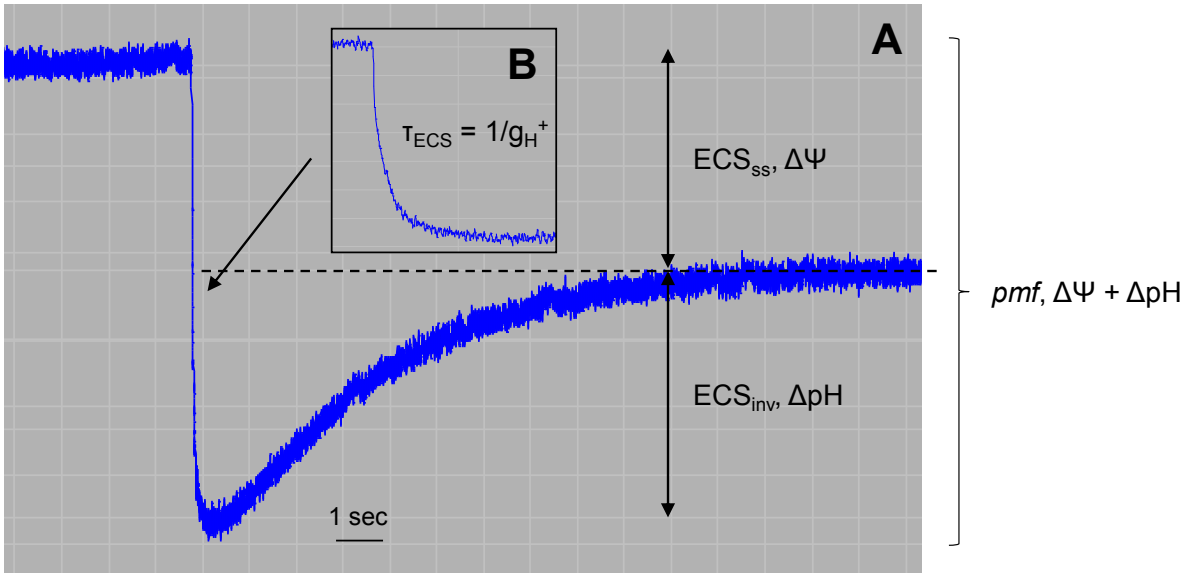

Figure 2.3 (A) Typical Dark-interval relaxation kinetic (DIRK), (B) Proton conductance through the ATPase. During the light-dark transition, a constant efflux of protons through the ATPase leads to a negative overshoot of the ECS signal compared to the steady state ECS in the dark (ECS_{inv}, ΔΨ). Due to counter ion movement, the ΔΨ is collapsed, thus reaching steady state (ECS_{ss}). The total amplitude of the ECS signal accounts for the chloroplastidal *pmf* in the light-dark transition. (B) Proton efflux through the ATPase can be analyzed by single exponential fit, acquiring the lifetime of the ECS signal (τ_{ECS}). The proton conductance (g_H^+) can be derived from the according rate constant.

The partition below the steady state (ECS_{inv}) accounts for the ΔpH portion of total *pmf*. The ECS in steady state (ECS_{ss}) complements the total *pmf*, giving the portion of the electric field component (ΔΨ). The decay of ECS can be expressed as single exponential, from which the lifetime of the ECS (τ_{ECS}) signal can be extracted. The proton conductance through the ATPase (g_{H^+}) is resembled in the according rate constant of τ_{ECS}.

The specific ECS unit for each sample was determined by applying a single turnover flash previous to each measurement. 10 flashes were averaged and the the ECS unit quantified. Initial *pmf* was determined during dark-light transition before switching on the actinic light source at 340, 825, or 1950 µmol photons m^{-2} s^{-1} for 30 min. Total *pmf* in the light was determined by analyzing the DIRK signal obtained in the light-dark transition. Arabidopsis wild type measurements were performed on individual plants, which one measurement per plant. For Arabidopsis mutants, multiple light-dark and dark-light transitions were measured at same sample as follows: (time in minutes; white bars: illumination, black bars: dark-phase):

15	0.5	5	0.5	5	0.5	5	0.5

Partitioning of the *pmf* into ΔΨ and ΔpH was calculated by measuring the steady state of signal recovery after 20-30 sec after the light-dark transition as described in Figure 2.3. Proton conductance was calculated from ECS decay (τ_{ECS}) as described (Figure 2.3). Lumen pH was calculated according to (Takizawa et al., 2007).

2.9 Spectrometric determination of PSII, PSI and Cyt b_6f

Thylakoids from *Arabidopsis thaliana* wild type plants were isolated as described (section 2.3). For the determination of the PSI content, thylakoids were diluted in 1.5 ml Measuring solution (P) to a concentration equivalent to 50 µmol chlorophyll. Samples were centrifuged for 45 sec at maximum speed. For the measurement, 1.2 ml of the supernatant were transferred into a disposable polystyrene cuvette (Sarstedt, Nümbrecht, Germany). 10 mM sodium ascorbate and 100 mM MV were added to the sample and mixed carefully before measurement. PSI was quantified using the P700 emitter/detector unit of a DUAL-PAM 100 (Walz, Effeltrich, Germany). Only fully dark-adapted samples were measured. Precautions were made that no trembling of the cuvette or the cuvette holder disturbed the sensitive measurement. After calibrating the P700 signal, a 200 ms saturation pulse was applied to the sample and the maximum amplitude of the signal was quantified. The dark baseline resembles the PSI in a fully reduced state, whereas at the maximal amplitude, PSI is in a completely oxidized state. PSI content was calculated as follows:

$$\Delta c = \frac{\frac{\Delta I}{I}}{(2.3 * \varepsilon * d)},$$

with ε = 2.53 cm² µmol^{-1}, specific for the Dual-PAM system used for the experiments.

PSI measuring solution (P)

0.2 % (w/v) beta-DM
30 mM KCl
10 mM $MgCl_2$
30 mM HEPES/KOH (pH 7.6)

The amounts of PSII and cytochrome b_6f were calculated from differential spectra measured with a photospectrometer in a range of 540-575 nm. In this approach absorption changes of cytochrome b_6, cyt f, cyt_{559} and cyt_{550} were measured at different oxidation states (see below). The differential spectra were fitted against reference spectra and the amount of cytochrome b_6f and PSII (cyt_{550}) was calculated.

For the measurements, dark adapted thylakoids from *Arabidopsis thaliana* were isolated as previously described (section 2.3). Thylakoids equivalent to 50 µmol of chlorophyll were incubated for 10 min in the high salt Measuring solution (Cyt) to ensure compete grana unstacking. After blanking, 1 mM potassium ferricyanide was added to the measuring cuvette to fully oxidize the cytochromes. After 1 min of incubation the spectra was measured (10 cycles). Hereafter, 10 mM sodium ascorbate was added to the sample to partially reduce the cytochromes. Samples were incubated for 5 min and measured again in a range of 540-575 nm (10 cycles). Finally, to fully reduce all cytochromes, a spatula tip of dithionite was added to the sample. The cuvette was sealed with paraffin oil (150 µl) to prevent reoxidation of the cytochromes by aerial oxygen. After 8 min of incubation on ice, the spectra were measured (10 cycles). Averages from all cycles of each treatment were used for calculating the amount of PSII (cyt_{550}) and Cyt b_6f.

Measuring solution (Cyt)

0.02 % (w/v) beta-DM
30 mM KCl
0.1 mM EDTA
30 mM HEPES/KOH (pH 7.6)

2.10 Lipid analysis

Lipids were extracted from total leaves according to a boiling water protocol, which was kindly provided by the workgroup of Prof. Dr. Peter Dörmann. Leaves (approximately 200 mg fresh weight) were harvested and immediately transferred into glass vials containing boiling water. Leaves were boiled for 20 min to inhibit all lipase activity. After transferring the leaves

into a fresh glass vial, 1 volume of Chloroform:Mehtanol (2:1) was applied and gently mixed. The green supernatant was transferred into a fresh glass vial and the leaf material was washed in a second step with 1 volume Chloroform:Mehtanol (1:2). The green supernatants were pooled and stored in a glass vial with Teflon cap at -20 °C. The leaf material was dried overnight in a drying chamber at 70 °C and dry weight was obtained the next day.
Samples were analyzed at the IMBIO in Bonn via mass spectrometry in the institute of Prof. Dr. Peter Dörmann, where further steps of lipid preparation were performed.

2.11 Microscopy

All light and electron microscopy studies were carried out by Dr. Michael Melzer in the Leibniz-Institute for plant genetics und crop research (IPK) in Gatersleben.

2.11.1 Light microscopy

Leaf cross sections were stained for 2 minutes at 60 °C with 1 % (v/v) methylene blue, 1 % (v/v) Azur II in a 1 % (v/v) aqueous borax solution. Samples were thereafter washed and dried. Cross sections were examined using a Zeiss Axiocam camera which was used in a Zeiss Axiovert 135 microscope (Zeiss, Oberkochen, Germany).

2.11.2 Transmission electron microscopy (TEM)

Transmission electron microscopy images were obtained with a FEI Tecnai Sphera G2 (FEI, Hillsboro, Oregon, USA) microscope, which uses a high voltage electron beam in order to create a black white image with high resolution. The high resolution is based on the wavelength of electrons, which is 100,000 times smaller compared to the wavelength of light, yielding in an increased total resolution compared to light microscopy. The image is created based on the number of electrons reaching the detector, which depends on the density of the mass of the sample. Areas of higher mass are darker compared to areas of lower mass.
Leaves from *Arabidopsis thaliana* plants, grown under different light conditions, were measured in a dark acclimated (overnight) and light acclimated (illumination with approximately 1000 µmol photons m^{-2} s^{-1} for 30 min) states. Additionally, samples were taken after 10 minutes of darkness after illumination. At each acclimation state, leaves were harvested, chopped, and fixed with Spurr fixation solution in a microwave using 150 W in the following sequence:
2x heating, 1 min
1x Cacodylate buffer, 45 sec
2x H_2O, 1 min

Samples were then stepwise dehydrated (20 min per step at room temperature) with increasing ethanol concentration reaching from 20 % to 100 % After dehydration, the samples were fixed in HM20 resin, again stepwise from 20 % to 100 % HM20. The samples were finally transferred in pre-polymerized galantine capsules and cooled to -35 °C. The resin was polymerized during 72 h in UV light at -35 °C.

Spurr fixation solution

2.0 % Formaldehyde

0.5 % Glutaraldehyde

50 mM Cacodylate buffer (pH 7.2)

2.11.3 Immunogold labeling

Immunogold labeling was used for semi-quantitative analysis of PsbS content in leaf tissues of plants from different growth conditions. Leaf sections (approx. 70 nm) were washed with 0.1 % BSA washing solution (150 mM phosphate buffer, pH 5.2, 0.5 % Tween-20, 0.1 % polyethylene glycol, 5 mM NH_4Cl) to minimize binding of non-specific proteins. The sections were incubated in diluted anti-PsbS antibody solution for 45 min and furthermore washed with washing solution with reduced BSA concentration (0.1 ng l^{-1}). 10 nm A-gold conjugates were added to the cross section and repeatedly washed with washing solution for 30 min. Contrasting of the sections was induced by adding LEICA EM STAIN (Leico Microsystems, Wetzlar, Germany) with uranyl acetate and lead citrate. Analysis of the samples was performed as previously described.

2.11.4 Confocal microscopy

Confocal microscopy (LSM 4000, Zeiss, Oberkochen, Germany) was used to detect auto fluorescence of chloroplasts in leaves of LL, NL, HL, and NatL grown *Arabidopsis thaliana* plants. Auto fluorescence was induced by using a red laser beam with 440 nm wavelength and detected between 680-700 nm. The advantage of confocal microscopy is an increased resolution due to subsequent scanning the sample areas, which are merged at the end of the scanning. Additionally, the resolution, primary of the z-axis (the depth of the sample), is enhanced by a so-called pinhole aperture, which prevents a decrease of resolution by reducing the scattering of non-directed light. Besides auto fluorescence, fluorescence markers, such as the green-fluorescent protein, can be detected via confocal microscopy (Cisek et al., 2009).

2.12 Chlorophyll a fluorescence transient (OJIP)

Chlorophyll a fluorescence transient is based on the so-called Kautsky effect (Kautsky and Hirsch, 1931) and can be used as a tool for measuring fluorescence states in PSII in a timescale of milliseconds. The nomenclature of this measurement O-J-I-P resembles the different fluorescence states, whereas O = origin, ground fluorescence (F_0); J and I = intermediate states based on the reduction of Q_A; P = peak, maximum fluorescence (Fm). *Arabidopsis thaliana* leaves were dark acclimated overnight. Measurements were performed with a Handy PEA device (Hansatech Instruments, Norfolk, UK). Dark acclimated leaves were illuminated for 1 sec with 3500 µmol photons m^{-2} s^{-1} with a gain multiplication of 0.5 to obtain the chlorophyll a fluorescence transient. Curves were analyzed on a logarithmic times scale.

2.13 Gas exchange measurements

Maximal CO_2 assimilation rate and light compensation points were calculated from light response curves of differently acclimated *Arabidopsis thaliana* plants obtained by gas exchange measurements (LI-COR-6400XT (LI-COR, Nebraska, USA)). A measuring chamber with an area of 2 cm² was used. Samples were measured under controlled CO_2 conditions: 400 ppm CO_2 with a flow of 300 µmol s^{-1} under 102.4 kPa. Temperature was set to constant 20 °C. Before measurement, plants were acclimated light acclimated for 15 min at 500 µmol photons m^{-2} s^{-1}. Light response curves were measured in the following steps from the highest to the lowest light intensity: 2000, 1500, 1000, 750, 500, 300, 150, 100, 50, 25, 25, 0 µmol photons m^{-2} s^{-1}. Leaves were acclimated for 3 min at each light intensity before measurement. The light quality consisted of 90 % red and 10 % blue light. The assimilation curves were fitted with Prism®, providing the maximum assimilation rate P_{max} and the light compensation point (LCP).

3 Results

3.1 Energy dissipation in *Monstera deliciosa* grown under low and natural high light

The evergreen hemi-epiphytic plant *Monstera deliciosa* is a climbing plant naturally growing under both very low light (LL) conditions (as found at the bottom of dense canopies) and high light (HL) conditions (at the top of the canopy). HL acclimated leaves of Monstera develop a drastically increased NPQ capacity compared to LL acclimated plants, which is accompanied by the accumulation of increased levels of PsbS and Zx (Demmig-Adams et al., 2006) and thus could be related to increased levels of qE and qZ quenching. However, a fraction of the increased NPQ capacity was found to be related to ΔpH-independent, sustained quenching processes (Demmig-Adams et al., 2006). To determine the molecular mechanisms, which contribute to the increased NPQ capacity in HL acclimated *Monstera deliciosa* plants, a combined approach involving ultrafast fluorescence spectroscopy and characterization of basic photosynthetic parameters, was chosen.

Manuscript draft

A highly efficient new photoprotection mechanism in higher plants grown under natural high light regime involves major thylakoid reorganization

A highly efficient new photoprotection mechanism in higher plants grown under natural high light regime involves major thylakoid reorganization

Suman Paul[1#)], Tobias Schumann[2)], Michael Reus[1)], Peter Jahns[2)], and Alfred R. Holzwarth[1,*)]

[1)] Max-Planck-Institute for Chemical Energy Conversion†, D-45470 Mülheim a.d. Ruhr, Germany

[3)] Biochemie der Pflanzen, Heinrich-Heine-Universität Düsseldorf, D-40225 Düsseldorf, Universitätsstr. 1, Germany

#) Present address: Fysiologisk botanik, Umeå Plant Science Centre, Umeå University, 901 87 Umeå, Sweden

Abbreviations: PS, photosystem; PSA, photosynthetic apparatus; RC, reaction center; NPQ, non-photochemical quenching; SI, supporting information;

Key words: thylakoid organization; lateral heterogeneity; non-photochemical quenching; fluorescence kinetics; evergreens; photosynthesis; light adaptation; photosynthesis;

Running title: Photoprotection mechanisms in plants

†) Previously known as the Max-Planck-Institute for Bioinorganic Chemistry

*) To whom correspondence should be addressed: Dr. Alfred Holzwarth, Max-Planck-Institute for Chemical Energy Conversion, Stiftstr. 34-36, D-45470 Mülheim a.d. Ruhr, Germany; e-mail: Alfred.Holzwarth@cec.mpg.de

Abstract

Non-photochemical quenching (NPQ) was studied by time-resolved fluorescence spectroscopy in intact leaves of the tropical evergreen *Monstera deliciosa* grown under either high light or low light conditions. Low light grown plants showed a spectrally and kinetically homogeneous photosystem II (PSII) pool and evidence for the same NPQ mechanisms and similar NPQ capacity as described previously for typical annual mesophytes like e.g. Arabidopsis. In contrast, natural high light grown Monstera not only showed evidence for the existence of two kinetically distinguishable (heterogeneous) PSII pools, but also exhibited a novel NPQ quenching mechanism that we term *spillover quenching*. This is the most efficient NPQ mechanism experimentally observed thus far in plants and contributes a larger fraction to the leaf's total quenching capacity in plants grown under natural high light than the two previously discovered "classical" NPQ mechanisms combined. It allows the plants to reach max. NPQ values of ca. 10, while the classical mechanisms only enable NPQ values of up to ca. 4. *Spillover quenching* thus constitutes a new, highly efficient photoprotective mechanism for PSII. The observed kinetically heterogeneous PSII pool and spillover quenching indicate a major structural reorganization of thylakoids upon high-light-acclimation of *Monstera deliciosa*. This light-induced reorganization abolishes the lateral segregation of PSII and PSI in high light grown plants and is particularly pronounced under NPQ conditions. Our data thus not only challenge the classical strict lateral segregation model of the photosystems in higher plants but also demonstrate that thylakoid structure reorganization is a fast and efficient process for both optimal long-term as well as short-term acclimation to variable light conditions thus strongly extending the photoprotection capacity well beyond the classical PSII intrinsic quenching mechanisms.

Introduction

To optimize photosynthesis while simultaneously preventing photo-oxidative damage, chloroplasts must adapt dynamically to rapidly and widely varying natural light levels. This involves short-term adjustments like state transitions [1,48] and thermal dissipation of excess excitation energy (assessed via non-photochemical quenching, NPQ) [21,38] as well as long-term acclimation [36,43] known to influence thylakoid structure [3,43]. The present understanding of higher plant thylakoid architecture involves two elements: Stacked, highly appressed membranes (grana) where photosystem II (PSII) is located, and extended non-appressed "stroma-lamellae" containing photosystem I (PSI) and the ATP synthase [4,7]. Little is known about possible functionally important structural changes in thylakoid organization during short-term acclimation such as NPQ activation. The present knowledge about thylakoid architecture is based mainly on structural information derived from dark-adapted plants, often grown under constant low light, rather than from plants grown under natural, highly variable light conditions that might induce a substantially different thylakoid structure and photoprotection capacity [2,6,16]. Optimal acclimation to widely varying light conditions may thus require highly dynamic light-induced thylakoid reorganizations [6]. Pronounced membrane stacking, and thus lateral segregation of the two photosystems may, in fact, be inconsistent with a highly dynamic membrane architecture required for efficient light acclimation [5,31]. Indeed, recent structural studies suggest that thylakoid membrane reorganization does occur during both short-term and long-term adjustments to high light exposure [12,27,30,31,41,52]. All of these data point to the possibility that plants in their photosynthetically active state in the light may have a substantially different thylakoid architecture than in their resting state in darkness.

Fast-growing annual species with high photosynthesis rates typically dissipate about half of the light they absorb at midday in sunny habitats to provide effective photoprotection against damage of the photosystems by excess light, while slow-growing evergreen species often dissipate over 90 % of the absorbed light under the same conditions [10]. Mechanistic analyses of photoprotective mechanisms have focused largely on the annual model species *Arabidopsis thaliana*. However, evergreen species exhibit up to three times higher maximal NPQ capacities than annual ones [10]. Yet, the underlying structural and/or molecular mechanism(s) of such drastically increased NPQ capacities remain unknown. At least two NPQ mechanisms are activated in PSII in the short-term, one associated with pH-dependent activation of the protein PsbS [37], and another associated with the formation of the xanthophyll pigment zeaxanthin [10,13,23,42]. Disagreement exists at present on whether the

two mechanisms cooperate synergistically in the same PSII antenna complex [22] or act independently in different antenna complexes [19,39]. While NPQ processes are generally considered to occur in PSII units independent of major reorganization of the thylakoid structure, both models propose minor structural changes in the (PSII-containing) grana stacks, either by minor reorganization of the peripheral antenna (LHCII) of PSII [26], and/or by detachment of a peripheral LHCII antenna from PSII [19].

Monstera deliciosa, a climbing (hemi-epiphytic) rainforest vine, is an excellent model of plant acclimation to contrasting light environments – as it thrives equally in the extremely low light environment on the rainforest floor and in full sunlight on top of the forest canopy [11]. Leaves from Monstera plants acclimated to full sunlight generate much higher maximum NPQ levels than shade-adapted leaves [11]. This higher NPQ capacity of sunlight-acclimated leaves is accompanied by increased levels of the PsbS protein and zeaxanthin [10,11]. To test whether the increased NPQ capacity is based on one or both of the known NPQ mechanisms (PsbS or zeaxanthin-dependent), or involves a novel additional mechanism, we characterized the molecular basis of the high NPQ capacity of *M. deliciosa* by comparing NPQ characteristics of low light grown (LL) plants with those of plants grown under natural, fluctuating high light (NatL plants). Using powerful ultrafast fluorescence methods for functional characterization we demonstrate a potent novel photoprotection mechanism based on major, and rapidly occurring reversible light-controlled thylakoid reorganization.

Methods

Plant material and growth conditions

Monstera deliciosa plants were obtained from a local garden center. Several cuttings were taken from one of the plants and were rooted and grown in soil (Floragard, Pflanzenerde) and fertilized with a liquid fertilizer optimized for evergreens once per week. Measurements were taken on the original plant and plants derived from cuttings. No significant differences beyond the variations occurring on different leaves of the same plant were observed in the parameters measured in this work.

The low light grown plants (LL plants) were grown at 40-50 μmol photons m^{-2} s^{-1} provided by an array of fluorescent tubes (Osram-L 65 W/25, Universal white) under a 12 h light/12 h dark cycle. The natural light grown plants (NatL plants) were grown exposed to natural sunlight (maximal average PFD = 1200-1400 μmol photons m^{-2} s^{-1}) behind a high glass window on the southeast side of the laboratory in Mülheim/Ruhr. The temperature in the laboratory where the LL plants were grown was kept constant at 20±2 °C. The temperature at which the NatL plants were grown varied between 20°C at night to a maximum of 24 °C on a

sunny day. All plants were long-term adapted for at least 3 months to the above conditions before any samples were taken. Fully developed leaves (4-6 weeks growth after onset of leaf unfolding) were used for the experiments and were taken only from the top of a shoot fully exposed to the above-mentioned light conditions without shading. The leaves were cut at the stem in the evening and were kept with the stem in water for dark-adaptation overnight. For a set of measurements, leaf sections were cut from the same leaf and treated as required. Lifetime measurements and global kinetic compartment analysis were carried out as described [19].

Pigment analysis

For pigment extraction, identical NPQ adapted leaf-parts were shock frozen and grinded by a beat mill system. The leaves were grinded for 2 x 30 s at 30 Hz. After grinding, 1 ml of acetone was added to each sample. Samples were stored over night at -20 °C to ensure full pigment extraction. The next day samples were centrifuged for 2 min. The supernatant was filtered through a 0.2 µm pore size filter and analyzed in a reversed-phase HPLC column system [14].

P700 oxidation state

The redox state of P700 was determined using the DUAL-PAM-100 (Walz, Effeltrich, Germany) and applying the saturation pulse method [32]. In brief, leaves were illuminated at different light intensities in the range from 20 to 1950 µmol photons m^{-2} s^{-1} and P700 absorbance changes were measured at 830 nm. After 3 min of illumination at each light intensity, the P700 oxidation state was derived from the P700 absorbance in presence of actinic light in relation to the absorbance of fully reduced and fully oxidized P700.

Steady state NPQ and relaxation kinetics

Actinic NPQ light was provided with red (635 nm peak wavelength, FWHM ca. 20 nm) high intensity LEDs for all data shown. In preliminary measurement series the maximal actinic light intensities yielding maximal saturating NPQ, which was however still fully reversible within maximally 2 h, were tested out. These maximal intensities were found to be ca. 300 µmol photons m^{-2} s^{-1} for LL plants (grown at 40-50 µmol photons m^{-2} s^{-1}, i.e. the actinic NPQ light intensity was 6-7 times growth intensity) and 2200-2400 µmol photons $m^{-2}s^{-1}$ for NatL plants (grown at natural variable light conditions, with maximal peak intensity around noon of 1200-1400 µmol photons $m^{-2}s^{-1}$). Application of significantly higher actinic light intensities did result in incomplete relaxation in particular for the LL grown leaves, reflecting photodamage. Since the present work focuses at an analysis of the kinetics at maximal reversible NPQ, i.e. plants devoid of photodamage, we did not apply still higher actinic

intensities throughout this work. The effects of actinic intensities yielding such photodamage will be described in a separate work.

Ultrafast fluorescence kinetics

Ultrafast lifetime measurements were carried out as described with the leaf sections held in a rotating cuvette, front-face excitation of the upper side of the leaf, using laser pulses of 663 nm and a repetition rate of 4 MHz [19,39]. Typically, lifetime measurements were started after 30 min of actinic illumination when the quenching had fully stabilized. Each set of lifetime measurements consisted of two different types of measurement: A time-resolved spectrum of the dark-adapted leaf with PSII reaction centers (RCs) closed by DCMU and very weak (≤5 μmol photons m^{-2} s^{-1}) background excitation. The DCMU treatment was carried out by mild vacuum incubation (3-4 times) in a 300 μM DCMU solution for 1 h. For achieving full PSII closure, as tested by fluorescence induction using a Hansatech *HandyPea* instrument and by fluorescence lifetime measurements, the lower epidermis of the leaves was mildly rubbed with extra-fine sandpaper (ISO/FEPA Grit designation: P400, average particle diameter: 35.0 μm) before DCMU incubation. To quickly close all PSII centers and achieve F'_{max} under (red high intensity LED array) NPQ conditions an additional focused blue (λ_{center} = 460 nm) high intensity LED light was applied. It provided additional high illumination for about 300 msec just before the illuminated sample spot entered the measuring beam in the rotating cuvette. This illumination was sufficient for closing all PS II RCs.

Data analysis

Kinetic data analysis and kinetic compartment modeling were performed as described [17,19]. For general explanation of kinetic models used for PSII and PSI and for details of data analysis and presentation see the Supporting information of [19]. Details for more complex kinetic models that were required for describing the data reported in this paper are discussed in the Results and Discussion sections.

Results

Steady state data

Fig. 1 shows the Fv/Fm values of dark-adapted LL and NatL grown Monstera leaves, and of leaves treated for 40 min. with actinic light to reach their maximal NPQ along with the respective relaxation kinetics. LL plants showed consistently higher F_v/F_m values in the dark-adapted leaf (0.83±0.02) vs. NatL plants which showed dark-adapted F_v/F_m values of 0.78±0.02. Upon actinic illumination, LL leaves showed a much smaller drop of F_v/F_m upon NPQ induction, equivalent to a much smaller NPQ_{max} of 3-4 vs NatL leaves (NPQ_{max} up to

10) (c.f. Fig. S1, Supplement; the numbers refer to the maximal NPQ values around 685 nm, see below). Both types of leaves showed a very rapid NPQ relaxation phase in the dark (time constant less than 2 minutes) which was not resolved in our measurements, followed by a much slower relaxation phase, which lasted ≤ 2 hours. At that time, the NPQ was fully relaxed.

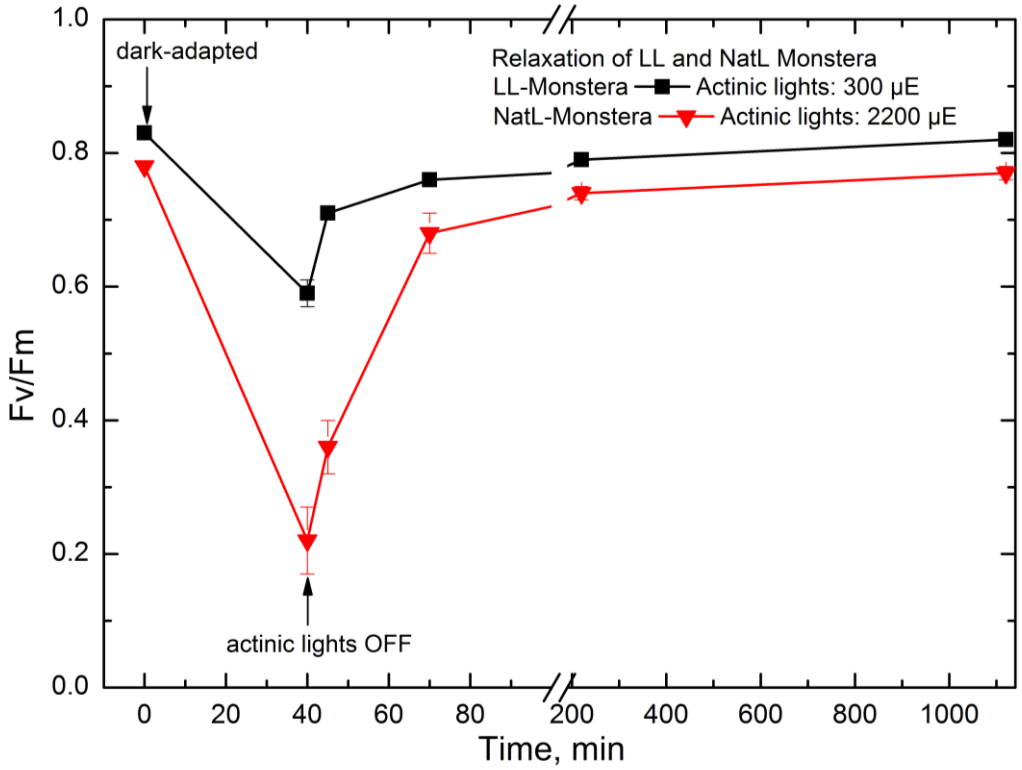

Fig. 1: Fv/Fm value in the dark, after NPQ induction in high light, and upon NPQ relaxation in the dark for LL and NatL grown Monstera leaves.

Fig. S1 (Supplement) shows the spectrally resolved NPQ induction kinetics (for details see [34,35]) for the two types of Monstera plants (LL and NatL grown resp.) using the same red actinic light intensity as applied for the other studies. The NPQ_{max} value is strongly wavelength dependent and differs largely in the two types of plan F_v/F_m values (Note that conventional instruments measure the average NPQ only above 720 nm, a range that is highly distorted by PSI fluorescence. Our instrument measures the wavelength resolved NPQ values across the whole emission range. The best range to characterize NPQ without serious distortions is at the maximum of PSII fluorescence, i.e. around 685 nm.)

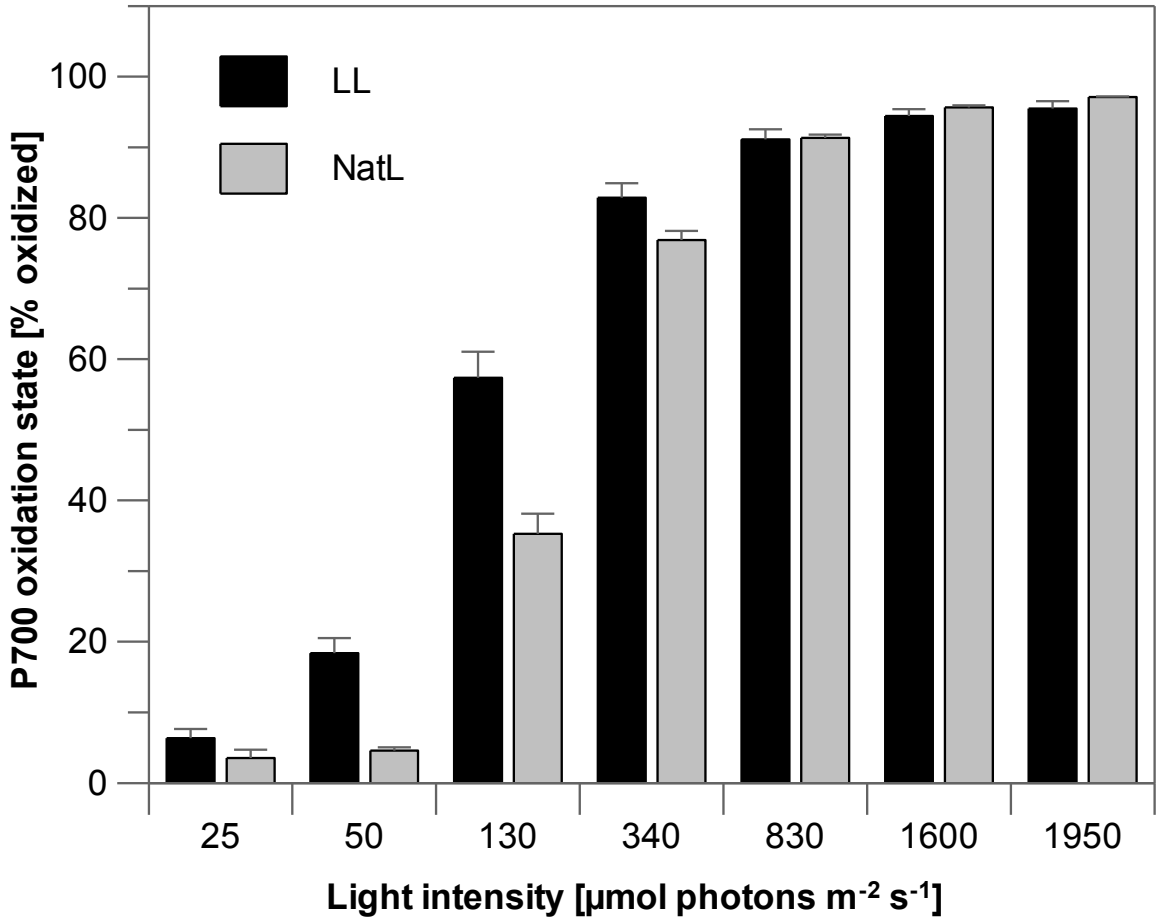

Fig. 2: P700 oxidation state for LL and NatL plants measured at different actinic light intensities.

The P700 oxidation state under light-adapted (NPQ) conditions is very important in the context of our photoprotection model in this study. It was determined for both types of plants as a function of actinic light intensity (Fig. 2). For LL plants the P700 oxidation states saturates at lower light intensities than for NatL plants. At ca. 800 µmol photons m^{-2} s^{-1} the oxidation states for both types of plants is saturated.

Xanthophyll cycle pigments were determined as a function of actinic illumination time. LL plants showed a much slower Zx formation and a smaller deepoxidation state (Fig. 3) as compared to NatL plants in agreement with earlier studies [11].

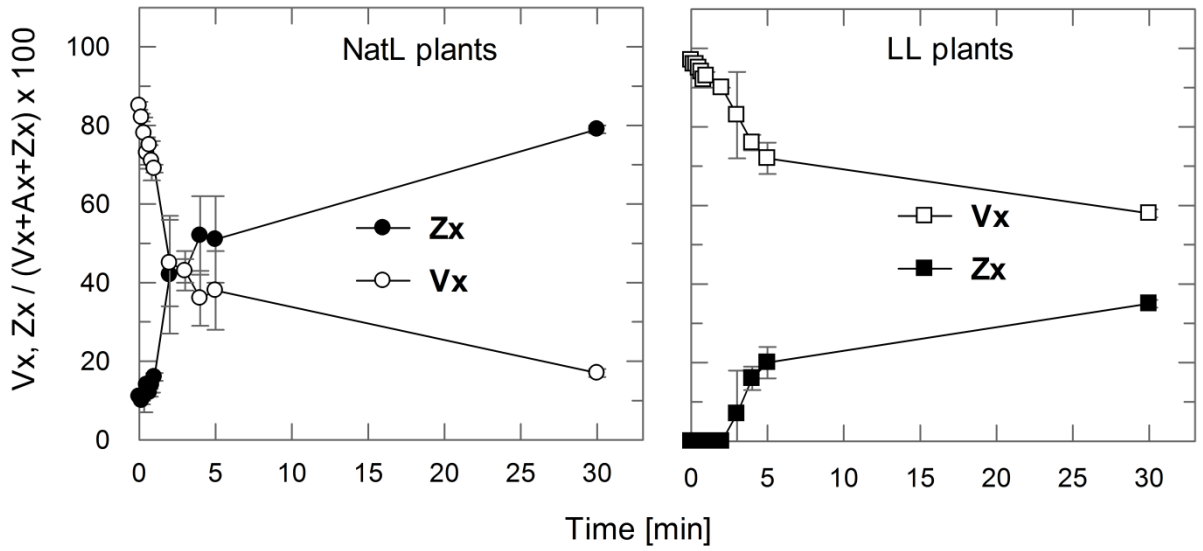

Fig. 3: Xanthophyll formation kinetics after switching on actinic NPQ light for Natl (left) and LL grown (right) plants.

Ultrafast lifetime measurements

Fluorescence lifetime measurements were carried out on leaves from LL plants for dark-adapted ($Fmax_{LL}$, PSII RCs closed) and quenched conditions under actinic light of 300 ($Fnpq_{LL}$) µmol photons m^{-2} s^{-1}. Natural high light-grown (NatL) plants were measured under dark-adapted ($Fmax_{NatL}$) and quenched conditions under actinic light of 2200 µmol photons m^{-2} s^{-1} ($Fnpq_{NatL}$). Fig. 4 shows typical fluorescence decays detected at 683 nm for these conditions.

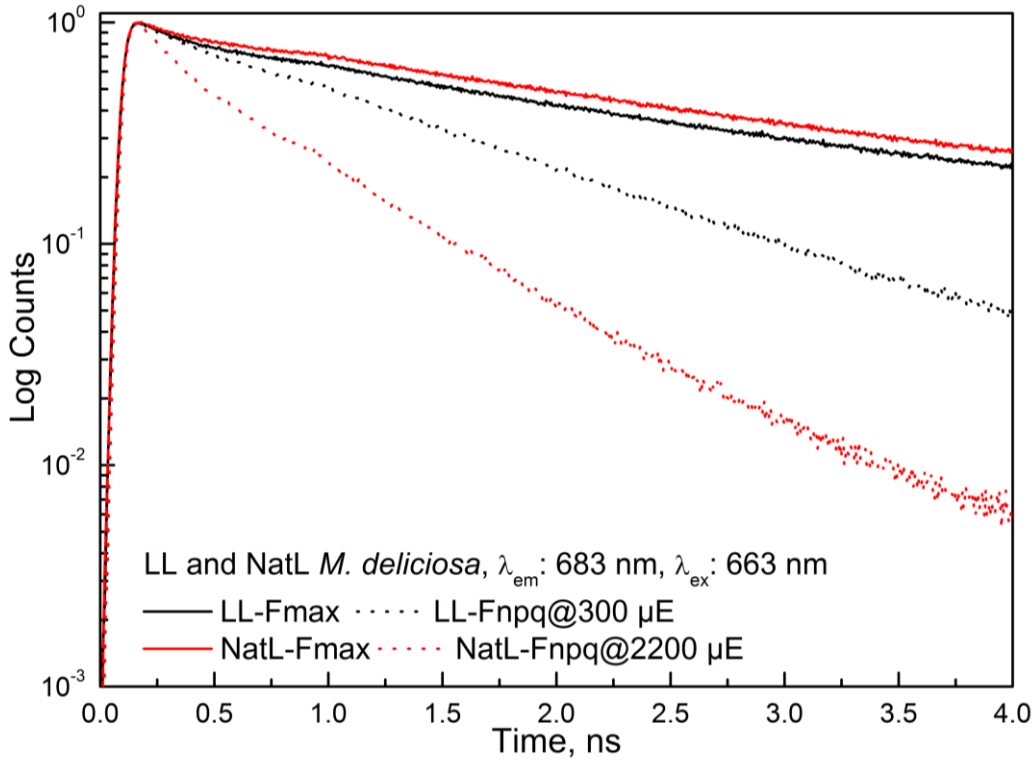

Fig. 4: Comparison of fluorescence decays (on a semi-logarithmic scale) of Monstera leaves from LL and NatL plants in unquenched (dark-adapted, F_{max}) and quenched conditions. λ_{exc} = 663 nm, λ_{det} = 683 nm

While the kinetics at F_{max} were similar for both types of leaves, albeit not identical, the kinetics in the quenched states differed strongly between LL and NatL plants. NatL plants were substantially more quenched as evidenced by the much shorter lifetimes, in agreement with the lower F_v/F_m values (Fig. 1) and the higher steady state NPQ values (Fig. S1). It is important to note that the pronounced differences in quenching between LL and NatL plants are not due to the different applied actinic light intensities used for LL versus NatL plants, since we had tested by steady state NPQ and Fv/Fm measurements (see above) that each set of plants had reached their saturating maximal reversible NPQ capacity at the respective value of actinic light employed. Note also that for LL plants the actinic light intensity applied for NPQ induction was actually 6-7 times the growth light intensity.

To gain detailed insight into the kinetics of quenching and to determine quenching locations and mechanisms, kinetic compartment analysis of the lifetime data was performed [17,19]. A very wide range of different kinetic models were initially tested on the data to determine whether they would be able to provide an optimal fit to the kinetics (the most important formal kinetic schemes that finally proved suitable for good fits are summarized in Fig. S2 and their characteristics are further discussed in the Supplement).

Initial analysis tested the same kinetic model successfully. The same kinetic scheme employed to describe dark-adapted and quenched kinetics for normal constant light grown Arabidopsis wild type and mutants leaves [19,39] was found to work successfully also for describing the kinetics of both dark-adapted and quenched LL grown Monstera plants. This kinetic scheme (both for quenched and unquenched conditions) for LL leaves involves a single homogeneous PSII pool, not involving any energy transfer from PSII to PSI (Fig. S2C). This model is thus consistent with a full lateral segregation of the two photosystems. The results of the kinetic analyses are shown as decay-associated fluorescence spectra (DAS) in Fig. 5.

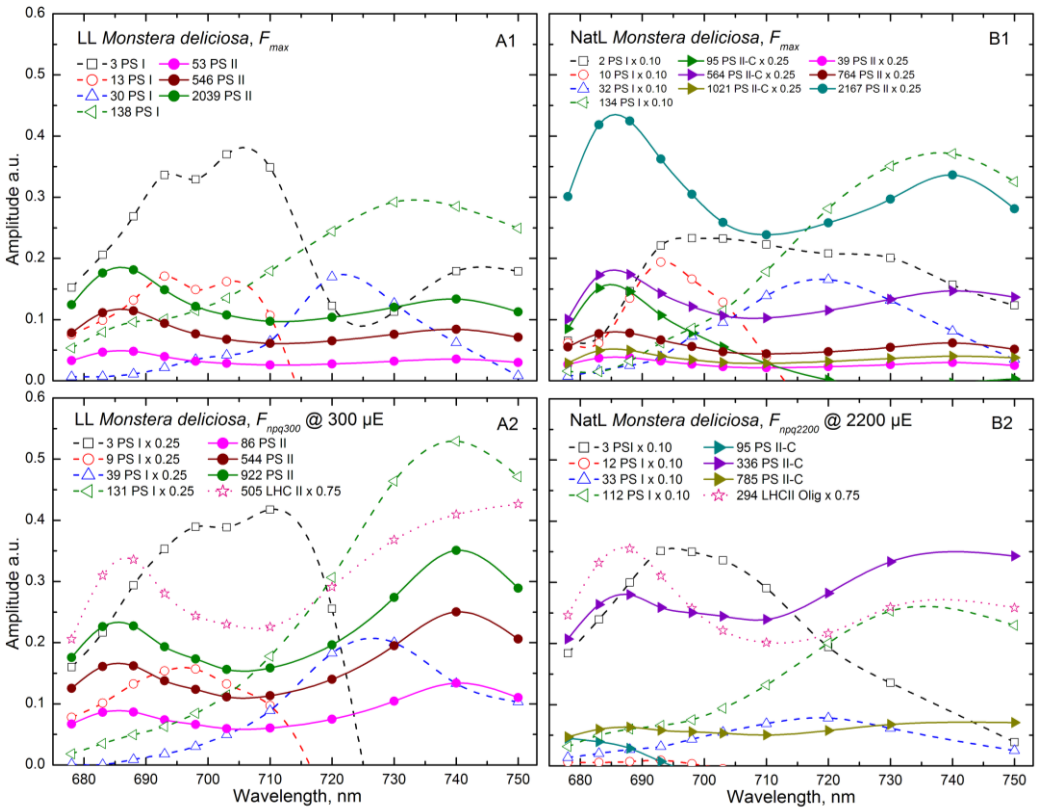

Fig. 5: Decay-associated spectra resulting from the kinetic compartment analysis of unquenched (A1, A2) and quenched (B1, B2) conditions of LL and NatL plants. The components labeled PSII belong to the unconnected (non-spillover) PSII, while those labeled PSII-c belong to the connected (spillover) PSII units. PSI components are shown dashed and the detached LHCII with a dotted line. For clarity of presentation only the positive amplitude parts are shown, which skips part of the PSI components.

These DAS plots also show the assignment of PSII and PSI kinetic components as provided by the kinetic compartment analysis. The resulting optimal rate constants for these models are given in Table 1. Derived parameters from the kinetic fits are provided in Tables 2 and 3.

Table 1: Rate constants (ns^{-1}) for the PSII and PSI kinetics in *Monstera deliciosa* leaves determined from the kinetic target analysis. For the meaning of the rate constants see Fig. S2. PSII-C: PSII fraction that is connected to the PSI-core via spillover energy transfer; k_t and k_{-t} are the forward and backward spillover rates from the PSII to the PSI core. The k_3 rate from the closed PSII units is fixed to 0.9 ns^{-1} [19]. The error limit in the rate constants are ±10%.

		PSII-C (connected)				**PSII unconnected**			**PSI**				
		k_D	k_{CS1}/k_{rec1}	k_1/k_2	k_t/k_{-t}	k_D	k_{CS1}/k_{rec1}	k_1/k_2	k_{r1}/k_{-r1}	k_{r2}/k_{-r2}	k_{CS}/k_{-CS}	k_4	**LHCII**
LL	Fmax	-	-	-	-	0.30	3.3/12	4.1/0.71	40/16	12/37	140/90	80	-
LL	$Fnpq_{300}$	-	-	-	-	1.8	1.6/8.2	2.1/0.72	80/19	21/110	119/62	134	2.4
NatL	Fmax	0.30	3.3/5.8	0.96/0.30	1.7/0.20	0.3	2.0/20	3.8/0.33	40/26	13/37	191/200	106	-
NatL	$Fnpq_{2200}$	1.03	2.2/6.1	1.9/0.9	1.8/0.31				38/52	15/62	170/30	70	3.40

Table 2: Average lifetime τ_{av} [ps] of the fluorescence decays for the *Monstera deliciosa* leaves grown under NatL and LL conditions were calculated from the kinetic data at 683 nm emission wavelength (excitation at 663 nm). The errors in the average lifetimes are ± 5 %; errors in the other values are ±10 %. NPQ values were calculated from the fluorescence decays at 683 nm according to the equation

$$NPQ = \frac{\tau av@Fmax}{\tau av@Fnpq} - 1$$

Also shown are the lifetimes [ps] of the component appearing under NPQ conditions assigned to functionally detached and quenched LHCII, along with the percentage of LHCII detachment as measured by the decrease in total PS II cross-section in the quenched vs. the unquenched state. PSII-C denotes the PSII fraction connected by spillover to PSI. For further meaning of the parameters refer to [19].

	LL	NatL
τ_{av} of PS II, ps		
F_{npq}	150	85
F_{max}	600	870
τ of quenched LHC II oligomers, ps	505	294
NPQ [a]	3.0	9.2
% of detached LHC II [b]	30	28

a) These numbers for the NPQ values derived from the lifetime measurements can be directly compared with those measured by conventional steady state NPQ induction. They fully agree within the error limits.

b) Measured as percentage of total absorption cross-section (at the excitation wavelength of 663 nm) of dark-adapted PSII that is detached as quenched LHCII

Table 3: Excitation vectors for the various antenna compartments resulting from kinetic compartment analysis for the time-resolved kinetic data of *Monstera deliciosa* leaves from plants grown under LL and NatL conditions. The suffix 'C' denotes the PS II units connected through energy-spillover with PSI. The errors are in the range of ±10 %.

	PSII-Ant/RC-C	**PSII-Ant/RC**	**PSI-Ant/RC**	**LHCII**
LL Fmax	-	0.80	1.0	-
LL $Fnpq_{300}$	-	0.65	1.0	0.25
NatL Fmax	0.40	0.60	1.0	-
NatL $Fnpq_{2200}$	0.30	-	1.0	0.20

For unquenched NatL plants the homogeneous PSII model fitting the kinetics of LL plants well was entirely unsuitable to satisfactorily describe the kinetics neither without (model S2 A) nor with (model S2 B) energy transfer ("spillover") from PSII to PSI. The unsatisfactory character of the homogeneously separated compartment PSII model (Fig. S2 C) for describing the kinetics in NatL leaves is demonstrated, for example, by the collection of residual plots of the kinetics shown in Fig. S3, which show large systematic deviations between the experimental and the model kinetics. We therefore tested the more complex kinetic models (Fig. S2 A and B). It turned out, that only a heterogeneous PSII pool model (model S2 A), with a fraction of about 60 % of PSII units in a separate ("non-spillover PSII") arrangement, and the remaining PSII fraction (denoted as PSII-C for "connected") requiring energy transfer ("spillover") to PSI was necessary for a good fit of the dark-adapted NatL plants. However, for fitting $Fnpq_{NatL}$, quenching kinetics of NatL plants, a homogeneous PSII pool, but requiring spillover from all PSII units to PSI (model S2 B), was required and sufficient for a good fit.

A common feature of both LL and NatL grown plants is that the quenched states revealed a pronounced increase in the rate constant of antenna deactivation k_D up to about 1.5 ns^{-1} (versus 0.3 ns^{-1} in the dark-adapted state, Table 1). This increase reflects the activation of the xanthophyll (Zx) dependent quenching [19,39,42]. Furthermore, a kinetic component was observed that reflects PsbS-dependent detachment of LHCII from the PSII super-complex [19,39] under NPQ conditions (indicated in the DAS plot as "LHCII detached"). The percentages of LHCII detachment (relative to total PSII absorption cross-sections) were in the range of 30-50 % (Table 1) and thus in line with previously observed detachment percentages in Arabidopsis leaves [19].

Table 2 further provides excitation probabilities (relative absorption cross-sections) of the various model compartments resulting from kinetic analysis. They represent a fairly good estimate of the (relative) total antenna sizes of PSII and PSI in the thylakoids. The data indicate a pronounced increase in the ratio of PSII to PSI absorption cross-sections in NatL vs. LL plants from a ratio of 0.75 to about 1.0, respectively. The PSI kinetic components and time-resolved spectra under all conditions (Fig. 5) behaved as is typical for higher plants, both in terms of kinetics as well as with respect to their spectra, i.e. they appear to be very similar to those observed previously in isolated intact PSI complexes [45] and in Arabidopsis leaves [19,39]. The PSII emission spectra both in the unquenched and in the quenched cases showed a substantially higher ratio of the far-red/red band intensities than the unquenched PSII

spectra. This is due to the high optical density of the Monstera leaves, which leads to large self-absorption in the wavelength range up to about 690 nm.

Discussion

In both, LL and NatL plants, the two previously described quenching mechanisms [19,23,39] are found to be operative upon high light adaptation. These two mechanisms are i) PsbS-dependent detachment of parts of the LHCII antenna of the PSII super-complex (Q1-type or qE quenching) and ii) zeaxanthin-associated quenching of the PSII antenna caused by increased rate constant of thermal dissipation in the antenna, k_D (Q2-type or qZ quenching). The fluorescence kinetics and quenching mechanisms of LL plants of Monstera thus were essentially the same as reported for wild-type Arabidopsis plants grown in constant light of 150 µmol photons m^{-2} s^{-1} [19]. Overall these NPQ effect for both LL and NatL plants a fully in line with a general NPQ model (4-state-2-site model) resulting from a wide range of NPQ studies on Arabidopsis w.t. and mutant plants as reviewed recently [18].

A novel NPQ mechanism

NatL plants exhibited an overall much higher capacity for quenching than LL plants, as already indicated by the steady state NPQ data (Figs. 1) and the much shorter fluorescence decay in time-resolved experiments (Fig. 4). They are fully consistent with previous studies using conventional NPQ measurements [11]. This increased quenching capacity of NatL plants is not explained by the above-mentioned two "classical" NPQ mechanisms, which show very characteristic features and changes in rate constants and kinetic components in the lifetime measurements. Taken as such, these two mechanisms (derived from simulations using the rate constants and other parameters given in Tables 1-3) would only be able to explain a maximal NPQ in the range of about 3-4 [19]. The drastically higher NPQ capacity observed for NatL plants is thus clearly related to the activation of a so far unknown NPQ mechanism, which is based on energy-spillover (i.e. energy transfer from PSII to PSI) and we thus propose to call this new mechanism "spillover quenching" (q_{SO}). This novel mechanism is the dominant quenching mechanism that drastically enhances maximal quenching in NatL plants vs. LL plants to a range of NPQ_{max} ca. 10 from NPQ_{max} 3-4, respectively, i.e. an increase by a factor of 3 (Note that this reflects a very strong increase in NPQ, since the NPQ scale is not linear). For NatL Monstera plants q_{SO} operates in addition and parallel to the previously described qE and qZ quenching mechanisms (Fig. 5, Fig. S2 B, and Table 1) while LL plants lack q_{SO} quenching (Fig. 5 and Fig. S2 C).

It is important to note that spillover, in a similar manner as direct antenna quenching by an increase in rate k_D (qZ quenching) [19], drains away excitation energy from PSII. Using the

detailed kinetic data provided in Table 1 it can be calculated that in a situation without spillover under NPQ conditions in NatL plants the PSII centers would still convert 19 % of the energy absorbed in PSII to radical pairs, which, under these conditions, would be largely converted to radical pair triplets and reactive oxygen species [34]. With the newly discovered spillover mechanism this percentage is however reduced to 9 %, i.e. a lowering of damaging species production by more than a factor of 2. Like the other two already known "classical" quenching mechanisms, q_{SO} is thus also highly effective in protecting PSII from potential damage under high light. Thus at 2200 µmol photons m^{-2} s^{-1}actinic light, q_{SO} contributes more than 50 % to the total quenching, and thus also a similar amount of total photoprotection of PSII. In this case, the expected Chl triplet yield in PSII (which is a measure for the damage potential under high light) was expected to be reduced to 4 %, from a non-quenched value of 25 % [34]. This underlines the very high and in fact dominant photoprotective capacity of q_{SO} in NatL grown plants.

The photochemical mechanism of spillover quenching

How can the underlying photochemistry of spillover quenching be understood? Efficient q_{SO} quenching requires a tight coupling of the antenna of PSII and PSI. Such a coupling gives rise to fast, preferentially downhill energy transfer from PSII to PSI with a rate k_t, that is nearly non-reversible due to (i) the low-energy antenna of PSI and (ii) the fast utilization of energy in PSI [51]. This drains away energy from PSII and thus acts as a PSII photoprotection mechanism (see above). This kind of efficient energy transfer from PSII to PSI is however only possible if the two photosystems are located next to each other in the same membrane. Spillover in a large percentage of PSII centers (in our case 100 % of the PSII centers are in this situation) is thus entirely incompatible with a lateral segregation model of the membrane.

At low light intensities, P700 is mostly in the reduced state (Fig. 2), and in that case, spillover would actually feed energy from PSII to PSI (Fig. S2). Thus, despite providing photoprotection to PSII, the energy drained from PSII by the q_{SO} mechanism is not lost as heat but could drive PSI. It can thus serve as a regulation mechanism that distributes the excitation energy between PSII and PSI as long as P700 is reduced. The small spillover effect present already in dark-adapted NatL grown Monstera is actually responsible for the lowered Fv/Fm value of NatL plants vs. LL plants (Fig. 1). However, at high actinic light intensities, the PSI-RC (reaction center) is mostly in the oxidized form of $P700^+$, as is typical for NPQ induced by high excess light. This is due to two effects: i) quenched PSII does not feed enough reducing equivalents to PSI via the electron transfer chain [33], and ii) the spillover further increases excitation pressure on PSI. This is confirmed by our measurements of the

P700 oxidation level in the quenched state (Fig. 2) showing a very high P700 oxidation state in NatL plants at moderate to high excitation intensities. In the $P700^+$ state, the PSI-RC is known to be a very efficient quencher, rapidly deactivating excited state energy into heat [50]. Thus q_{SO} quenching is, in essence, in most cases indirect non-photochemical quenching of PSII via oxidized PSI. q_{SO} quenching operating in NatL-grown plants in fact has a Janus face character. In the close interaction, "spillover" arrangement of PSII and PSI units, the controlled interplay between spillover and actual quenching in PSI under different light conditions thus provides important opportunities for balancing energy between PSII and PSI on the one hand (at lower light intensities), and for drastically increasing the efficiency of NPQ on the other hand (at high actinic light intensities).

Implications for thylakoid structural reorganization

The discovery of spillover complexes of PSII in higher plants has far-reaching implications with respect to thylakoid organization and high light-induced structural reorganizations of the photosynthetic membrane. Spillover-rates from PSII to PSI reach up to 1.8 ns^{-1} in NatL plants, which is actually very high, since this rate is comparable to the effective rate of trapping and charge separation in the PSII-RC (c.f. Table S1) [20,40,46]. Such a high-energy spillover rate between the large PSII-associated and PSI-associated antenna units is only possible over very short distances of their respective peripheral antenna chromophores, which must be in the distance range < 1 nm. Thus, the occurrence of spillover actually demands that PSII and PSI antenna units must be in direct contact with each other in the thylakoid membrane, a situation inconsistent with the prevailing lateral segregation model of the two photosystems [4]. Since NatL plants already show an about 40 % fraction of PSII units involved in spillover in the dark-adapted state, our data in fact demand that unquenched NatL plants of Monstera have a thylakoid organization where a large fraction (about 40 %) of PSII complexes is in direct contact in the same membrane with PSI complexes. This fraction of PSII involved in spillover (PSII-C in Fig. S2) increases to 100 % upon high light exposure leading to NPQ induction. Our findings thus imply that in NatL plants, a substantial light-induced reorganization of the thylakoid membrane must occur upon transition from the dark-adapted unquenched state to the quenched state. The observed fluorescence kinetics in the NPQ state of NatL plants can only be explained if all PSII units are in direct close contact with a PSI complex in the same membrane under high actinic light. This means that lateral segregation of PSII and PSI must be completely abolished under thermal dissipation (NPQ) conditions in NatL plants. Lateral segregation into PSII containing grana stacks and PSI

containing stroma-exposed unstacked thylakoid regions is brought about by grana membrane stacking forces (see below more details). Grana stacking does not allow PSI to move into the stacking region and mix with PSII due to its large extra-membraneous protein extrusion part. Likewise, mixing of PSII with PSI in the same membrane region can only occur if grana stacking is substantially loosened up, i.e. if intermembrane distances in the grana increase sufficiently.

Our findings on the spillover quenching effects in NatL grown plants, and the lack of such effects in LL grown plants, are in full agreement with the results of recent thylakoid structural analysis by electron microscopy on Monstera plants grown under the same conditions [12]. The EM analysis of dark-adapted LL-leaves revealed tall stacks of up to over 100 firmly appressed thylakoids as previously described for LL-grown evergreens from the family (Araceae) [8] to which Monstera belongs, and much less tall stacks (ranging between about 20 to 30 discs) for NatL-plants. LL-thylakoids remained largely appressed upon exposure to actinic high light. In contrast, high light exposure of NatL leaves induced a substantial change in thylakoid organization. The previously tightly appressed thylakoids largely widened their intermembrane separation under NPQ irradiation to an extent that PSI migration into the previously tight grana stacks appears possible.

The homogenous PSII pool, not connected to PSI in both dark- and light-acclimated states of LL- plants indicated by the fluorescence lifetime analysis, is consistent with the tight stacking of the large grana regions (and thus complete lateral segregation of the two photosystems) in both states [12]. In NatL-plants which showed much smaller grana stacks, however, about 40 % of PSII units were already found involved in spillover even in the dark-adapted state. This fraction increased to 100 % in the light-acclimated state. This result implies that unquenched NatL-leaves of Monstera have a thylakoid organization with a substantial fraction of PSII complexes in direct neighborhood to, and in energy-transfer contact with, PSI complexes. This finding is consistent with the much less pronounced and looser grana stacking in NatL- versus LL-plants, which is further reduced strongly upon short-term acclimation to high light. Thus, the reduced stacking in light adapted NatL thylakoids (Table 3) supports the increase of the fraction of PSII involved in spillover to 100 % upon NPQ induction in NatL-plants. While LL and NatL plants already show pronounced differences in the thylakoid grana stacking, a rapid light-induced reorganization of the thylakoid membrane takes place in NatL-plants upon transition from the dark-adapted, unquenched state, to the quenched state. LL grown plants apparently lack the potential for such a light-induced grana stacking modification. The reasons for this difference are unclear.

Recent data however indicate that grana stacks and the ability for thylakoid reorganization may be controlled by such factors as the level of thylakoid protein phosphorylation, and possibly the levels of Zx and PsbS in the membrane [4,6,29,30,47,49].

The prevailing notion is that lateral segregation of PSII and PSI units into different parts of the thylakoid membrane is a direct consequence of membrane stacking in the appressed (grana) regions of the thylakoids – caused by complex interactions between surface charges of protein complexes such as LHCII [5]. PSI is forced out of the stacked membrane regions due to both surface charge interaction and its large extra-membraneous stroma-exposed parts [7,9]. This implies that membrane appression and lateral segregation of the two photosystems reflect in fact just the two opposite sides of the same coin. We are thus led to conclude that in the dark adapted state of NatL plants the degree of membrane stacking must already be substantially reduced compared to LL plants. This could happen for example by partial unfolding of grana margins. The further conclusion from our data under this assumption is, that functional membrane stacking, leading to separation of PSII and PSI, is essentially abolished in the quenched state of NatL plants. The PSII super-complexes cannot be located in grana and at the same time be located directly next to a PSI complex. This situation is described by the schemes of thylakoid architecture in different states shown in Fig. 6. In this context it is of note that Rozak et al. [44] already reported pronounced and rapid reversible alterations in thylakoid appression of spinach upon changes in high light intensity using electron microscopy, albeit with relatively low resolution, but similar in their effects to Monstera leaves under different irradiation conditions [12].

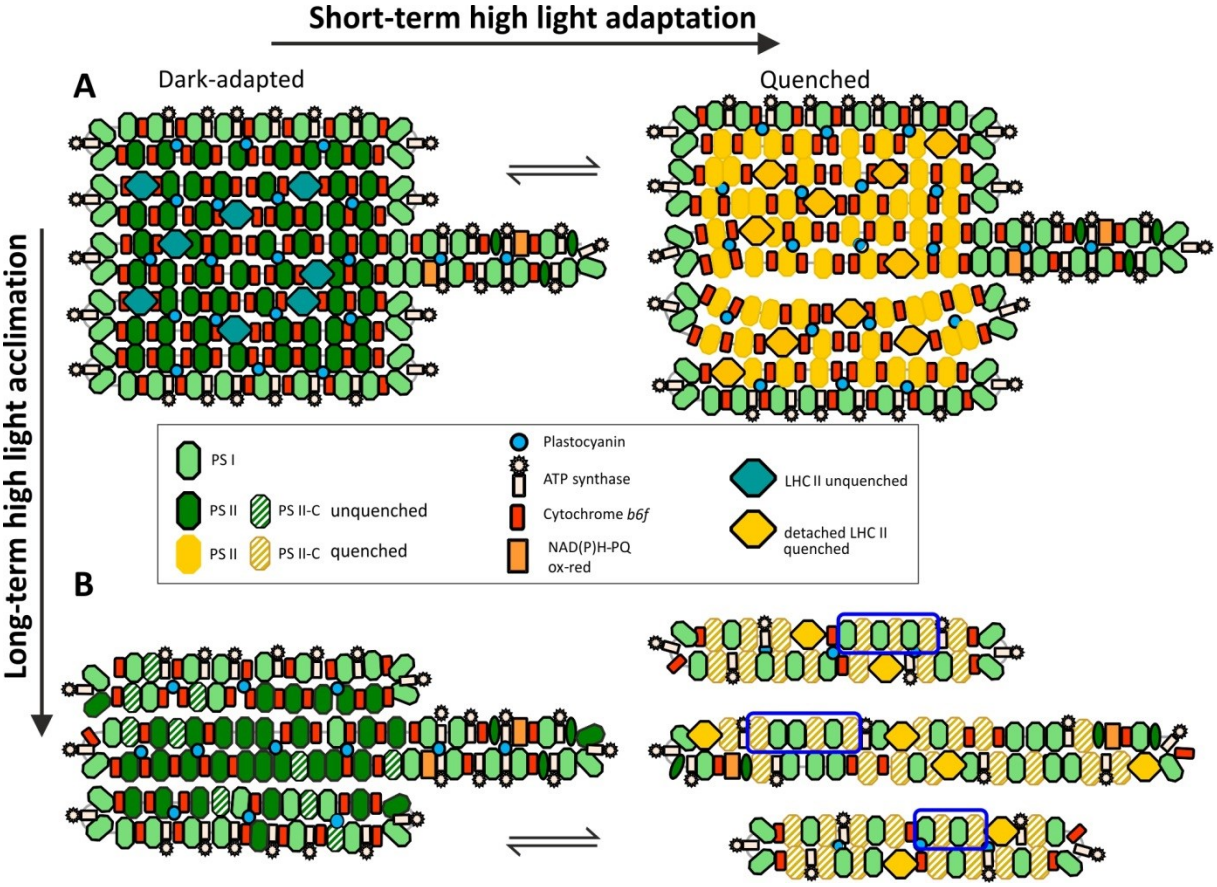

Fig. 6: Cartoons showing thylakoid structural arrangements of LL plants (A, top) and NatL plants (B, bottom) in their dark-adapted unquenched (left) and the high-light adapted quenched states (right). In LL plants which have a pronounced grana stacking in the dark-adapted state, no grana unstacking occurs in the quenched state and PSII and PSI units are strictly separated. NatL plants show smaller grana stacks with partially unstacked thylakoids and thus partially mixed PSII and PSI units already in the dark-adapted state. In the quenched state further unstacking occurs, leading to a complete mixing of PSII and PSI units in the same membrane region in high light. Three of the high efficiency Q_{SO} quenching units formed under these conditions in NatL plants are highlighted by the blue boxes in B (right). Note that these thylakoid cartoon models are not meant to show exact details of the structural (re)arrangement of thylakoid membrane components. They summarize and combine however the functional data in this work and the results of a recent electron microscopy study on thylakoid structure on Monstera plants grown under the same conditions [12]. The cartoons highlight the striking functional changes occurring upon short-term and long-term adaptation to different light conditions which drastically influence the functional organization, as evidenced by the kinetic data. The basic thylakoid protein distribution shown (dark-adapted LL plants, A) is based on the PSA organization of dark-adapted LL Arabidopsis [9] since our time-resolved data lead to the same conclusions for Arabidopsis [19] and LL grown Monstera. The blue-green diamonds in the dark-adapted structures represent the quasi-crystalline arrays of LHCII that have been found in the thylakoid structure of Arabidopsis, while the yellow diamonds in the quenched structures represent the detached and quenched LHCII complexes [19]. This scheme shows only the four extreme situations of the thylakoid architecture suggested by our data. Intermediate architectures will exist both for long-term as well as for short-term adaptation.

We should note that time-resolved fluorescence measurements, as the basis of our conclusions, are not capable to provide detailed structural information. Rather, they provide – in addition to the characterization of the internal processes of energy transfer, charge separation, and quenching, important functional information about the relative orientation and interaction of the two photosystems. This selective nature of the information provided by this method is crucial in the present context. Thus, our data are able to unravel important and

highly selective information on the structural organization of the thylakoid membranes in which these photosynthetic complexes are imbedded. In addition to its ability to distinguish clearly between a spillover situation and other types of quenching, which is not possible with any other method to the best of our knowledge, this non-invasive method works equally well in the photosynthetically active "energized state" of the membrane as well as in the dark-adapted state. This method thus gives crucial information about the functional, as well as structural, organization of the photosystems in the membrane and of any related changes in this organization to external effects like e.g. light stress.

LL-plants lack the ability for structural reorganization

Our results indicate that LL-leaves of Monstera lack the ability for rapid thylakoid reorganization and thus develop no q_{SO}. LL-leaves thus achieve only a maximal NPQ capacity of 2.5-3, which is in the range observed for laboratory-grown wild type Arabidopsis and other annual higher plants that develop in high light [15,37]. One may thus ask the question what is the reason for this lack of thylakoid reorganization of LL plants in contrast to NatL plants. Do higher levels of PsbS or zeaxanthin [11] promote thylakoid reorganization in NatL-plants and thus enable or enhance the q_{SO} quenching mechanism? The L17 mutant of Arabidopsis is a PsbS overexpressor and shows enhanced NPQ (of the qE or Q1-type [19]), with a higher total NPQ capacity than wild type [37]. Despite the higher PsbS level and a corresponding higher level of LHCII detachment from PSII, this mutant did not exhibit the quenching shown here to be associated with rapid thylakoid structural reorganization in NatL-leaves of Monstera [19]. PsbS alone is thus unlikely to be the major factor providing thylakoid structural plasticity under NatL conditions. Likewise, also analysis of the zeaxanthin enriched Arabidopsis *npq2* mutant did not reveal any indications for activation of q_{SO} quenching [19]. Thus, neither increased PsbS nor zeaxanthin levels alone are able to promote thylakoid membrane reorganization required for spillover-based quenching, although it cannot be excluded that PsbS and Zx together may support membrane reorganization in NatL-plants [12]. However, the more rapid and more efficient conversion of violaxanthin to zeaxanthin in NatL leaves (Fig. 3) support the view that a generally altered organization of the thylakoid membrane in NatL leaves [28,30,52] facilitates the release and diffusion of violaxanthin in the lipid phase of the thylakoid membrane, which are supposed to be the rate-limiting steps in zeaxanthin formation [24].

Conclusions

The observation of spillover quenching as a novel and highly efficient photoprotective thermal dissipation of excess energy (NPQ) mechanism in higher plants challenges the present concepts on both NPQ as well as on functional thylakoid architecture in several ways. With respect to NPQ, it suggests that our understanding of NPQ mechanisms and function has to be broadened. Our findings imply that thermal dissipation (NPQ) can no longer be considered to be merely a local phenomenon centered in the PSII antenna alone. Rather, NPQ should be considered as a property determined and affected by overall thylakoid architecture. As a thylakoid-wide regulation mechanism, it must synchronize well with other regulatory mechanisms both, at the functional and the structural level, to ensure efficient functioning of the photosynthetic apparatus and optimal photoprotection. With respect to thylakoid architecture, the observation of spillover quenching challenges the concept of lateral heterogeneity of the photosystems as a general structural and operational principle. Apparently, growth light environments and other factors exist, under which it is advantageous for the photosynthetic apparatus to give up lateral segregation of the photosystems and the associated division into appressed grana and interconnecting stroma thylakoid and to mix PSII and PSI in the same membrane region. It is thus an interesting challenge to understand the external influences and internal regulation mechanisms that determine and control the thylakoid structures of higher plants to find their balance between the extremes of strict lateral segregation of photosystems and their complete mixing in the same membrane region. Recent data clearly indicate that low light conditions favor extended grana stacking [25]. Our results emphasize the notion of a highly dynamic nature of thylakoid structure (see e.g. [6] for a recent discussion), rather than the presently prevailing more static picture of thylakoid organization [30,52]. The extreme lateral segregation model might represent an organization optimal primarily under light limiting conditions [25]. It is important to note that the presently available direct structural information from electron microscopy studies is limited to the non-energized state of the thylakoids (i.e. the dark-adapted state). Direct structural information on thylakoid architecture in the energized state in high light is essentially lacking so far. Non-invasive indirect methods that are, however, highly sensitive to the functional organization of the photosystems, as for example *in vivo* ultrafast fluorescence spectroscopy as applied here, thus provide important insights in the interplay between the functional and the structural organization of the photosynthetic apparatus. Our results emphasize the demand for future electron microscopy studies of thylakoid architecture in the energized state and in response to both long-term and short-term light adaptation processes.

Acknowledgements

This work was supported by grants to ARH (Deutsche Forschungsgemeinschaft DFG grant HO-924/3-1 and the EU Training and Research Network "Harvest") and to PJ (Deutsche Forschungsgemeinschaft DFG grant JA 665/9-1).

Reference List

1. J.F. Allen, State transitions--a question of balance, Science 299 (2003) pp. 1530-1532.

2. P. Alter, A. Dreissen, F.L. Luo, and S. Matsubara, Acclimatory responses of Arabidopsis to fluctuating light environment: comparison of different sunfleck regimes and accessions, Photosynth. Res. 113 (2012) pp. 221-237.

3. J.M. Anderson, Photoregulation of the composition, function, and structure of thylakoid membranes, Ann. Rev. Plant Physiol. 37 (1986) pp. 93-136.

4. J.M. Anderson, Lateral heterogeneity of plant thylakoid protein complexes: early reminiscences, Philos. Trans. R. Soc. Lond B Biol. Sci. 367 (2012) pp. 3384-3388.

5. J.M. Anderson, W.S. Chow, and J. De Las Rivas, Dynamic flexibility in the structure and function of photosystem II in higher plant thylakoid membranes: the grana enigma, Photosynth Res. 98 (2008) pp. 575-587.

6. J.M. Anderson, P. Horton, E.H. Kim, and W.S. Chow, Towards elucidation of dynamic structural changes of plant thylakoid architecture, Philos. Trans. R. Soc. Lond B Biol. Sci. 367 (2012) pp. 3515-3524.

7. B. Andersson and J.M. Anderson, Lateral heterogeneity in the distribution of chlorophyll-protein complexes of the thylakoid membranes of spinach chloroplasts, Biochim. Biophys. Acta 593 (1980) pp. 427-440.

8. W.S. Chow, E.H. Kim, P. Horton, and J.M. Anderson, Granal stacking of thylakoid membranes in higher plant chloroplasts: the physicochemical forces at work and the functional consequences that ensue, Photochem. Photobiol. Sci. 4 (2005) pp. 1081-1090.

9. J.P. Dekker and E.J. Boekema, Supramolecular organization of thylakoid membrane proteins in green plants, Biochim. Biophys. Acta 1706 (2005) pp. 12-39.

10. B. Demmig-Adams, C.M. Cohu, O. Muller, and W.W. Adams, III, Modulation of photosynthetic energy conversion efficiency in nature: from seconds to seasons, Photosynth. Res. 113 (2012) pp. 75-88.

11. B. Demmig-Adams, V. Ebbert, D.L. Mellman, K.E. Mueh, L. Schaffer, C. Funk, C.R. Zarter, I. Adamska, S. Jansson, and W.W. Adams, Modulation of PsbS and

flexible vs sustained energy dissipation by light environment in different species, Physiologia Plantarum 127 (2006) pp. 670-680.

12. B. Demmig-Adams, O. Muller, J.J. Stewart, C.M. Cohu, and W.W.I. Adams, Chloroplast thylakoid structure in evergreen leaves employing strong thermal energy dissipation, J. Photochem. Photobiol. B: Biology in press (2015).

13. B. Demmig-Adams, K. Winter, A. Krüger, and F.-C. Czygan, Photoinhibition and zeaxanthin formation in intact leaves. A possible role of the xanthophyll cycle in the dissipation of excess light energy, Plant Physiol. 84 (1987) pp. 218-224.

14. A. Färber, A.J. Young, A.V. Ruban, P. Horton, and P. Jahns, Dynamics of xanthophyll-cycle activity in different antenna subcomplexes in the photosynthetic membranes of higher plants, Plant Physiol. 115 (1997) pp. 1609-1618.

15. T. Golan, X.-P. Li, P. Müller-Moulé, and K.K. Niyogi, Using Mutants to Understand Light Stress Acclimation in Plants, in: G.C. Papageorgiou and Govindjee (Eds.), Chlorophyll a Fluorescence: A Signature of Photosynthesis, Advances in Photosynthesis and Respiration Vol.19, Springer, Dordrecht, 2004, pp. 525-554.

16. M. Herbstová, S. Tietz, C. Kinzel, M.V. Turkina, and H. Kirchhoff, Architectural switch in plant photosynthetic membranes induced by light stress, Proc. Natl. Acad. Sci. U. S. A 109 (2012) pp. 20130-20135.

17. A.R. Holzwarth, Data Analysis of Time-Resolved Measurements, in: J. Amesz and A.J. Hoff (Eds.), Biophysical Techniques in Photosynthesis. Advances in Photosynthesis Research, Kluwer Academic Publishers, Dordrecht, 1996, pp. 75-92.

18. A.R. Holzwarth and P. Jahns, Non-Photochemical Quenching Mechanisms in Intact Organisms As Derived From Ultrafast-Fluorescence Kinetic Studies, in: B. Demmig-Adams, G. Garab, W.W.I. Adams, and Govindjee (Eds.), Non-Photochemical Quenching and Thermal Energy Dissipation In Plants, Algae and Cyanobacteria, vol. 40, Advances in Photosynthesis and Respiration, Springer, Dordrecht, 2014, pp. 129-156.

19. A.R. Holzwarth, Y. Miloslavina, M. Nilkens, and P. Jahns, Identification of two quenching sites active in the regulation of photosynthetic light-harvesting studied by time-resolved fluorescence, Chem. Phys. Lett. 483 (2009) pp. 262-267.

20. A.R. Holzwarth, M.G. Müller, M. Reus, M. Nowaczyk, J. Sander, and M. Rögner, Kinetics and mechanism of electron transfer in intact photosystem II and in the isolated reaction center: Pheophytin is the primary electron acceptor, Proc. Natl. Acad. Sci. USA 103 (2006) pp. 6895-6900.

21. P. Horton, Optimization of light harvesting and photoprotection: molecular mechanisms and physiological consequences, Philos. Trans. R. Soc. Lond B Biol. Sci. 367 (2012) pp. 3455-3465.

22. P. Horton, M. Wentworth, and A.V. Ruban, Control of the light harvesting function of chloroplast membranes: The LHCII-aggregation model for non-photochemical quenching, FEBS Lett. 579 (2005) pp. 4201-4206.

23. P. Jahns and A.R. Holzwarth, The role of the xanthophyll cycle and of lutein in photoprotection of photosystem II, Biochim. Biophys. Acta, Bioenerg. 1817 (2012) pp. 182-193.

24. P. Jahns, D. Latowski, and K. Strzalka, Mechanism and regulation of the violaxanthin cycle: the role of antenna proteins and membrane lipids, Biochim. Biophys. Acta 1787 (2009) pp. 3-14.

25. H. Jia, J.R. Liggins, and W.S. Chow, Acclimation of leaves to low light produces large grana: the origin of the predominant attractive force at work, Philos. Trans. R. Soc. Lond B Biol. Sci. 367 (2012) pp. 3494-3502.

26. M.P. Johnson, T.K. Goral, C.D. Duffy, A.P. Brain, C.W. Mullineaux, and A.V. Ruban, Photoprotective energy dissipation involves the reorganization of Photosystem II light-harvesting complexes in the grana membranes of spinach chloroplasts, Plant Cell 23 (2011) pp. 1468-1479.

27. M. Khatoon, K. Inagawa, P. Pospisil, A. Yamashita, M. Yoshioka, B. Lundin, J. Horie, N. Morita, A. Jajoo, Y. Yamamoto, and Y. Yamamoto, Quality control of photosystem II: Thylakoid unstacking is necessary to avoid further damage to the D1 protein and to facilitate D1 degradation under light stress in spinach thylakoids, J. Biol. Chem. 284 (2009) pp. 25343-25352.

28. H. Kirchhoff, Architectural switches in plant thylakoid membranes, Photosynth. Res. (2013).

29. H. Kirchhoff, Diffusion of Molecules and Macromolecules in Thylakoid Membranes, 2014, pp. 495-502.

30. H. Kirchhoff, Structural changes of the thylakoid membrane network induced by high light stress in plant chloroplasts, Philos. Trans. R. Soc Lond B Biol Sci 369 (2014) p. 20130225.

31. H. Kirchhoff, C. Hall, M. Wood, M. Herbstová, O. Tsabari, R. Nevo, D. Charuvi, E. Shimoni, and Z. Reich, Dynamic control of protein diffusion within the granal thylakoid lumen, Proc. Natl. Acad. Sci. USA 108 (2011) pp. 20248-20253.

32. C. Klughammer and U. Schreiber, An improved method, using saturating light-pulses, for the determination of photosystem I quantum yield iia P700+-absorbency changes at 830 nm, Planta 192 (1994) pp. 261-268.

33. D.M. Kramer, The photonic"smart grid" of the chloroplast in action, Proc. Natl. Acad. Sci. USA 107 (2010) pp. 2729-2730.

34. P.H. Lambrev, Y. Miloslavina, P. Jahns, and A.R. Holzwarth, On the relationship between non-photochemical quenching and photoprotection of photosystem II, Biochim. Biophys. Acta, Bioenerg. 1817 (2012) pp. 760-769.

35. P.H. Lambrev, M. Nilkens, Y. Miloslavina, P. Jahns, and A.R. Holzwarth, Kinetic and spectral resolution of multiple nonphotochemical quenching components in *Arabidopsis* leaves, Plant Physiol. 152 (2010) pp. 1611-1624.

36. T.-Y. Leong and J.M. Anderson, Light-quality and irradiance adaption of the composition and function of pea-thylakoid membranes, Biochim. Biophys. Acta 850 (1986) pp. 57-63.

37. X.-P. Li, P. Müller-Moulé, A.M. Gilmore, and K.K. Niyogi, PsbS-dependent enhancement of feedback de-excitation protects photosystem II from photoinhibition, Proc. Natl. Acad. Sci. USA 99 (2002) pp. 15222-15227.

38. Z. Li, S. Wakao, B.B. Fischer, and K.K. Niyogi, Sensing and responding to excess light, Ann. Rev. Plant Biol. 60 (2009) pp. 239-260.

39. Y. Miloslavina, S. DeBianchi, L. Dall'Osto, R. Bassi, and A.R. Holzwarth, Quenching in *Arabidopsis thaliana* mutants lacking monomeric antenna proteins of photosystem II, J. Biol. Chem. 286 (2011) pp. 36830-36840.

40. Y. Miloslavina, M. Szczepaniak, M.G. Müller, J. Sander, M. Nowaczyk, M. Rögner, and A.R. Holzwarth, Charge separation kinetics in intact photosystem II core particles is trap-limited. A picosecond fluorescence study, Biochemistry 45 (2006) pp. 2436-2442.

41. R. Nevo, D. Charuvi, O. Tsabari, and Z. Reich, Composition, architecture and dynamics of the photosynthetic apparatus in higher plants, Plant J 70 (2012) pp. 157-176.

42. M. Nilkens, E. Kress, P. Lambrev, Y. Miloslavina, M. Müller, A.R. Holzwarth, and P. Jahns, Identification of a slowly inducible zeaxanthin-dependent component of non-photochemical quenching of chlorophyll fluorescence generated under steady-state conditions in *Arabidopsis*, Biochim. Biophys. Acta-Bioenergetics 1797 (2010) pp. 466-475.

43. C.B. Osmond, What Is Photoinhibition? Some Insights From Comparisons of Shade and Sun Plants, in: N.R. Baker and J.R. Bowyer (Eds.), Photoinhibition of Photosynthesis: From the molecular mechanism to the field, Environmental plant biology, BIOS Scientific Publishing, Oxford, 1994, pp. 1-24.

44. P.R. Rozak, R.M. Seiser, W.F. Wacholtz, and R.R. Wise, Rapid, reversible alterations in spinach thylakoid appression upon changes in light intensity, Plant Cell Environ. 25 (2002) pp. 421-429.

45. C. Slavov, M. Ballottari, T. Morosinotto, R. Bassi, and A.R. Holzwarth, Trap-limited charge separation kinetics in higher plant photosystem I complexes, Biophys. J. 94 (2008) pp. 3601-3612.

46. M. Szczepaniak, J. Sander, M. Nowaczyk, M.G. Müller, M. Rögner, and A.R. Holzwarth, Charge separation, stabilization, and protein relaxation in photosystem II core particles with closed reaction center, Biophys. J. 96 (2009) pp. 621-631.

47. M. Tikkanen and E.M. Aro, Integrative regulatory network of plant thylakoid energy transduction, Trends Plant Sci 19 (2014) pp. 10-17.

48. M. Tikkanen, M. Grieco, and E.M. Aro, Novel insights into plant light-harvesting complex II phosphorylation and 'state transitions', Trends Plant Sci. 16 (2011) pp. 126-131.

49. M. Tikkanen, M. Suorsa, P.J. Gollan, and E.-M. Aro, Post-genomic insight into thylakoid membrane lateral heterogeneity and redox balance, FEBS Lett. 586 (2012) pp. 2911-2916.

50. H.-W. Trissl, Determination of the quenching efficiency of the oxidized primary donor of photosystem I, $P700^{+}$: Implications for the trapping mechanism, Photosynth. Res. 54 (1997) pp. 237-240.

51. H.-W. Trissl and C. Wilhelm, Why do thylakoid membranes from higher plants form grana stacks?, Trends. Biochem. Sci. 18 (1993) pp. 415-419.

52. M. Yoshioka-Nishimura, D. Nanba, T. Takaki, C. Ohba, N. Tsumura, N. Morita, H. Sakamoto, K. Murata, and Y. Yamamoto, Quality Control of Photosystem II: Direct Imaging of the Changes in the Thylakoid Structure and Distribution of FtsH Proteases in Spinach Chloroplasts Under Light Stress, 2014, pp. 1255-1265.

Supplementary data

Steady state NPQ analysis was performed using a home-built wavelength resolving fluorescence induction spectrometer [2]. Actinic light adaptation for NPQ measurements was carried out using an array of red (λ_{center} = 635 nm) high intensity light-emitting diodes. The steady state NPQ results are shown in Fig. S1 providing both the spectrally resolved maximal NPQ data as well as the steady state fluorescence spectrum (Fmax emission spectrum, all PSII centers closed, normalized) of the dark-adapted unquenched leaves.

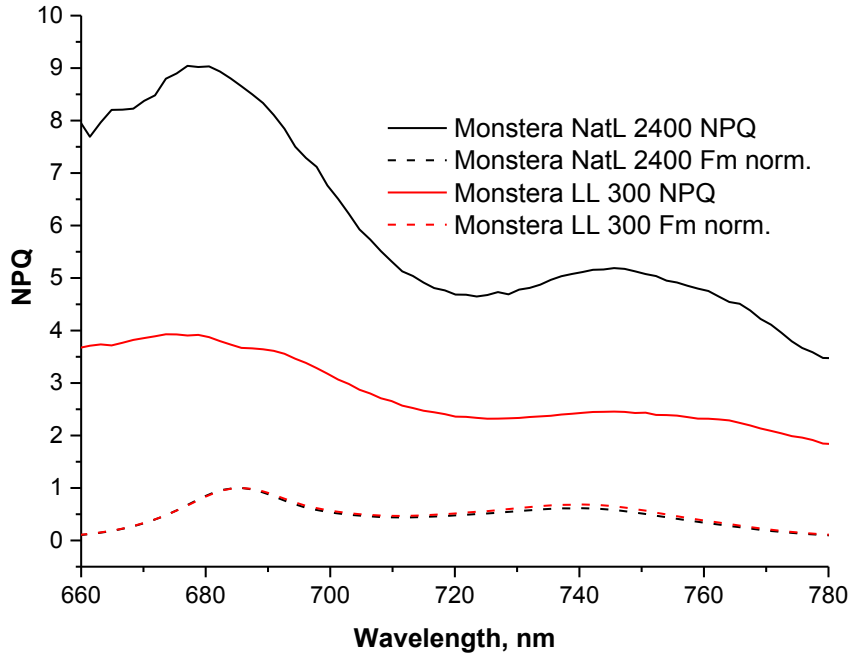

Fig. S1: Wavelength-resolved maximal NPQ values (full lines) and steady state emission spectra of unquenched *Monstera* leaves at Fmax (all PSII centers closed by light, dashed lines). Note that the NPQ spectrum of the LL plant is much broader than for the NatL plant and peaks below 680 nm, whereas the spectrum of the NatL plant has its quenching peak at 680 nm. Also the amplitude ratio of the far-red/red band is very different for the two plant conditions.
NPQ is defined as NPQ = (F_{max}/F'_{max})-1

The wavelength resolved steady state NPQ measurements (for details see [2] indicate that the NPQ values are actually pronouncedly wavelength dependent. They show a maximal NPQ value of 9.5±1 at the maximum of the PSII emission around 685 nm for NatL plants vs. 3.5±0.5 for LL plants. Note that conventional instruments employed for NPQ measurements (like e.g. the PAM instrument of Walz) measure the average NPQ values at wavelengths above 720 nm only. Accordingly, our NPQ values in that range should be compared with results measured with conventional instruments. NPQ in that long wavelength range is, however, reduced strongly by PSI emission. The most precise NPQ value for PSII is obtained at the maximum of PSII emission in the range 680-685 nm where PSI emission is very low.

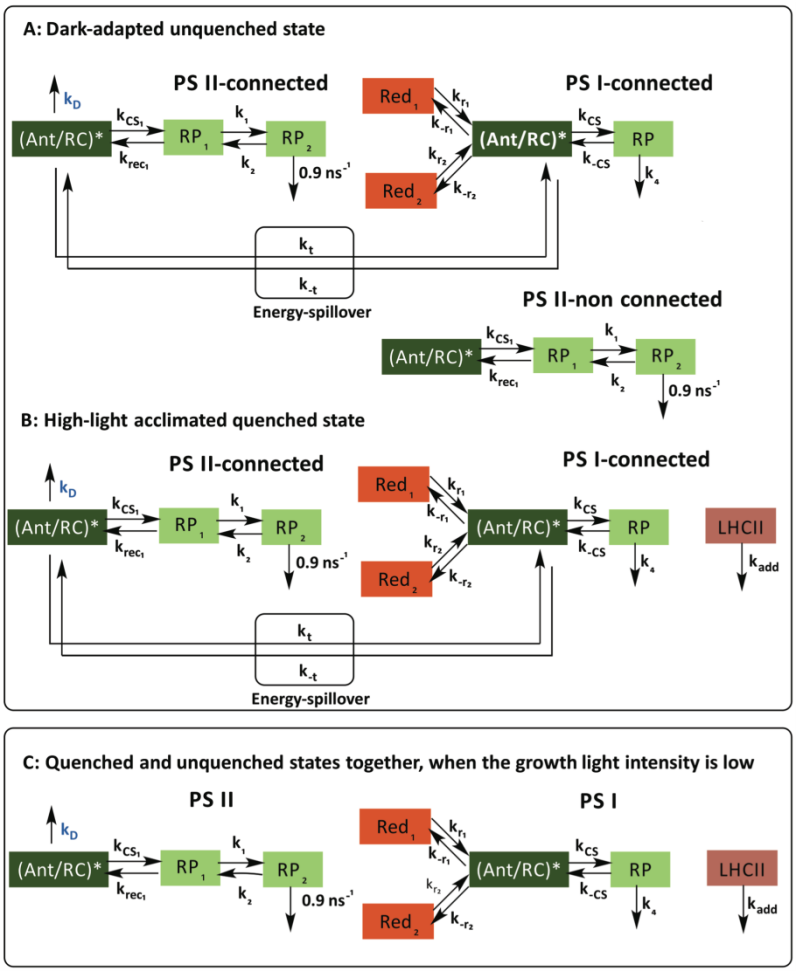

Fig. S2: Alternative kinetic compartment models proving successful for describing the quenching kinetics for the various light adaptation conditions. The compartment models for PSI and PSII units follow those that have been demonstrated on isolated intact PSI and PSII complexes [4-6] and on *Arabidopsis* intact leaves [1,3]. The compartment labeling is as follows: Ant/RC*: antenna/reaction center excited states of PSII or PSI; RPx: radical pairs; LHCII: functionally detached and quenched light-harvesting complex II from PSII.

The model S2 A is a heterogeneous PSII model, with one of the different PSII pools involved in spillover. This model requires part of the PSII units to be in direct contact with PSI units. The model turned out to be adequate for fitting the kinetics of dark-adapted NatL grown leaves. The model S2 B is a homogeneous PSII model with spillover. All the PSII units are in direct spillover contact with PSI units. This model proved adequate for fitting the kinetis of NatL grown plants in the NPQ condition. Both models S2 A and S2 B are inconsistent with a strict lateral segregation of PSII and PSI in different membrane areas, i.e. they are incompatible with the conventional granum/stroma-exposed region model for thylakoids of higher plants. The model S2 C is the standard separate PSII and PSI units model. The two photosystems are not involved in direct energy transfer (spillover) among each other. This model is consistent with the strict lateral segregation model of the thylakoid membrane. The model is adequate to perfectly describe the kinetics of both dark-adapted as

well as NPQ-adapted LL grown Monstera leaves. It had been developed earlier for describing the kinetics of normal grown Arabidopsis leaves [1].

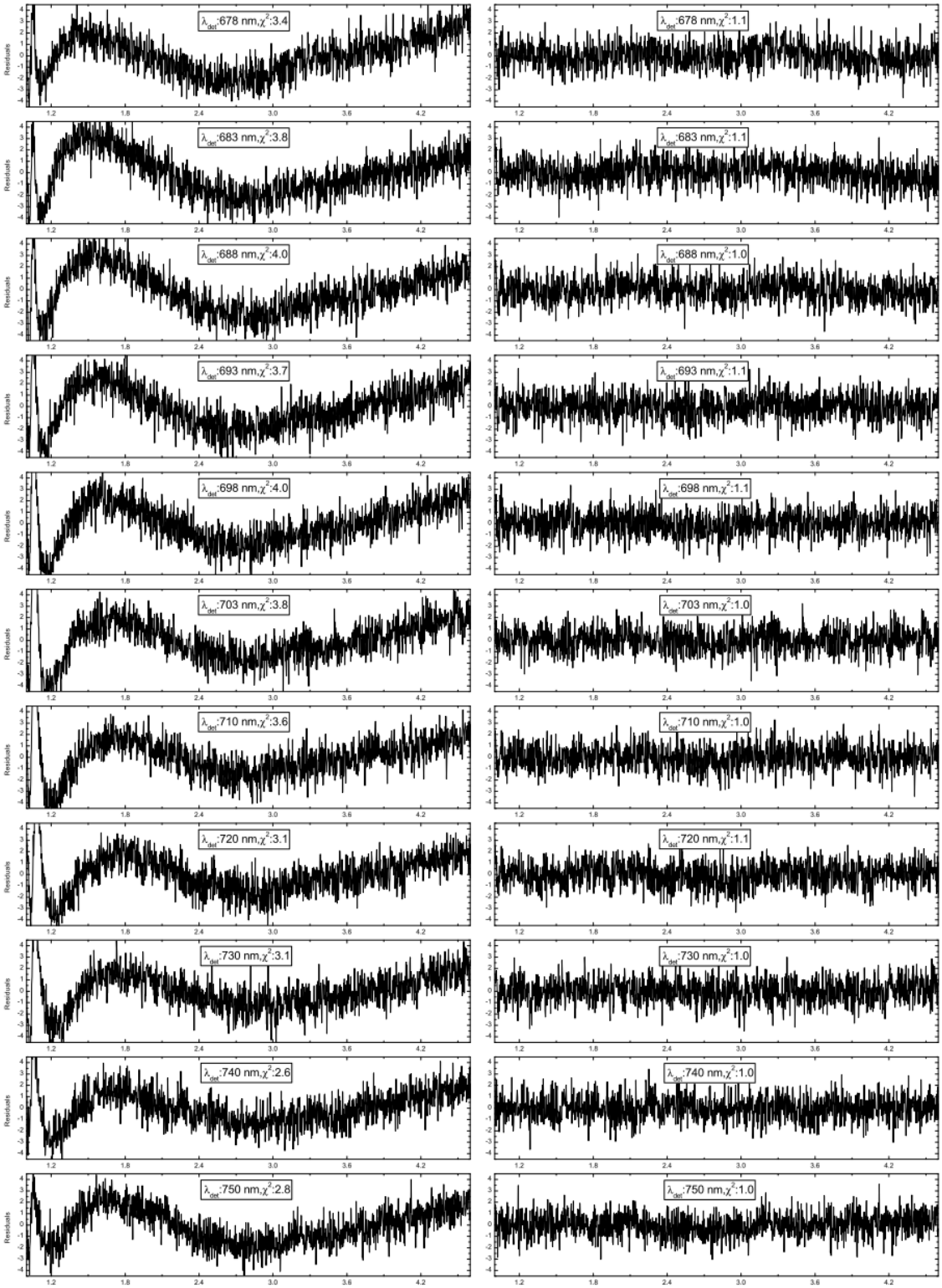

Fig. S3: Comparison of residual plots from global compartment analysis of the kinetics of dark-adapted NatL grown plants. F_{max} kinetics using a homogeneous spillover PSII model (Fig. S2 B) (left, global χ^2 = 3.7) vs. a heterogeneous PSII model (spillover + non-spillover PSII, right, global χ^2 = 1.08) (Fig. S2A).

Reference List

1. A.R. Holzwarth, Y. Miloslavina, M. Nilkens, and P. Jahns, Identification of two quenching sites active in the regulation of photosynthetic light-harvesting studied by time-resolved fluorescence, Chem. Phys. Lett. 483 (2009) pp. 262-267.

2. P.H. Lambrev, M. Nilkens, Y. Miloslavina, P. Jahns, and A.R. Holzwarth, Kinetic and spectral resolution of multiple nonphotochemical quenching components in *Arabidopsis* leaves, Plant Physiol. 152 (2010) pp. 1611-1624.

3. Y. Miloslavina, S. DeBianchi, L. Dall'Osto, R. Bassi, and A.R. Holzwarth, Quenching in *Arabidopsis thaliana* mutants lacking monomeric antenna proteins of photosystem II, J. Biol. Chem. 286 (2011) pp. 36830-36840.

4. Y. Miloslavina, M. Szczepaniak, M.G. Müller, J. Sander, M. Nowaczyk, M. Rögner, and A.R. Holzwarth, Charge separation kinetics in intact photosystem II core particles is trap-limited. A picosecond fluorescence study, Biochemistry 45 (2006) pp. 2436-2442.

5. C. Slavov, M. Ballottari, T. Morosinotto, R. Bassi, and A.R. Holzwarth, Trap-limited charge separation kinetics in higher plant photosystem I complexes, Biophys. J. 94 (2008) pp. 3601-3612.

6. C. Slavov, E. El-Mohsnawy, M. Rögner, and A.R. Holzwarth, Trapping kinetics in isolated cyanobacterial PS I complexes, Chem. Phys. 357 (2009) pp. 163-170.

Author contributions

T.S. performed the measurements of P700 oxidation kinetics and xanthophyll cycle activity, and analyzed the data. T.S. contributed to writing of parts of the manuscript concerning the P700 and xanthophyll data.

3.2 Energy dissipation in HL acclimated Arabidopsis NPQ mutant plants

Energy-spillover quenching (q_{SO}) was shown to contribute greatly to the NPQ capacity of natural HL grown *Monstera deliciosa* plants. However, it remained unclear whether q_{SO} acts as an autonomously active quenching mechanism independent from qE (PsbS dependent) or qZ (Zx dependent). Since this question can be answered satisfactorily only by comparative time-resolved fluorescence measurements on PsbS and Zx deficient mutants, the characteristics of q_{SO} quenching was investigated in corresponding HL acclimated *Arabidopsis thaliana* mutants. For this purpose, time-resolved measurements were conducted using the PsbS deficient mutant *npq4*, the PsbS over-expressing line *L17*, and the Zx deficient *npq1* mutant.

The time-resolved fluorescence decays in the dark-acclimated F_{max} state and in the light-acclimated F_{NPQ} state are shown in Figure 3.1. No differences were observed in the F_{max} state when comparing wild type and mutant plants. In the light acclimated F_{NPQ} state, an accelerated decay, indicating the activation of quenching processes, was found in all genotypes (Figure 3.1 dotted lines). The *L17* mutant showed the fastest decay of the fluorescence signal (= most efficient energy quenching), followed by the WT and finally by the two mutants with reduced NPQ capacity (*npq4* and *npq1*). Both mutations, that effect either activation of Q1 (*npq4*) or Q2 (*npq1*) exhibited the same effect on overall fluorescence decay.

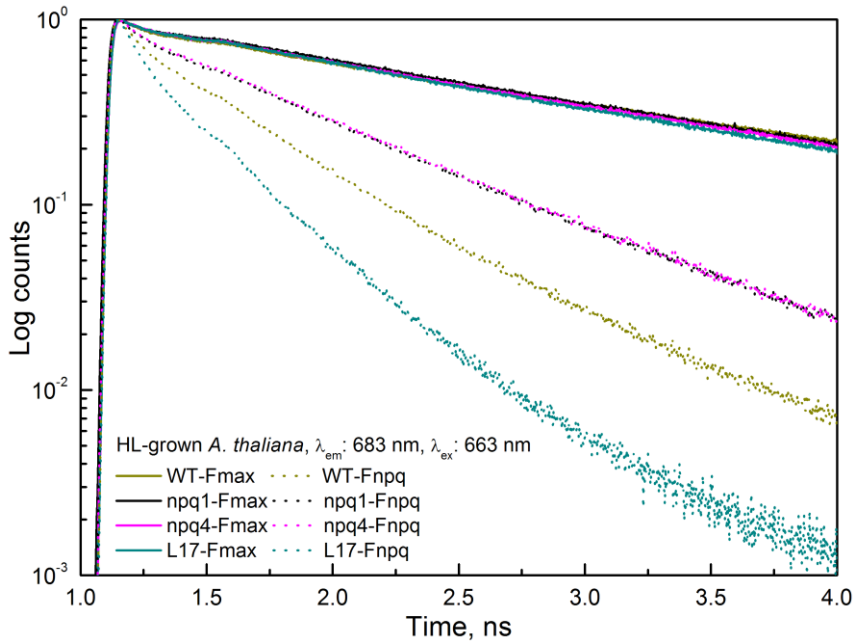

Figure 3.1 Fluorescence decay in *Arabidopsis thaliana* wild type and mutant plants. Maximum fluorescence in unquenched, closed PSII RC upon DCMU treatment in the dark (solid lines), and quenched states in light acclimated leaves (dotted lines) are shown.

Decay associated spectra (DAS) were derived from kinetic compartment analysis of the fluorescence decay traces (Figure 3.2). Under F_{max} conditions, only in WT, *L17* and *npq4* plants (Figure 3.2 A, C, E), but not in *npq1* plants (Figure 3.2 G), a heterogeneous PSII pool

was required for satisfactory describing the DAS, as indicated by the three components labelled as connected PSII (PSII-C) in addition to the typical, unconnected PSII components (PSII). Thus, the HL induced formation of a heterogeneous PSII pool, or more precisely the presence of a PSII pool connected to PSI, occurs independent of the PsbS protein, but not independent of Zx.

In the light-acclimated F_{NPQ} state, only connected PSII RCs were found in the WT and *L17* mutant (Figure 3.2 B, D), indicating the activation of q_{SO} quenching as in HL acclimated Monstera plants (see chapter 3.1). In the *npq4* mutant, however, a heterogeneous pool of connected and unconnected PSII was maintained in the light-acclimated state (Figure 3.2 F). This indicates that PsbS might be required for switching a heterogeneous pool of PSII and PSII-C to a homogeneous PSII-C pool, and thus for the activation of q_{SO}. Light-activation of the Q1 site (= appearance of the component 'LHCII Olig'), which is related to the detachment of LHCII complexes, was only found in WT, *L17* and *npq1* (Figure 3.2 B, D, F), but not in *npq4* (Figure 3.2 F), as has been shown earlier for NL grown plants (Holzwarth et al., 2009). This demonstrates again the requirement of PsbS protein for the conformational changes that lead to the detachment of the LHCII antenna upon illumination and thus the activation of Q1.

Kinetic target analysis was performed to determine the rate constants for the assigned PSII kinetic components (Table 3.1). The rate constant k_D describes the effective non-radiative deactivation rate and thus is a direct measure of NPQ in the PS II-attached antenna related to the quenching site Q2 (Holzwarth et al., 2009). In the unquenched F_{max} state, k_D was identical in all genotypes with a value of 0.3 ns^{-1} in both unconnected PSII ($k_{D\_max,\ PSII}$) and connected PSII ($k_{D\_max,\ PSII\text{-}C}$). In the quenched F_{NPQ} state, k_D was strongly increased in WT (1.6 $^{ns-}$1, connected PSII), *L17* (1.1 ns^{-1}, connected PSII), and in *npq4* (1.5 ns^{-1}, unconnected PSII), but not in *npq1* (0.4 ns^{-1}, unconnected PSII). The unchanged k_D in *npq1* plants confirms that Q2 cannot be activated in absence of Zx (Holzwarth et al., 2009).

The total NPQ was similar in the *npq4* and *npq1* mutant, 1.7 and 1.6, respectively, but strongly increased in *L17* plants (NPQ = 5.1), in comparison to WT plants with an NPQ of 3.1. These values were in agreement with the NPQ capacity that was calculated based on PAM measurements (data not shown).

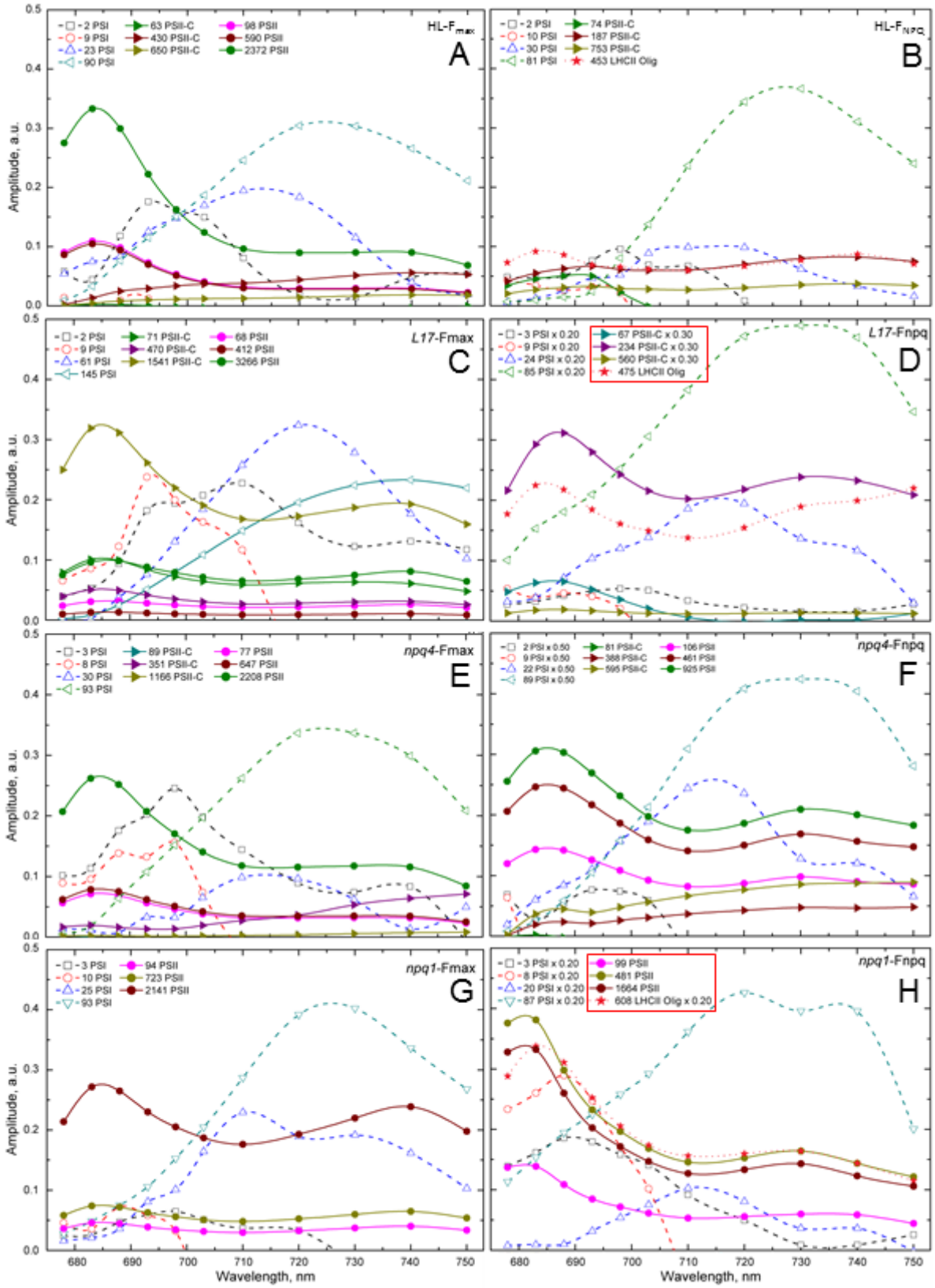

Figure 3.2 Decay associated spectra for WT, L17, *npq4*, and *npq1* mutants in a F_{NPQ} state (A, C, E, G) and in a F_{max} state (B, D, F, H) with closed PSII RC upon DCMU treatment in dark acclimated leaves. Spectral properties of PSI are shown in dotted lines, PSII related DAS are shown in solid lines. Rate constants are indicated in the top left corner of each graph. Red boxes indicate quenching with and without Zx. Measurements and analysis was performed by Dr. Suman Paul.

Table 3.1 Average lifetimes and rate constants of F_{max} and F_{NPQ} components in HL grown *Arabidopsis thaliana* plants. The upper part shows the average lifetime (τ_{av}) [ps] of the fluorescence decay measurements shown in Figure 3.2. The middle part shows the rate constants k_D [ns^{-1}] for PSII antenna deactivation under F_{max} and F_{NPQ} conditions, as well as the average lifetime for the PSII kinetic. Two pools of PSII RC exist, unconnected (PSII) and connected (PSII-C) RC, the latter allowing for energy-spillover. The lower part shows the lifetime τ [ps] of the detached PSII antenna, the site of Q1-type quenching. The respective contribution of the detached antenna (LHCII) and at PSII (NPQ_{PSII}) to the total NPQ is indicated. Errors in the rate constants were within ± 10 %.

	WT	L17	*npq4*	*npq1*
τ_{av}, ps @ 686 nm (F_{NPQ})	320	220	510	540
τ_{av}, ps @ 686 nm (F_{max})	1320	1360	1400	1380
Total NPQ	3.1	5.2	1.7	1.6
$k_{D\_max,\ PSII}$, ns^{-1}	0.3	0.3	0.3	0.3
$k_{D\_NPQ,\ PSII}$, ns^{-1}	-	-	1.5	0.4
$\tau_{av,\ PSII}$, ps (F_{max})	1020	1249	977	987
$\tau_{av,\ PSII}$, ps (F_{NPQ})	-	-	497	748
$k_{D\_max,\ PSII\text{-}C}$, ns^{-1}	0.3	0.3	0.3	-
$k_{D\_NPQ,\ PSII\text{-}C}$, ns^{-1}	1.6	1.1	0.5	-
$\tau_{av,\ PSII\text{-}C}$, ps ($F_{max}$)	374	694	535	-
$\tau_{av,\ PSII\text{-}C}$, ps ($F_{NPQ}$)	338	287	355	-
k_{D_LHCII} [ns^{-1}]	2.21	2.11	-	1.6
Lifetime τ [ps] of detached antenna component	453	475	-	608
Detached antenna cross-section relative to total PSII antenna (%)	40	20	-	66

The detachment of LHCII was more pronounced in *npq1* mutants (66 % reduction of the PSII antenna cross section) than in the WT (40 % reduction), however it was reduced in *L17* (20 % reduction). Quenching in detached LHCII was more efficient in *L17* than in *npq1* as reflected by the corresponding lifetimes (Table 3.1).

In conclusion, these time-resolved measurements show that spillover quenching (q_{SO}) can be activated in HL grown Arabidopsis plants, as has been shown before for Monstera plants grown under natural HL conditions. The activation of q_{SO} is thus not a specific feature of evergreen plants or a specific response to natural HL conditions. Moreover, activation of q_{SO} can be activated independent of the activation of Q2, but likely not independent of the activation of Q1 (and thus of PsbS). Since the activation of q_{SO} is accompanied by structural reorganization of the thylakoid membrane (see chapter 3.1), it is tempting to speculate that PsbS plays a critical role in the regulation of the membrane organization.

3.3. Characterization of Arabidopsis plants to different growth light intensities

To understand the acclimation of the photosynthetic apparatus to high light and particularly the processes leading to the acquirement of a high NPQ capacity, the acclimation of *Arabidopsis thaliana* wild-type plants to different light regimes was investigated. The plants were thoroughly characterized regarding structural and physiological properties in context with photosynthetic light utilization.

3.3.1 Morphological and structural characterization

3.3.1.1 Plant growth and leaf characteristics

Arabidopsis thaliana wild type (WT) plants were grown under different light intensities: Low light (LL, 25 µE), normal light (NL, 100 µE), high light (HL, 500 µE) and natural light (NatL, 10-1200 µE). The phenotype of the plants is shown in Figure 3.3. LL plants showed the smallest size in rosette diameter and the leaves were thin and of round shape. In comparison to LL plants, the leaves of normal light (NL) grown plants showed an oval shape with increased leaf area. However, less leaves were developed in comparison to LL plants of similar rosette diameter. With further increasing growth light intensity (HL), the leaf and plant size increased.

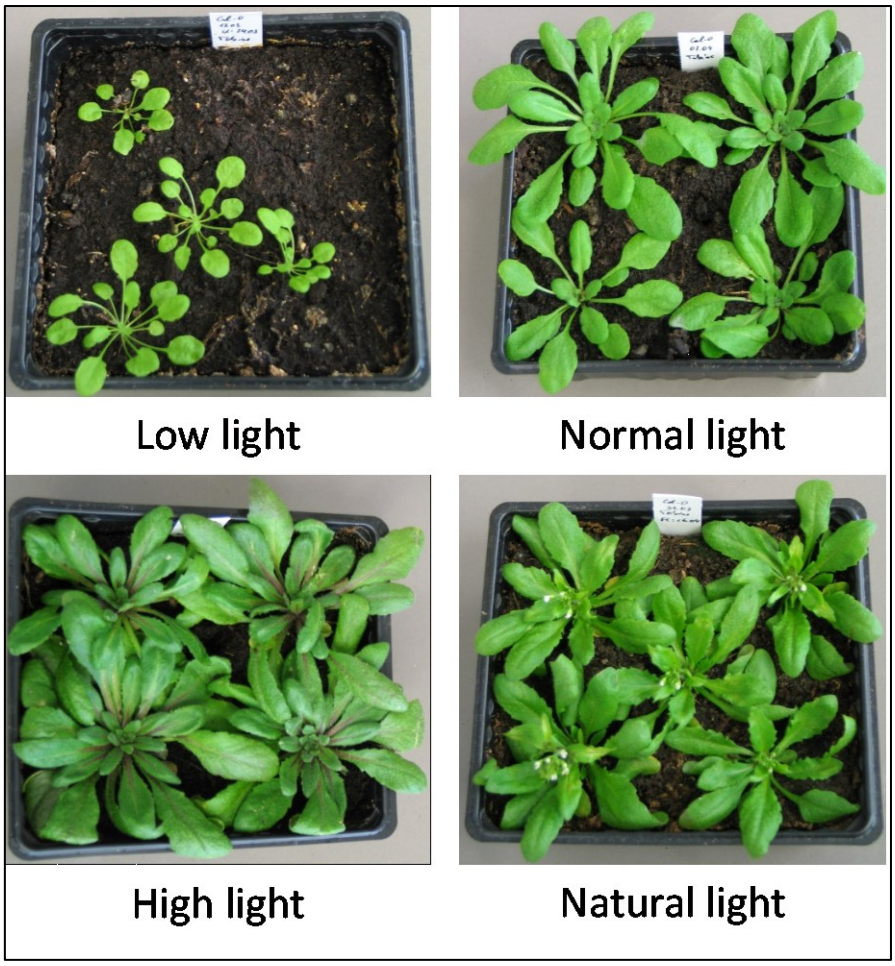

Figure 3.3 Growth phenotypes of Low light (LL), Normal light (NL), High light (HL) and Natural light (NatL) grown plants. Representative, six weeks old plants are shown.

The leaf color of NatL plants was darker than that of LL and NL plants, but lighter in comparison to HL plants, indicating intermediate or shared properties of LL and HL growth conditions on the level of leaf development. The most striking phenotypical feature of NatL plants in comparison to the other growth conditions was the presence of flowers (Figure 3.3 Natural light). Since all plants had the same age, fluctuating light conditions obviously triggered early flowering (Figure 3.3).

Phenotypical observations revealed an intermediate leaf growth in NatL, which combines characteristics of NL and HL plants. For further characterization, leaves were cut from the plants and general growth parameters, such as the leaf area, fresh and dry weights were determined (Figure 3.4).

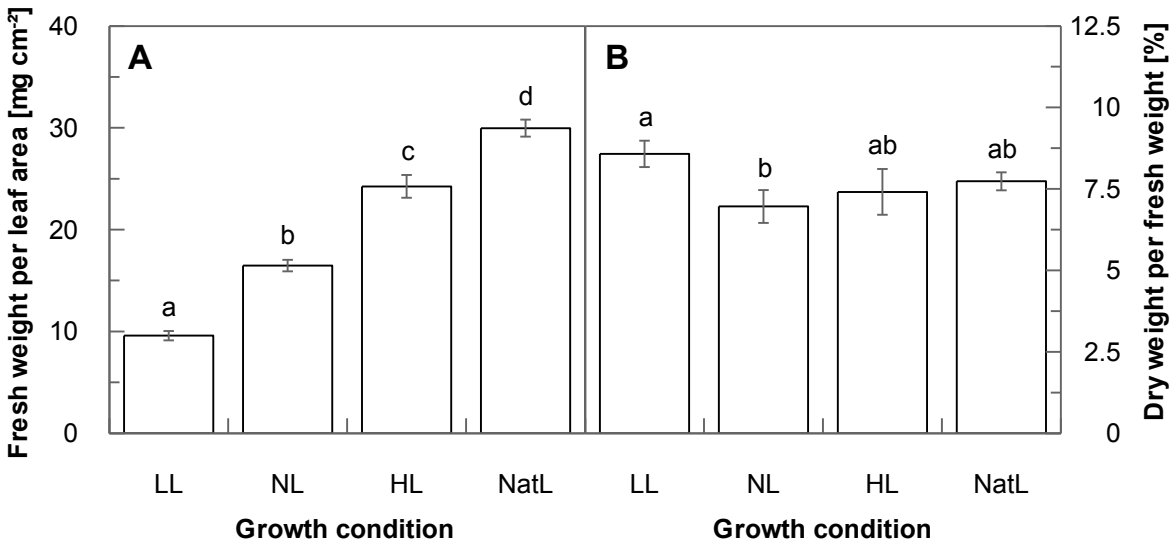

Figure 3.4 Leaf parameters of LL, NL, HL, and NatL grown plants. (A) fresh weight per leaf area, (B) dry weight per fresh weight in percent. Mean and standard error of six independent samples are shown. Significant differences are indicated.

As expected, the lowest fresh weight (10 mg per cm^2) was determined for LL plants (Figure 3.4). With increasing growth light intensity the fresh weight increased to 15 mg per cm^2 in NL plants and 25 mg per cm^2 in HL plants. The highest fresh weight was determined in NatL plants, with 30 mg per cm². Very similar differences were observed on DW basis resulting in a similar DW content of 7-9 % for all growth conditions (Figure 3.4 B), which indicates a similar leaf structure without pronounced differences in cell wall thickness. The accumulation of higher mass in NatL plants as compared to HL plants indicates a higher light use efficiency in NatL grown plants, since the mean light intensity under NatL conditions (about 150 µmol photons m^{-2} s^{-1}) was much lower than under HL conditions (about 500 µmol photons m^{-2} s^{-1}). Light microscopy images of leaf cross sections were analyzed to evaluate whether the differences in the fresh weight could be simply explained with differences in the leaf thickness. All light and electron microscopy measurements presented in this work were performed by Dr. Michael Melzer at the „Leibniz-Institut für Pflanzengenetik und Kulturpflanzenforschung Gatersleben“.

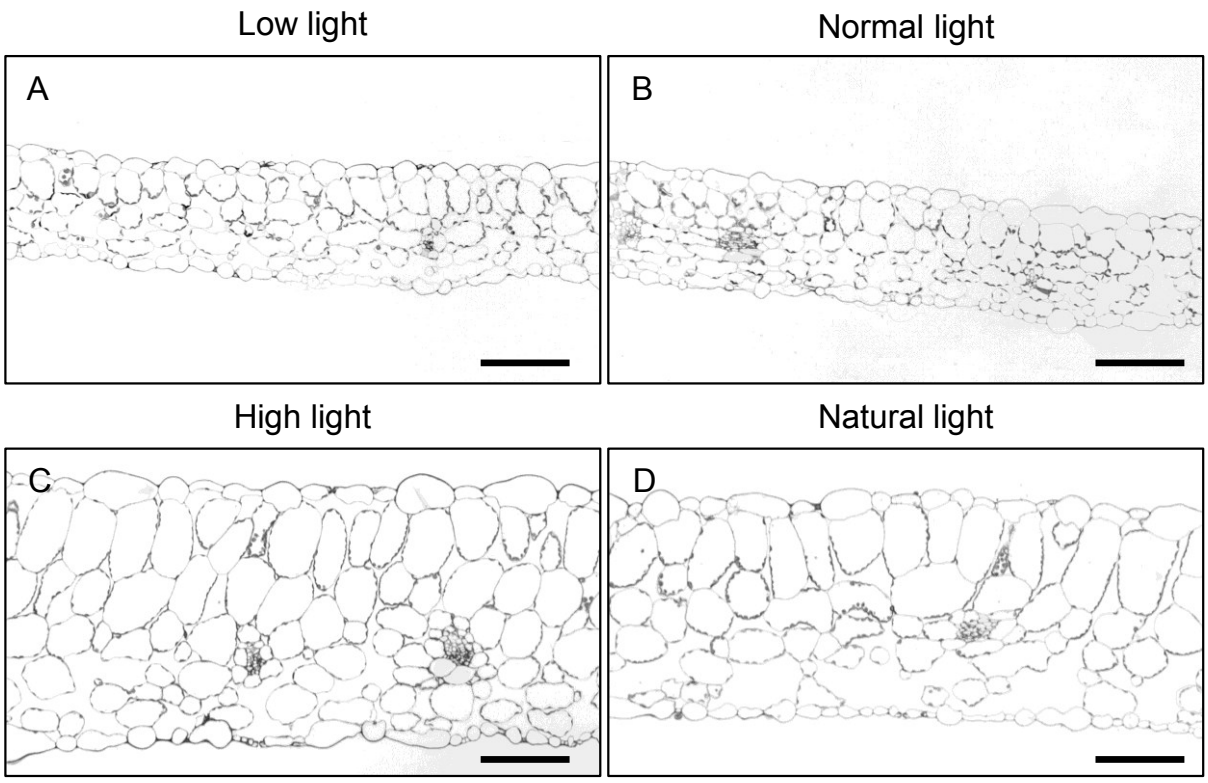

Figure 3.5 Light microscopy images of leaf cross sections of LL (A), NL (B), HL (C), and NatL (D) plants. Scale bar indicates 50 µm. Small, dark structures in the cells are chloroplasts.

Different growth light conditions resulted in clear differences in leaf thickness. The thickness of leaves from LL and NL grown plants was similar, but significantly reduced by about 50 % as compared to leaves from HL and NatL grown plants, which also showed similar leaf thickness (Figure 3.5). On average, the leaf thickness of LL and NL plants was 80 µm in contrast to HL and NatL plants with 160 µm leaf thickness (Figure 3.6 A). The stepwise, light dependent increase in fresh and dry weight with increasing growth light intensity (Figure 3.4) can thus not be explained simply by differences in leaf thickness. Increased thickness of the leaves was not due to increased number of cells, but rather due to cell elongation, resulting in the formation of a more pronounced palisade parenchyma in HL and NatL plants (compare Figure 3.5). Thus, when normalized to the area of the leaf cross section, the number of cells was reduced by more than 50 % in HL and NatL plants in comparison to LL and NL plants. On average 1 x 10^5 cells per cm² were found in HL and NatL plants, compared to 2.5 x 10^5 cells in LL and NL plants (Figure 3.6 B).

Chloroplasts were visible in all mesophyll cells. However, more chloroplasts were found in the adaxial side of the leaf, i.e. the palisade parenchyma, and the number of chloroplasts per cell increased with increasing growth light intensity (Figure 3.5).

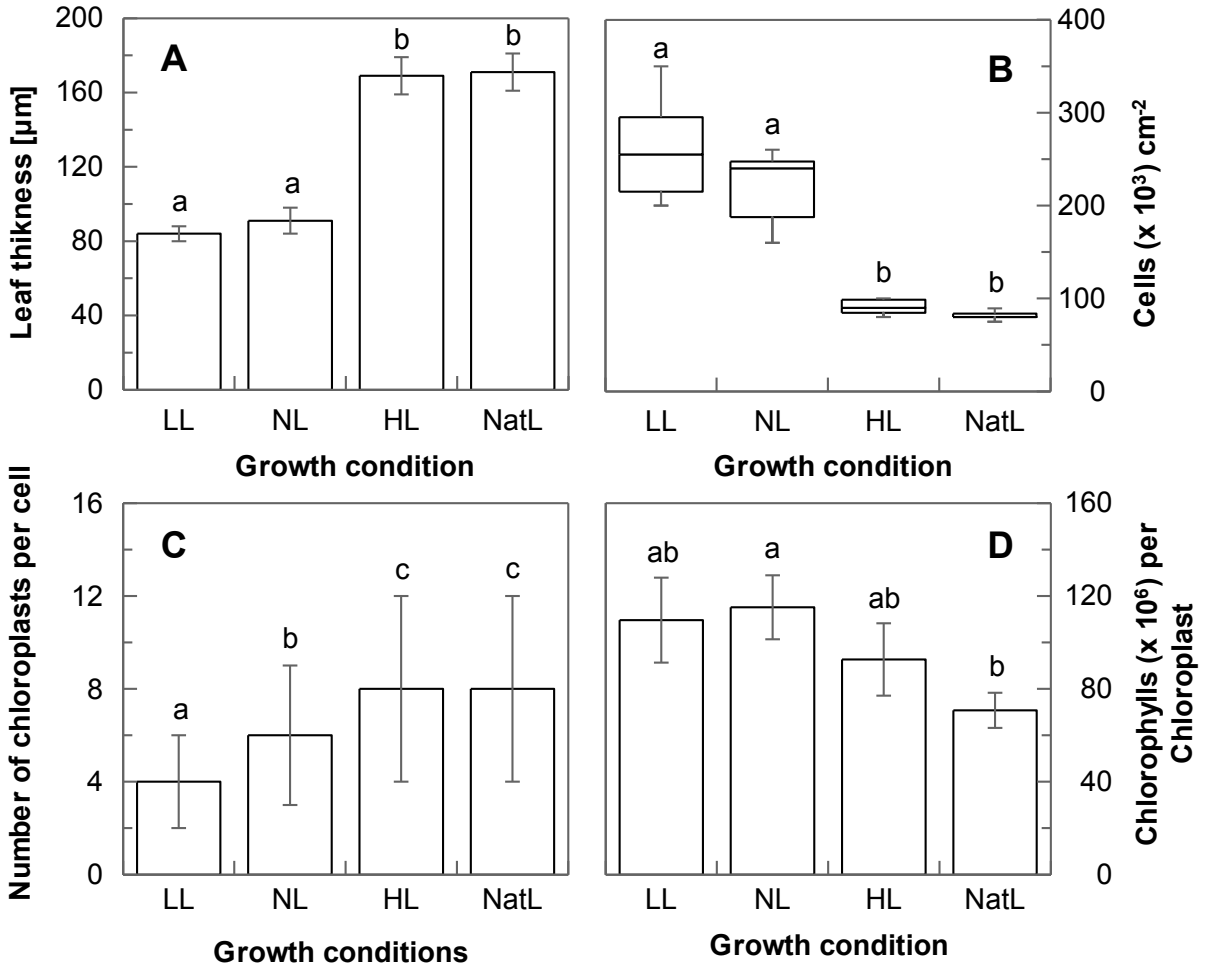

Figure 3.6 Analysis of light microscopy images shown in Figure 3.5. (A) Leaf thickness, (B) the number of cells per cm² leaf area, and (C) the number of chloroplasts per cell were quantified. Additionally the number of Chl per chloroplast, based on chloroplast isolation experiments, was calculated (D). Significant differences are indicated. Mean and standard error of at least six images are shown.

For photosynthetic efficiency, the number of chloroplasts per cell and the amount of Chl per chloroplast are important parameters. However, exact quantification of the number of chloroplasts was not trivial for two reasons: (i) the leaf cross sections were two-dimensional, thus chloroplasts which were not in the cutting level could not be counted, and (ii) no chloroplasts were found in the center of cells, indicating that non-membrane attached chloroplasts might have been lost during the preparation (Figure 3.5). Under the assumption that the loss of chloroplasts was comparable in all samples from all growth conditions, the number of chloroplasts was quantified in relation to the number of chloroplasts per cell in NL plants, which was arbitrarily set to a value of 1 (Figure 3.6 C). In comparison to NL plants, where 6 chloroplasts were found per cell on average, in LL plants only 4 chloroplasts per cell were calculated. On the contrary, in HL and NatL plants the number of chloroplasts per cell was increased 8. Analysis of isolated chloroplasts from all growth conditions revealed a difference in size of the chloroplasts. Since the size could not be quantified satisfactorily, due to the three-dimensionality of the chloroplast, rather the amount of Chl per chloroplast was

determined. As opposed to the number of chloroplasts per cell, which increased with increasing growth light intensity, the amount of Chl per chloroplast decreased (Figure 3.6 D). However, significant differences in the amount of Chl per chloroplast were only found between NL and NatL grown plants (Figure 3.6 D). The amount of Chl per chloroplast varied between 80 (x 10^6) in NatL plants and 120 (x 10^6) in NL plants.

3.3.1.2 Chloroplast quantification via confocal microscopy imaging

Since the number of chloroplasts could not be quantified satisfactorily in the light microscopy images (see also discussion), confocal microscopy was used as alternative method to visualize the chloroplasts. The advantage of using confocal microscopy instead of light microscopy is the use of intact cells. Due to the autofluorescence of the chloroplasts, no pretreatment for visualization is required. Figure 3.7 shows cells of LL, NL, HL, and NatL grown plants in the dark and after 30-60 min illumination. In line with the data derived from light microscopic images, the number of chloroplasts per cell increased with increasing growth light intensity. In LL plants, less chloroplasts were found in the cell, compared to other growth conditions. NL and HL plants showed similar amounts of chloroplasts per cell, however, the highest number of chloroplasts was found in NatL grown. The latter was in clear contrast to the results obtained via light microscopic imaging, where the same amount of chloroplasts was determined in HL and NatL plants (Figure 3.6 C).

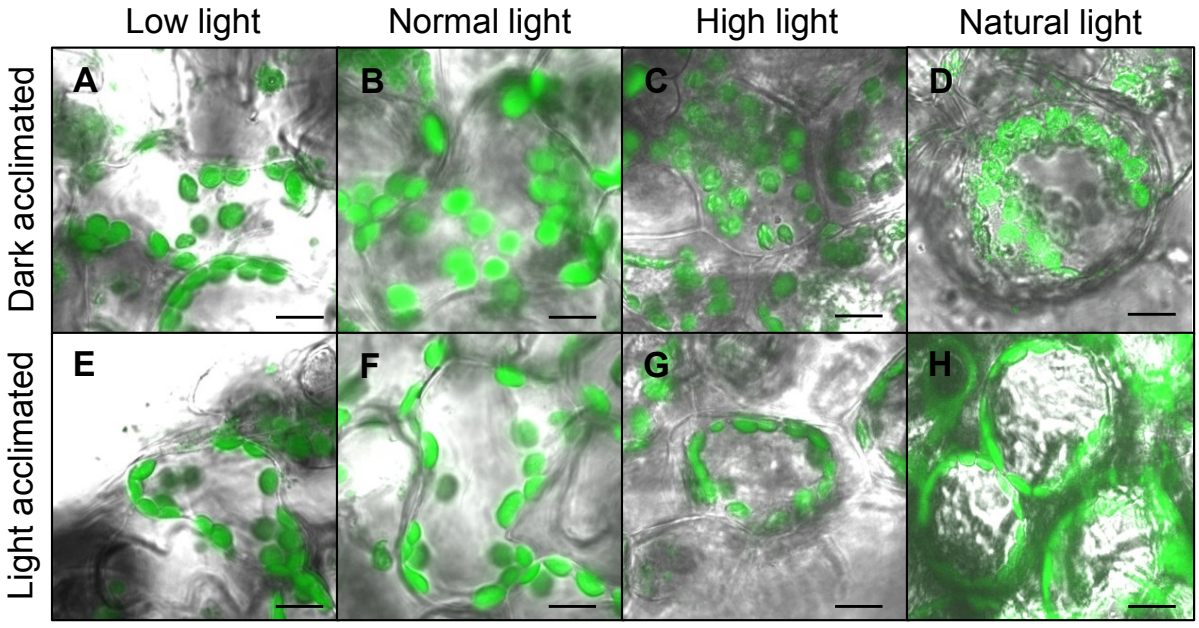

Figure 3.7 Confocal microscopy images of LL, NL, HL and NatL leaf cells with chloroplasts in dark acclimated (A-D) and light acclimated states (E-H). Auto fluorescence, induced via excitation at 420 nm and detected at 720 nm, of chloroplasts is shown in false color. Scale bar indicate 20 µm.

Chloroplasts from LL, NL, and HL plants were rather oval, whereas the shape of dark acclimated NatL chloroplasts was round. In the dark acclimated state, chloroplasts were randomly distributed across the cell in all plants. In the light acclimated state, chloroplasts

were attached to the cell walls averted from the light source. This light induced chloroplast movement was observed independently from the growth light condition.

3.3.1.3 Thylakoid membrane structure and lipid body quantification

To assess possible differences in thylakoid membrane organization, the chloroplast structure was further investigated by transmission electron microscopy. Representative images from dark acclimated leaves are shown in Figure 3.8. Chloroplasts from LL plants showed the highest density of thylakoid membranes in comparison to those from other growth conditions. In general, more and thicker grana stacks were detectable, which were connected by a large number of stroma lamellae (Figure 3.8 LL). On average 5-9 membranes were found per grana stack (Figure 3.9 B). With increasing growth light intensity, the amount of thylakoid membranes as well as the extent of grana stacks decreased. Also in chloroplasts from NL plants, various stroma lamellae interconnected the separated grana stacks, which were still the dominating structure of the thylakoid membrane. However, the number of membranes per grana stack was not significantly reduced in NL grown plants compared to LL grown plants (Figure 3.9 B).

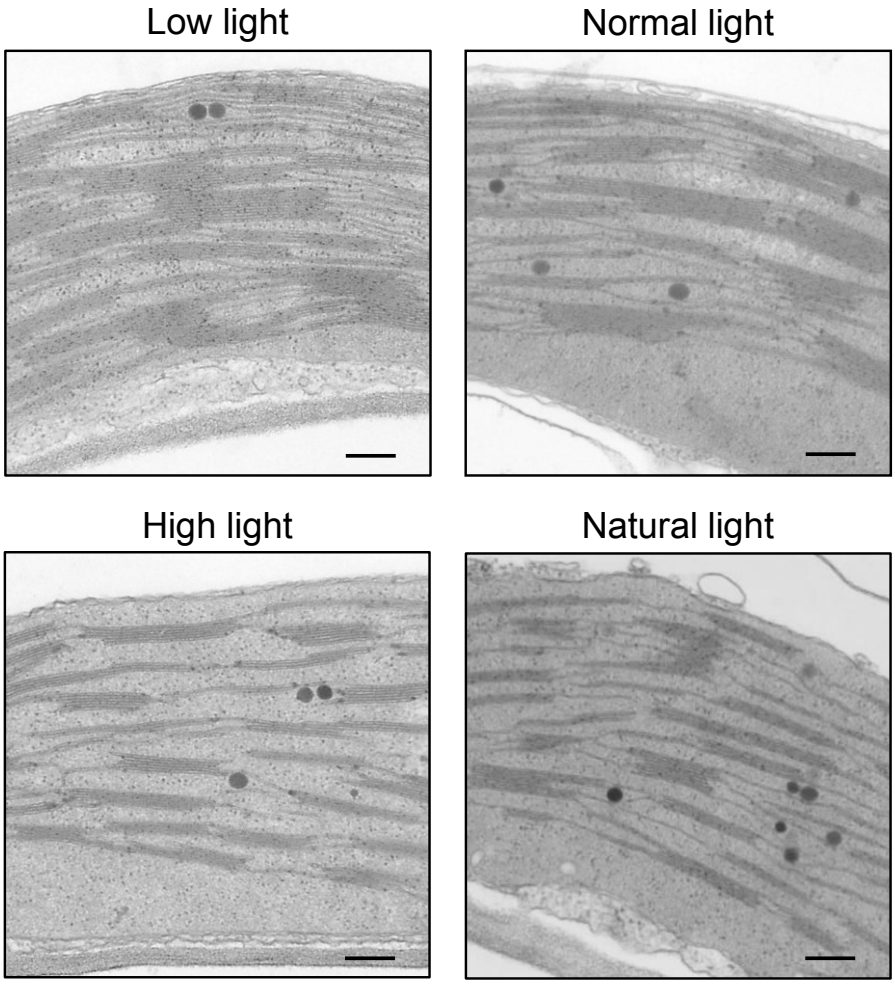

Figure 3.8 Typical transmission electron microscopy images. Images show the structure of the thylakoid membrane. Round structures are lipid droplets. Bars indicate 200 nm.

In contrast to LL and NL, the overall amount of thylakoid membranes and the overall degree of grana stacking was strongly reduced in HL plants, so that the relative fraction of stroma exposed membranes increased. Grana stacks in HL plants consisted typically of only three membranes. In NatL plants, the thylakoid membrane system was similar to that in HL plants, but the number of membranes per grana stacks was significantly increased by 25 %, consisting of four membranes. However, NatL grown plants consists of both, thicker grana stacks, as well as thinner grana (compare Figure 3.8), therefore the average number of membranes per grana might be slightly misleading.

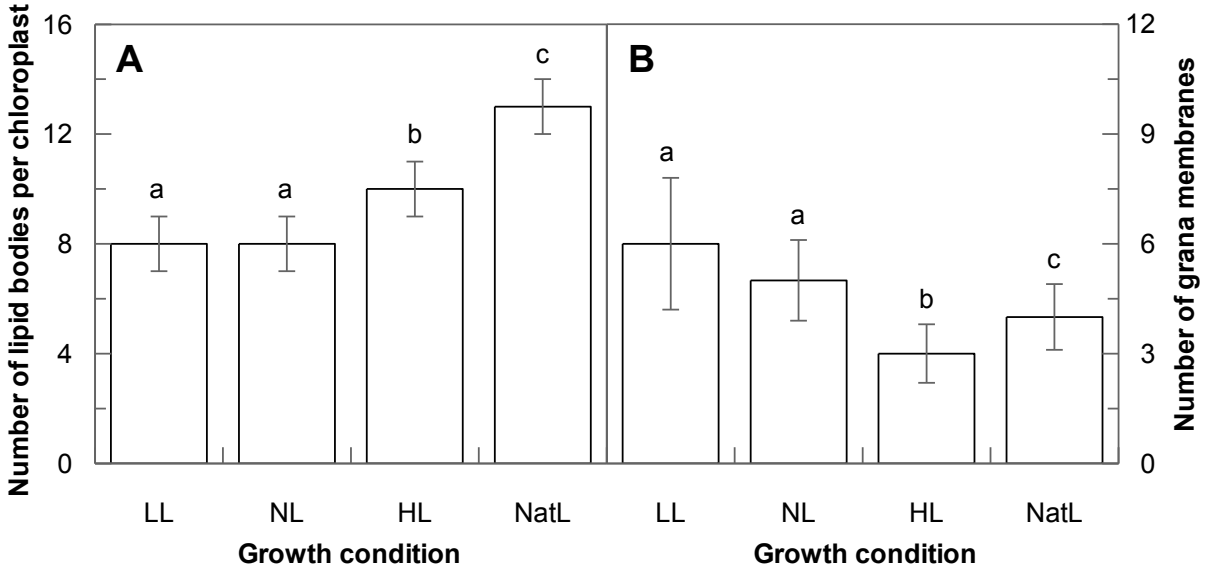

Figure 3.9 (A) Number of lipid bodies per chloroplast in LL, NL, HL, and NatL plants and (B) Absolute number of membranes of the grana stacks. Stacks were also used for quantification results shown in Figure 3.11. Significant differences are indicated.

Another striking difference among the chloroplasts from different growth conditions was found with respect to the number of lipid droplets. In chloroplasts, three types of lipid droplets exist, differing in their fatty acid composition and the integration and/or interaction with proteins: (i) plastoglobuli, (ii) plastoglobuli-like particles, and (iii) lipid-protein-particles (Smith et al., 2000). Since the droplets were not isolated and analyzed, the differentiation between these possible candidates was not possible, so that they will be referred to as “lipid droplets” only. As shown in Figure 3.9 A, the number of lipid droplets was comparable in LL and NL plants, where eight lipid droplets were found per chloroplast. The number increased to 10 in HL plants and was highest in NatL plants, where 12 droplets were found per chloroplast.

In summary, the overall membrane organization showed typical differences in LL, NL and HL grown plants. NatL plants showed mainly characteristics of HL plants, though grana stacks were thicker and more comparable to LL plants with the difference, that the amount of grana margins was increased with respect to the total grana width.

3.3.1.4 Light induced thylakoid membrane dynamics

Possible rearrangement of the thylakoid membrane structure upon short-term acclimation to high light was again assessed via transmission electron microscopy, since it has been shown for Monstera plants that the flexibility of the grana membrane was correlated with the appearance of q_{SO} quenching. Chloroplast from dark acclimated leaves (Figure 3.8) were compared with those from light acclimated leaves (30 minutes of illumination at 1500 to 2000 µmol photons m^{-2} s^{-1}) and subsequently re-darkened (for 10 min) leaves. These experimental conditions were chosen to obtain information about possible structural changes in relation to the induction and relaxation of NPQ processes. Representative images of dark acclimated, light acclimated and re-darkened thylakoid membrane structures are shown in Figure 3.10.

Images from dark acclimated chloroplasts were similar to those shown in Figure 3.8. For LL and NL plants, the membrane structure in the light acclimated state did not differ from that in the dark acclimated state (Figure 3.10 B). The grana stacks remained tightly appressed and no changes were visible in the organization of the stroma lamellae. Consequently, also no structural changes occurred upon re-darkening of LL and NL plants (Figure 3.10 C and F).

In contrast to LL and NL plants, HL plants exhibited light dependent structural changes in the organization of grana stacks. Here, clear unstacking of grana was observed after 30 minutes of illumination. Again, no differences in the stromal thylakoid membrane were observed. The unstacking was not reversible in the 10 minutes post illumination (Figure 3.10 I). NatL plants also showed a light dependent grana unstacking, however the unstacking was more pronounced than in HL plants (Figure 3.10 K). Furthermore, membrane unstacking was rapidly reversible, as indicated in the partial restacking observed in the relaxation period (Figure 3.10 L). In comparison to other growth light conditions, NatL plants showed a high accumulation of starch in the ten minutes of relaxation light treatment (Figure 3.10 L). The structural properties of thylakoid membranes in plants from different growth conditions were statistically analyzed for significance in the observed changes.

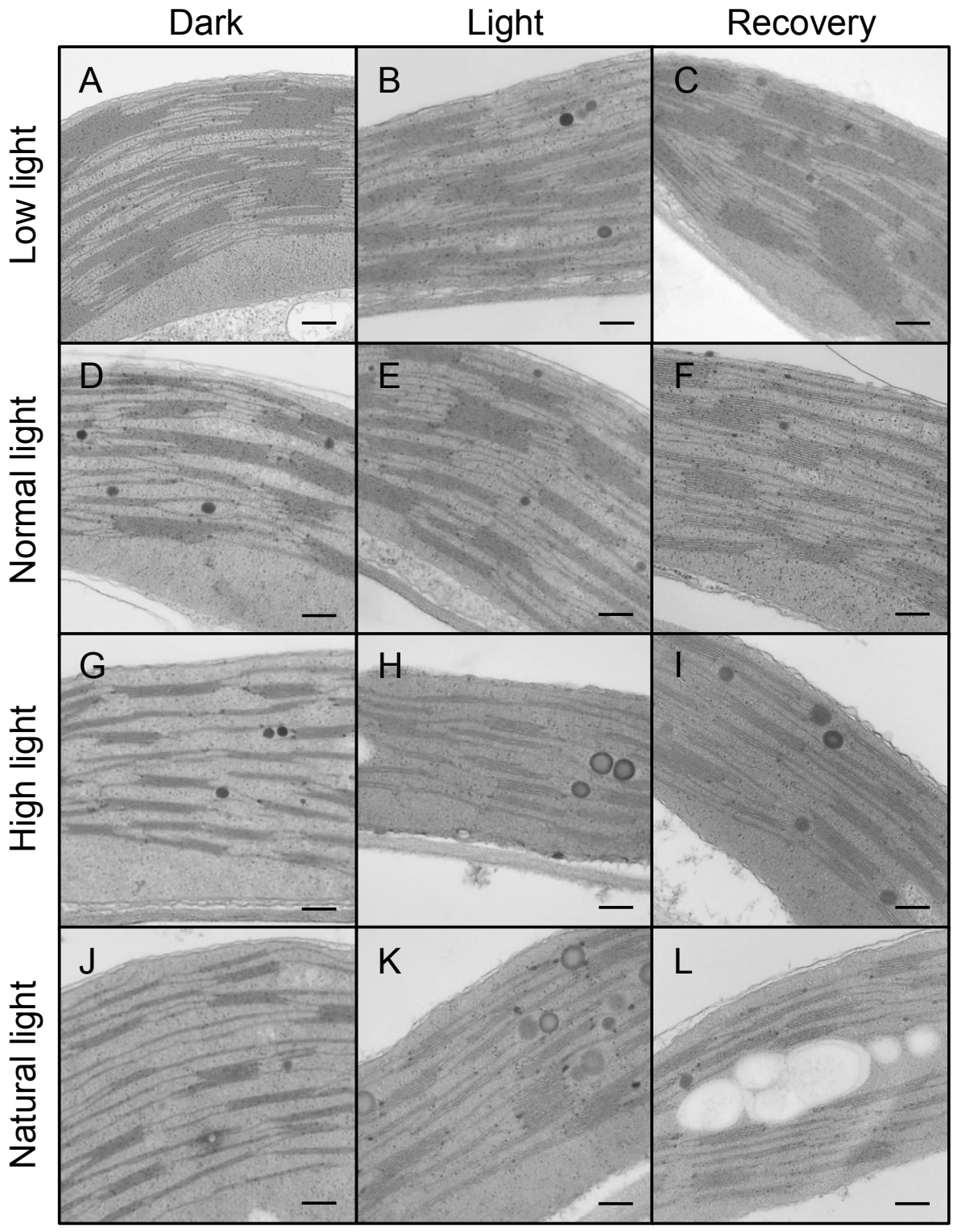

Figure 3.10 Transmission electron micrographs of chloroplasts. Images from LL (A-C), NL (D-F), HL (G-I), and NatL (J-L) plants in a dark- and light acclimated state, as well as after ten minutes of relaxation in the dark. Scale bars indicate 200 nm.

The average number of grana membranes per µm of height ranged between 40 and 50 under all growth conditions (Figure 3.11). Upon illumination, LL grown plants showed no significant change in grana height (Figure 3.11 A) or grana width (Figure 3.11 B), but rather an increased stacking than unstacking became visible upon illumination. In NL plants, a

significant unstacking, as indicated by the number of membranes per µm of granum, was only observed in the dark recovery phase after illumination, but not in the light-acclimated state.

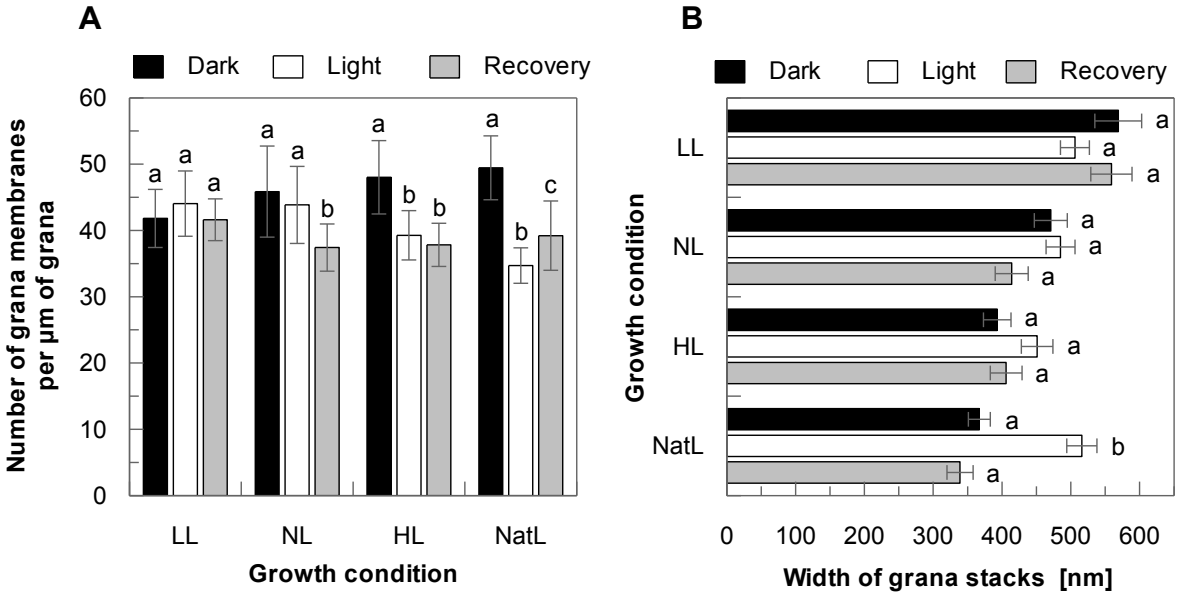

Figure 3.11 Structural changes in the grana of thylakoid membranes upon 30 minutes of HL illumination a 10 minutes post-illumination recovery phase in LL, NL, HL, and NatL plants. Analysis is based on transient electron images as exemplarily shown in Figure 3.10. (A) Light dependent changes in height, as well as the changes in width (B) are shown. Significant differences amongst one growth condition are indicated.

A significant unstacking of the grana stacks upon illumination was observed in HL plants. Here, the number of membranes per µm of granum decreased from 50 in the dark to 40 in the light, thus the height of the grana was increased by 20 %. Also, NatL plants showed unstacking of the grana stacks, however 30 % increase in space per membrane was quantified. As opposed to HL plants, partial restacking of grana was observed during the ten minutes post-illumination period, thus representing an unique feature of NatL plants. The width of grana stacks, however, decreased with increasing growth light intensity, from 500 nm in LL plants to 400 nm in HL and NatL. Only NatL plants showed a significant broadening of the grana stacks of about 35 % parallel to unstacking. Also this broadening was reversible in the ten minutes of post-illumination. It should be noted, that the effect of unstacking, coupled with a broadening of the grana stack, was found as a trend (though not statistically significant) in all growth conditions, except for LL plants, where light-induced grana stacking was paralleled by narrowing of the grana width. One could assume that unstacking is realized by a simultaneous narrowing of the grana stacks, which was clearly not observed, as had been described by (Kirchhoff, 2013).

Obviously, the tight packing of grana stacks found in LL and NL plants prevents the light dependent grana unstacking. Only in HL and NatL grown plants, a structural rearrangement of the membrane in response to high light was possible, likely correlated to the reduced

degree of grana stacking. However, more pronounced unstacking was observed in NatL plants, even though the grana stacks found in NatL plants were thicker compared to those in HL plants. Thus growth under fluctuating light conditions leads to an increased flexibility of thylakoid membranes.

3.3.1.5 Lipid composition

One possibility for altering the membrane flexibility are changes in the lipid composition of the thylakoid bilayer. The ratio of saturated to unsaturated fatty acids is a key determinant for membrane flexibility. A membrane containing in the majority saturated lipids is rather flexible, whereas poly-unsaturated bilayers were shown to be rather rigid (Niemelä et al., 2009).

In order to test the hypothesis of an altered lipid composition of thylakoid membrane, total lipid extracts were isolated from leaves of LL, NL, HL, and NatL plants, and analyzed in cooperation with Prof. Dr. Peter Dörmann (IMBIO, University Bonn).

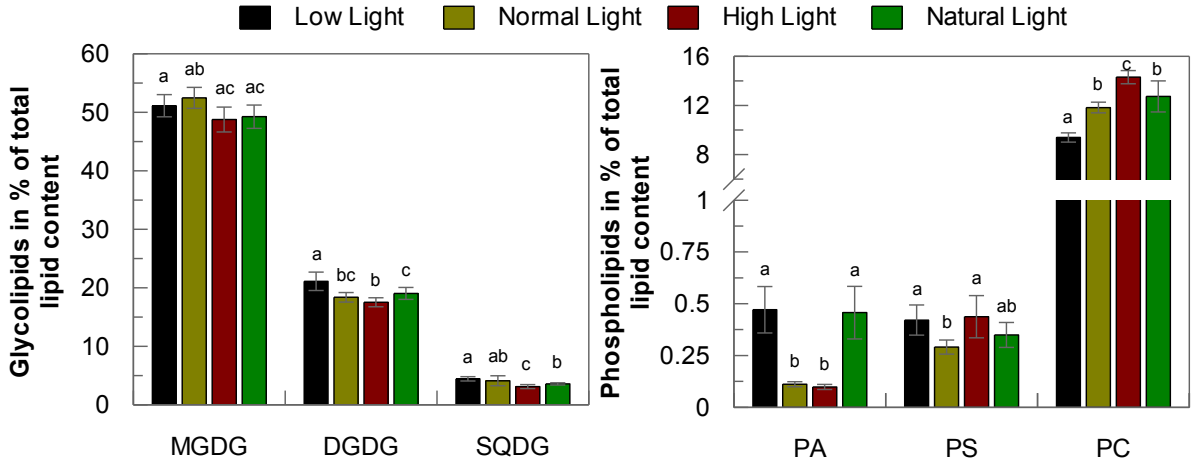

Figure 3.12 Lipid compositions of leaves harvested from LL, NL, HL, and NatL grown *Arabidopsis thaliana* plants. Shown is the relative amount of glycolipids (A) and phospholipids (B) of the total amount of lipids isolated. Mean and standard deviation of five independent samples is shown. MGDG: Monogalactosyldiacylglycerol; DGDG: Digalactosyldiacylglycerol; SQDG: Sulfoquinovosyldiacylglycerols; PA: Phosphatidic acid; PS: Phosphatidylserine; PC: Phosphatidylcholine. Measurements and analysis were performed in cooperation with Dr. P. Dörmann (IMBIO, Bonn)

Figure 3.12 shows the relative content of the different glycolipids and phospholipids. The proportional contribution of glycolipids to the total amount of lipids was similar among all growth conditions (Figure 3.12 A). About 75 % of the lipids in leaves were glycolipids, with MGDG (50 %) being the major constituent, followed by DGDG (20 %) and SQDG (5 %), which is in line with previous findings (Wang and Benning, 2012). The remaining 25 % of total lipids in leaves were assigned to phospholipids, with phosphatidylcholine (PC) being the major component (12-16 %). Phosphatidylinositol, phosphatidylglycerine, and phosphatidylethanolamine each represented about 4 % of the total amount of lipids independent from the growth condition (and therefore not shown in Figure 3.12), while only 0.1-0.5 % of the total lipids were made up by phosphatidic acid (PA) and phosphatidylserine

(PS). The most pronounced differences in response to different growth light conditions at the level of membrane lipids was found for phospholipids (Figure 3.12 B). The amount of PC, for example, was increased in chloroplasts with increasing growth light intensity, while the PC content in NatL grown plants was similar to that of NL grown plants. In contrast to PC, the amount of PA was highest in LL and NatL grown plants, while the amount of PS was significantly lower only in NL grown plants in comparison with LL and HL grown plants. The majority of lipids, i.e. glycolipids, was unaltered among the different growth conditions (Figure 3.12 A). In conclusion, no clear light-dependent effect on the composition of glyco- and phospholipids were found in response to the different growth conditions, Therefore, differences in the lipid composition as key player for the observed membrane flexibility was rather unlikely.

3.3.1.6 Quantification of PSII, PSI and Cyt b_6f

The relative amounts of grana and stroma lamellae to the thylakoid membrane were not correlated with changes in the lipid composition of the thylakoid membrane. In fact, the organization of the membrane as grana or stroma lamellae is more connected to lateral segregation of complexes of the photosynthetic electron transport chain. As described in the introduction, PSII and its antenna is localized in the grana regions, whereas PSI can only be found in the grana margins and the stroma lamellae. The growth phenotype of plants grown under different light conditions differed, indicating differences in the composition of the components involved in the photosynthetic electron transport. For this reason, PSII, PSI and the Cyt b_6f complex, were quantified in plants from different growth light conditions on basis of their activity in isolated thylakoids, derived from spectrophotometric measurements. For methodological details see section 2 “Material and methods”.

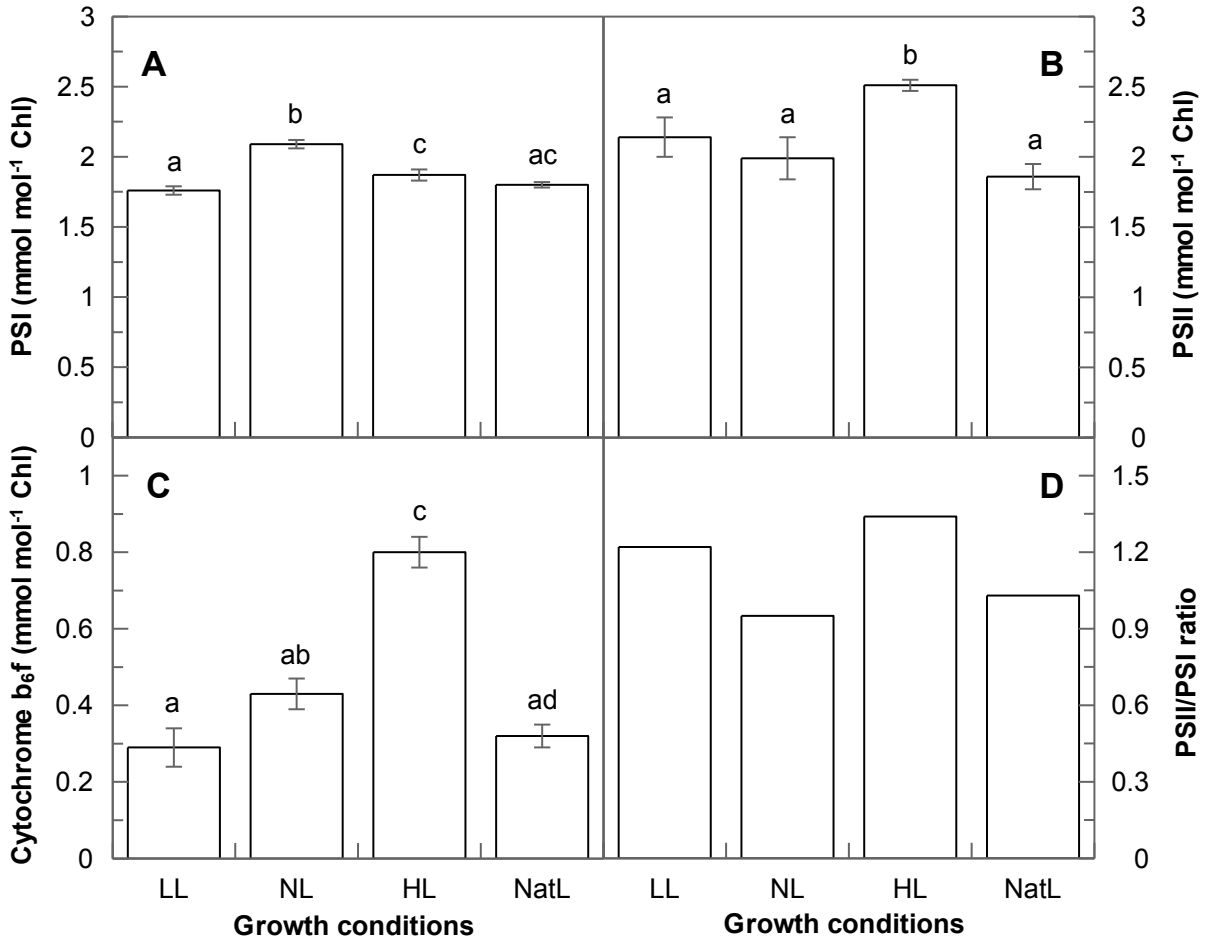

Figure 3.13 Components of the photosynthetic LET chain; (A) PSI, (B) PSII, and (C) Cyt b_6f. Amounts are given in mmol protein complex per mol Chl. Significant differences are indicated. (D) PSII/PSI ratio.

No pronounced differences in the PSI and PSII content on Chl basis were determined among plants from different growth conditions (Figure 3.13). In general, the amount of PSI (1.7 to 2 mmol per mol Chl) was slightly lower compared to that of PSII (2.0 to 2.5 mmol per mol Chl) giving rise to PSII / PSI ratios between 1.0 and 1.4 (Figure 3.13 D). In NL plants, significantly more PSI was found in comparison to other growth light conditions (Figure 3.13 A), whereas PSII was most abundant in HL plants (Figure 3.13 B). NatL plants showed PSI amounts comparable to LL and HL, but lower amounts of PSII compared to HL. In contrast, the amount of Cyt b_6f varied strongly (in the range from 0.3 to 0.8 mmol Cyt b_6f per mol Chl) and showed a positive correlation with increasing growth light intensity. In HL plants, about 2-3 fold higher levels of Cyt b_6f were determined in comparison with plants from all other growth conditions (Figure 3.13 C). This particular response of the Cyt b_6f content to different growth light intensities has been reported before (Leong and Anderson, 1984). The low Cyt b_6f content determined for NatL plants thus suggests a rather LL acclimated electron transport chain at least on basis of the abundance of protein complexes. Fluctuating light conditions include HL and LL periods likewise, hence the resulting NL-like stoichiometry of LET protein complexes in NatL grown plants resembled an acclimation towards both conditions.

3.3.1.7 Pigment composition

Acclimation to different growth light conditions should further result in different pigment composition, mainly related to changes in the PSII antenna size. Therefore, the pigment composition of leaves from plants grown under different growth light conditions was analyzed via HPLC (Figure 3.14). Changes in the PSII antenna size should be reflected by changes in the amount of pigments bond specifically by antenna proteins or RC proteins, though parallel changes in the PSII / PSI ratio will superimpose such changes. In particular, the Chl a/b ratio is a reliable indicator of the accumulation of antenna proteins, since Chl b is bound by antenna proteins only, so that an increase of the Chl a/b ratio can be expected upon reduction of the PSII antenna size. In line with this prediction, LL plants showed the lowest Chl a/b ratio of 3.5 and the Chl a/b ratio increased with increasing growth light intensities (Figure 3.14 E). NL plants showed a slightly higher Chl a/b ratio of about 3.6, whereas a more pronounced increase was found for HL plants (Chl a/b ratio of 4.5). In NatL plants, a similar Chl a/b ratio as in NL plants was determined, indicating a medium-large antenna size.
The acclimation to different growth light intensities was also reflected on the level of carotenoids. Nx, which is exclusively bound to one specific binding site in LHCII, showed highest accumulation in LL grown plants (34 mmol per mol Chl), while 31-32 mmol Nx per mol Chl were found for plants from other growth conditions (Figure 3.14 A). This 10 % higher Nx level in LL plants again indicates a higher number of LHCII in these plants compared to plants from the other growth conditions. The amount of Lut, however, was similar under all growth light conditions, and ranged from 90 mmol per mol Chl in NL plants to 94 mmol per mol Chl in HL plants (Figure 3.14 B). Lut is bound to all antenna proteins of both photosystems, and occupies two binding sites in LHCII and one binding site in LHCI. Therefore, the amount of Lut was three times higher than the relative amount of Nx, when normalized on a Chl basis (Figure 3.14 B).

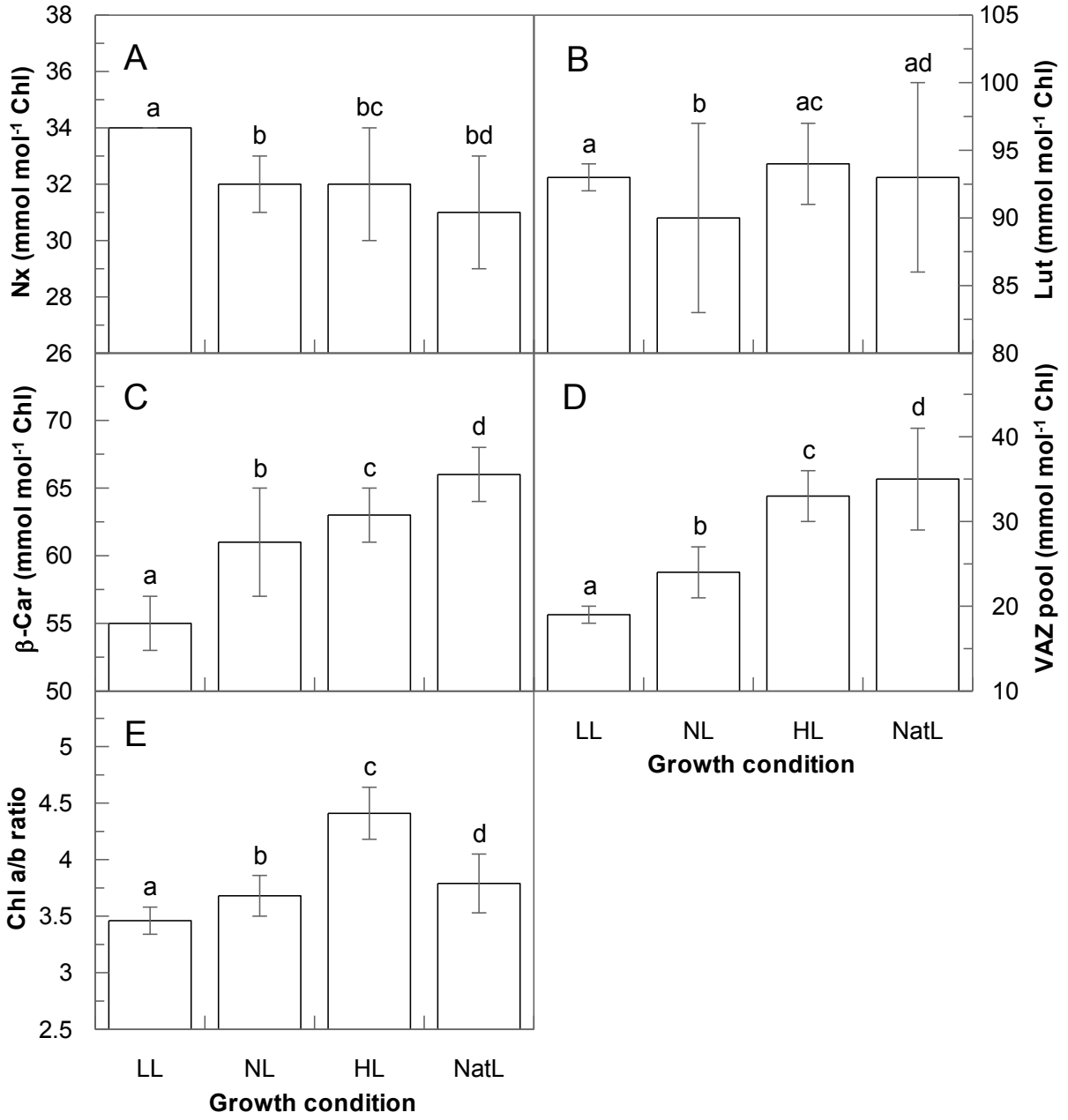

Figure 3.14 Pigments (mmol pigment per mol Chl). (A) Neo, (B) Lut, (C) β-Car, (D) Xanthophyll pigment pool size, Vx + Ax + Zx (E) Chl a/b ratio in LL, NL, HL, and NatL plants. Mean and standard deviation of at least 35 samples are shown. Significant differences are indicated.

β-Car is bound to the RCs of both PSII and PSI, and thus is an indicator of the photosystem content. As expected, LL plants showed the lowest β-Car content (55 mmol β-Car per mol Chl), while increasing amounts were determined with increasing growth light intensities (NL plants: 61 mmol β-Car per mol Ch; HL plants: 63 mmol β-Car per mol Ch). However, the highest amount of β-Car was found in NatL plants (65 mmol per mol Chl), which does not correspond to the rather low Chl a/b ratio (Figure 3.14 E) and the RC content (Figure 3.13) and may thus rather be related to the low PSII / PSI ratio.

The pool size of the xanthophyll cycle pigments Vx, Ax and Zx (= VAZ-pool) serves as a general indicator of light acclimation, since the VAZ pool size is typically positively correlated

with high light stress. In agreement with this notion, LL plants showed the lowest VAZ pool size of 20 mmol per mol Chl. With increasing growth light intensity, the size of the VAZ pool increased to 25 mmol per mol Ch in NL plants, over 33 mmol per mol Ch in HL plants, to 35 mmol per mol Chl in NatL plants (Figure 3.14 D), and thus showed a similar trend as observed for the β-Car content (Figure 3.14 C).

No pronounced differences in the amount of Nx and Lut were found among plants from different growth conditions, however the amount of Nx decreased with increasing growth light intensity and was lowest in NatL grown plants. On the contrary, the amount of β-Car and the VAZ pool size increased with increasing growth light intensity and were highest in NatL grown plants. The chlorophyll a/b ratio indicated similar antenna size of NL and NatL grown plants.

3.3.1.8 Summary of morphological and structural properties

The following table (Table 3.2) provides an overview over the morphological and structural properties of *Arabidopsis thaliana* wild type plants grown under constant LL, NL, and HL plants, and natural fluctuating light grown NatL plants. Within the table, a color code provides information about similarities or differences among the different growth conditions. Each growth condition has its individual color (LL: yellow, NL: orange, HL: red, NatL: green). Similarities among different growth conditions are indicated by the same color.

The phenotype of Arabidopsis plants altered with different growth light conditions in the leaf size and rosette density and diameter (Figure 3.3). NatL plants showed NL-like plant growth. However, the leaf thickness was comparable in LL and NL plants, as well as in HL and NatL plants, where leaf thickness was increased two-fold (Figure 3.5 and 3.6). With increasing growth light intensity, the fresh weight per leaf area increased and was highest in NatL grown plants, whereas the dry weight to fresh weight ratio was unaltered among the different growth conditions (Figure 3.4). The lipid composition was largely unaltered, and the observed differences did not show a specific light dependent pattern (Figure 3.12).

The thylakoid membrane structure altered depending on the growth conditions, with higher degree of grana stacking in low light conditions (Figure 3.9 B). With increasing growth light intensity, the number of grana decreased. NatL grown plants showed mostly HL-like thylakoid membrane structure (Figure 3.8). Thick grana stacks (LL and NL) were unable to undergo structural changes in the short-term upon illumination with high light, whereas HL and NatL grown plants showed an unstacking of the grana stacks. NatL plants showed additionally partial restacking of the membranes upon 10 minutes of redarkening after illumination. The change in the height of grana stacks was accompanied by a change in width in NatL plants, however a significant change in the grana width could not be observed for the other growth conditions (Figure 3.11). The amount of Chl per chloroplast decreased

with increasing growth light conditions and was comparable in LL and NL plants, and in HL and NatL grown plants (Figure 3.6 D).

Table 3.2 Summary of differences and similarities among plants from different growth conditions concerning their leaf morphology, chloroplast structure and protein and pigment content. Individual colors are provided for each growth condition (LL = yellow, NL = orange, HL = red, NatL = green). Similarities between growth conditions are indicated by using the same color. FW: fresh weight, DW: dry weight, Neo: Neoxanthin, Lut: Lutein, β-Car: β-carotene, VAZ: xanthophyll cycle pool pigments.

		LL	NL	HL	NatL
Leaf morphology	Thickness				
	FW per cm²				
	DW/FW (%)				
	No of Chloroplasts				
	Lipid composition				
Chloroplast and thylakoid membrane	Grana structure				
	Grana Unstacking				
	Grana Restacking				
	Change in width				
	Chl/Chloroplast				
Protein complexes	PSII				
	PSI				
	Cyt b_6f				
Pigment composition (mmol pigment per mol Chl)	Chl a/b				
	Neo				
	Lut				
	β-Car				
	VAZ				

PSII and PSI amounts were mainly unaltered among the different growth conditions. However the amount of cyt b_6f was strongly increased in HL plants, compared to the other growth conditions (Figure 3.13).

The pigment composition was diverse and differed dependent on the respective carotenoid. No major differences were found in the amount of Nx and Lut among the different plants (Figure 3.14 A, B), while the amount of β-Car and VAZ pool pigments increased with increasing growth light intensity and were highest in NatL grown plants (Figure 3.14 C, D). The Chl a/b ratio increased with increasing growth light intensity in accordance with a decrease in the amount of LHCII per PSII RC. NL and NatL grown plants showed similar Chl a/b ratios, indicating a comparable antenna size (Figure 3.14 E).

NatL plants were similar to HL grown plants at the level of leaf morphology and thylakoid membrane organization and dynamics. However, the amount of Cyt b_6f and the Chl a/b ratio indicate NL-like features of electron transport, including LHCII. Simultaneously, the amount of protective carotenoids, i.e. β-Car and VAZ pool, were increased in NatL grown plants.

3.3.2 CO_2 assimilation and photosynthetic electron and proton transport

The impact of different growth light regimes on photosynthetic performance was investigated in intact leaves by applying gas exchange measurements and different spectroscopic approaches.

3.3.2.1 Photosynthetic CO_2 assimilation

Light response curves were measured to characterize the key parameters of photosynthetic CO_2 assimilation. These measurements could not be conducted for LL plants, because the leaves were too small for the leaf clamp, which had to be used for the experiment. Mismatching of the reference and sample cuvette was the consequence, making measurements impossible.

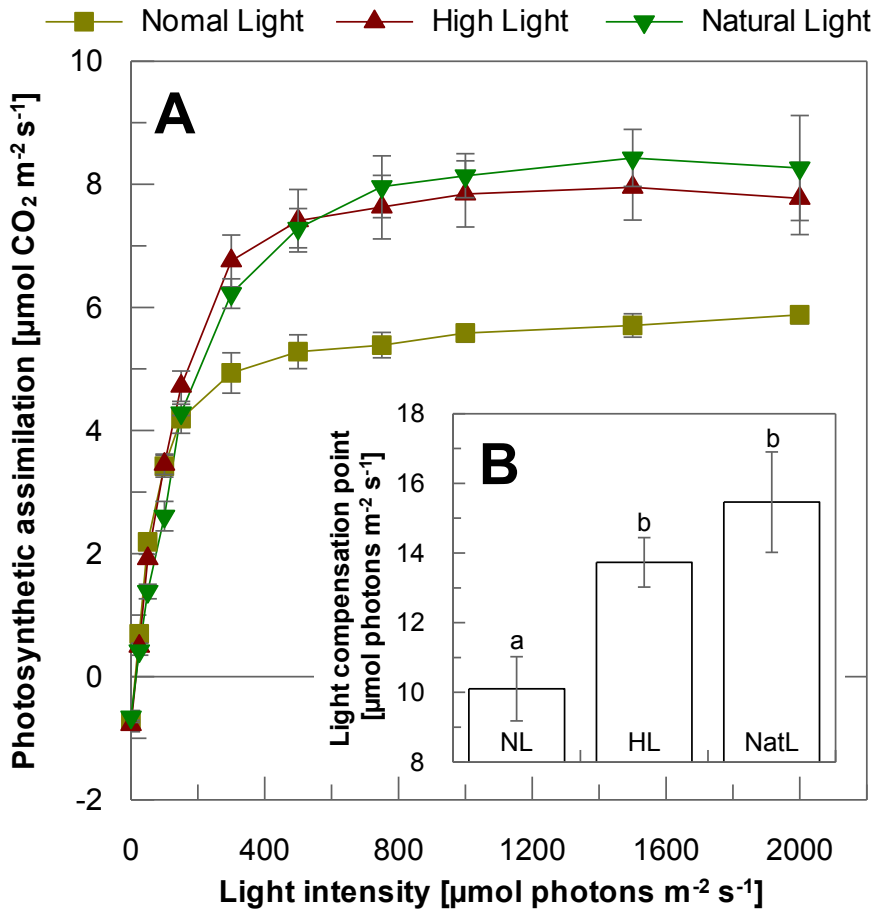

Figure 3.15 (A) Light response curves of NL, HL, and NatL grown plants, in the range of 0 to 2000 µmol photons m^{-2} s^{-1} and (B) Light compensation point calculated from fitted assimilation curves. Mean and standard errors are shown. Significant differences are indicated. Due to experimental restrictions, LL plants could not be measured.

Therefore, only data for NL, HL and NatL plants were determined. For NL plants, the maximum photosynthetic assimilation rate of about 5 µmol CO_2 m^{-2} s^{-1} was reached at a light intensity of 500 µmol photons m^{-2} s^{-1}. Above this intensity, only a slight further increase was detectable (Figure 3.15). In contrast to that, HL and NatL plants both showed a maximum photosynthetic assimilation rate of about 8 µmol CO_2 m^{-2} s^{-1}, which was reached at about 500

µE in HL plants and at 700 µmol photons m^{-2} s^{-1} in NatL plants (Figure 3.15). Below 400 µE, the assimilation rate in HL plants increased somewhat faster in response to light intensities than in NatL plants, though the maximum value was similar in both cases. In relation to the growth light intensities (NL: 100 µE; NatL: mean value of 150 µE), the saturation of assimilation was reached at higher light intensities in NL (500 µE) and NatL (700 µE) plants. In HL plants, however, the maximum assimilation rate was reached at the growth light intensity of 500 µmol photons m^{-2} s^{-1}. This indicates that photosynthesis in HL plants was nearly light-saturated during growth, whereas NL and NatL plants did not use the full photosynthetic capacity during growth. By fitting the assimilation curves as a single exponential increase, the light compensation points for NL, HL, and NatL plants were calculated (Figure 3.15 B). In NL plants, the light compensation point was lowest with about 10 µmol photons m^{-2} s^{-1}. HL plants, which had to cope with five times higher light intensities than NL plants, showed a slightly, but significant higher compensation point of about 13.5 µmol photons m^{-2} s^{-1}. NatL plants showed the highest light compensation point of about 15 µmol photons m^{-2} s^{-1}, which was, however, statistically not significantly different from that of HL plants (Figure 3.15 B). This high light compensation point of NatL plants suggest, that rather transient high light intensities up to 1,500 µE (see section 2.1) than the mean growth light intensity (150 µmol photons m^{-2} s^{-1}) determines the light compensation point.

3.3.2.2 PSII oxidation state

Apart from the overall CO_2 assimilation rate, the redox state of the photosynthetic electron transport chain is an important indicator for the acclimation of photosynthesis to different light conditions. At the level of PSII, the fraction of so-called open RCs is defined by the parameter qL, which can be derived from Chl fluorescence measurements (Kramer et al., 2004b). qL is proportional to the fraction of oxidized Q_A and therefore represents the fraction of active or “open” PSII RCs and hence indicates the reduction state of the PSII acceptor side.

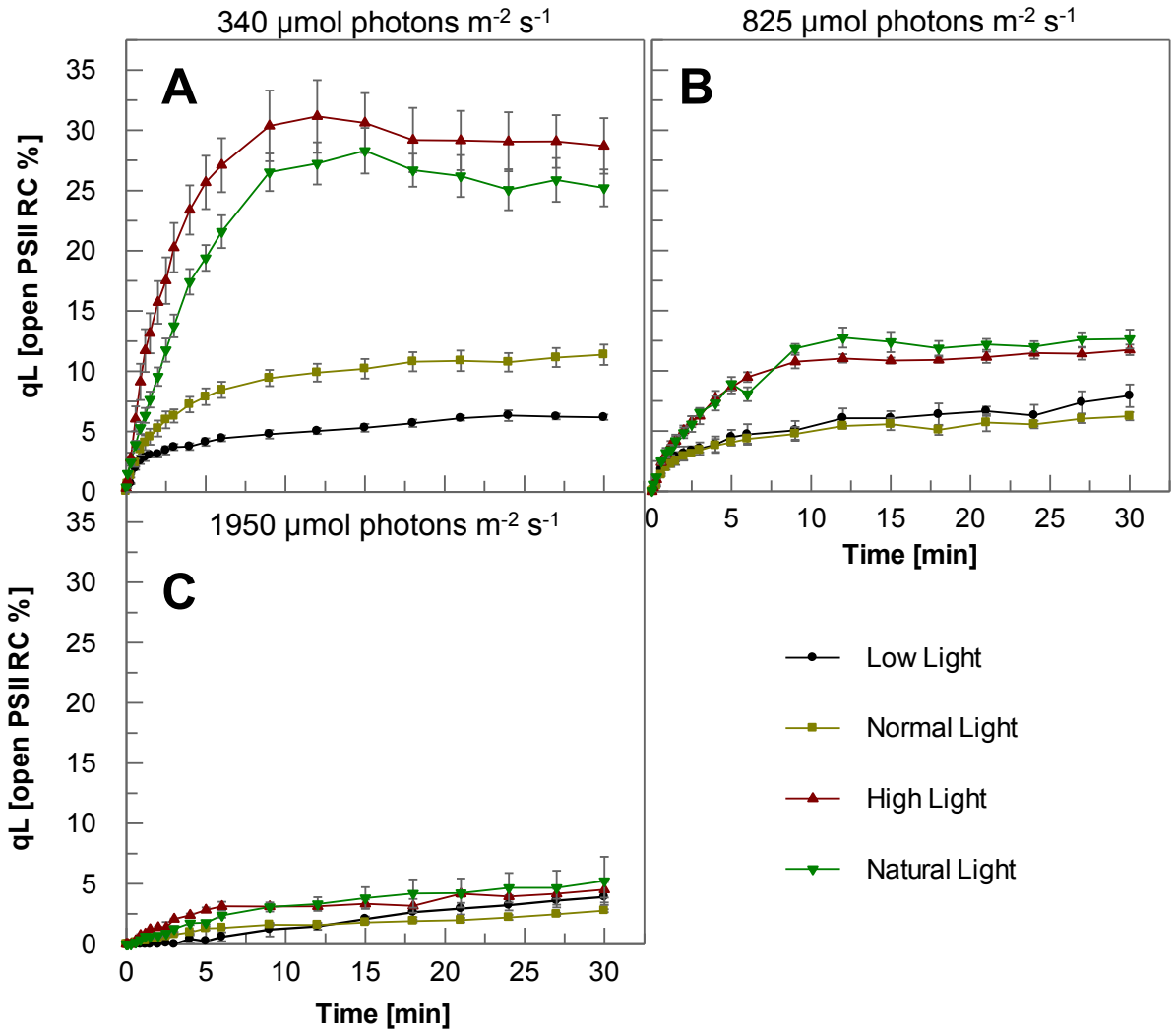

Figure 3.16 Amount of open PSII RC (qL) in percent of total amount of PSII RC during 30 minutes of illumination. LL, NL, HL, and NatL plants were illuminated. Leaves were illuminated with (A) 340 µmol photons m^{-2} s^{-1}, (B) 825 µmol photons m^{-2} s^{-1}, and (C) 1950 µmol photons m^{-2} s^{-1} actinic light intensity. Mean and standard deviation of six independent samples are shown.

qL was determined at three representative light intensities of 340, 825 and 1950 µE, to obtain information about the redox state of the electron transport chain at moderately and highly saturating light intensities (Figure 3.16). At 340 µmol photons m^{-2} s^{-1}, a light intensity just below the saturation of CO_2 assimilation (Figure 3.15), HL plants showed the largest fraction of open PSII RC (30 %) followed by NatL plants with approximately 25 % of open PSII RC, while In NL and LL plants, qL was decreased to 10 % and 5 %, respectively (Figure 3.16 A). This indicates, that particularly in LL plants the PQ pool (and hence Q_A) is almost fully reduced at 340 µmol photons m^{-2} s^{-1}. As expected, qL remained at this low level in LL plants at 825 µmol photons m^{-2} s^{-1}, whereas qL was reduced in all other plants (Figure 3.16 B). While qL in NL plants dropped to the same low level (5 %) as in LL plants, the fraction of open PSII RC was reduced to about 10 % in HL and NatL plants. Obviously, the PQ pool is still not fully reduced in HL and NatL plants at this light intensity though CO_2 assimilation is already saturated. At light intensities that strongly exceed the intensity required for saturation

of CO_2 assimilation (here: 1950 µmol photons m^{-2} s^{-1}), qL remained at low levels (< 5 %) in plants from all growth light conditions (Figure 3.16 C). Only during the initial 5 minutes of illumination, a faster increase in qL was detectable in HL and NatL plants, but similar values were reached after about 20 min of illumination in all plants. In contrast to the two other light intensities, no clear saturation of qL was visible at longer illumination time, so that qL slowly increased to values of about 5 % at the end of the illumination period of 30 min. It should be noted, that this slow increase might be an artefact related to the very high light intensity rather than representing a real increase of the fraction of open centers, e.g. due to activation of photoprotective mechanisms.

3.3.2.3 Rates of linear electron transport (ETR)

The determination of the PSII quantum yield (Φ PSII) further allowed an estimation of ETR and thus provides information of overall electron transport from PSII to PSI in plants from the different growth conditions. ETRs were derived from the same curves as used for qL determination (Figure 3.16) and the results are summarized in Figure 3.17.

In general, the ETR increased with increasing actinic light intensity in plants from all growth conditions. The ETR in LL plants increased from 20 (at 345 µE) to 40 µmol electrons m^{-2} s^{-1} (at 825 µE and 1950 µE), while in NL plants ETRs of 40 µmol electrons m^{-2} s^{-1} were determined at all actinic light intensities. In contrast, the ETR in HL plants increased from 70 (at 345 µE) to 80 µmol electrons m^{-2} s^{-1} (at 825 µE and 1950 µE) and in NatL plants from 60 (at 340 µE) to 80 µmol electrons m^{-2} s^{-1} (at 825 µE). At the highest light intensity (1950 µE) the ETR was again reduced to 60 µmol electrons m^{-2} s^{-1} in NatL grown plants.

The generally higher ETR in HL and NatL grown plants in comparison with LL and NL plants indicates a higher quantum yield in HL and NatL plants, consistent with the larger fraction of open RCs (qL) determined above (Figure 3.16). The increase of the ETR at an actinic light intensity of 825 µE implies that the low fraction of open PSII RCs (Figure 3.16) did not limit LET, in agreement with the literature (Walters, 2005). No further acceleration in electron transport was observed when using 1950 µmol photons m^{-2} s^{-1}, compared to 825 µmol photons m^{-2} s^{-1}, indicating a saturation of the linear electron transport at 825 µmol photons m^{-2} s^{-1}.

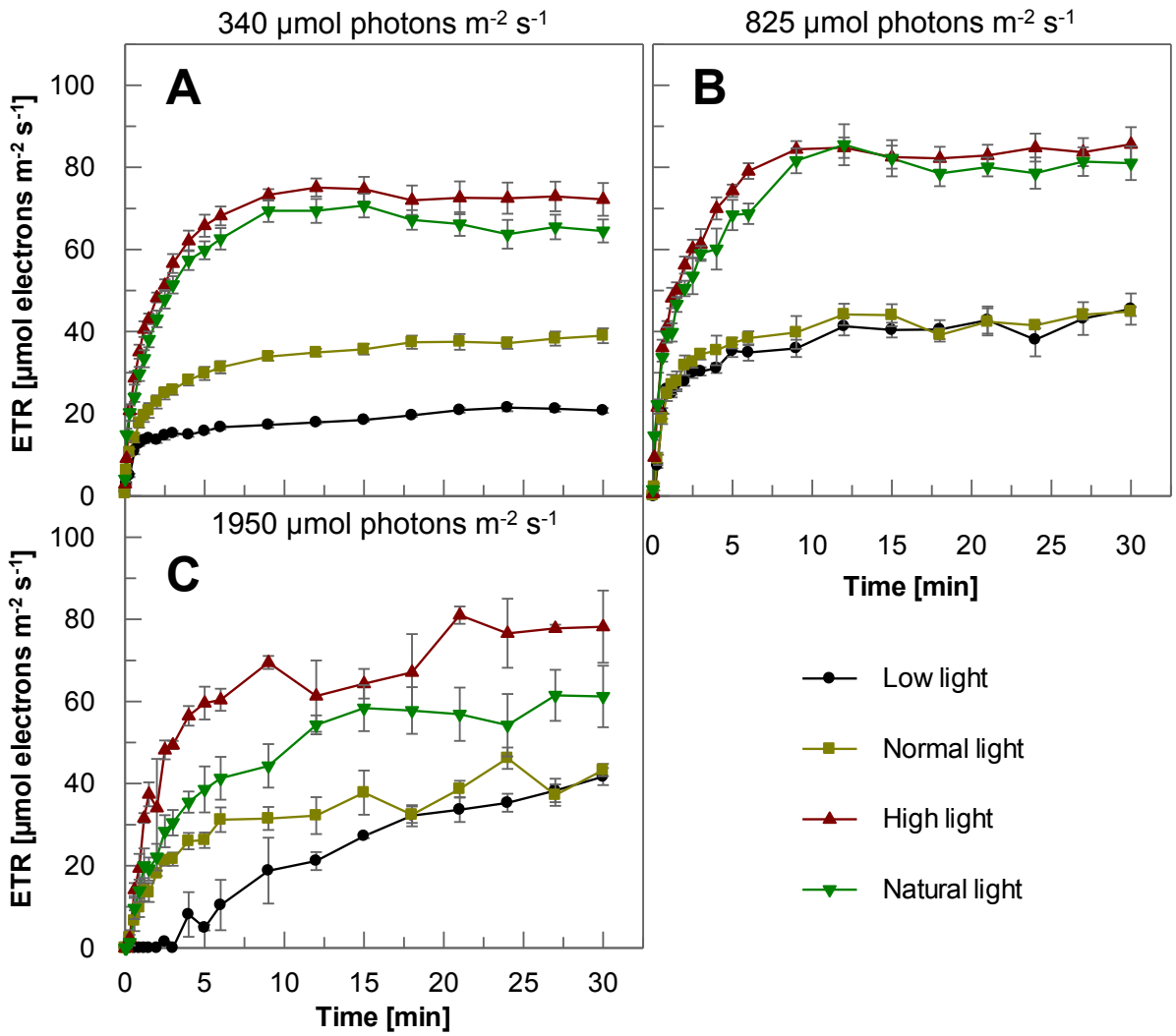

Figure 3.17 Electron transport rates (ETRs) of LL, NL, HL, and NatL plants illuminated with 340 (A), 825 (B), and 1950 (C) µmol photons m^{-2} s^{-1} for 30 minutes. Mean and standard error of at least three independent samples are shown.

3.3.2.4 PSI oxidation state

The redox state of PSI at a given actinic light intensity reflects the ratio of PSI oxidation (due to excitation) and reduction (due to linear electron flow from PSII), so that highly oxidized PSI indicates a limitation of PSI re-reduction by electrons provided from linear electron transport through Cyt b_6f. Therefore, PSI is typically more reduced at low light intensities and more oxidized at high light intensities. The light intensity at which the transition to a high oxidation state of PSI occurs is thus an indicator for the acclimation of linear electron transport to different light intensities.

At low light intensity (Figure 3.18, 53 µmol photons m^{-2} s^{-1}), a relatively high oxidation state of PSI (about 20 %) was observed in LL and NatL plants, while the PSI pool of NL and HL plants was almost completely reduced at this light intensity (Figure 3.18). Generally, with increasing light intensity the fraction of oxidized PSI increased in all plants, but clearly different light dependencies were found for the different plants. At 166 µmol photons m^{-2} s^{-1}, LL and NL plants showed the highest inactivation of PSI among all plants, with 80 % and

60 %, respectively, followed by NatL plants (45 %) and HL plants (20 %). At further increasing light intensity, NatL plants showed similar PSI oxidation states as HL plants, and LL plants showed similar PSI oxidation states as NL plants. However, at all higher light intensities (> 166 photons m^{-2} s^{-1}), HL/NatL plants showed significantly lower PSI oxidation states than LL/NL plants (Figure 3.18). At 340 µmol photons m^{-2} s^{-1} the PSI oxidation state in HL and NatL was in the range of 60 %, while values of 90 % and 80 % were determined in LL and NL plants, respectively. At 825 µmol photons m^{-2} s^{-1} the oxidation state of PSI in HL and NatL plants increased to 80 %, and to 90-95 % in LL and NL plants. At the highest light intensity (1950 µmol photons m^{-2} s^{-1}) LL and NL plants showed 95 % oxidation of PSI, as opposed to HL and NatL, where about 90 % oxidized PSI was found. The similarity of LL and NL plants as well as of HL and NatL plants at the three highest light intensities is in line with the observations for the PSII oxidation state (Figure 3.16) and the electron transport rates (Figure 3.17). It is worth to note, however, that the level of PSI oxidation in NatL plants was similar to those of LL plants at low light intensities, but similar to HL plants at higher light intensities. This suggests that NatL plants share properties of both LL and HL plants, which likely reflects the ability of NatL plants to efficiently cope with a broad variety of light intensities.

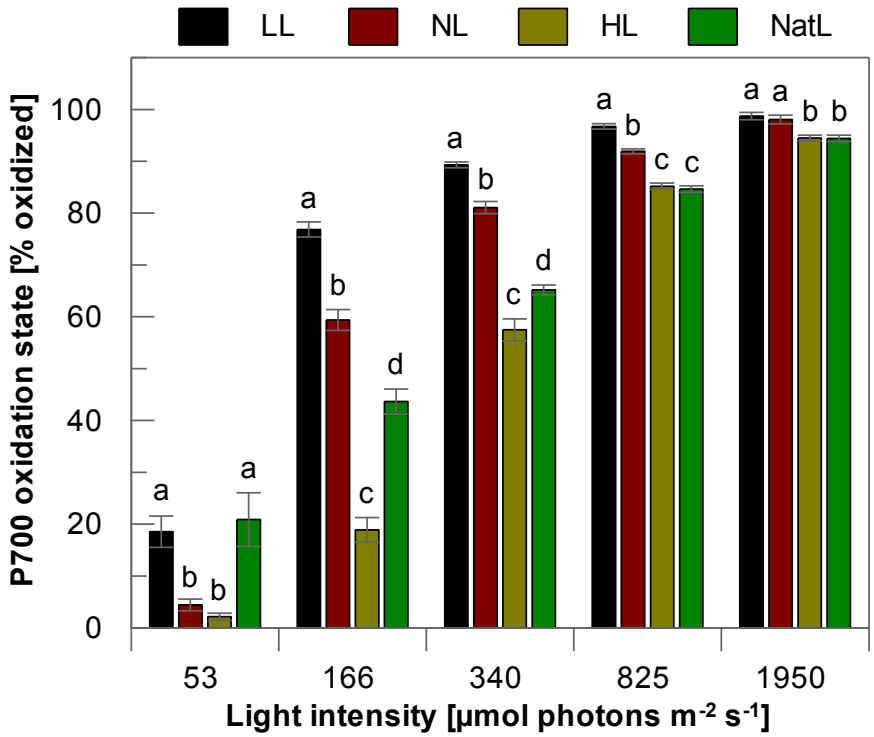

Figure 3.18 P700 oxidation state in LL, NL, HL, and NatL plants at five different illumination intensities. The P700 oxidation state is an indicator for the relative amount of oxidized, closed, and therefore inactive PSI RC in relation to the whole PSI RC pool. Mean and standard error of at least five independent samples are shown. Significant differences are indicated.

3.3.2.5 Chl a fluorescence induction (OJIP transients)

A general estimation of the characteristics of electron transfer processes and their according rates is provided in the so called OJIP measurements (Stirbet and Govindjee, 2011). In this method, the dynamics of the Chl a fluorescence increase from F_0 to Fm is monitored within two seconds of illumination at a time resolution of 10 µs. Different transient phases in the overall Chl fluorescence rise can be distinguished, as shown in Figure 3.19. In this experiment, only the increase to the P level (= Fm) was measured, while the subsequent fluorescence decay phases, termed S, M and T, were not analyzed. In short, the O-J phase is termed photochemical phase, since its kinetics is strongly dependent on the intensity of the applied light. States J-I-P were shown to be strongly dependent on the temperature, thus termed as thermal phase. O-J kinetics contain information about the reduction of Q_A in PSII. The further reduction of the PQ pool can be interpreted in the J-I rise, where at the plateau of the I phase, electrons are transferred onto PC. Finally, the transfer to the final acceptor in PSI is shown in the I-P phase. In summary, the kinetics of the different transitions reflect the reduction of the electron transfer chain at different levels.

The OJIP transients determined in LL, NL, HL, and NatL plants are summarized in Figure 3.19 A. The overall reduction was fastest in LL plants. This was true for both, the intra-PSII transfer, within PSII (Figure 3.19 B, O-J), and in particular the inter-PSII transfer, from PSII to the PQ pool (Figure 3.19 C, J-I). Intermediate kinetics were found for NL plants, while HL and NatL plants showed slowest reduction of both Q_A (O-J) and PC (J-I), although a distinct plateau of the I phase was not clearly distinguishable from the J-P transient (Figure 3.19 C).

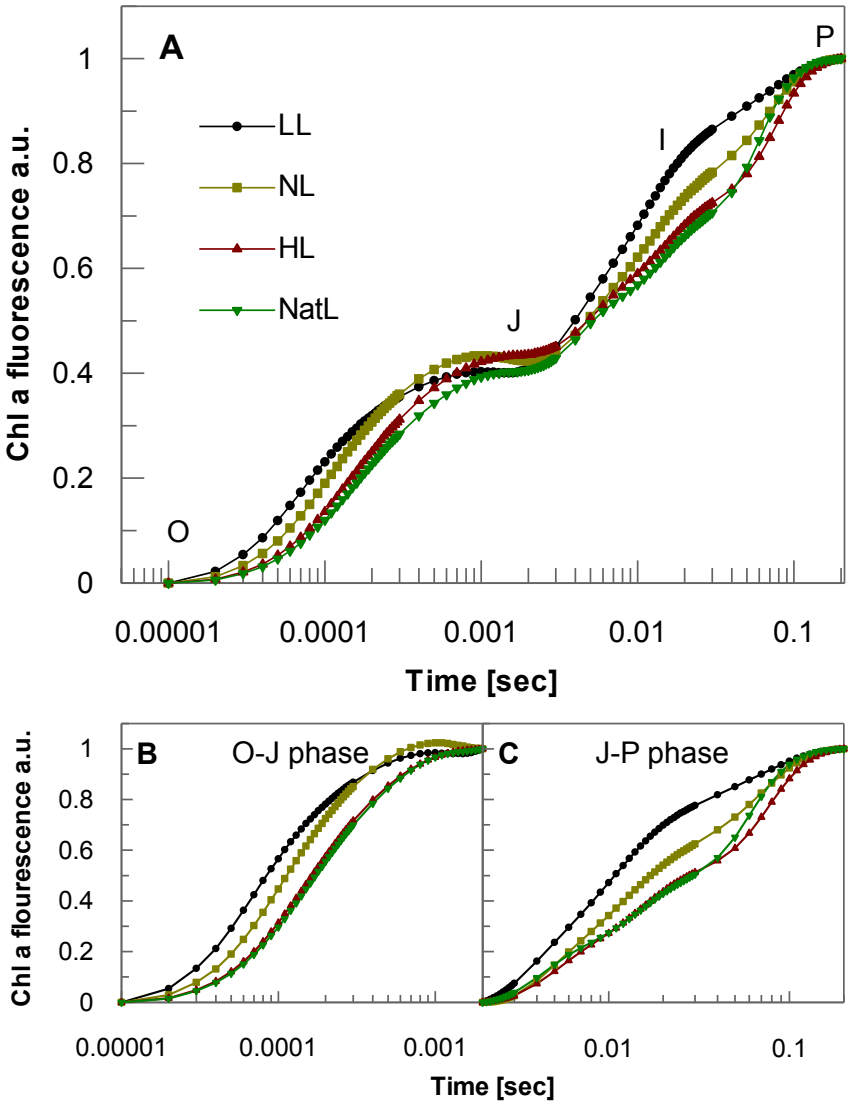

Figure 3.19 (A) Measurements of the Chl a fluorescence transient in LL, NL, HL, and NatL grown plants. (B) Normalization of the total amplitude of all growth conditions from O to the J phase. (C) Normalization of the total amplitude of all growth conditions from J to P phase. Normalization in (B) and (C) allows for direct comparison of the fluorescence kinetics. O, original fluorescence, comparable F_0; J and I, intermediate states; P, fluorescence peak, comparable to F_M. Mean of ten measurements is shown, standard deviation was < 0.04.

The kinetics of Q_A reduction are known to depend on the antenna size of PSII (Malkin et al., 1981) with a larger antenna leading to a faster Q_A reduction. Applied to the acquired data this suggests, that LL plants possess the largest functional antenna, followed by NL plants and finally HL and NatL plants, which showed very similar O-J kinetics (Figure 3.19 B). However, the strict dependence on the antenna size is only given when electron transfer from Q_A to Q_B is blocked, e.g. upon addition of DCMU. The same order of kinetics was found for the J-I-P transient, which is likely determined by the PQ pool size and the amount of Cyt b_6f. The obtained data thus support the view that HL and NatL plants have the highest electron transport capacity from PSII to PSI, and LL plants the lowest, in agreement with the above data (Figure 3.17).

3.3.2.6 Total proton motive force (*pmf*) in dark and light acclimated states

In addition to the electron transport characteristics, key parameters of proton transport were analyzed. For that, spectrophotometric measurements of the light-induced electrochromic shift (ECS) at 515 nm were performed, from which basic information about the proton motif force (*pmf*), the driving force for ATP synthesis, can be derived (see Methods, section 2.8.3 for details). Besides the extent of the *pmf*, the corresponding partitioning in ΔpH and ΔΨ, and also the proton conductance g_{H^+} can be estimated from the P515 measurements (Cruz et al., 2001; Takizawa et al., 2007). In Figure 3.20 the extent of the total *pmf* at three different light intensities is shown for plants grown under the different light conditions.

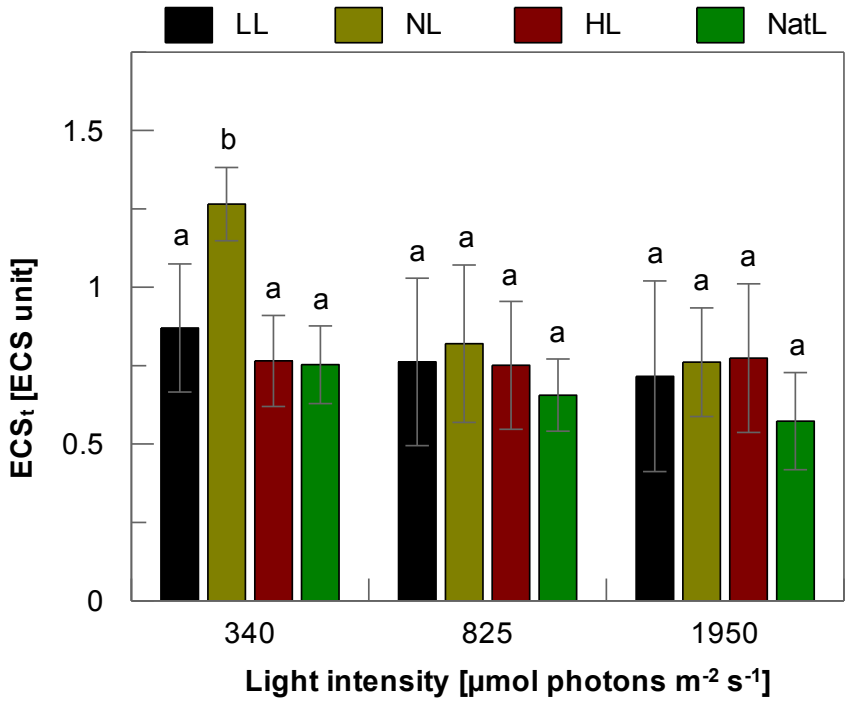

Figure 3.20 Total *pmf* in the light-dark transition, expressed in ECS units. Samples were illuminated with the according light intensity for 30 minutes. Mean and standard deviation of at least five independent samples are shown. Significant differences are indicated.

The total *pmf* in a stable, light acclimated state of photosynthesis was derived from rapid absorption changes during the light-dark transition after 30 minutes illumination, and is expressed as ECS_t normalized on the ECS unit obtained by single turnover flash previous to the measurement. In LL plants, a total *pmf* in the light about 0.8 was found for all actinic light intensities, indicating a saturation of the *pmf* at the lowest intensity used. The same was true for the plants from other growth light conditions, where similar *pmf* was determined for all light intensities. Except for the pmf determined in NL plants at 340 µmol photons m^{-2} s^{-1}, no significant differences among the growth conditions were found. It should be noted, however, that the differences between plants from different growth conditions do not necessarily reflect a proportional difference in the *pmf,* since the ECS signal is based on absorption changes of

carotenoids, so that altered optical properties and differences in the carotenoid content may influence the amplitude of the absorption changes.

More specific information, however, can be derived from further analyses of the ECS signal, providing estimates of the *pmf* partitioning into ΔpH and ΔΨ, the proton conductance of the ATP synthase (gH^+) and the lumen pH.

3.3.2.7 Partitioning of the pmf into ΔpH and ΔΨ

In order to estimate the partitioning of the *pmf* into ΔpH and ΔΨ, the respective dark-interval relaxation kinetics (DIRK) of the ECS signal during the light-dark transition were analyzed,

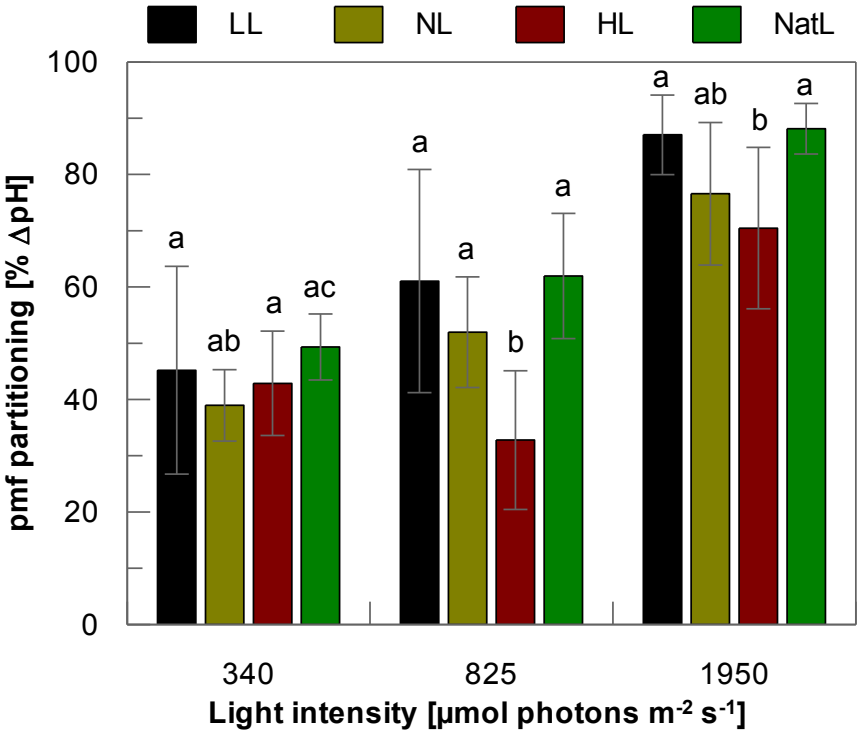

Figure 3.21 Proton motive force partitioning, indicated as percent of ΔpH on ECS_t after 30 minutes of actinic light illumination with 340, 825, and 1950 µmol photons m^{-2} s^{-1}. Partitioning was derived from the same curves which were analyzed for total *pmf* determination (Figure 3.20). Mean and standard deviation of at least five independent samples are shown. Significant differences are indicated.

At 340 µmol photons m^{-2} s^{-1}, the fraction of the total *pmf* stored as ΔpH ranged between 40 and 50 % in plants from all growth conditions (Figure 3.21). With increasing actinic light intensity, the ΔpH fraction increased, except for HL at 825 µmol photons m^{-2} s^{-1}, where a similar partitioning was found in comparison to the lower light intensity of 340 µmol photons m^{-2} s^{-1}. The highest fraction of ΔpH (90 %) was found in LL and NatL grown plants at an intensity of 1950 µmol photons m^{-2} s^{-1}, while somewhat lower fractions were determined for NL (75 %) and HL (70 %) plants (Figure 3.21). Thus, under all light conditions, the *pmf* partitioning in LL and NatL plants was similar and showed the largest fraction of the total *pmf* stored as ΔpH, whereas the lowest contribution of ΔpH relative to the total *pmf* was found in HL plants.

3.3.2.8 Proton conductance and lumen pH

The steady state *pmf* is characterized by a constant influx and efflux of protons into and out of the thylakoid lumen. The influx of protons is dependent on the rate of electron transport, while the efflux is mainly controlled by the activity of the ATPase. A simple non-invasive approach to determine the rate of proton efflux through the ATPase is the proton conductance (g_H^+), which can be derived from the kinetics of the decay of the ECS signal measured at 515 nm after switching off the actinic light. Fitting of this decay with a mono-exponential function thus allows determining the rate constant g_H^+ for proton flux through the ATP synthase.

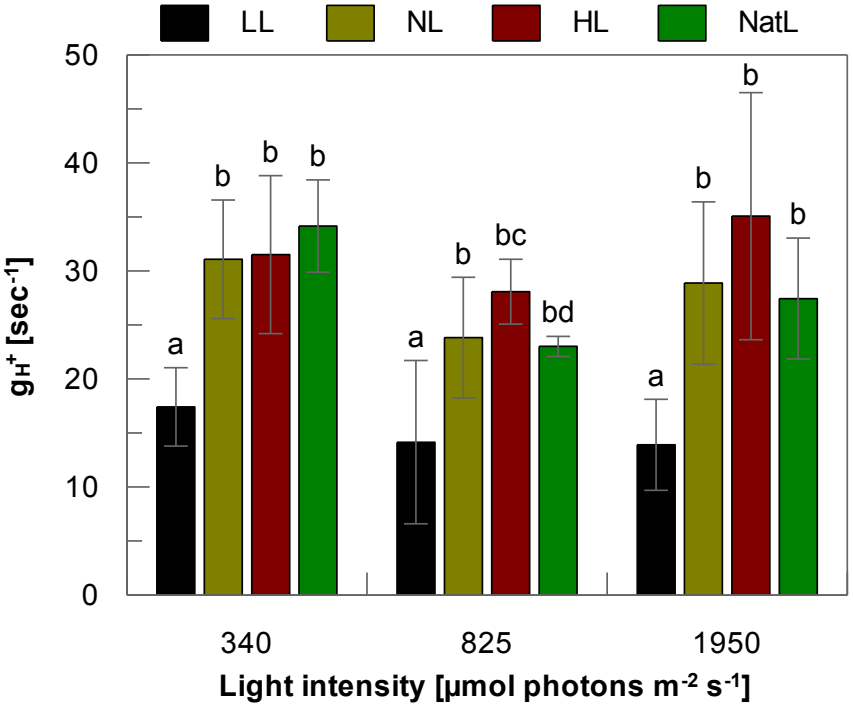

Figure 3.22 Proton conductance (g_H^+) after 30 minutes of illumination in LL, NL, HL, and NatL plants. Same curves analyzed for total *pmf* were used (Figure 3.20). Significant differences are indicated.

In LL plants, g_H^+ was under all actinic light conditions significantly lower than in plants from the other growth light conditions, and reached values between 13 and 17 sec^{-1}. NL, HL and NatL plants did not show statistically significant differences in g_H^+ at either actinic light intensity, and g_H^+ ranged between 25 and 35 sec^{-1}. Thus, proton conductance was about twofold higher in NL, HL and NatL plants as compared to LL plants. This result is in accordance with the differences in the total *pmf* and supports the proportionality of the total *pmf* and g_H^+.

On basis of the total *pmf* and the fraction of the *pmf* stored as ΔpH it is further possible to estimate the lumen pH, when taking into account further assumptions, such as estimates for the pmf_d (112 mV) and the stromal pH (7.8) (for details see (Takizawa et al., 2007).

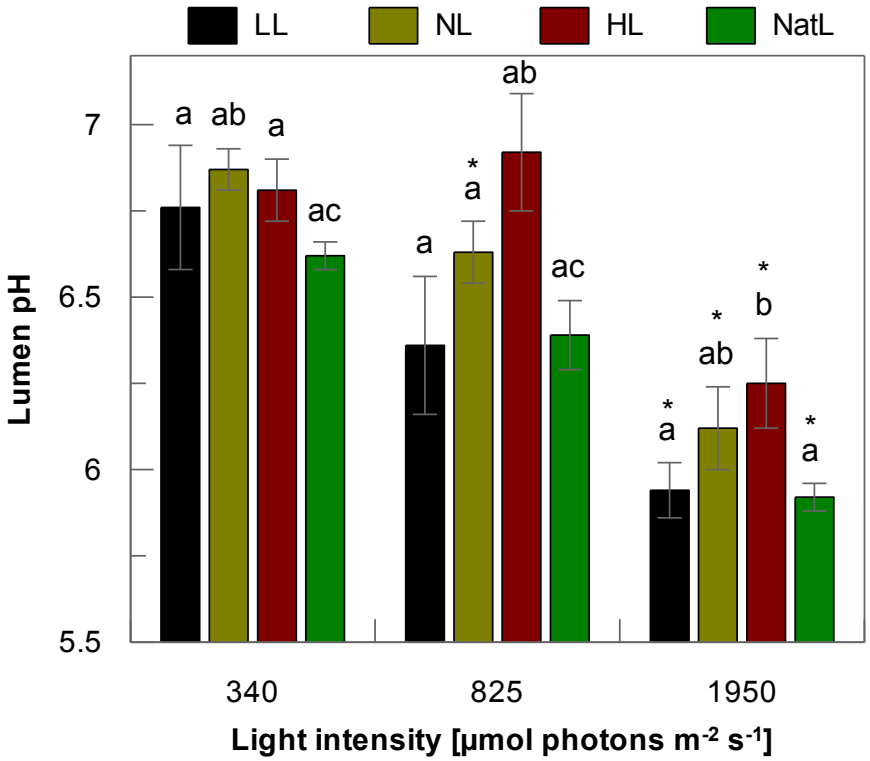

Figure 3.23 Lumen pH after 30 minutes of illumination with 340, 825, and 1950 µmol photons m^{-2} s^{-1} in LL, NL, HL, and NatL plants. Calculations were performed according to (Takizawa et al., 2007). Same curves were analyzed as described previously (Figure 3.21, 3.22). Mean and standard error of at least five independent samples are shown. Significant differences among growth conditions at one light intensity are indicated with letters, significant changes of the growth conditions among different light intensities are indicated with asterisks.

In Figure 3.23, estimates of the steady-state lumen pH at the end of 30 minutes of illumination at 340, 825, and 1950 µmol photons m^{-2} s^{-1} are shown. As expected, the lumen pH decreased with increasing light intensity, though for most conditions no statistically significant differences were found among the plants from different growth conditions. At an actinic light intensity of 340 µmol photons m^{-2} s^{-1}, the lumen pH was calculated with about 6.75 in all plants. At higher light intensities, LL and NatL plants generally showed stronger acidification of the lumen than NL and HL plants. At 825 µmol photons m^{-2} s^{-1}, the lumen pH in LL and NatL plants decreased to 6.5 in contrast to NL and HL plants, where lumen acidification remained nearly unchanged as compared to the lowest light intensity (Figure 3.23). A further decrease in lumen pH was determined at 1950 µmol photons m^{-2} s^{-1}, where the values decreased to pH 5.9 in both LL and NL plants, and to pH 6.1 and 6.2 in NL and HL plants, respectively.

3.3.2.9 Summary of photosynthetic capacity, and electron and proton

According to the observed growth phenotype (see section 3.3), the CO_2 assimilation rate in plants from different growth conditions altered. Higher maximum assimilation rates (P_{max}) were found for HL and NatL grown plants as compared to NL grown plants (Figure 3.15 A).

The higher P_{max} in HL and NatL plants was accompanied by an increased light compensation point as compared to NL grown plants (Figure 3.15 B).

The fraction of open PSII RC (qL) at 340 and 825 µmol photons m^{-2} s^{-1} illumination intensity was higher in HL and NatL grown plants, compared to LL and NL grown plants, however, qL generally decreased with increasing actinic light intensity. At 1950 µmol photons m^{-2} s^{-1}, no differences in the fraction of open PSII RC were found among the different plants (Figure 3.16).

Table 3.3 Summary of the CO_2 assimilation, photosynthetic efficiency, as well as proton motive force. Individual colors are provided for each growth condition (LL = yellow, NL = orange, HL = red, NatL = green). Similarities between growth conditions are indicated by using the same color. P_{max}: maximum CO_2 assimilation rate, LCP: light-compensation point.

		LL	NL	HL	NatL
Photosynthetic efficiency	P_{max}				
	LCP				
	qL				
	ETR				
	P700				
	OJIP				
proton motive force	ECS_t				
	ΔpH portion on *pmf*				
	g_H^+				
	Lumen pH				

In line with a higher fraction of open PSII RC, the ETR in HL and NatL grown plants was increased two-fold at 340 and 825 µmol photons m^{-2} s^{-1}, compared to LL and NL grown plants. Maximum rates of around 90 electrons m^{-2} s^{-1} were measured for HL and NatL grown plants, whereas LL and NL grown plants reached ETRs of 30-40 at 825 µmol photons m^{-2} s^{-1}. NatL grown plants showed characteristic of both, LL and HL grown plants with regard to PSI oxidation at different actinic light intensities. Here, NatL plants showed LL-like, higher PSI oxidation state at lower light intensities, however lower, HL-like maximum PSI oxidation state at higher light intensities (Figure 3.18).

The OJIP data showed fastest Q_A reduction in LL grown plants, and slower Q_A reduction in HL and NatL grown plants. However, the J-I-P transient confirmed the overall higher electron transport capacity of HL and NatL grown plants, which was faster in HL and NatL grown plants, compared to LL and NL grown plants (Figure 3.19).

Measurements on the total *pmf* showed comparable values in NL, HL and NatL grown plants, whereas the total *pmf* in LL plants was decreased by 50 % under all actinic light conditions (Figure 3.20). However, the ΔpH portion of the total *pmf* was higher in LL and NatL grown plants, compared to NL and HL plants (Figure 3.21). As shown for the total *pmf*, the proton

conductance (g_{H^+}) was comparable in NL, HL, and NatL grown plants, and decreased in LL grown plants (Figure 3.22).

With increasing growth light intensity, the lumen pH decreased in all plants, except for HL grown plants, where no differences in lumen acidification between 340 and 825 µmol photons m^{-2} s^{-1} were found (Figure 3.23). LL and NatL grown plants showed the lowest lumen pH upon illumination, which was in line with the *pmf* partitioning.

Overall NatL grown plants were most similar to HL grown plants in most of the analyzed aspects, however NatL grown plants also exhibited features from LL grown plants, as shown in the P700 oxidation pattern and the *pmf* partitioning.

3.3.3 Energy dissipation

The dissipation of absorbed light energy as heat (= non-photochemical quenching, NPQ) comprises different components, which can be activated on different timescale and which differ in the underlying mechanism and molecular requirements. Under most natural conditions, the energy-dependent qE mechanism and the Zx-dependent qZ mechanism represent the dominating NPQ processes that are activated upon short-term acclimation to high light. On basis of the time-resolved fluorescence measurements on Monstera plants, an additional, spillover-based mechanism (q_{SO}) has been characterized in plants acclimated to natural high light conditions. In this chapter, the NPQ properties of Arabidopsis plants grown under different light conditions are characterized, including the critical regulatory factors of NPQ, PsbS and Zx.

3.3.3.1 Quantification of PsbS protein

The PsbS protein is an essential regulator of qE, and the amount of PsbS has been shown to be positively correlated with qE (Li et al., 2000). Two approaches were chosen to obtain information about the amount of PsbS in plants from different growth light conditions: Western Blot analyses of total protein extracts and immunogold labeling of ultrathin leaf sections.

3.3.3.1.1 Western Blot analysis

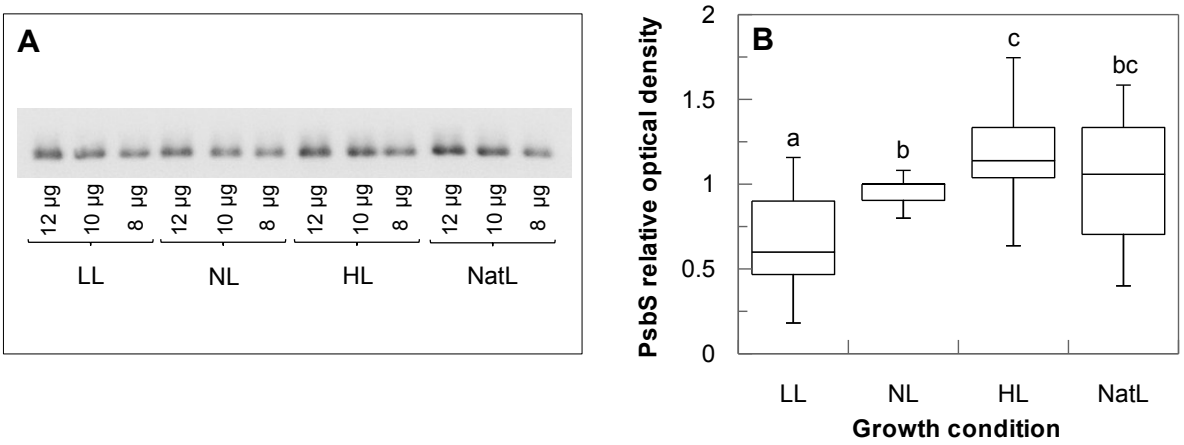

Figure 3.24 Quantification of the PsbS protein via Western Blot analysis. For each growth condition, three different concentrations of total protein extract were loaded. Band intensity was quantified as described in section 2.8 (A) Representative Westernblot used for the quantification (B) Box plot analysis of quantified details. The horizontal line indicates the median, the boxes represent the distribution of 50 % of the data points. Error bars indicate lower and upper quartiles. Five different blots were used for quantification. Significant differences are indicated.

Figure 3.24 summarizes the results of the Western blot analyses. Total protein extract was loaded in three different concentrations (12, 10, and 8 µg) for each growth condition. Only blots with linear correlation of the different protein concentration per growth condition were used for analysis. The normalized quantification is shown in Figure 3.24 B. In LL plants, the amount of PsbS was reduced to 60 % of the levels in NL plants. On the contrary, the PsbS amount was increased in HL plants to 125 % of the levels in NL plants. NatL plants showed slightly higher PsbS amounts than NL plants, but lower amounts than in HL plants. Significant differences were only found for LL and HL plants, but not for NatL plants.

3.3.3.1.2 Immunogold labeling

Immunogold labeling provides information about the localization and amount of the protein of interest. However, the significance of the data strongly depends on the specificity of the antibody and the accessibility of the antibody to the respective epitope. The PsbS specific antibody used here did not show any cross-reaction with other proteins upon immunogold labelling of chloroplasts from the PsbS deficient *npq4* mutant and increased labelling in the PsbS over-expressing line *L17* (Viviana Correa Galvis, unpublished results).

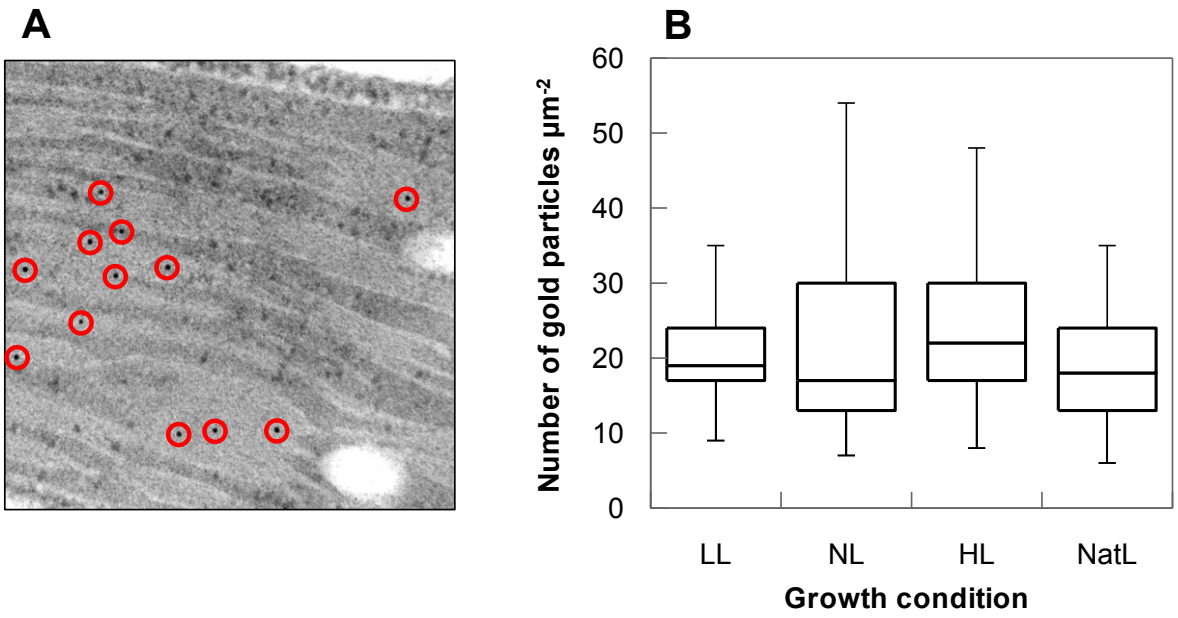

Figure 3.25 Quantification of the PsbS protein via immunogold labeling. (A) Typical transmission electron micrograph of a chloroplast from NatL plants. The thylakoid membranes are shown in light gray, stromal areas in dark gray. The gold particles are located to the thylakoid membrane system (red circles). (B) Box plot showing the amount of gold particles normalized on the area of 1 µm².

The number of gold particles was quantified in TEM images, exemplarily shown for a leaf from NatL grown plants (Figure 3.25 A). In total, 60-80 samples from dark- and light acclimated leaves were analyzed. The gold particles were found to be randomly distributed within the thylakoid membrane in all types of plants, so that no allocation of gold particles to different parts of the membrane, i.e. grana stacks, grana margins or stroma lamellae was possible. Since no differences were found between dark- and light-adapted samples, all data obtained were pooled. On basis of immunogold labeling, no significant differences in the amount of PsbS were found between the different growth conditions (Figure 3.24 B). Independent of the growth conditions, mean values between 17 and 22 gold particles per µm² were found, with an extremely high variation in the amount of gold particles in NL and HL plants (Figure 3.25 B). These results were not in line with the PsbS quantification based on Western blot analysis (Figure 3.24), likely due to general limitations of immungold labeling.

3.3.3.2 Steady state NPQ

As mentioned before, the PsbS protein is required for the activation of the NPQ, more precisely for the qE mechanism of NPQ. In Figure 3.26 the NPQ induction during 30 illumination and NPQ relaxation in a subsequent 30 min dark period is shown for plants grown under different light conditions. During 30 minutes of illumination, not only qE is activated, but also qZ and qI. It has previously been shown, that qE and qZ act in separated quenching centers, termed Q1 and Q2. Q1 has been assigned to quenching in detached LHCII, which is only dependent on the action of PsbS and thus reflects qE. On the other

hand, Q2 is localized in antenna proteins attached to PSII core, where excess energy is quenched in a Zx dependent way, giving rise to qZ (Holzwarth et al., 2009). The photoinhibitory quenching qI is generated in parallel with qZ, but is – in contrast to qE which relaxes within 2-5 minutes and qZ, which relaxes within 5-30 minutes – characterized by very slow relaxation kinetics, and thus irreversible during a 30 min dark relaxation period. For quantification of the different NPQ components, the NPQ amplitude which relaxed within 30 min has been assigned to the sum of qE and qI and the remaining NPQ was assigned to qI. The values derived from these analyses are summarized in Table 3.4.

Figure 3.26 A shows NPQ dynamics of LL, NL, HL, and NatL plants illuminated with 340 µmol photons m^{-2} s^{-1}. LL and NL plants showed similar NPQ dynamics during both, light induction and dark relaxation with a maximum NPQ of 1.3. However the remaining non-reversible NPQ (= qI) was slightly higher in LL plants (0.4) in comparison with plants from all other growth conditions (about 0.2) (Table 3.4). At 340 µmol photons m^{-2} s^{-1}, HL and NatL plants showed significantly higher NPQ induction than LL and NL plants. While NatL plants exhibited a higher maximal NPQ than HL plants (2.4 vs 2.1, respectively), the kinetics of NPQ induction were faster in HL plants (Figure 3.26 A). The increased NPQ in NatL plants could be assigned to an increased qE capacity in comparison with HL plants (Table 3.4)

At 825 µmol photons m^{-2} s^{-1}, a 30-50 % higher maximum NPQ was observed in all plants (Figure 3.26 B, Table 3.4). Again, the induction of NPQ in LL and NL plants was similar. The somewhat higher maximum NPQ value in LL plants (2.3) as compared to NL plants (1.8) was mainly due a linear increase of the NPQ after about 10 min of illumination, which was likely related to photoinhibition, as indicated by the much higher amplitude of qI in LL plants (1.06) than in NL plants (0.77) (Table 3.4). Also HL and NatL plants revealed similar NPQ dynamics at 825 µmol photons m^{-2} s^{-1}, with slightly higher maximum NPQ in NatL (2.8) than in HL plants (2.7) (Figure 3.26 B, Table 3.4). Despite the higher maximum NPQ in HL and NatL plants, the contribution of photoinhibition to the overall NPQ was smaller compared to LL and NL plants, resulting in a much higher capacity for rapidly reversible (qE + qZ) quenching in HL and NatL plants (about 2.2) in comparison with LL and NL plants (about 1.2) (Table 3.4).

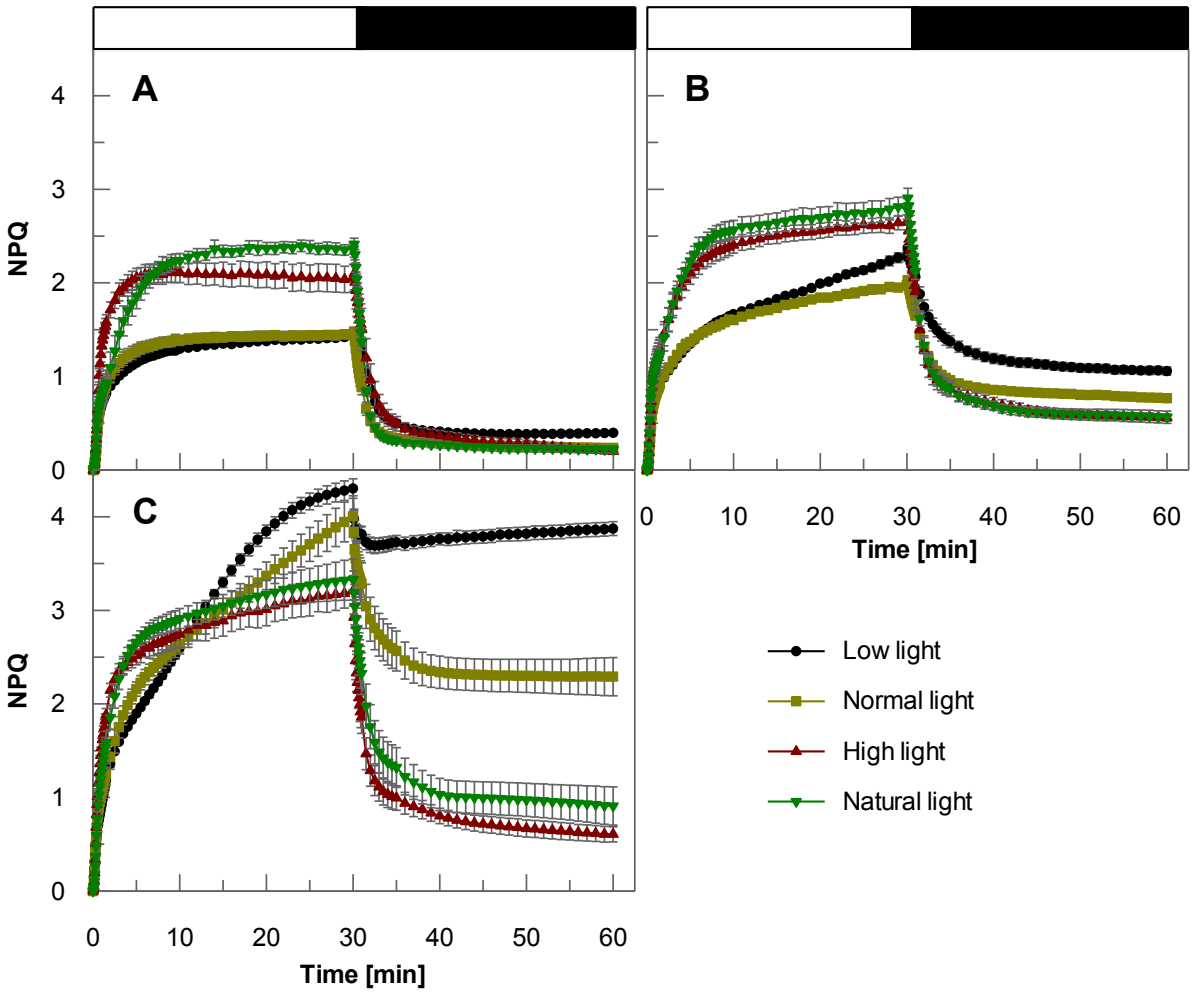

Figure 3.26 NPQ measurements calculated from Chl fluorescence traces measured by a Dual-PAM system. LL, NL, HL, and NatL plants were illuminated with three different actinic light intensities: (A) 340, (B) 825, and (C) 1950 µmol photons m^{-2} s^{-1}. NPQ fluorescence was measured for 30 minutes in the light (indicated by white bars) and a following 30 minute dark period (indicated by black bars). Mean and standard deviation are shown for six independent samples.

A further increase of the actinic light intensity to 1950 µmol photons m^{-2} s^{-1} lead to a further increase in NPQ in plants from all growth conditions. LL plants showed the highest NPQ induction with 4.25, however 80 % of the observed quenching was due to irreversible photoinhibitory qI quenching (3.26C, Table 3.4). NL plants showed a maximum NPQ of 4.0, which was likewise predominantly related to a pronounced increase of the qI component. In contrast, HL and NatL plants showed a similar maximum NPQ of 3.3 and 3.6, respectively, which was predominantly based on qE-type quenching, as can be derived from the rapid dark-relaxation of NPQ. The pronounced increase of rapidly inducible and relaxing quenching in HL and NatL plants can thus be predominantly assigned to an increased qE capacity (Figure 3.26 C, Table 3.4), in agreement with the increased levels of PsbS determined via Western blot analysis (Figure 3.24). The photoprotective effect of a high qE capacity is visible from the much lower qI in HL and NatL plants as compared to LL and NL plants (Table 3.4). The NPQ analyses thus support the view that acclimation to fluctuating light conditions increases the capacity of pH-regulated qE quenching.

The capacity for reversible qE + qZ –type quenching in each growth condition mainly remained unchanged among different illumination intensities, except for LL plants at 1950 µmol photons m^{-2} s^{-1}. Here, the capacity was somewhat reduced, however the used light intensity was 80 x higher compared to the growth light intensity. With increasing growth light conditions, the capacity increased from an NPQ of about 1.0 in LL over 1.4 in NL to an NPQ capacity of 2.6 and 2.8 in HL and NatL plants. Thus, the overall quenching capacity was only determined by the growth light condition, but independent from the actinic light intensity. However, higher actinic light intensities modified the kinetics NPQ induction (compare Figure 3.26 A and B HL). Overall, the amplitude of the NPQ, which increased with increasing growth light intensity, was in line with the biochemically determined PsbS content (Figure 3.24), as also shown in other works (Ballottari et al., 2007).

Table 3.4 Quantitative analysis of different NPQ components. The parameters were calculated from the traces shown in Figure 3.26. qE + qZ represent the reversible components of NPQ in the time frame measured, qI is the irreversible part of NPQ. Mean values +/- SE are shown.

	340 µmol photons m^{-2} s^{-1}		825 µmol photons m^{-2} s^{-1}		1950 µmol photons m^{-2} s^{-1}	
	qE + qZ	qI	qE + qZ	qI	qE + qZ	qI
LL	1.03 ± 0.02	0.40 ± 0.01	1.23 ± 0.02	1.06 ± 0.04	0.83 ± 0.11	3.40 ± 0.13
NL	1.21 ± 0.05	0.23 ± 0.03	1.21 ± 0.06	0.77 ± 0.03	1.71 ± 0.05	2.29 ± 0.16
HL	1.85 ± 0.12	0.2 ± 0.03	2.09 ± 0.07	0.56 ± 0.04	2.60 ± 0.10	0.61 ± 0.08
NatL	2.15 ± 0.07	0.22 ± 0.04	2.23 ± 0.15	0.56 ± 0.07	2.85 ± 0.09	0.98 ± 0.20

The clear discrimination of the qE and qZ components was not possible without detailed kinetics analyses, but it is known that the contribution of qZ to the rapidly relaxing NPQ is rather low and typically in the range of 0.3-0.5 only (Nilkens et al., 2010). However, possible differences in the contribution of Zx to quenching may also be estimated by analyzing the extent and kinetics of Zx formation.

3.3.3.3 Xanthophyll conversion

The conversion of Vx to Zx under the same experimental conditions as used for the NPQ measurements is shown in Figure 3.27. At 340 µmol photons m^{-2} s^{-1}, LL and NatL plants showed similar Vx convertibility (Figure 3.27 A). Within 30 minutes, about 40 % of the VAZ pool pigments were converted to Zx. The conversion was relatively slow (half rise time of about 10 min) in comparison to NL and HL plants (half rise time of about 5 min). Moreover, about 50 % of the VAZ pool was convertible to Zx in NL and HL plants (Figure 3.27 A). The same characteristics of Zx formation was also visible upon illumination at 850 µmol photons m^{-2} s^{-1} (Figure 3.27 B). However, more pronounced differences among plants from different growth conditions were detectable at the highest light intensity of 2000 µmol photons m^{-2} s^{-1} (Figure 3.27 C). HL grown plants showed an increased conversion of Vx to Zx (about 60 % of

the total VAZ pool) and the formation of Zx was slightly accelerated in LL plants, while the conversion of Vx to Zx remained unchanged in NL and NatL plants. The reconversion of Zx to Ax and Vx in during the subsequent dark period showed no pronounced differences among the different plant types (Figure 3.27). It should be noted, however, that the information on the back reaction was limited, since only the Zx content at the end of the dark phase has been determined.

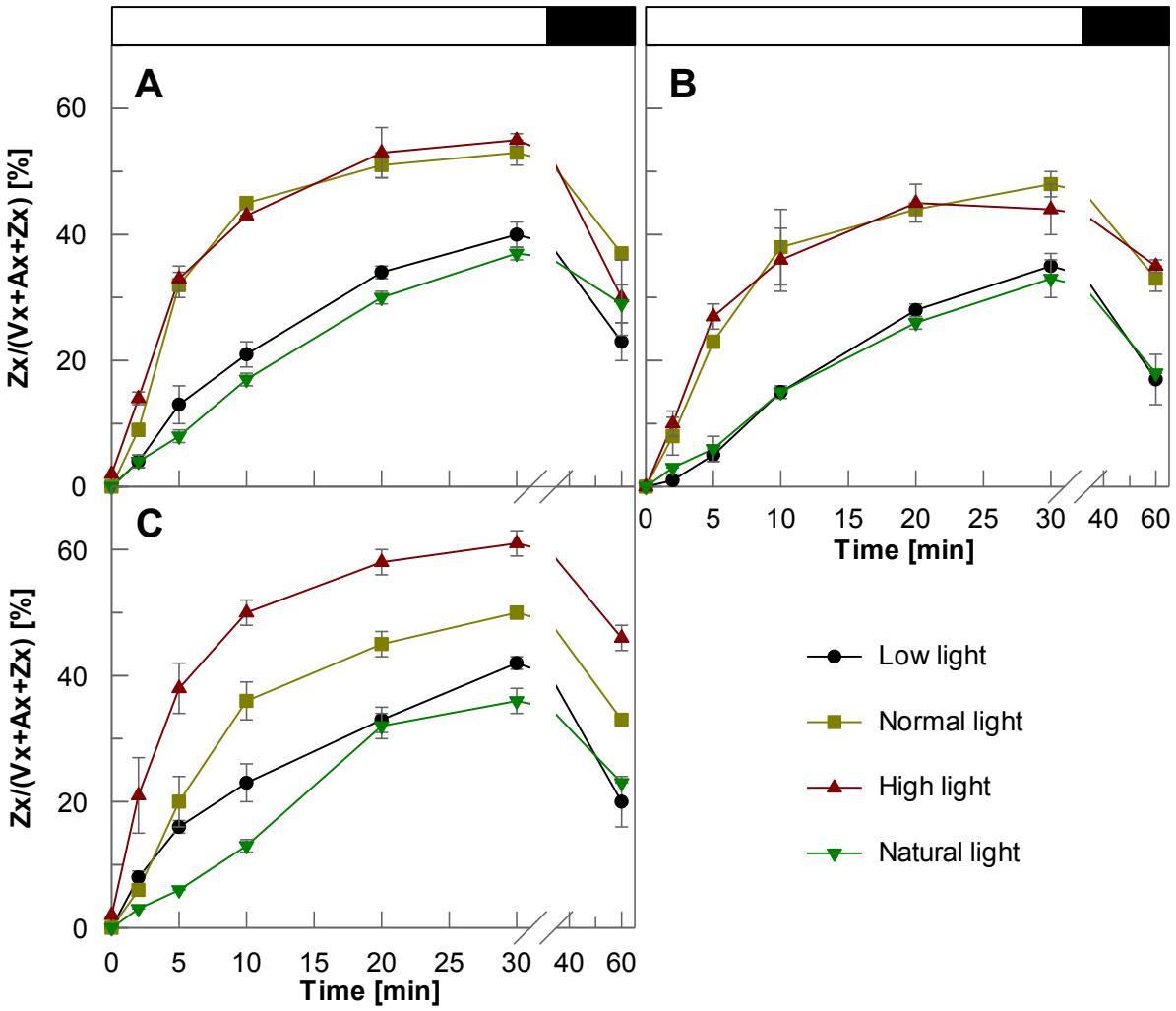

Figure 3.27 Convertibility of the VAZ pool indicated as portion of zeaxanthin of the VAZ pool in percent during 30 minutes (white bars) of illumination and after 30 minutes of relaxation (black bars). Zeaxanthin content is shown for LL, NL, HL, and NatL plants at illumination intensities of (A) 350, (B) 850, and (C) 2000 µmol photons m^{-2} s^{-1}. Mean and standard error of at least three independent measurements are shown.

The overall lower conversion rate in LL and NatL grown plants is in line with the assumption of a larger PSII antenna size in these two types of plants (based on Chl a/b ratios, Figure 3.14 E). Protein bound xanthophylls have been shown to be less convertible in comparison to non-protein bound Zx (Jahns, 1995; Jahns et al., 2009). In contrast, the larger VAZ pool size (Figure 3.14 D) and the lower LHCII content (Figure 3.14 E) in HL plants suggest that the pool of non-protein bound xanthophylls is increased, resulting in more rapid conversion of Vx to Zx (Figure 3.27). The slow and incomplete conversion of Vxto Zx in NatL plants in

together with the high level of rapidly reversible NPQ (Figure 3.26, Table 3.4) indicates that particularly the Zx-independent qE component of NPQ is increased in these plants.

3.3.3.4 Transient NPQ

Zx is known to be modulate the maximum qE-capacity and the NPQ kinetics (Ruban and Horton, 1999). The faster qE quenching observed at higher actinic light intensities in HL plants (Figure 3.26) might be due to a faster conversion of Vx to Zx under the same conditions. However, the convertibility of the VAZ pool could not explain the fast qE induction in NatL plants, since the conversion of the VAZ pool was rather slow compared to HL plants (Figure 3.27). More detailed analysis of qE induction at low actinic light intensities might provide more information about the underlying molecular mechanism. When starting from the fully dark-adapted state, low light is known to induce a transient NPQ only, which is related to the transient buildup of a high ΔpH, due to a delay in light activation of the ATP synthase and the enzymes in the Calvin-Benson cycle (Finazzi et al., 2004; Kalituho et al., 2007). After full light activation of the ATP synthase (typically after a few minutes of illumination), the proton concentration in the lumen decreases rapidly under low light conditions and thus NPQ mechanisms are deactivated. The transient NPQ induction in LL, NL, HL and NatL plants is shown in Figure 3.28.

The peak in early transient NPQ induction was reached after 30 to 60 seconds upon illumination. The fastest, but weakest response (NPQ = 0.2, Figure 3.28) was found in LL plants. It should be noted, however, that the actinic light intensity used for LL plants had to be reduced to 13 µmol photons m^{-2} s^{-1}, since higher light intensities (as the light intensity of to 53 µmol photons m^{-2} s^{-1} used for all other plants) already induced a stable NPQ in these plants. This lower light intensity might alter the kinetics of NPQ induction. In all other plants, the maximum of the transient NPQ was reached after about 1 min of illumination. NL and HL showed similar maximum values of 0.35 and 0.38, respectively, but the relaxation kinetic was slightly faster in HL plants (Figure 3.28). In contrast, NatL plants showed a nearly two-fold higher amplitude (about 0.68) of the transient NPQ response in comparison to NL and HL plants.

At the end of 10 min illumination, similar steady-state NPQ values were detectable for all plants. However, in LL and HL a transient decrease of the NPQ below this steady state value was observed in the time range of 2-5 min (Figure 3.28), which might reflect differences in the activation of the ATP synthase, resulting in different transient pH values in the thylakoid lumen. Upon re-darkening, the most rapid decay of NPQ was found in NatL plants, as observed before for the relaxation of the steady-state NPQ (Figure 3.26).

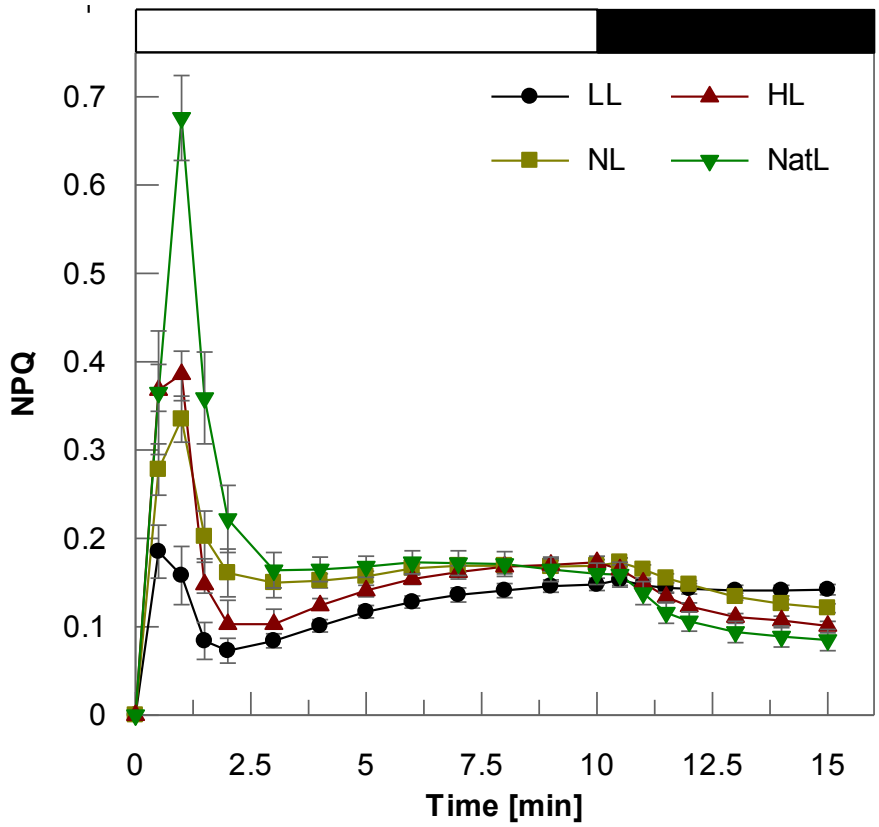

Figure 3.28 Transient NPQ induction in LL, NL, HL, and NatL plants during ten minutes of illumination (white bar) and five minutes of dark relaxation (black bar). NPQ was induced at 53 µmol photons m^{-2} s^{-1} in NL, HL, and NatL plants and with 13 µmol photons m^{-2} s^{-1} in LL plants. Mean and standard deviation of six independent measurements are shown.

The differences in the extent of the transient NPQ is obviously not correlated with the kinetics of Zx formation. Thus, either differences in the PsbS content (which is highest in HL and NatL plants, Figure 3.24) or other properties related to HL acclimation are responsible for the increased NPQ capacity in NatL plants. To evaluate possible differences in the activation of the two quenching sites Q1 and Q2, or the possible activation of spillover quenching (q_{SO}) upon acclimation to NatL conditions, time-resolved fluorescence measurements were performed.

3.3.3.5 Time-resolved fluorescence measurements

The contribution and characteristics of different NPQ processes (such as qE and qZ) was further investigated by time-resolved fluorescence spectroscopy. Applying this approach to intact leaves from Arabidopsis WT and mutant plants, two different quenching sites have been characterized earlier (Holzwarth et al., 2009). Quenching site Q1 was found to be PsbS dependent and to be related to the detachment and aggregation of parts of the LHCII antenna, while site Q2 was Zx dependent and related to antenna proteins that remained bound to the PSII reaction center (Holzwarth et al., 2009). In addition, this method further identified spillover quenching (q_{SO}) as efficient additional energy dissipation mechanism active in Monstera plants adapted to natural high light (see 3.1). Applying this method to

Arabidopsis WT plants grown under NL, HL and NatL conditions should provide further insights into the quenching mechanisms activated in response to various growth light conditions. Unfortunately, it was not possible to perform these measurements with LL plants due to the small leaf size of these plants. Typical fluorescence decay kinetics obtained for the dark-adapted (F_{max} condition) and light-adapted (F_{NPQ} condition) are shown exemplarily for the wavelength of 686 nm in Figure 3.29. In the dark adapted state (F_{max}), all plants showed similar fluorescence decay kinetics (average lifetimes (τ_{av}) of about 1.3 ns, Table 3.5), indicating similar photochemical properties of dark-adapted PSII. An accelerated decay was found in the light-adapted state (F_{NPQ}), reflecting the induction of NPQ in all cases. In comparison with NL plants (τ_{av} = 380 ps), however, a slightly faster decay was found for HL plants (τ_{av} = 320 ps) and much faster decay for NatL plants (τ_{av} = 130 ps). These lifetimes corresponded to NPQ values of 2.6 (NL plants), 3.1 (HL plants) and 8.5 (NatL plants). For NL and HL plants, the NPQ values were somewhat higher but still similar to those derived from steady state fluorescence measurements (Figure 3.26), while the NPQ value was much higher for NatL plants. This discrepancy is related to the fact that steady state NPQ values are determined from fluorescence emitted at wavelength > 720 nm, while the NPQ values obtained from time-resolved measurements were derived from the fluorescence at 686 nm. Obviously, the NPQ at this PSII specific wavelength is much higher in the red region as compared to the far-red region.

For more detailed analysis, the decay-associated spectra (DAS), which carry both, spectral and kinetic information, were derived from kinetic compartment analysis (see 1.4.3). DAS for NL, HL and NatL grown Arabidopsis plants in the F_{max} and F_{NPQ} states are shown in Figure 3.29. The kinetics analysis typically results in the identification of 4 components related to PSI (characterized by very short lifetimes in the range from 4-100 ps) and 3 or more components related to PSII. Since the NPQ processes occur in PSII and thus affect PSII components only, all further discussions and analyses are restricted to PSII related spectra. PSII related spectra (Figure 3.29 solid lines) show a characteristic peak maximum at 683 nm and a second local maximum in the far-red region (at about 740 nm). As pointed out in section 3.1, models including also PSII pools connected to PSI were comparatively tested to determine best fits of the data. In NL and NatL plants, a model assuming a homogenous PSII pool of unconnected RC was sufficient for fitting the acquired data in both the dark and light acclimated state (Figure 3.29 A + B, and E + F). Additionally, a specific LHCII antenna component, which is attached to the PSII core, was identified in the dark acclimated state of NL and NatL plants (Figure 3.29 A and E; LHCII attached), while a component related to detached LHCII was apparent in the light acclimated state in all types of plants. Detachment of parts of the LHCII antenna was accompanied by a shortening of the respective lifetimes (from 990 to 292 ps in NL plants and from 686 to 233 ps in NatL plants), indicating the light-

induced quenching in LHCII upon detachment. This detached antenna component was formerly identified as the PsbS dependent quenching site Q1 (Holzwarth et al. 2009) which has been assigned to the PsbS-dependent qE component of NPQ (Nilkens et al. 2010; Jahns and Holzwarth, 2012). Light activation of the Zx dependent quenching site Q2 (assigned to antenna proteins bound to the PSII RC core) was visible from the shortening of the lifetime of the slowest PSII component (about 2-2.4 ns), which represents the dominating PSII component in the dark-adapted state of all types of plants. In NL plants, the lifetime was reduced from about 2.2 ns under F_{max} conditions (Figure 3.29 A) to about 840 ps under F_{NPQ} conditions (Figure 3.29 B), in NatL plants from about 2.1 ns (F_{max}; Figure 3.29 E) to about 700 ps (F_{NPQ}; Figure 3.29 F) and in HL plants from about 2.4 ns to about 750. In all cases, this strong reduction of the lifetime in the F_{max} state indicates the activation of Zx-dependent NPQ, most likely identical with the qZ component of NPQ (Nilkens et al. 2010; Jahns and Holzwarth, 2012).

In contrast to NL and NatL plants, it was required to assume a heterogeneous PSII pool to obtain satisfying fits of the data measured with HL plants in the dark acclimated state (Figure 3.29 C; PSII and PSII-C). Furthermore, no additional LHCII component was found in HL plants under F_{max} conditions (Figure 3.29 C), indicating a smaller PSII antenna size in comparison with NL and NatL plants, in agreement with former observations (Figure 3.14 E, Table 3.2). In contrast to the typical, unconnected PSII pool (as present in NL and NatL plants) which is separated from PSI, the pool of PSII RC connected to PSI (PSII-C) has to be located in membrane regions where also PSI is localized, i.e. in the grana margins or in stroma lamellae. As already shown for high light grown Monstera plants (section 3.1), connected PSII-RC allow for direct energy transfer between PSII and PSI via their connected antenna complexes, which explains the pronounced emission of far-red fluorescence at 740 nm in the respective PSII related spectra (Figure 3.29 D, arrow).

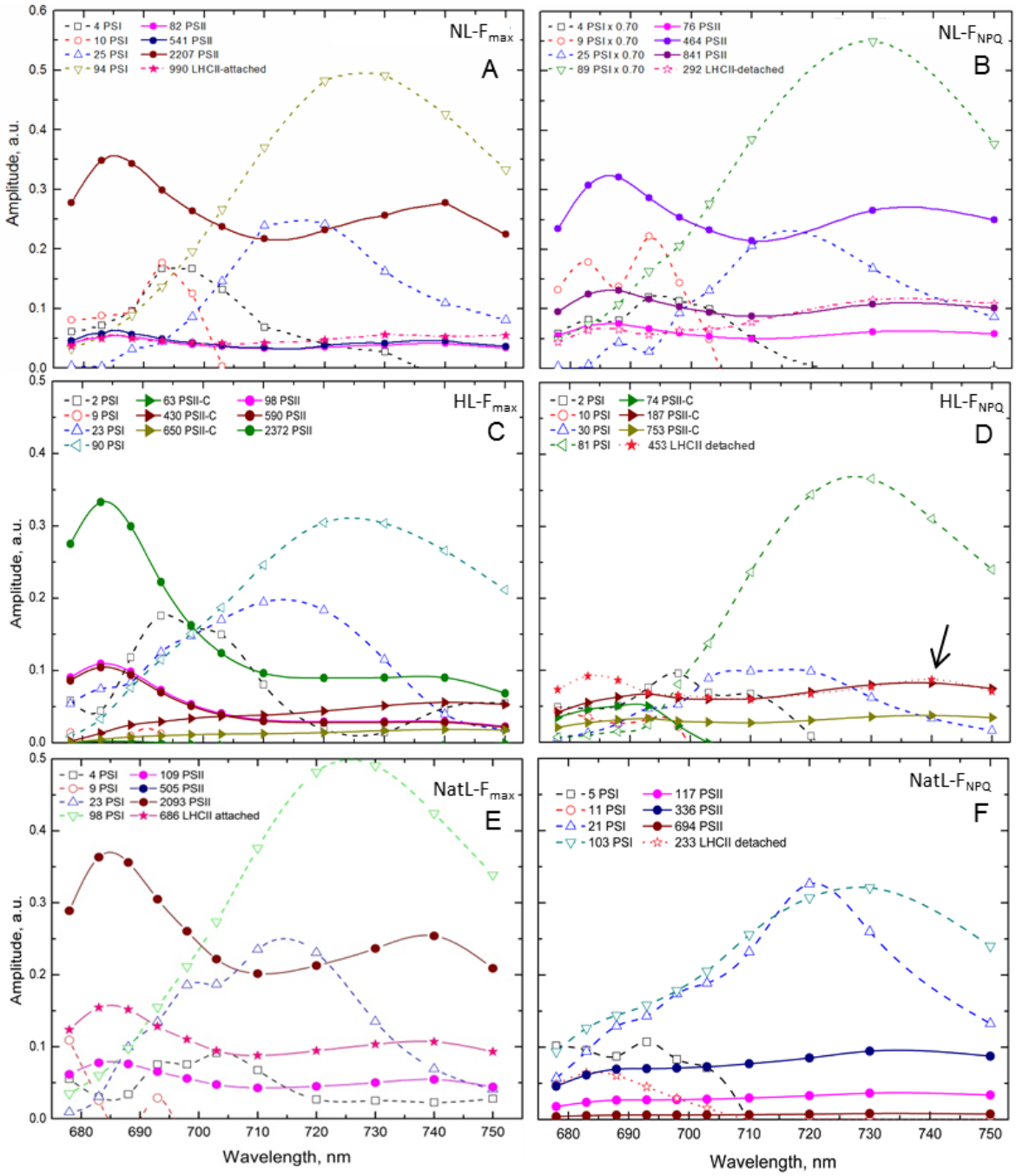

Figure 3.29 Decay associated spectra (DAS) of NL, HL, and NatL grown Arabidopsis plants in dark acclimated and DCMU treated state with closed PSII RC (F_{max}) (A, C, and E). Spectra in a quenching active, light acclimated state are shown in B, D, and F (F_{NPQ}). Rates constants for the according spectra are shown in the upper left corner of each Figure. PSI components are shown in dotted lines, PSII related spectra are show in solid lines. Measurements were performed and analyzed by Dr. Suman Paul.

In the light acclimated state (F_{NPQ}), all PSII RC were connected to PSI (Figure 3.29 D; only PSII-C), allowing for effective energy-spillover quenching q_{SO} as in high light grown Monstera plants (section 3.1). In addition to q_{SO}, also the activation of the quenching sites Q1 (= detachment of LHCII trimers, Figure 3.29 D) and Q2 (as indicated by the absence of the long-lived 2 ns component of PSII, Figure 3.29 D) was observed in HL plants.

Table 3.5 Average lifetimes and rate constants of F_{max} and F_{NPQ} components in NL, HL, and NatL grown *Arabidopsis thaliana* plants. The upper part shows the average lifetime (τ_{av}) [ps] of the fluorescence decay measurements shown in Figure 3.29. The middle part shows the rate constants k_D [ns^{-1}] for PSII antenna deactivation under F_{max} and F_{NPQ} conditions, as well as the average lifetime for the PSII kinetic. Two pools of PSII RC exist, unconnected (PSII) and connected (PSII-C) RC, the latter allowing for energy-spillover. The lower part shows the lifetime τ [ps] of the detached PSII antenna, the site of Q1-type quenching. The respective contribution of the detached antenna (LHCII) and at PSII (NPQ_{PSII}) to the total NPQ is indicated. Errors in the rate constants were within ± 10 %.

	NL	HL	NatL
τ_{av}, ps @ 686 nm (F_{max})	1380	1320	1240
τ_{av}, ps @ 686 nm (F_{NPQ})	380	320	130
Total NPQ	2.6	3.1	8.5
$k_{D\ max,\ PSII}$, ns^{-1}	0.3	0.3	0.3
$k_{D\ NPQ,\ PSII}$, ns^{-1}	1.8	-	3.2
$\tau_{av,\ PSII}$, ps (F_{max})	943	1020	902
$\tau_{av,\ PSII}$, ps (F_{NPQ})	460	-	382
$k_{D\ max,\ PSII\text{-}C}$, ns^{-1}	-	0.3	-
$k_{D\_NPQ,\ PSII\text{-}C}$, ns^{-1}	-	1.6	-
$\tau_{av,\ PSII\text{-}C}$, ps ($F_{max}$)	-	374	-
$\tau_{av,\ PSII\text{-}C}$, ps ($F_{NPQ}$)	-	338	-
k_{D_LHCII}, ns^{-1}	3.4	2.21	4.3
Lifetime τ [ps] of detached antenna component	292	453	233
Detached antenna cross-section relative to total PSII antenna (%)	30	40	30

These analyses thus support the conclusion, that spill-over quenching (q_{SO}) is only activated in HL plants. The increased NPQ capacity of NatL plants is therefore not due to spillover quenching, but rather to a more efficient quenching at Q1 and Q2. The kinetic features of the energy dissipation processes on basis of the kinetic target analysis are summarized in Table 3.5. The rate constant k_D represents the effective rate of non-photochemical inactivation of PSII and therefore is a direct measure of NPQ in the PS II-attached antenna. The increase of k_D corresponds to the activation of Q2 (Holzwarth et al., 2009). In NL and NatL plants, k_D increased by a factor of about 6 and 10, respectively, while a 5-fold increase was found for the connected PSII-C in HL plants (Table 3.5). Activation of Q1 led to a 30-40 % decrease of the functional PSII cross-section in all plants. However, the quenching in detached LHCII complexes was most efficient in NatL plants (k_{D_LHCII} = 4.3) followed by NL plants (k_{D_LHCII} = 3.4) and HL plants (k_{D_LHCII} = 2.2).

3.3.3.6 Summary of energy dissipation properties and mechanisms

The overall NPQ capacity and the underlying mechanisms were characterized. Western Blot analysis showed an increase in the amount of PsbS proteins with increasing growth light

intensity. NatL grown plants were found to accumulate high levels of PsbS similar to HL grown plants (Figure 3.24 B). Specific localization of the PsbS protein in grana or margin regions was assessed via immunogold labelling, however, no light dependent differences could be derived (Figure 3.25 B).

Table 3.6 Summary of the quenching abilities of LL, NL, HL, and NatL grown plants. Individual colors are provided for each growth condition (LL = yellow, NL = orange, HL = red, NatL = green). Similarities between growth conditions are indicated by using the same color.

		LL	NL	HL	NatL
Non-photochemical quenching (NPQ)	Westernblot PsbS				
	Immunogold PsbS				
	NPQ (qE+qZ)				
	VAZ convertibility				
	Transient NPQ				
Time-resolved measurements	Energy-spillover				
	Additional LHCII				
	Antenna quenching				

Xanthophyll conversion and thus Zx formation in NatL plants was similar to that in LL plants, but clearly different from that in NL and HL plants (Figure 3.27). These data support the view, that rather the overall antenna size than the VAZ pool size determines Vx convertibility

NatL plants showed like HL plants a much higher NPQ capacity than LL and NL plants, which could be related to rapidly reversible quenching processes. This high NPQ capacity led to a much lower degree of photoinhibition upon high light stress in comparison with LL and NL plants (Figure 3.26, Table 3.4). NatL plants further showed the highest transient NPQ among all types of plants, indicating a very efficient activation of qE-type quenching (Figure 3.28).

Time-resolved fluorescence measurements showed that only in HL plants spillover quenching (q_{SO}) can be activated (Figure 3.29). The high capacity of rapidly reversible NPQ in NatL plants can thus be assigned to a more efficient activation of quenching sites Q1 and Q2 (Table 3.5).

4 Discussion

The characterization of acclimation processes of NatL grown plants revealed new insights into the regulation of light utilization in the context of light dependent regulation of thylakoid membrane dynamics. Morphological and functional similarities of NatL grown plants to both, LL and HL plants, provide the basis for the exceptionally high acclimation potential of NatL plants to both, low and high light intensities. Among all tested parameters, the very high dynamic of the thylakoid membrane organization might represent the key factor for the high acclimation capacity observed in NatL grown plants. In this context, particularly the architecture of the grana stacks, especially their ratio of core to margin regions, seems to be crucial. Even though membrane unstacking has been shown to correlate with a new type of non-photochemical quenching (spillover quenching, q_{SO}), which was identified in HL grown *A. thaliana* and *M. deliciosa* plants, q_{SO} was not active in NatL grown plants. The high NPQ capacity in NatL grown plants was thus not based on q_{SO}, like in HL grown plants, but rather on a highly effective qE mechanism.

4.1 Relevance of acclimation studies

When analyzing the light acclimation of plants one has to discriminate between long- and short-term acclimation. Typically, long-term responses are related to the growth phenotype and plant morphology (Weston et al., 2000; Murchie, 2004) as well as protein stoichiometries (Anderson and Osmond, 1987; Schöttler et al., 2011). Long-term responses are usually controlled by hormone signaling (Mateo et al., 2006). Short-term responses, on the other hand, are responses towards quickly changing parameters (Walters and Horton, 1994) and were shown to be mainly redox regulated (Escoubas et al., 1995; Fey et al., 2005; Queval and Foyer, 2012), which has an impact on e.g. protein phosphorylation (Allen, 1992). However, the activation of NPQ mechanisms through protonation of antenna proteins (including PsbS) is regulated by the ΔpH (Li et al., 2004).

In this work, the short- and long-term acclimation of plants to different light intensities was studied. Plants grown under constant light conditions in a growth chamber were compared to plants grown under natural, fluctuating light conditions. The focus of the work was the characterization of NPQ properties/mechanisms that are activated in the short-term in response to high light.

The acclimation of plants to constant light conditions and its impact on the photosynthetic apparatus are very well characterized (Leong and Anderson, 1984; Bailey et al., 2001; Ballottari et al., 2007; Alter et al., 2012). Under field conditions, however, especially light is a very variable parameter that includes both, long-term (on a daily or seasonal basis) and

short-term (sun flecks due to shading or clouding) variations. Related to this complexity, it is still unclear how plants keep track on experienced light levels and how this experience is memorized and implemented in the acclimation state (Walters, 2005; Retkute et al., 2015). In context with NPQ, the importance of applying natural light conditions to evaluate the impact of NPQ on plant fitness has been demonstrated by quantifying the number of produced seeds under controlled and field conditions in Arabidopsis WT and NPQ deficient mutant plants (Külheim et al., 2002). Under controlled conditions, the number of seeds produced per plant was similar in WT and mutant plants, while under field conditions the seed production was drastically reduced in the NPQ deficient *npq4* and *npq1* mutants (Külheim et al., 2002).

In recent studies, artificial high light fluctuations have been used to simulate naturally occurring sun flecks in canopies, in order to study their impact on the photosynthetic electron transport chain and CO_2 assimilation (Yin and Johnson, 2000; Wagner et al., 2008; Alter et al., 2012; Tessmer et al., 2013; Armbruster et al., 2014). However, Yin and Johnson demonstrated in their work, that both, intensity and frequency of the applied pulses had an marked influence on the acclimation response (Yin and Johnson, 2000), underlining that the outcome of such experiments may not be reliable and thus not suitable to describe the situation in natural light grown plants.

In this work, plants grown under natural light conditions outside of the lab have been used to establish field conditions. Outdoors, however, the growth conditions of NatL plants differed from lab conditions in more aspects than simply the fluctuation of light. To evaluate the comparability of the different growth conditions, several factors need to be taken into account:

1) Water availability: To exclude differences in growth caused by water stress, NatL plants were grown under a balcony, where plants were watered manually just as under lab conditions, to accomplish optimal soil humidity.
2) Temperature stress: Temperature changes have the most dramatic effect on the lipid composition, including the membrane systems of chloroplasts (Szymanski et al., 2014). Therefore, the lipid composition of NatL and control plants was analyzed to examine any temperature related changes. The data showed no difference in the lipid composition of plants grown under controlled lab conditions and NatL plants (Figure 3.12). Besides the lipid data, temperature diagrams, which were based on climate measurements from the local weather station, were analyzed. The temperature during the growing seasons was between 15 and 25 °C (see Figure 2.2), which was comparable to the temperature conditions in the lab (20 °C).

3) Light: The light intensity, under which NatL plants were grown, was measured with a light sensor (see Figure 2.1). The median of the light intensity was 150 µmol photons m^{-2} s^{-1}, with lower and upper quartiles of 66 and 288 µmol photons m^{-2} s^{-1}, respectively. Highest light intensities were in the range of 1800 µmol photons m^{-2} s^{-1}, but such extreme high light periods were rather rare and of short duration. Differences in the light quality would only have an impact on the PSII to PSI ratio, rather than other photosynthetic parameters like CO_2 assimilation (Chow et al., 1990; Horton et al., 1996). However, the spectral properties of the light source used for constant light conditions is adapted to the natural spectrum of the sun, hence no severe impact of the light quality was expected.
4) Reproducibility: Another major concern with field measurements is the reproducibility of the data. NPQ measurements were performed during both growing seasons to check for comparability. In both years the NPQ induction and relaxation kinetics were comparable (Figure 4.1).

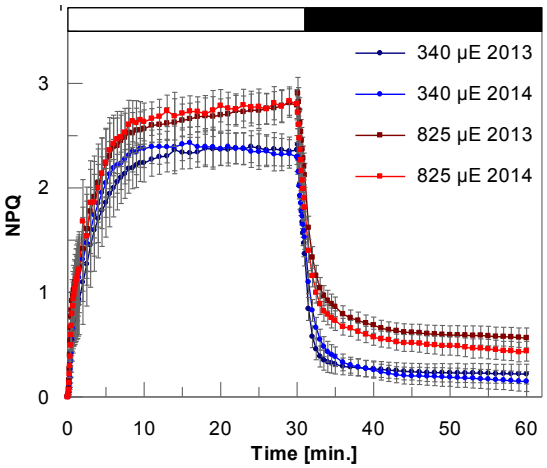

Figure 4.1 NPQ measured in NatL grown plants in the years 2013 and 2014. Comparable NPQ was induced at 30 min illumination of 340 and 825 µmol photons m^{-2} s^{-1}.

In conclusion, the different growth conditions used in this work provide a reliable basis for studying long-term acclimation to different growth light regimes. Apart from characterization of basic key parameters, particularly the impact of different long-term acclimation states on the capacity of short-term acclimation to high light intensities in terms of NPQ was of interest. For that, the response of the different plants to 30 min of illumination at three different light intensities (340, 825, and 1950 µmol photons m^{-2} s^{-1}) were characterized. These intensities were chosen to provide light intensities that significantly exceed the growth light intensity.

4.2 Plant morphology and chloroplast movement

Long-term acclimation to different growth light intensities is reflected by the growth and morphological properties of plants (Weston et al., 2000; Murchie, 2004). Indeed, leaves of HL and NatL grown plants were thicker than LL and NL leaves, because of bigger parenchyma cells in HL and NatL plants (Figure 3.3). In terms of photoprotection, chloroplast movement is very (cost) efficient way to control the amount of absorbed (excess) light (Kasahara et al., 2002). Chloroplast movement can be used to increase light harvesting under limiting light

conditions (accumulation response) and to decrease light absorption under HL stress conditions (avoidance response) (Kasahara et al., 2002; Wada et al., 2003). The increased cell depth observed in HL and NatL plants, might provide more space for the movement of chloroplasts, compared to LL and NL plants, and thus might allow for a stronger avoidance response under HL conditions (Figure 3.7).

Despite chloroplast movement, the photosynthetic machinery is acclimated towards different light conditions at different levels. An important difference among the plants on the protein level was found for LHCII, which accumulated to higher levels in LL and NatL plants, as compared to HL plants (Figure 3.14 E). LHCII complexes are involved in both, light-harvesting and energy dissipation, and have thus a significant impact on the acclimation towards different light conditions.

However, not only morphological properties, but also especially efficient quenching mechanisms are necessary for the survivability of plants under excess light conditions. The impact of long-term acclimation to high light on energy dissipation was studied in two plant species: *M. deliciosa* and *A. thaliana*. For Monstera plants acclimated to natural high light, a new quenching mechanism was found, termed energy-spillover (q_{SO}), which drastically increased the quenching capacity, compared to LL acclimated Monstera plants. To clarify, whether activation of q_{SO} is a specific acclimation response of evergreen species, or plants acclimated to either fluctuating or high light, experiments in differentially acclimated Arabidopsis plants were conducted.

4.3 Quenching capacity and mechanisms

Plants acclimated to different growth light conditions, showed pronounced differences in the NPQ capacity. Under constant light conditions, the capacity of rapidly reversible NPQ (qE and qZ) increased with increasing growth light intensity (Figure 3.26, Table 3.4). Interestingly, NatL grown plants showed the highest NPQ capacity of all plants at all actinic light intensities (Figure 3.26), quite similar to HL plants. However, the median light intensity of NatL was at 150 µmol photons m^{-2} s^{-1} and thus rather in the range of NL than of HL. Hence, the quenching capacity of NatL plants was not related to the median growth light intensity but to the fluctuation of light. In comparison to HL (500 µmol photons m^{-2} s^{-1}), the highest NatL intensities were in the range of 1500-2000 µmol photons m^{-2} s^{-1}. The increased NPQ capacity in NatL plants is thus triggered by the maximum light intensity, rather than by the median growth light intensity.

The transiently induced NPQ at non-saturating light intensities provides information on the induction and reversibility of the initial qE response (Figure 3.28). Compared to other growth conditions, the maximum transient NPQ in NatL plants was increased 2-fold, which indicates a very rapid and efficient activation of qE in plants subjected to fluctuating light conditions.

Time-resolved measurements also identified a very strong quenching in the detached antenna of PSII in NatL grown plants, as opposed to NL or HL grown plants (Table 3.5). Both results indicate, that the high quenching capacity in HL and NatL grown plants is likely based on the different mechanisms.

The rapidly reversible part of NPQ (qE) mainly depends on three factors: the PsbS protein, the lumen pH, and the xanthophyll Zx (Demmig-Adams and Adams 1996; Li et al., 2000; Li et al., 2004). These parameters have been analyzed in differentially acclimated plants to further understand the quenching mechanisms that might be responsible for the different quenching capacities.

4.3.1 PsbS Protein

The PsbS protein is essential for the induction of qE (Li et al., 2000) and triggers pH-regulated conformational changes in the antenna of PSII, which lead to a detachment of LHCII from PSII. Quantification of PsbS by means of Western Blot analysis revealed that the amount of PsbS protein increased with increasing growth light intensity, which was in line with the literature (Demmig-Adams et al., 2006; Ballottari et al., 2007). When normalized to total protein, comparable amounts of PsbS protein were found in HL and NatL grown plants (Figure 3.24). Normalized to Chl, however, the amount of PsbS per Chl was decreased in NatL plants as compared to HL plants (Figures 3.6 D and 3.24). Hence, the high NPQ capacity in NatL grown plants cannot be explained simply by the amount of PsbS protein.

4.3.2 ΔpH

The protonation of the PsbS protein triggers the conformational changes in the light harvesting antenna of PSII (Li et al., 2004). Upon illumination, the thylakoid lumen is acidified, which leads to the protonation of PsbS and thus to the activation of NPQ processes. The lumen pH depends on the ratio of proton influx (from linear electron transport, Figure 3.17) and proton efflux through the ATPase (g_H^+, Figure 3.22). Furthermore, the partitioning of the proton motive force, the driving force for ATP synthesis (Capaldi and Aggeler, 2002), is a key regulator for the lumen acidification. It has been proposed that the role of *pmf* partitioning is the establishment of a lumen pH that is sufficient for ATP synthesis, while it is still in range for efficient qE modification (Kramer et al., 1999; Cruz et al., 2001). However, since both components of the *pmf* are equal driving forces for the ATP synthesis (Wiedenmann et al., 2008), regulating the extent of qE quenching might be the primary function of the *pmf* partitioning.

No differences in the total *pmf* were found among plants from different growth conditions after 30 min of illumination at different actinic light intensities (Figure 3.20), but *pmf* partitioning into ΔpH and ΔΨ fraction differed (Figure 3.21). In HL plants, the fraction stored

as ΔpH was lower than in LL and NatL grown plants, which both showed a high fraction of ΔpH. A high ΔpH fraction of *pmf* allows for enhanced lumen acidification, which would increase the NPQ induction through protonation of PsbS. Indeed, estimation of the luminal pH on basis of the ECS data supported a lower lumen pH in LL and NatL plants than in HL plants at all actinic light intensities (Figure.3.23). The values of the luminal pH calculated in this work were in line with the literature (Kramer et al., 1999). The higher ΔpH fraction of the total *pmf* in NatL plants might thus explain the faster and stronger qE response in comparison with HL plants (Figure 3.28). Moreover, the less pronounced lumen acidification in HL plants could also explain the reduced quenching efficiency in the detached antenna of PSII (k_{D_LHCII}, ns^{-1}, Table 3.5), supporting the view that the detachment of LHCII trimers cannot be the main component of NPQ in HL plants.

4.3.3 Zeaxanthin

Zx fulfills a dual role in photo-protection: bound to LHCs, Zx deactivates ^{1}Chl* and allosterically enhances qE type quenching (Demmig-Adams et al., 1990; Horton et al., 2008; Johnson et al., 2008a), and as free pigment it supports the detoxification of ROS as an antioxidant (Havaux et al., 2005; Havaux et al., 2007; Johnson et al., 2007). Generally, the VAZ pool size was increased in HL and NatL grown plants, compared to LL and NL grown plants (Figure 3.14 D). However, the conversion of Vx to Zx was much faster in HL plants, compared to NatL plants (Figure 3.27). This might be due to a different distribution of Vx in HL and NatL grown plants. It has been shown, that the convertibility of Vx is strongly dependent on the ratio of free (fast convertibility) to protein bound (slow convertibility) pigments (Jahns et al., 2001; Wehner et al., 2006; Jahns and Holzwarth, 2012). Thus, in NatL grown plants, with an increased amount of LHCII complexes (Figure 3.14), most of the Vx molecules might be bound to antenna proteins, which would explain the slow conversion of Vx to Zx upon illumination. Binding of Zx to LHCII is known to enhance qE quenching (Horton et al., 2008). Therefore, increased binding of Zx to LHCII likely contributes to the overall strong qE response in NatL plants (Table 3.5, Figure 3.28). By contrast, the fast conversion of xanthophylls in HL grown plants indicates that a significant amount of Zx is present as free pigment, which is rather involved in ROS scavenging than contributing to qE.

4.4 The role of energy-spillover

Energy-spillover q_{SO} explained the increased NPQ capacity in Monstera plants acclimated to natural high light (section 3.1). In Arabidopsis, energy-spillover quenching was found in HL acclimated plants, but not in NatL grown plants (Figure 3.29, Table 3.5). Hence, q_{SO} is not a mechanism that is specific for evergreen plants, but represents an acclimation towards constant high light, rather than fluctuating conditions with short HL peaks. q_{SO} in HL

acclimated Arabidopsis plants also explains the high quenching capacity (Figure 3.26, Table 3.4) in comparison to LL and NL plants, since the quenching was not attributed to very effective qE quenching (Table 3.5, Figure 3.28).

The mechanism of q_{SO} was further investigated in HL acclimated Arabidopsis mutants deficient in either the qE (*npq4* mutant) or the qZ (*nqp1* mutant) component of NPQ (Figure 3.2, Table 3.1). In the PsbS-deficient *npq4* mutant, energy-spillover was found, although not the entire pool of PSII was connected to PSI in a light acclimated state. This indicates that PsbS is not essential for, but PsbS might be involved in regulation of q_{SO}. In contrast, Zx deficient *npq1* mutants did not show any energy-spillover quenching (Table 3.1), suggesting that Zx plays a major role in activation of q_{SO}.

4.5 The grana structure determines the quenching mechanism

Even though the 2D structure of grana stacks is known for many years, the exact 3D structure is still under debate. Two models have been proposed: the fork-model and the helical model (Arvidsson and Sundby, 1999; Mustárdy and Garab, 2003; Shimoni et al., 2005), however, reliable evidence for one of the models still needs to be provided. In addition, the function of grana membranes as pure tool for lateral segregation of PSII and PSI has been challenged. Due to the 3D structure that grana provide (Mullineaux, 2005), as opposed to a linear 2D membrane system existing in stroma lamellae, the light harvesting antenna of PSII can be shared among several PSII RC. The advantage of a shared antenna is the distribution of excitation energy, which leads to faster trapping of energy and thereby reduces the probability of ROS formation.

Precondition for energy-spillover quenching is the localization of PSII and PSI in close proximity, to allow for direct energy transfer from the antenna of PSII to PSI (see section 3.1). However, lateral segregation is realized via grana formation, since PSII and LHCII are found in the grana stacks, whereas PSI and LHCI are found in the margins and stroma lamellae. Thus only in plants with very small grana stacks energy-spillover should be allowed.

In this work, the membrane structure in *A. thaliana* was analyzed by electron microscopy. TEM images showed grana dominated thylakoid membrane structure in LL plants, which is in line with previous observations (Anderson, 1986). With increasing growth light intensity, the number and size of grana decreased (Figure 3.8). HL plants showed only thin and narrow grana stacks interconnected with long regions of stoma lamellae, as characterized before (Anderson, 1986). Indeed, q_{SO} was only found in HL plants with stroma dominated thylakoid membrane structure, but not in NatL grown plants. The grana structure of NatL plants showed both, LL and HL features. The overall membrane organization was more similar to HL plants, but the grana stacks in NatL plants contained more membrane layers than in HL

plants. In comparison to LL plants, however, grana stack in NatL plants were smaller in both width and height, resulting in an increased ratio of margins to grana cores.

4.5.1 The role of the antenna size in grana formation

It is known that the antenna size of PSII strongly depends on the growth light conditions. With increasing growth light intensity the amount of LHCII per PSII decreases (Dekker and Boekema, 2005). The Chl a/b ratio is a reasonable estimate for changes in the ratio of reaction center to antenna size proteins (Mishra et al., 2012). Since the stoichiometry of PSI and LHCI is constant (Ballottari et al., 2007), changes in the Chl a/b ratio reflect predominantly changes in the PSII:LHCII ratio, apart from changes in the PSII:PSI ratio. As expected, the Chl a/b ratio was found to increase with increasing light intensities (Figure 3.14 E), which reflects the reduction of the amount of LHCII per PSII RC. Since LHCII is predominantly bound in the grana stacks at PSII and supposed to be involved in grana formation (Anderson and Andersson, 1988; Melis, 1991), these results also support the observed thylakoid membrane structure. Whether the height of grana stacks is determined by the amount of LHCII could not be determined in this work, however, the amount of LHCII complexes correlates with the thickness of grana stacks (Figures 3.8 and 3.14 E).

4.5.2 Other factors

Besides the putative role of LHCII complexes in the formation of grana, at least one other protein was found to be involved in the buildup of the grana structure. CURT1, which is involved in the formation of grana, was found in the margins of the grana stacks (Armbruster et al., 2013; Pribil et al., 2014). The amount of CURT1 proteins regulates the width of the grana stacks, hence the expression of CURT1 might determine the overall width of the stacks. However, the interplay of the factors, which determine or control the overall grana structure, remains to be studied.

4.6 Thylakoid membrane flexibility allows for rapid short-term acclimation towards changing light conditions

The overall structure of the grana membrane resulting from long-term acclimation likely determines whether energy-spillover is possible or not. However, an increase in the fraction of connected PSII RC in Arabidopsis and Monstera plants was accompanied by the unstacking (short-term response) of grana stacks (Demmig-Adams et al., 2015) (Figure 3.11 and Table 3.5). Hence, not only the overall structure, but also the flexibility of the membrane is directly involved in short-term acclimation to high light. However, grana unstacking did not necessary lead to energy-spillover quenching, as demonstrated in NatL grown plants that

showed the most significant unstacking, but no energy-spillover. Since the unstacking of the membrane in HL plants regulated the extent of q_{SO} quenching, one could assume a similar regulatory role of the unstacking in energy dissipation for NatL grown plants. Most likely, the unstacking might provide space for LHCII migration, which would allow a very fast fine-tuning of light harvesting and energy dissipation (Tikkanen et al., 2012). This assumption is in line with a proposed faster qE quenching due to unstacking (Herbstova et al., 2012; Pribil et al., 2014), as was also found here in the steady state and transient NPQ measurements (Figures 3.26 and 3.28).

No grana unstacking was observed in LL and NL grown plants and neither q_{SO}, nor a very effective qE mechanism were found in either of them (Figure 3.26 and Table 3.5). The reason for this inflexibility might be related to the size of the grana stacks. Generally, the formation of grana stacks involves two competing forces (attraction and repulsion) that control the degree of stacking and unstacking of the grana (Barber and Chow, 1979). The majority of attraction forces in the grana stacks are based on LHCII interactions. Across the gap of two adjacent thylakoid membrane layers in a granum, van-der-Waals forces between hydrogen bonds of different LHCII lead to stacking. These forces are very weak, however with increasing number of LHCII in the grana stack, the sum of interactions create a strong attraction force (Chow et al., 1991). Cyt b_6f and PSI, on the other hand, have no effect on grana formation (Clausen et al., 2014; Manara et al., 2014). In LL plants, additional LHCII-trimers were found (indicated by the Chl a/b ratio and the OJIP transient, Figures 3.14 E and 3.19). The role of these additional (weakly coupled) LHCII trimers is still unclear, however the accumulation of PSII and LHCII complexes in LL plants is known to lead to the formation of dense protein arrays (so called LHCIIb domains) (Boekema et al., 2000), in which the repulsion forces between two adjacent membranes are reduced (Chow et al., 1988). The strong attraction forces in the core of grana in LL and NL plants might be responsible for the inability to unstack the grana membranes upon illumination, which in turn might reduce the photochemical and non-photochemical responses towards higher light intensities.

However, the light dependent stacking and unstacking of membranes (short-term response) might not only determined by the amount of LHCII complexes, but rather based on short-term modification of the proteins such as phosphorylation (Kirchhoff, 2013) and protonation (Clausen et al., 2014). Unstacking via protonation might be realized not only by direct protonation of LHCII, but also indirectly by the PsbS dependent detachment of LHCII, which might reduce the attraction forces in the grana stack, and could thus lead to unstacking. Protein phosphorylation, on the other hand, might unstack membranes through the negative charges that accumulate with the phosphate group along the membranes (Kirchhoff, 2013). The impact of protonation upon lumen acidification and phosphorylation on grana unstacking was tested in HL acclimated *pgr1* (unable to form a stable proton gradient) and *stn7* (no

phosphorylation of LHCII) mutants. No light-dependent unstacking of grana was detectable in the *pgr1* or *stn7* mutant (data not shown). This observation is in line with previous reports for the effect of phosphorylation on grana unstacking (Herbstova et al., 2012; Clausen et al., 2014) and indicates that both, protonation and phosphorylation are important for the ability to unstack.

In summary, the structure of the thylakoid membrane and the ratio of grana core to margin fractions determine the flexibility of the membrane, which is important for the enhancement of NPQ. Protonation and phosphorylation are both necessary for grana unstacking and hence for the full connection of PSII to PSI upon induction of energy-spillover in HL plants. In NatL plants, however, unstacking might accelerate the diffusion of LHCII complexes and by that qE quenching.

4.6.1 Mechanisms of membrane unstacking

Unstacking of membranes requires a mechanism, which allows for an increase of the amount of margin fractions, which is the consequence of grana unstacking. These changes could be realized either by a simultaneous narrowing of the grana stack while unstacking, or by the rapid incorporation of lipids into the thylakoid membrane. In addition, the lipid composition might be critical for grana unstacking. In this work, the lipid content of the chloroplast membrane was analyzed from plants of all growth conditions. However, no differences in the composition of glycolipids were found among plants of different growth conditions (Figure 3.12 A). Overall the molar stoichiometry between the glyco- and phospholipids were in line with the literature (Webb and Green, 1991; Dörmann and Benning, 2002; Kirchhoff et al., 2002; Pribil et al., 2014), except for PC which was increased 2-fold compared to an earlier study on spinach (Webb and Green, 1991). Since no differences in the lipid composition were found between LL/NL and HL/NatL grown plants, the lipid composition can be excluded as key parameter, which determines the capability of grana unstacking.

Upon illumination, changes in both the height and the width of grana stacks were quantified (Figure 3.11). Narrowing of grana stacks (indicated by a decrease in width upon illumination) was not observed under any growth conditions. On the contrary, further broadening of the membrane was determined in NatL plants (Figure 3.11 B). Hence, also simultaneous narrowing of the membrane while unstacking can be excluded.

The third possibility to allow for grana unstacking is the temporal enlargement of the membrane by the incorporation of lipids. Newly synthesized lipids as a possible explanation seemed unlikely, due to the fast dynamics of membrane unstacking (30 mins). However, a possible reservoir for those lipids represent lipid droplets that were found attached to the grana stacks (Figure 3.8). Indeed more lipid droplets were found in NatL grown plants, which showed the highest membrane flexibility (Figure 3.9 A). The accumulation of lipid droplets in

the chloroplast has previously been reported with respect to HL acclimation (Lichtenthaler, 2007). Different types of lipid droplets exist: (i) plastoglobuli, (ii) plastoglobuli-like particles, and (iii) lipid-protein particles (Smith et al., 2000). However, discrimination between these lipid droplets was not possible in this work. Plastoglobuli mainly consist of storage lipids such as triacylglycerols (Tevini and Steinmüller, 1985) and are therefore not suitable as reservoir for interchangeable lipids for the thylakoid membrane. Most likely, lipid-protein particles might be involved in thylakoid membrane interactions, since they consist of glycolipids and catabolites of photosynthetic proteins (Ghosh et al., 1994; Smith et al., 1997), which indicates a direct interaction with the thylakoid membrane system. In this work, the high flexibility in NatL grown plants correlated with a significant increase in the chloroplastidal lipid bodies. An involvement of lipid bodies in the unstacking of membranes is thus likely and finds further support in the literature, where a possible involvement of lipid droplets in membrane flexibility is stated (Austin et al., 2006; Haferkamp et al., 2010).

4.7 Model for light acclimation processes at the membrane level

Under natural conditions, the ability to acclimate towards changing light determines the fitness and survivability of plants. Analysis of the acclimation response of field-grown plants is therefore essential for the understanding of the underlying processes. This work showed that acclimation to NatL conditions provides a higher flexibility of photochemical and non-photochemical processes than acclimation to constant light conditions. In particular, the high NPQ capacity of NatL plants was found to rely on a different mechanism than in plants grown under constant high light. Strikingly, the different specific properties of all plants correlated with the underlying grana structure and flexibility. In the following, a summarizing overview of long- and short-term acclimation processes in plants from the respective growth conditions and their underlying grana structure are depicted in Figure 4.2.

Starting from a proplastid (center of Figure 4.2), chloroplasts develop differently in dependence of the growth light conditions. Three scenarios are highlighted in the model, two of them related to artificial, constant growth light intensities typically used in the lab. Here, two extreme cases are shown, acclimation to constant HL (A) and LL (B). In contrast to these artificial conditions, acclimation of plants to natural, fluctuating light conditions is shown (Figure 4.2 C). The architecture of the grana membranes typically reflects long-term responses (red arrows) to the growth light condition. The content of the black boxes show short term responses in the low light or dark acclimated state (left side of the box) and in the HL acclimated state (right side of the box).

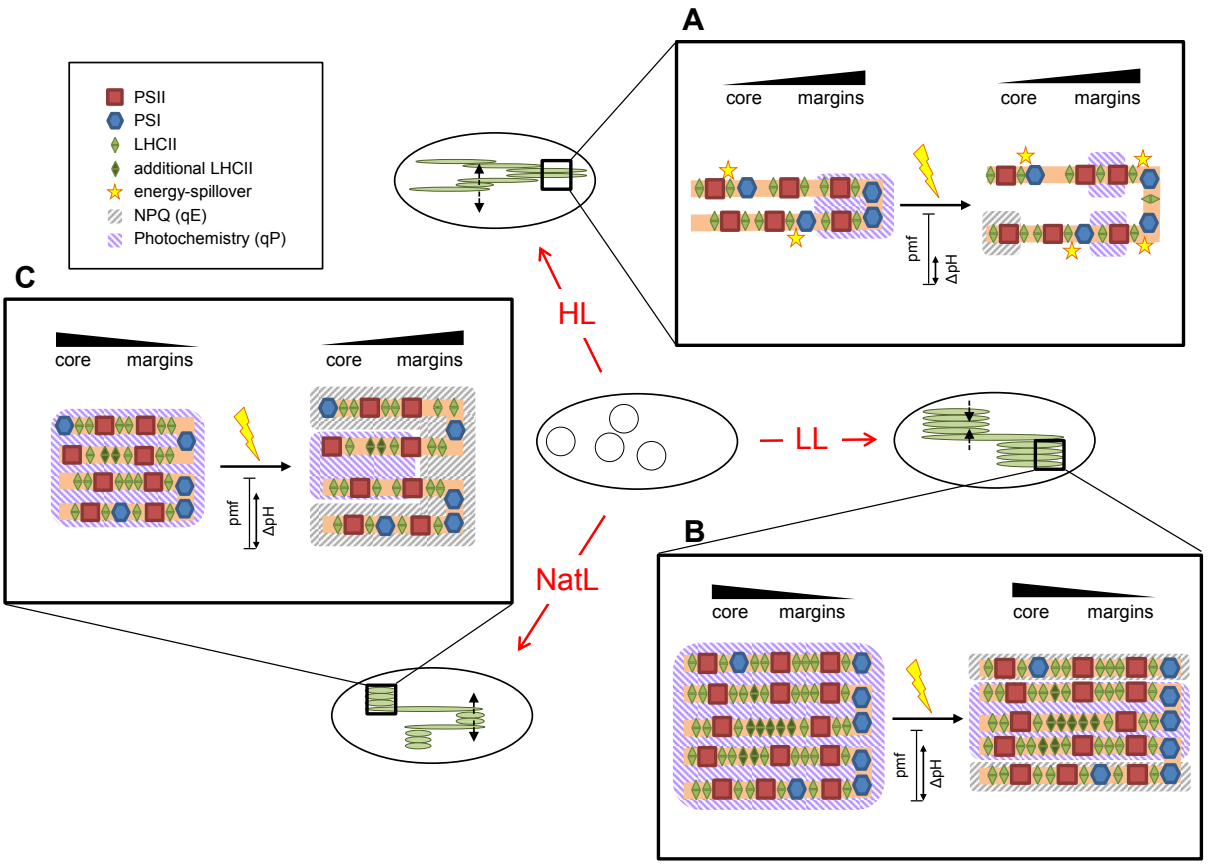

Figure 4.2 Model for light acclimation processes at the membrane level. (A) LL plants, (B) HL plants and (C) NatL plants. Red arrows indicate long-term acclimation processes, black symbols short-term acclimation processes. In each box, the dark or low light acclimated state is shown on the left side, illumination is indicated by the yellow flash. The high light acclimated state is shown on the right side of each box. For clarity, LHCI, ATPase and Cyt b_6f were excluded from the model. Hatched grey areas indicate qE type quenching, hatched blue areas high photochemical activity and yellow stars the proposed sites of spillover quenching q_{SO}.

The thylakoid membrane system in HL plants is dominated by long stroma lamellae, which connect thin and short grana stacks, so that the majority of membranes of a granum can be classified as “margins” or stroma exposed regions. Grana stacks are not thick enough to contain any core regions and thus lateral segregation of PSII and PSI is minimal (Figure 4.2 A). This leads to partial energy-spillover quenching between adjacent PSII and PSI RC (Figure 4.2 A). In HL plants, energy-spillover in connected PSII RC reduces the efficiency of photochemistry due to a constitutive quenching of excitation energy in PSI (see section 3.1). On the contrary, the thylakoid membrane in LL plants is densely packed with LHCIIs and dominated by thick grana stacks, which are connected by only short sections of stroma lamellae and expand over long regions in the chloroplast (Figure 4.2 B). Additional LHCIIs (Figure 4.2 B, dark green) lead to an enhanced stacking and maximize light harvesting under low light conditions. Due to the thickness of the grana stacks the ratio of core:margin fractions is high. NatL grown plants showed characteristics of both LL and HL plants, long stroma lamellar regions, comparable to HL and thicker grana stacks, comparable to LL.

However, the grana stacks were more narrow compared to LL, leading to a decreased core:margin ratio.

In HL plants, the acclimation towards HL intensities leads to an unstacking of the thylakoid membrane. The unstacking further leads to the full connection of PSII to PSI, maximizing the quenching via energy-spillover. The fraction of *pmf* stored as ΔpH is low, thereby keeping the chloroplast in a “light-harvesting” state. Due to the low lumen acidification, only a weak qE response is triggered in HL plants (Figure 4.2 A, grey hatched area). The illumination of LL plats with HL intensities does not lead to membrane unstacking, thus the grana remains in a core dominated state (Figure 4.2 B). The *pmf* is dominated by the ΔpH fraction (Figure 3.21), which leads to a strong acidification of the thylakoid lumen (Figure 3.22). The low lumen pH activates qE, however detachment of LHCII from PSII is limited due to the stacked membrane structure, which limits the qE response. Only in the grana margins, where the diffusion space for LHCII trimers is increased, detachment of LHCII trimers is possible. Because of the packed grana stacks, the chloroplast is forced to stay in a “light-harvesting” state, without having the possibility to quench the energy in the core region. The excess of excitation energy in the grana core leads to strong photoinhibition upon longer high light exposure (Figure 3.26, Table 3.4). In NatL grown plants, membrane unstacking was observed upon HL acclimation (Figure 4.2 C). The unstacking increases the margin fraction of the granum, thereby switching from a “light-harvesting state” into a “quenching state”. Comparable to LL plants, the fraction of *pmf* stored as ΔpH is high (Figure 3.21), resulting in a low lumen pH (Figure 3.23). The strong acidification of the thylakoid lumen leads to a strong qE response and fast detachment of LHCIIs from the PSII RC, which are released in the extended margin regions (Table 3.5).

Closing up, in NatL grown plants the very rapid light-dependent switch from core dominated (light-harvesting state) to margin dominated (quenching state) grana might allow for the acclimation towards quickly changing light intensities. However, the exact regulation and the involved signals in membrane unstacking remain to be elucidated.

5.1 Summary

Long- and short-term acclimation to varying environmental conditions is essential for the survivability of plants. Sunlight represents not only the ultimate energy source for photosynthesis, but also an important and highly dynamic stress factor. Under most natural conditions, the amount of absorbed light energy exceeds the capacity that can be utilized in photosynthesis, giving rise to the formation of reactive oxygen species and thus photo-oxidative stress. The dissipation of excess light energy as heat (= non-photochemical quenching, NPQ) in the antenna of photosystem II (PSII) is an efficient photoprotective mechanisms to minimize photo-oxidative damage. The NPQ capacity of plants varies substantially in response to different growth light conditions. In this work, the acclimation of plants to different growth light conditions was studied from the morphological to the molecular level, aiming at the identification of parameters or mechanisms that determine different NPQ capacities. The experimental work was focused on the comparative analysis of plants grown either under controlled lab conditions (LL: low light, NL: normal light, and HL: high light) or under natural, fluctuating light (NatL). In the evergreen plant *Monstera deliciosa*, which is known to develop an extremely high NPQ capacity under HL, a new and very efficient quenching mechanism was identified, which was based on energy transfer from PSII to PSI, and thus was termed energy spillover quenching (q_{SO}). Spillover quenching was only activated in Monstera plants acclimated to natural HL conditions, but not in LL grown Monstera plants. Activation of q_{SO} was accompanied by highly dynamic changes in the thylakoid membrane structure, indicating that q_{SO} activation requires light-dependent unstacking of grana membranes. Acclimation of *Arabidopsis thaliana* plants to HL and NatL was also accompanied by a strongly increased NPQ capacity in comparison to LL and NL grown plants. Interestingly, the increased NPQ capacity was also based on q_{SO} quenching in HL plants, but not in NatL grown plants, which showed an increased capacity of pH-regulated qE quenching. Detailed characterization of plants from different growth conditions corroborated the known morphological, physiological and biochemical properties of LL, NL and HL plants. NatL plants, however, were shown to combine properties of both LL and HL grown plants, leading to very efficient light utilization. Strikingly, the high qE capacity of NatL plants, correlated with increased dynamics of thylakoid membrane reorganization upon short-term acclimation to excess light. In conclusion, the thylakoid membrane organization and particularly the light-dependent and reversible unstacking of grana membranes likely represent the key parameters that provide the basis for the high acclimation capacity to rapidly changing LL and HL conditions of NatL grown plants in comparison to plants grown under constant light conditions.

5.2 Zusammenfassung

Die kurz- und langfristige Anpassung an variable Umweltbedingungen ist essentiell für die Überlebensfähigkeit von Pflanzen. Sonnenlicht ist nicht nur die unverzichtbare Energiequelle für die Photosynthese, sondern stellt gleichzeitig einen wichtigen und sehr dynamischen Stressfaktor dar. Unter den meisten natürlichen Bedingungen übersteigt die Menge an absorbierter Lichtenergie die Kapazität der Nutzbarkeit in der Photosysnthese, was zur Bildung von reaktiven Sauerstoffspezies und damit zu photo-oxidativem Stress führt. Die Abführung der überschüssigen Lichtenergie in Form von Wärme (= nicht-photochemische Löschung, NPQ) in den Antennen von Photosystem II (PSII) ist ein effizienter photprotektiver Mechanismus, um photo-oxidative Schädigungen zu minimieren. Die NPQ Kapazität von Pflanzen variiert erheblich in Abhängigkeit von der Lichtintensität während des Wachstums. In der vorliegenden Arbeit wurde die Anpassung von Pflanzen an verschiedene Lichtintensitäten von der morphologischen bis zur molekularen Ebene untersucht, mit dem Ziel, diejenigen Parameter bzw. Mechanismen zu identifizieren, welche die unterschiedlichen NPQ Kapazitäten bestimmen. Die Untersuchungen zielten auf die vergleichende Analyse von Pflanzen, die unter kontrollierten Laborbedingungen (LL: Schwachlicht, NL: Normallicht, HL: Starklicht) oder unter natürlichen, fluktuierenden Lichtbedingungen (NatL) gewachsen waren. In der immergrünen Pflanze *Monstera deliciosa*, die dafür bekannt ist unter HL Bedingungen eine ausgesprochen hohe NPQ Kapazität auszubilden, wurde ein neuartiger und sehr effizienter NPQ-Mechanismus identifiziert, der auf dem Energietransfer von PSII zu PSI beruhte und daher als ‚*spillover quenching*' (q_{SO}) bezeichnet wurde. *Spillover quenching* wurde nur in Monstera Pflanzen aktiviert, die an natürliche HL Bedingungen angepasst waren, nicht jedoch in LL gewachsenen Pflanzen. Die Aktivierung von q_{SO} ging einher mit hoch-dynamischen Änderungen in der Struktur der Thylakoidmembranen, was dafür spricht, dass die Aktivierung von q_{SO} einer Licht-regulierten Entstapelung der Thylakoidmembran bedarf. Auch die Anpassung von *Arabidopsis thaliana* Pflanzen an HL und NatL ging mit einer stark erhöhten NPQ Kapazität gegenüber LL und NL Pflanzen einher. Interessanterweise beruhte die erhöhte NPQ Kapazität in HL Pflanzen auch auf dem q_{SO} Mechnismus, jedoch war in NatL Pflanzen eine erhöhte Kapazität des pH-regulierten qE Mechanismus dafür verantwortlich. Die detaillierte Charakterisierung der Pflanzen, die unter unterschiedlichen Lichtbedingungen gewachsen waren, bestätigte die bekannten morphologischen, physiologischen und biochemischen Eigenschaften von LL, NL und HL Pflanzen. NatL Pflanzen waren dabei durch kombinierte Eigenschaften von LL und HL Pflanzen charakterisiert, die eine sehr effiziente Lichtnutzung in NatL Pflanzen ermöglichten. Interessanter Weise korrelierte die hohe qE Kapazität von NatL Pflanzen mit einer erhöhten Dynamik der Thylakoidmembran in der kurzfristigen Antwort auf überschüssiges

Lichtenergie. Zusammengefasst lässt sich sagen, dass die Organisation der Thylakoidmembran und insbesondere die lichtregulierte, reversible Entstapelung der Granamembranen wahrscheinlich die Schlüsselparameter sind, welche die Grundlage für die hohe Kapazität der Anpassung an schnell wechselnde LL und HL Bedingungen von NatL Pflanzen im Vergleich mit Pflanzen, die unter Laborbedingungen angezogen wurden, bilden.

6 References

Albertsson P (2001). A quantitative model of the domain structure of the photosynthetic membrane. Trends Plant Sci **6** (8): 349–354.

Allen JF (1992). Protein phosphorylation in regulation of photosynthesis. Biochim Biophys Acta **1098**: 275–335.

Alter P, Dreissen A, Luo F, and Matsubara S (2012). Acclimatory responses of *Arabidopsis* to fluctuating light environment: comparison of different sunfleck regimes and accessions. Photosynth Res **113** (1-3): 221–237.

Amunts A, Drory O, and Nelson N (2007). The structure of a plant photosystem I supercomplex at 3.4 Å resolution. Nature **447** (7140): 58–63.

Amunts A, and Nelson N (2008). Functional organization of a plant Photosystem I: Evolution of a highly efficient photochemical machine. Plant Physiol Biochem **46** (3): 228–237.

Amunts A, Toporik H, Borovikova A, and Nelson N (2010). Structure Determination and Improved Model of Plant Photosystem I. J Biol Chem **285** (5): 3478–3486.

Anderson, JM, and Osmond, CB (1987). Shade-sun responses: compromises between acclimation and photoinhibition: In: Photoinhibition (Amsterdam: Elsevier).

Anderson JM (1986). Photoregulation of the Composition, Function, and Structure of Thylakoid Membranes. Annu. Rev. Plant Physiol. **37**: 93–136.

Anderson JM (1992). Cytochrome b_6f complex: Dynamic molecular organization, function and acclimation. Photosynth Res **34**: 341–357.

Anderson JM, and Andersson B (1988). The dynamic photosynthetic membrane and regulation of solar energy conversion. Trends Biochem Sci **13** (9): 351–355.

Anderson JM, Chow WS, and Park Y (1995). The grand design of photosynthesis: Acclimation of the photosynthetic apparatus to environmental cues. Photosynth Res **46**: 129–139.

Armbruster U, Carrillo LR, Venema K, Pavlovic L, Schmidtmann E, Kornfeld A, Jahns P, Berry JA, Kramer DM, and Jonikas MC (2014). Ion antiport accelerates photosynthetic acclimation in fluctuating light environments. Nat Comms **5** (5439): 1–8.

Armbruster U, Labs M, Pribil M, Viola S, Xu W, Scharfenberg M, Hertle AP, Rojahn U, Jensen PE, Rappaport F, Joliot P, Dörmann P, Wanner G, and Leister D (2013). Arabidopsis CURVATURE THYLAKOID1 Proteins Modify Thylakoid Architecture by Inducing Membrane Curvature. The Plant Cell **25** (7): 2661–2678.

Arnon DI (1949). Copper Enzymees in Isolated Chloroplasts. Polyphenoloxidase in *Beta Vulgaris*. Plant Physiol. **24** (1): 1–15.

Arvidsson PO, and Sundby C (1999). A model for the topology of the chloroplast thylakoid membrane. Aust J Plant Physiol **26**: 687–694.

Aspinall-O'Dea M, Wentworth M, Pascal A, Robert B, Ruban AV, and Horton P (2002). In vitro reconstitution of the activated zeaxanthin state associated with energy dissipation in plants. PNAS **99** (25): 16331–16335.

Austin JR, Frost E, Vidi P, Kessler F, and Staehelin A (2006). Plastoglobules Are Lipoprotein Subcompartments of the Chloroplast That Are Permanently Coupled to Thylakoid Membranes and Contain Biosynthetic Enzymes. Plant cell online **18** (7): 1693–1703.

Avenson TJ, Ahn TK, Zigmantas D, Niyogi KK, Li Z, Ballottari M, Bassi R, and Fleming GR (2008). Zeaxanthin Radical Cation Formation in Minor Light-harvesting Complexes of Higher Plant Antenna. J Biol Chem **283** (6): 3550–3558.

Avenson TJ, Cruz JA, Kanazawa A, and Kramer DM (2005). Regulating the proton budget of higher plant photosynthesis. PNAS **27** (102): 9709–9713.

Bailey S, Walters RG, Jansson S, and Horton P (2001). Acclimation of Arabidopsis thaliana to the light environment: the existence of separate low light and high light responses. Planta **213** (5): 794–801.

Ballaré CL (1999). Keeping up with the neighbours: phytochrome sensing and other signalling mechanisms. Trends Plant Sci **4** (3): 97–102.

Ballottari M, Dall'Osto L, Morosinotto T, and Bassi R (2007). Contrasting Behavior of Higher Plant Photosystem I and II Antenna Systems during Acclimation. J Biol Chem **282** (12): 8947–8958.

Barber J, and Chow WS (1979). A Mechanism for Controlling the Stacking and Unstacking of Chloroplast Thylakoid Membranes. FEBS Letters **105** (1): 5–10.

Beisel KG, Jahnke S, Hofmann D, Koppchen S, Schurr U, and Matsubara S (2010). Continuous Turnover of Carotenes and Chlorophyll a in Mature Leaves of Arabidopsis Revealed by $^{14}CO_2$ Pulse-Chase Labeling. Plant Physiol. **152** (4): 2188–2199.

Bellafiore S, Barneche F, Peltier G, and Rochaix J (2005). State transitions and light adaptation require chloroplast thylakoid protein kinase STN7. Nature **433**: 892–895.

Bendall DS (1982). Photosynthetic cytochromes of oxygenic organisms. Biochim Biophys Acta **683**: 119–151.

Bennoun P, and Levine RP (1967). Detecting Mutants That Have Impaired Photosynthesis by Their Increased Level of Fluorescence. Plant Physiol. **42**: 1284–1287.

Ben-Shem A, Frolow F, and Nelson N (2003). Crystal structure of plant photosystem I. Nature **426**: 630–635.

Bergantino E, Sandonà D, Cugini D, and Bassi R (1998). The photosystem II subunit CP29 can be phosphorylated in both C3 and C4 plants as suggested by sequence analysis. Plant Mol Biol **36**: 11–22.

Bergantino E, Segala A, Brunetta A, Terado E, Rigoni F, Giacometti GM, and Szabò I (2003). Light- and pH-dependent structural changes in the PsbS subunit of photosystem II. Proc Natl Acad Sci USA **100** (25): 15265–15270.

Björkman O, and Demmig B (1987). Photon yield of O_2 evolution and chlorophyll fluorescence characteristics at 77 K among vascular plants of diverse origins. Planta **170**: 489–504.

Björkman, O. (1981). Responses to Different Quantum Flux Densities. Encyclopedia of Plant Physiology **Physiological Plant Ecology I**: 57–107.

Boekema EJ, van Breemen, Jan F.L, van Roon H, and Dekker JP (2000). Arrangement of photosystem II supercomplexes in crystalline macrodomains within the thylakoid membrane of green plant chloroplasts. J Mol Biol **301** (5): 1123–1133.

Bonardi V, Pesaresi P, Becker T, Schleiff E, Wagner R, Pfannschmidt T, Jahns P, and Leister D (2005). Photosystem II core phosphorylation and photosynthetic acclimation require two different protein kinases. Nature **437** (7062): 1179–1182.

Caffarri S, Kouřil R, Kereïche S, Boekema EJ, and Croce R (2009). Functional architecture of higher plant photosystem II supercomplexes. EMBO J **28** (19): 3052–3063.

Capaldi RA, and Aggeler R (2002). Mechanism of the F1F0-type ATP synthase, a biological rotary motor. Trends Biochem Sci **27** (3): 154–160.

Cavalier-Smith T (2000). Membrane heredity and early chloroplast evolution. Trends Plant Sci **5** (4): 174–182.

Chazdon RL (1986). Light Variation and Carbon Gain in Rain Forest Understorey Palms. J Ecol **74**: 995–1012.

Chazdon RL, and Pearcy RW (1986). Photosynthetic responses to light variation in rainforest species: II. Carbon gain and photosynthetic efficiency during lightflecks. Oecologia **69**: 524–531.

Chow WS, Kim E, Horton P, and Anderson JM (2005). Granal stacking of thylakoid membranes in higher plant chloroplasts: the physicochemical forces at work and the functional consequences that ensue. Photochem. Photobiol. Sci. **4** (12): 1081.

Chow WS, Melis A, and Anderson JM (1990). Adjustments of photosystem stoichiometry in chloroplasts improve the quantum efficiency of photosynthesis. PNAS **87**: 7502–7506.

Chow WS, Miller C, and Anderson JM (1991). Surface charges, the heterogeneous lateral distribution of the two photosystems, and thylakoid stacking. Biochim Biophys Acta - Bioenergetics **1057** (1): 69–77.

Chow WS, Qian L, Goodchild DJ, and Anderson JM (1988). Photosynthetic acclimation of Alocasia macrorrhiza (L.) G. Don to growth irradiance: structure, function and composition of chloroplasts. Aust J Plant Physiol **15**: 107–122.

Cisek R, Spencer L, Prent N, Zigmantas D, Espie GS, and Barzda V (2009). Optical microscopy in photosynthesis. Photosynth Res **102** (2-3): 111–141.

Clausen CH, Brooks MD, Li T, Grob P, Kemalyan G, Nogales E, Niyogi KK, and Fletcher DA (2014). Dynamic Mechanical Responses of Arabidopsis Thylakoid Membranes during PSII-Specific Illumination. Biophys. J. **106** (9): 1864–1870.

Croce R, Müller MG, Bassi R, and Holzwarth AR (2001). Carotenoid-to-Chlorophyll Energy Transfer in Recombinant Major Light-Harvesting Complex (LHCII) of Higher Plants. I. Femtosecond Transient Absorption Measurements. Biophys. J. **80**: 901–915.

Crouchman S, Ruban AV, and Horton P (2006). PsbS enhances nonphotochemical fluorescence quenching in the absence of zeaxanthin. FEBS Letters **580** (8): 2053–2058.

Cruz JA, Sacksteder CA, Kanazawa A, and Kramer DM (2001). Contribution of Electric Field (Δψ) to Steady-State Transthylakoid Proton Motive Force (pmf) in Vitro and in Vivo. Control of pmf Parsing into Δψ and ΔpH by Ionic Strength. Biochemistry **40** (5): 1226–1237.

Dall'Osto L, Caffarri S, and Bassi R (2005). A Mechanism of Nonphotochemical Energy Dissipation, Independent from PsbS, Revealed by a Conformational Change in the Antenna Protein CP26. The Plant Cell **17** (4): 1217–1232.

Danielsson R, Albertsson P, Mamedov F, and Styring S (2004). Quantification of photosystem I and II in different parts of the thylakoid membrane from spinach. Biochim Biophys Acta - Bioenergetics **1608** (1): 53–61.

de la Torre WR, and Burkey KO (1990a). Acclimation of barley to changes in light intensity: chlorophyll organization. Photosynth Res **24**: 117–125.

de la Torre WR, and Burkey KO (1990b). Acclimation of barley to changes in light intensity: photosynthetic electron transport activity and components. Photosynth Res **24**: 127–136.

Dekker JP, and Boekema EJ (2005). Supramolecular organization of thylakoid membrane proteins in green plants. Biochim Biophys Acta - Bioenergetics **1706** (1-2): 12–39.

Demmig-Adams B, and Adams WW (1992). Photoprotection and Other Responses of Plants to High Light Stress. Annu. Rev. Plant Physiol. Plant. Mol. Biol. (Annual Review of Plant Physiology) **43**: 599–626.

Demmig-Adams B, and Adams WW (1996). The role of xanthophyll cycle carotenoids in the protection of photosynthesis. Trends Plant Sci **1** (1): 21–26.

Demmig-Adams B, Adams WW, Heber U, Neimanis S, Winter K, Krüger A, Czygan F-C, Bilger W, and Björkman O (1990). Inhibition of Zeaxanthin Formation and of Rapid

Changes in Radiationless Energy Dissipation by Dithiothreitol in Spinach Leaves and Chloroplasts. Plant Physiol. **92**: 293–301.

Demmig-Adams B, Ebbert V, Mellman DL, Mueh KE, Schaffer L, Funk C, Zarter CR, Adamska I, Jansson S, and Adams WW (2006). Modulation of PsbS and flexible vs sustained energy dissipation by light environment in different species. Physiol Plant **127** (4): 670–680.

Demmig-Adams B, Muller O, Stewart JJ, Cohu CM, and Adams WW (2015). Chloroplast thylakoid structure in evergreen leaves employing strong thermal energy dissipation. J. Photochem. Photobiol. **152** (Pt B): 357–366.

Dörmann P, and Benning C (2002). Galactolipids rule in seed plants. Trends Plant Sci **7** (3): 112–118.

Dörmann P, Hoffmann-Benning S, Balbo I, and Benning C (1995). Isolation and Characterization of an Arabidopsis Mutant Deficient in the Thylakoid Lipid Digalactosyl Diacylglycerol. The Plant Cell **7**: 1801–1810.

Escoubas J, Lomas M, LaRosche J, and Falkowski PG (1995). Light intensity regulation of cab gene transcription is signaled by redox state of the plastoquinone pool. PNAS **92**: 10237–11241.

Färber A, Young AJ, Ruban AV, and Jahns P (1997). Dynamics of Xanthophyll-Cycle Activity in Different Antenna Subcomplexes in the Photosynthetic Membranes of Higher Plants. Plant Physiol. **115**: 1609–1618.

Fey V, Wagner R, Bräutigam K, Wirtz M, Hell R, Dietzmann A, Leister D, Oelmuller R, and Pfannschmidt T (2005). Retrograde Plastid Redox Signals in the Expression of Nuclear Genes for Chloroplast Proteins of Arabidopsis thaliana. J Biol Chem **280** (7): 5318–5328.

Finazzi G (2002). Redox-Coupled Proton Pumping Activity in Cytochrome b_6f As Evidenced by the pH Dependence of Electron Transfer in Whole Cells of *Chlamydomonas reinhardtii*. Biochemistry **41** (23): 7475–7482.

Finazzi G, Johnson GN, Dall'Osto L, Joliot P, Wollman F, and Bassi R (2004). A zeaxanthin-independent nonphotochemical quenching mechanism localized in the photosystem II core complex. PNAS **101** (33): 12375–12380.

Formaggio E, Cinque G, and Bassi R (2001). Functional Architecture of the Major Light-harvesting Complex from Higher Plants. J Mol Biol **314**: 1157–1166.

Foyer CH, and Noctor G (2009). Redox regulation in photosynthetic organisms: signaling, acclimation, and practical implications. Antioxidants & Redox Signaling **11**: 861–905.

Galvez-Valdivieso G, and Mullineaux PM (2010). The role of reactive oxygen species in signalling from chloroplasts to the nucleus. Physiol Plant **138** (4): 430–439.

Ganeteg U, Külheim C, Andersson J, and Jansson S (2004). Is Each Light-Harvesting Complex Protein Important for Plant Fitness? Plant Physiol. **134** (1): 502–509.

Genty B, Briantais J, and Baker NR (1989). The relationship between the quantum yield of photosynthetic electron transport and quenching of chlorophyll fluorescence. Biochim Biophys Acta **990**: 87–92.

Ghosh S, Hudak KA, Dumbroff EB, and Thompson JE (1994). Release of photosynthetic protein catabolites by blebbing from thylakoids. Plant Physiol. **106**: 1547–1553.

Gilmore AM, and Yamamoto HY (1991). Resolution of lutein and zeaxanthin using a non-endcapped, lightly carbon-loaded C 1 8 high-performance liquid chromatographic column. Journal of Chromatography (543): 137–145.

Green BR, Pichersky E, and Kloppstech K (1991). Chlorophyll a/b-binding proteins: an extended family. Trends Biochem Sci **16** (5): 181–186.

Guskov A, Kern J, Gabdulkhakov A, Broser M, Zouni A, and Saenger W (2009). Cyanobacterial photosystem II at 2.9-Å resolution and the role of quinones, lipids, channels and chloride. Nat Struct Mol Biol **16** (3): 334–342.

Haehnel W (1984). Photosynthetic Electron Transport in Higher Plants. Annu. Rev. Plant Physiol. **35**: 659–693.

Haferkamp S, Haase W, Pascal AA, van Amerongen H, and Kirchhoff H (2010). Efficient Light Harvesting by Photosystem II Requires an Optimized Protein Packing Density in Grana Thylakoids. J Biol Chem **285** (22): 17020–17028.

Hager A (1969). Lichtbedingte pH-Erniedrigung in einem Chloroplasten-Kompartiment als Ursache der enzymatischen Violaxanthin- -> Zeaxanthin-Umwandlung; Beziehungen zur Photophosphorylierung. Planta **89**: 224–243.

Härtel H, Lokstein H, Dörmann P, Grimm B, and Benning C (1997). Changes in the Composition of the Photosynthetic Apparatus in the Galactolipid-Deficient *dgd1* Mutant of *Arabidopsis thaliana*. Plant Physiol. **115**: 1175–1184.

Härtel H, Lokstein H, Dörmann P, Trethewey RN, and Benning C (1998). Photosynthetic light utilization and xanthophyll cycle activity in the galactolipid deficient *dgd1* mutant of *Arabidopsis thaliana*. Plant Physiol Biochem **36** (6): 407–417.

Hauska G, Hurt E, Gabellini N, and Lockau W (1983). Comparative Aspects of Quinol-Cytochrome c /Plastocyanin Oxidoreductases. Biochim Biophys Acta **726**: 97–133.

Havaux M, Dall'Osto L, and Bassi R (2007). Zeaxanthin Has Enhanced Antioxidant Capacity with Respect to All Other Xanthophylls in Arabidopsis Leaves and Functions Independent of Binding to PSII Antennae. Plant Physiol. **145** (4): 1506–1520.

Havaux M, Eymery F, Porfirova S, Rey P, and Dörmann P (2005). Vitamin E Protects against Photoinhibition and Photooxidative Stress in *Arabidopsis thaliana*. Plant cell online **17** (12): 3451–3469.

Havaux M, and Niyogi KK (1999). The violaxanthin cycle protects plants from photooxidative damage by more than one mechanism. PNAS **96**: 8762–8767.

Herbstova M, Tietz S, Kinzel C, Turkina MV, and Kirchhoff H (2012). Architectural switch in plant photosynthetic membranes induced by light stress. PNAS **109** (49): 20130–20135.

Hideg E, Kálai T, Hideg K, and Vass I (1998). Photoinhibition of Photosynthesis in Vivo Results in Singlet Oxygen Production Detection via Nitroxide-Induced Fluorescence Quenching in Broad Bean Leaves. Biochemistry **37**: 11405–11411.

Hirth M, Dietzel L, Steiner S, Ludwig R, Weidenbach H, Pfalz J, and Pfannschmidt T (2013). Photosynthetic acclimation responses of maize seedlings grown under artificial laboratory light gradients mimicking natural canopy conditions. Front. Plant Sci. **4** (334): 1–12.

Holt NE, Zigmantas D, Vulkanas L, Li X, Niyogi KK, and Fleming GR (2005). Carotenoid Cation Formation and the Regulation of Photosynthetic Light Harvesting. Science **307** (5708): 430–433.

Holzwarth AR, and Jahns P (2014). Non-Photochemical Quenching Mechanisms in Intact Organisms as Derived from Ultrafast-Fluorescence Kinetic Studies. In Non-Photochemical Quenching and Energy Dissipation in Plants, Algae and Cyanobacteria, B. Demmig-Adams, G. Garab, W. Adams III, and Govindjee, eds (Dordrecht: Springer Netherlands), pp. 129–156.

Holzwarth AR, Miloslavina Y, Nilkens M, and Jahns P (2009). Identification of two quenching sites active in the regulation of photosynthetic light-harvesting studied by time-resolved fluorescence. Chem. Phys. Lett. **483** (4-6): 262–267.

Hope AB (2000). Electron transfers amongst cytochrome f, plastocyanin and photosystem I: kinetics and mechanisms. Biochim Biophys Acta - Bioenergetics **1456** (1): 5–26.

Horton P, Johnson MP, Perez-Bueno ML, Kiss AZ, and Ruban AV (2008). Photosynthetic acclimation: Does the dynamic structure and macro-organisation of photosystem II in higher plant grana membranes regulate light harvesting states? FEBS Journal **275** (6): 1069–1079.

Horton P, Ruban AV, and Walters RG (1996). Regulation of Light Harvesting in Green Plants. Annu. Rev. Plant Biol. **47**: 655–684.

Jahns P (1995). The Xanthophyll Cycle in Intermittent Light-Crown Pea Plants. Plant Physiol. **108**: 149–156.

Jahns P, Graf M, Munekage Y, and Shikanai T (2002). Single point mutation in the Rieske iron–sulfur subunit of cytochrome b6/f leads to an altered pH dependence of plastoquinol oxidation in Arabidopsis. FEBS Letters **519** (1-3): 99–102.

Jahns P, and Holzwarth AR (2012). The role of the xanthophyll cycle and of lutein in photoprotection of photosystem II. Biochim Biophys Acta - Bioenergetics **1817** (1): 182–193.

Jahns P, Latowski D, and Strzalka K (2009). Mechanism and regulation of the violaxanthin cycle: The role of antenna proteins and membrane lipids. Biochim Biophys Acta - Bioenergetics **1787** (1): 3–14.

Jahns P, Wehner A, Paulsen H, and Hobe S (2001). De-epoxidation of Violaxanthin after Reconstitution into Different Carotenoid Binding Sites of Light-harvesting Complex II. J Biol Chem **276** (25): 22154–22159.

Jarvis P, Dörmann P, Peto CA, Lutes J, Benning C, and Chory J (2000). Galactolipid deficiency and abnormal chloroplast development in the *Arabidopsis MGD synthase 1* mutant. PNAS **97** (14): 8175–8179.

Johnson GN, Young AJ, Scholes JD, and Horton P (1993). The dissipation of excess excitation energy in British plant species. Plant Cell Environ **16**: 673–679.

Johnson MP, Davison PA, Ruban AV, and Horton P (2008a). The xanthophyll cycle pool size controls the kinetics of non-photochemical quenching in *Arabidopsis thaliana*. FEBS Letters **582** (2): 262–266.

Johnson MP, Havaux M, Triantaphylides C, Ksas B, Pascal AA, Robert B, Davison PA, Ruban AV, and Horton P (2007). Elevated Zeaxanthin Bound to Oligomeric LHCII Enhances the Resistance of Arabidopsis to Photooxidative Stress by a Lipid-protective, Antioxidant Mechanism. J Biol Chem **282** (31): 22605–22618.

Johnson MP, Perez-Bueno ML, Zia A, Horton P, and Ruban AV (2008b). The Zeaxanthin-Independent and Zeaxanthin-Dependent qE Components of Nonphotochemical Quenching Involve Common Conformational Changes within the Photosystem II Antenna in Arabidopsis. Plant Physiol. **149** (2): 1061–1075.

Johnson MP, and Ruban AV (2009). Photoprotective Energy Dissipation in Higher Plants Involves Alteration of the Excited State Energy of the Emitting Chlorophyll(s) in the Light Harvesting Antenna II (LHCII). J Biol Chem **284** (35): 23592–23601.

Junge W, Sielaff H, and Engelbrecht S (2009). Torque generation and elastic power transmission in the rotary F_OF_1-ATPase. Nature **459** (7245): 364–370.

Kalituho L, Beran KC, and Jahns P (2007). The Transiently Generated Nonphotochemical Quenching of Excitation Energy in Arabidopsis Leaves Is Modulated by Zeaxanthin. Plant Physiol. **143** (4): 1861–1870.

Kasahara M, Kagawa T, Oikawa K, Suetsugu N, Miyao M, and Wada M (2002). Chloroplast avoidance movement reduces photodamage in plants. Nature **420** (6917): 829–832.

Kautsky H, and Hirsch M (1931). Neue Versuche zur Kohlensäureassimilation. Naturwissenschaften **19** (48): 964.

Kirchhoff H (2013). Architectural switches in plant thylakoid membranes. Photosynth Res **116** (2-3): 481–487.

Kirchhoff H (2014). Diffusion of molecules and macromolecules in thylakoid membranes. Biochim Biophys Acta - Bioenergetics **1837** (4): 495–502.

Kirchhoff H, Hall C, Wood M, Herbstova M, Tsabari O, Nevo R, Charuvi D, Shimoni E, and Reich Z (2011). Dynamic control of protein diffusion within the granal thylakoid lumen. PNAS **108** (50): 20248–20253.

Kirchhoff H, Mukherjee U, and Galla H (2002). Molecular Architecture of the Thylakoid Membrane: Lipid Diffusion Space for Plastoquinone. Biochemistry **41** (15): 4872–4882.

Klimmek F, Ganeteg U, Ihalainen JA, van Roon H, Jensen PE, Scheller HV, Dekker JP, and Jansson S (2005). Structure of the Higher Plant Light Harvesting Complex I: In Vivo Characterization and Structural Interdependence of the Lhca Proteins. Biochemistry **44** (8): 3065–3073.

Klughammer C, and Schreiber U (2008). Saturation Pulse method for assessment of energy conversion in PS I. PAN **1**: 11–14.

Knapp AK, and Smith WK (1989). Influence of Growth Form on Ecophysiological Responses to Variable Sunlight in Subalpine Plants. Ecology **70** (4): 1069–1082.

Kono M, Noguchi K, and Terashima I (2014). Roles of the Cyclic Electron Flow Around PSI (CEF-PSI) and O_2-Dependent Alternative Pathways in Regulation of the Photosynthetic Electron Flow in Short-Term Fluctuating Light in *Arabidopsis thaliana*. Plant Cell Physiol **55** (5): 990–1004.

Kono M, and Terashima I (2014). Long-term and short-term responses of the photosynthetic electron transport to fluctuating light. J. Photochem. Photobiol. **137**: 89–99.

Kovacs L, Damkjaer J, Kereiche S, Ilioaia C, Ruban AV, Boekema EJ, Jansson S, and Horton P (2006). Lack of the Light-Harvesting Complex CP24 Affects the Structure and Function of the Grana Membranes of Higher Plant Chloroplasts. Plant cell online **18** (11): 3106–3120.

Kramer DM, Avenson TJ, and Edwards GE (2004a). Dynamic flexibility in the light reactions of photosynthesis governed by both electron and proton transfer reactions. Trends Plant Sci **9** (7): 349–357.

Kramer DM, Cruz JA, and Kanazawa A (2003). Balancing the central roles of the thylakoid proton gradient. Trends Plant Sci **8** (1): 27–32.

Kramer DM, Johnson GN, Kiirats O, and Edwards GE (2004b). New fluorescence parameters for the determination of Q_A redox state and excitation energy fluxes. Photosynth Res **79**: 209–218.

Kramer DM, and Sacksteder CA (1998). A diffused-optics flash kinetic spectrophotometer (DOFS) for measurements of absorbance changes in intact plants in the steady-state. Photosynth Res **56**: 103–112.

Kramer DM, Sacksteder CA, and Cruz JA (1999). How acidic is the lumen? Photosynth Res **60**: 151–163.

Krause, GH, and Jahns, P. (2003). Light-Harvesting Antennas in Photosynthesis: Pulse Amplitude Modulated Chlorophyll Fluorometry and its Application in Plant Science.

Krause, GH, and Jahns, P. (2004). Non-photochemical Energy Dissipation Determined by Chlorophyll Fluorescence Quenching. Characterization and Function.

Krause GH (1973). The high-energy state of the thylakoid system as indicated by chlorophyll fluorescence and chloroplast shrinkage. Biochim Biophys Acta - Bioenergetics **292** (3): 715–728.

Krause GH, Vernotte C, and Briantais J (1982). Photoinduced quenching of chlorophyll fluorescence in intact chloroplasts and algae. Resolution into two components. Biochim Biophys Acta - Bioenergetics **679** (1): 116–124.

Küchler M, Decker S, Hörmann F, Soll J, and Heins L (2002). Protein import into chloroplasts involves redox-regulated proteins. EMBO J **21** (22): 6136–6145.

Külheim C, Ågren J, and Jansson S (2002). Rapid Regulation of Light Harvesting and Plant Fitness in the Field. Science **297** (5578): 91–93.

Laemmli UK (1970). Cleavage of Structural Proteins during the Assembly of the Head of Bacteriophage T4. Nature **227**: 680–685.

Lee J, Kim DH, and Hwang I (2014). Specific targeting of proteins to outer envelope membranes of endosymbiotic organelles, chloroplasts, and mitochondria. Front. Plant Sci. **5** (173): 1-11.

Leong TY, and Anderson JM (1984). Adaptation of the thylakoid membranes of pea chloroplasts to light intensities. II. Regulation of electron transport capacities, electron carriers, coupling factor (CF_1) activity and rates of photosynthesis. Photosynth Res **5**: 117–128.

Li X, Björkman O, Shih C, Grossmann AR, Rosenquist M, Jansson S, and Niyogi KK (2000). A pigment-binding protein essential for regulation of photosynthetic light harvesting. Nature **403**: 391–395.

Li X, Gilmore AM, Caffarri S, Bassi R, Golan T, Kramer DM, and Niyogi KK (2004). Regulation of Photosynthetic Light Harvesting Involves Intrathylakoid Lumen pH Sensing by the PsbS Protein. J Biol Chem **279** (22): 22866–22874.

Lichtenthaler HK (2007). Biosynthesis, accumulation and emission of carotenoids, α-tocopherol, plastoquinone, and isoprene in leaves under high photosynthetic irradiance. Photosynth Res **92** (2): 163–179.

Lichtenthaler HK, Buschmann C, Döll M, Fietz H, Bach T, Kozel U, Meier D, and Rahmsdorf U (1981). Photosynthetic activity, chloroplast ultrastructure, and leaf characteristics of high-light and low-light plants and of sun and shade leaves. Photosynth Res **2**: 115–141.

Lichtenthaler HK, and Schindler C (1992). Studies on the photoprotective function of Zx at high-light conditions. Photosynth Res **4**: 517–520.

Liu Z, Yan H, Wang K, Kuang T, Zhang J, Gui L, An X, and Chang W (2004). Crystal structure of spinach major light-harvesting complex at 2.72 Å resolution. Nature **428**: 287–292.

Lowry OH, Rosenbrough NJ, Farr AL, and Randall RJ (1951). Protein Measurement with the Folin Phenol Reagent. J Biol Chem **193** (1): 265–275.

Malkin S, Armond PA, Mooney HA, and Fork DC (1981). Photosystem II Photosynthetic Unit Sizes from Fluorescence Induction in Leaves: Correlation to Photosynthetic Capacity. Plant Physiol. **67**: 570–579.

Manara A, DalCorso G, Leister D, Jahns P, Baldan B, and Furini A (2014). AtSIA1 AND AtOSA1: two Abc1 proteins involved in oxidative stress responses and iron distribution within chloroplasts. New Phytol **201** (2): 452–465.

Mateo A, Funck D., Mühlenbock P, Kular B, Mullineaux PM, and Karpinski S (2006). Controlled levels of salicylic acid are required for optimal photosynthesis and redox homeostasis. J Exp Bot **57** (8): 1795–1807.

Mehler AH (1951). Studies on Reactions of Illuminated Chloroplasts.: I. Mechanism of the Reduction of Oxygen and Other Hill Reagents. Arch Biochem Biophys **33** (1): 65–77.

Melis A (1991). Dynamics of photosynthetic membrane composition and function. Biochim Biophys Acta - Bioenergetics **1058** (2): 87–106.

Melis A (1999). Photosystem-II damage and repair cycle in chloroplasts: what modulates the rate of photodamage in vivo? Trends Plant Sci **4** (4): 130–135.

Miloslavina Y, Szczepaniak M, Müller MG, Sander J, Nowaczyk M, Rögner M, and Holzwarth AR (2006). Charge Separation Kinetics in Intact Photosystem II Core Particles Is Trap-Limited. A Picosecond Fluorescence Study †. Biochemistry **45** (7): 2436–2442.

Miloslavina Y, Wehner A, Lambrev PH, Wientjes E, Reus M, Garab G, Croce R, and Holzwarth AR (2008). Far-red fluorescence: A direct spectroscopic marker for LHCII oligomer formation in non-photochemical quenching. FEBS Letters **582** (25-26): 3625–3631.

Mishra Y, Jänkänpää HP, Kiss AZ, Funk C, Schröder WP, and Jansson S (2012). Arabidopsis plants grown in the field and climate chambers significantly differ in leaf morphology and photosystem components. BMC Plant Biol **12** (6): 1-18.

Mitchell P (1961). Coupling of Phosphorylation to Electron and Hydrogen Transfer by a Chemi-Osmotic Type of Mechanism. Nature **191**: 144–148.

Mittler R, Vanderauwera S, Gollery M, and van Breusegem F (2004). Reactive oxygen gene network of plants. Trends in Plant Science **9** (10): 490–498.

Morosinotto T, Ballottari M, Klimmek F, Jansson S, and Bassi R (2005). The Association of the Antenna System to Photosystem I in Higher Plants. J Biol Chem **280** (35): 31050–31058.

Müller MG, Lambrev P, Reus M, Wientjes E, Croce R, and Holzwarth AR (2010). Singlet Energy Dissipation in the Photosystem II Light-Harvesting Complex Does Not Involve Energy Transfer to Carotenoids. Chem. Eur. J. of Chem. Phys. **11** (6): 1289–1296.

Müller P, Li X, and Niyogi KK (2001). Non-Photochemical Quenching. A Response to Excess Light Energy. Plant Physiol. **125**: 1558–1566.

Mullineaux CW (2005). Function and evolution of grana. Trends Plant Sci **10** (11): 521–525.

Murata N (1969). Control of excitation transfer in photosynthesis. II. Magnesium ion-dependent distribution of excitation energy between two pigment systems in spinach chloroplasts. Biochimica et Biophysica Acta (BBA) - Bioenergetics **189** (2): 171–181.

Murata N, and Sugahara K (1969). Control of excitation transfer in photosynthesis. III. Light-induced decrease of chlorophyll a fluorescence related to photophosphorylation system in spinach chloroplasts. Biochim Biophys Acta - Bioenergetics **189** (2): 182–192.

Murchie EH (2004). Acclimation of photosynthesis to high irradiance in rice: gene expression and interactions with leaf development. J Exp Bot **56** (411): 449–460.

Mustárdy L, and Garab G (2003). Granum revisited. A three-dimensional model ? where things fall into place. Trends Plant Sci **8** (3): 117–122.

Niemelä PS, Hyvönen MT, and Vattulainen I (2009). Atom-scale molecular interactions in lipid raft mixtures. Biochimica et Biophysica Acta (BBA) - Biomembranes **1788** (1): 122–135.

Nilkens M, Kress E, Lambrev PH, Miloslavina Y, Müller MG, Holzwarth AR, and Jahns P (2010). Identification of a slowly inducible zeaxanthin-dependent component of non-photochemical quenching of chlorophyll fluorescence generated under steady-state conditions in Arabidopsis. Biochim Biophys Acta - Bioenergetics **1797** (4): 466–475.

Oelze M, Kandlbinder A, and Dietz K (2008). Redox regulation and overreduction control in the photosynthesizing cell: Complexity in redox regulatory networks. Biochim Biophys Acta **1780** (11): 1261–1272.

Ögren E, and Sundin U (1996). Photosynthetic responses to variable light: a comparison of species from contrasting habitats. Oecologia **106**: 18–27.

Ort DR (2001). When There Is Too Much Light. Plant Physiol. **125**: 29–32.

Page M, Sultana N, Paszkiewicz K, Florance H, and Smirnoff N (2012). The influence of ascorbate on anthocyanin accumulation during high light acclimation in Arabidopsis thaliana: further evidence for redox control of anthocyanin synthesis. Plant Cell Environ **35** (2): 388–404.

Papageorgiou G, and Govindjee (1968a). Light-Induced Changes in the Fluorescence Yield of Chlorophyll a In Vivo I. Anacystis nidulans. Biophys. J. **8**: 1299–1315.

Papageorgiou G, and Govindjee (1968b). Light-Induced Changes in the Fluorescence Yield of Chlorophyll a In Vivo II. Chlorella Pyrenoidosa. Biophys. J. **8**: 1316–1328.

Paulsen H, Rümler U, and Rüdiger W (1990). Reconstitution of pigment-containing complexes from light-harvesting chlorophyll a/b-binding protein overexpressed in *Escherichia coli*. Planta **181**: 204–211.

Pearcy RW, and Calkin HW (1983). Carbon dioxide exchange of C_3 and C_4 tree species in the understory of a Hawaiian forest. Oecologia **58**: 26–32.

Peterman EJ, Monshouwer R, van Stokkum, IHM, van Grondelle R, and van Amerongen H (1997). Ultrafast singlet excitation transfer from carotenoids to chlorophylls via different pathways in light-harvesting complex II of higher plants. Chem. Phys. Lett. **264** (3-4): 279–284.

Pfannschmidt T (2003). Chloroplast redox signals: how photosynthesis controls its own genes. Trends Plant Sci **8** (1): 33–41.

Plumley FG, and Schmidt GW (1987). Reconstitution of chlorophyll a/b light-harvesting complexes: Xanthophyll-dependent assembly and energy transfer. PNAS **84**: 146–150.

Pollard DFW (1970). The effect of rapidly changing light on the rate of photosynthesis in largetooth aspen (*Populus grandidentata*). Can J Bot **48** (4): 823–829.

Pribil M, Labs M, and Leister D (2014). Structure and dynamics of thylakoids in land plants. J Exp Bot **65** (8): 1955–1972.

Qin X, Suga M, Kuang T, and Shen J (2015). Structural basis for energy transfer pathways in the plant PSI-LHCI supercomplex. Science **438** (6238): 989–995.

Queval G, and Foyer CH (2012). Redox regulation of photosynthetic gene expression. Phil. Trans. R. Soc. B **367** (1608): 3475–3485.

Rachmilevitch S, Lambers H, and Huang B (2008). Short-term and long-term root respiratory acclimation to elevated temperatures associated with root thermotolerance for two Agrostis grass species. J Exp Bot **59** (14): 3803–3809.

Reifarth F, Christen G, Seeliger AG, Dörmann P, Benning C, and Renger G (1997). Modification of the Water Oxidizing Complex in Leaves of the *dgd1* Mutant of *Arabidopsis*

thaliana Deficient in the Galactolipid Digalactosyldiacylglycerol. Biochemistry **36** (39): 11769–11776.

Retkute R, Smith-Unna SE, Smith RW, Burgess AJ, Jensen OE, Johnson GN, Preston SP, and Murchie EH (2015). Exploiting heterogeneous environments: does photosynthetic acclimation optimize carbon gain in fluctuating light? J Exp Bot **66** (9): 2437–2447.

Roden JS, and Pearcy RW (1993). Effect of leaf flutter on the light environment of poplars. Oecologia **93**: 201–207.

Ruban AV, Berera R, Ilioaia C, van Stokkum, Ivo H M, Kennis JTM, Pascal AA, van Amerongen H, Robert B, Horton P, and van Grondelle R (2007). Identification of a mechanism of photoprotective energy dissipation in higher plants. Nature **450** (7169): 575–578.

Ruban AV, and Horton P (1999). The Xanthophyll Cycle Modulates the Kinetics of Nonphotochemical Energy Dissipation in Isolated Light-Harvesting Complexes, Intact Chloroplasts, and Leaves of Spinach. Plant Physiol. (119): 531–542.

Ruban AV, and Johnson MP (2009). Dynamics of higher plant photosystem cross-section associated with state transitions. Photosynth Res **99** (3): 173–183.

Ruban AV, Wentworth M, Yakushevska AE, Andersson J, Lee PJ, Keegstra W, Dekker JP, Boekema EJ, Jansson S, and Horton P (2003). Plants lacking the main lightharvesting complex retain photosystem II macro-organization. Nature **421**: 648–652.

Sacksteder CA, and Kramer DM (2000). Dark-interval relaxation kinetics (DIRK) of absorbance changes as a quantitative probe of steady-state electron transfer. Photosynth Res **66** (1-2): 145–158.

Schleiff E, and Becker T (2010). Common ground for protein translocation: access control for mitochondria and chloroplasts. Nat Rev Mol Cell Biol **12** (1): 48–59.

Schofield O, Grzymski J, Moline M, and Jovine R (1998). Impact of temperature acclimation on photosynthesis in the toxic red-tide dinoflagellate *Alexandrium fundyense* (Ca28). J. Plankton Res. **20** (7): 1241–1258.

Schöttler MA, Albus CA, and Bock R (2011). Photosystem I: Its biogenesis and function in higher plants. J Plant Physiol **168** (12): 1452–1461.

Schöttler MA, and Tóth SZ (2014). Photosynthetic complex stoichiometry dynamics in higher plants: environmental acclimation and photosynthetic flux control. Front. Plant Sci. **5** (188): 1–15.

Schreiber U, Schliwa U, and Bilger W (1986). Continuous recording of photochemical and non-photochemical chlorophyll fluorescence quenching with a new type of modulation fluorometer. Photosynth Res **10**: 51–62.

Seelert H, Poetsch A, Dencher NA, Engel A, Stahlberg H, and Müller DJ (2000). Proton-powered turbine of a plant motor. Nature **405**: 418–419.

Seemann JR, Sharkey TD, Wang JL, and Osmond CB (1987). Environmental Effects on Photosynthesis, Nitrogen-Use Efficiency, and Metabolite Pools in Leaves of Sun and Shade Plants. Plant Physiol. **84**: 796–802.

Shimoni E, Rav-Hon O, Ohad I, Brumfeld V, and Reich Z (2005). Three-Dimensional Organization of Higher-Plant Chloroplast Thylakoid Membranes Revealed by Electron Tomography. Plant cell online **17** (9): 2580–2586.

Siefermann-Harms D (1985). Caroetenoids in photosynthesis. I. Localization in photosynthetic membranes and light-harvesting function. Biochim Biophys Acta **811**: 325–335.

Slavov C, Ballottari M, Morosinotto T, Bassi R, and Holzwarth AR (2008). Trap-Limited Charge Separation Kinetics in Higher Plant Photosystem I Complexes. Biophys. J. **94** (9): 3601–3612.

Smith MD, Ghosh S, Dumbroff EB, and Thompson JE (1997). Characterization of Thylakoid-Derived Lipid-Protein Particles Bearing the Large Subunit of Ribulose-1,5-Bisphosphate Carboxylase/Oxygenase. Plant Physiol. **115**: 1073–1082.

Smith MD, Licatalosi DD, and Thompson JE (2000). Co-Association of Cytochrome f Catabolites and Plastidy-Lipid-Associated Protein with Chloroplast Lipid Particles. Plant Physiol. **124**: 211–221.

Spetea C, and Schoefs B (2010). Solute transporters in plant thylakoid membranes: Key players during photosynthesis and light stress. Commun Integr Biol **3** (2): 122–129.

Standfuss J, van Scheltinga, Anke C T, Lamborghini M, and Kühlbrandt W (2005). Mechanisms of photoprotection and nonphotochemical quenching in pea light-harvesting complex at 2.5 Å resolution. EMBO J **24**: 919–928.

Stirbet A, and Govindjee (2011). On the relation between the Kautsky effect (chlorophyll a fluorescence induction) and Photosystem II: Basics and applications of the OJIP fluorescence transient. J. Photochem. Photobiol. **104** (1-2): 236–257.

Szymanski J, Brotman Y, Willmitzer L, and Cuadros-Inostroza A (2014). Linking Gene Expression and Membrane Lipid Composition of Arabidopsis. The Plant Cell **26** (3): 915–928.

Takizawa K, Cruz JA, Kanazawa A, and Kramer DM (2007). The thylakoid proton motive force in vivo. Quantitative, non-invasive probes, energetics, and regulatory consequences of light-induced pmf. Biochim Biophys Acta - Bioenergetics **1767** (10): 1233–1244.

Telfer A (2002). What is β-carotene doing in the photosystem II reaction centre? Phil. Trans. R. Soc. B **357** (1426): 1431–1440.

Tessmer OL, Jiao Y, Cruz JA, Kramer DM, and Chen J (2013). Functional approach to high-throughput plant growth analysis. BMC Syst Biol **7** (6): 1–13.

Tevini M, and Steinmüller D (1985). Composition and function of plastoglobuli II. Lipid composition of leaves and plastoglobuli during beech leaf senescence. Planta **163**: 91–96.

Tikkanen M, Grieco M, Nurmi M, Rantala M, Suorsa M, and Aro E (2012). Regulation of the photosynthetic apparatus under fluctuating growth light. Phil. Trans. R. Soc. B **367** (1608): 3486–3493.

Triantaphylidès C, and Havaux M (2009). Singlet oxygen in plants: production, detoxification and signaling. Trends in Plant Science **14** (4): 219–228.

Umena Y, Kawakami K, Shen J, and Kamiya N (2011). Crystal structure of oxygen-evolving photosystem II at a resolution of 1.9 Å. Nature **473** (7345): 55–60.

Vainonen JP, Hansson M, and Vener AV (2005). STN8 Protein Kinase in *Arabidopsis thaliana* Is Specific in Phosphorylation of Photosystem II Core Proteins. J Biol Chem **280** (39): 33679–33686.

Vass I, and Styring S (1993). Characterization of Chlorophyll Triplet Promoting States in Photosystem II Sequentially Induced during Photoinhibition. Biochemistry **32**: 3334–3341.

Vollmar M, Schlieper D, Winn M, Buchner C, and Groth G (2009). Structure of the c_{14} Rotor Ring of the Proton Translocating Chloroplast ATP Synthase. J Biol Chem **284** (27): 18228–18235.

Wada M, Kagawa T, and Sato Y (2003). Chloroplast Movement. Annu. Rev. Plant Biol. **54** (1): 455–468.

Wagner B, Goss R, Richter M, Wild A, and Holzwarth AR (1996). Picosecond time-resolved study on the nature of high-energy-state quenching in isolated pea thylakoids different localization of zeaxanthin dependent and independent quenching mechanisms. J. Photochem. Photobiol. **36** (3): 339–350.

Wagner R, Dietzel L, Bräutigam K, Fischer W, and Pfannschmidt T (2008). The long-term response to fluctuating light quality is an important and distinct light acclimation mechanism that supports survival of *Arabidopsis thaliana* under low light conditions. Planta **228** (4): 573–587.

Walters RG (2005). Towards an understanding of photosynthetic acclimation. J Exp Bot **56** (411): 435–447.

Walters RG, and Horton P (1994). Acclimation of *Arabidopsis thaliana* to the light environment: Changes in composition of the photosynthetic apparatus. Planta **195**: 248–256.

Wang Z, and Benning C (2012). Chloroplast lipid synthesis and lipid trafficking through ER–plastid membrane contact sites. Biochem. Soc. Trans. **40** (2): 457–463.

Webb MS, and Green BR (1991). Biochemical and biophysical properties of thylakoid acyl lipids. Biochim Biophys Acta - Lipids and Lipid Metabolism **1060**: 133–158.

Wehner A, Grasses T, and Jahns P (2006). De-epoxidation of Violaxanthin in the Minor Antenna Proteins of Photosystem II, LHCB4, LHCB5, and LHCB6. J Biol Chem **281** (31): 21924–21933.

Wehner A, Storf S, Jahns P, and Schmid, V. H. R. (2004). De-epoxidation of Violaxanthin in Light-harvesting Complex I Proteins. J Biol Chem **279** (26): 26823–26829.

Weston E, Thorogood K, Vinti G, and López-Juez E (2000). Light quantity controls leaf-cell and chloroplast development in *Arabidopsis thaliana* wild type and blue-light-perception mutants. Planta **211**: 807–815.

Whitmarsh J, and Cramer WA (1977). Kinetics of the photoreduction of cytochrome b-559 by Photosystem II in chloroplasts. Biochim Biophys Acta - Bioenergetics **460** (2): 280–289.

Wiedenmann A, Dimroth P, and von Ballmoos C (2008). Δψ and ΔpH are equivalent driving forces for proton transport through isolated F0 complexes of ATP synthases. Biochim Biophys Acta - Bioenergetics **1777** (10): 1301–1310.

Wild A, Höpfner M, Rühle W, and Richter M (1986). Changes in the stoichiometry of PSII as an adaptive response to High-Light and Low-Light Conditions during Growth. Z Naturforsch **41**: 597–603.

Wraight CA, and Crofts AR (1970). Energy-Dependent Quenching of Chlorophyll a Fluorescence in Isolated Chloroplasts. Eur J Biochem **17**: 319–327.

Yakushevska AE, Jensen PE, Keegstra W, van Roon H, Scheller VH, Boekema EJ, and Dekker JP (2001). Supermolecular organization of photosystem II and its associated lightharvesting antenna in *Arabidopsis thaliana*. Eur J Biochem **268**: 6020–6028.

Yamamoto YH, Wang Y, and Kamite L (1977). A Chloroplast Absorbance Change from Violaxanthin De-Epoxidase. A Possible Component of 515 nm Changes. Biochem Biophys Res Commun **42** (1): 37–42.

Yang D, Webster J, Adam Z, Lindahl M, and Andersson B (1998). Induction of Acclimative Proteolysis of the Light-Harvesting Chlorophyll a/b to Elevated Light Intensities. Plant Physiol. **118**: 827–834.

Yin ZH, and Johnson GN (2000). Photosynthetic acclimation of higher plants to growth in fluctuating light environments. Photosynth Res **63**: 97–107.

7 Acknowledgements

I would like to thank my supervisor Prof. Dr. Peter Jahns for the opportunity to work in his group on this research project. Thank you Peter, for your guidance throughout the doctoral research phase, your invaluable counsil and your support, especially in times of desperation and disorientation. I am very greatful to my co-supervisor, Prof. Dr. Georg Groth, for his support and patience towards the end of my thesis.

I want to thank our collaborators at the Max-Planck Institute at Mülheim a.d. Ruhr for their contribution on the time-resolved measurements. I also want to thank Dr. Michael Melzer for the collaboration and his wonderful microscopy pictures. Also my thanks to Dr. Mark Aurel Schöttler and Dr. Stefan Hobe who helped me with parts of my work, and of course for their hospitality.

My special thanks to the AG Jahns group: To Nadine “Hase” Schwarz for sharing her knowledge at the beginning of my research phase, and for her laughter and friendship. To Lena “Sonnenschein” Brückle for being the most unbreakable person I know. We really missed you. To Lazar “Elchjunge” Pavlovic for his understanding and his friendship throughout our doctoral research phase and beyond. To Maria “Mutti” Graf for simply being the “Mutti” and of course for the best Verlängtern in the whole wide world. To Philipp “Zippie” Zache, who was an enrichment for the workgroup with his calm attitude and his great sense of humor, and of course for his friendship. To Petra “Petruschka” Redekopp for her moral support and her bright personality. To Andreas Hussner for the opportunity to work with him and for the nice discussions about world politics and everything else.
My very special thanks to Viviana “Vivi” Correa Galvis who, besides being that type of colleague everybody wishes to be blessed with, enriched my life in so many ways. Muchas gracias mi vida por todo, MUACK!
I would also like to thank our former Bachelor student Sabine “Sebaine” Schleker, who I was allowed to co-supervise, for her support: A bright future lies in front of you. I would also like to thank all the former members in this workgroup who crossed my path throughout this wonderful time.

An dieser Stelle möchte ich meiner Familie danken. Vielen tausend Dank für eure Unterstützung durch diese, nicht immer ganz so leichte, Zeit. Ihr seid die besten Eltern die man sich nur wünschen kann! Auch nach fast vier Jahren des rumdokterns fehlen mir die Worte meine Liebe und Dankbarkeit in Worte zu fassen.